BEHAVIOUR OF COMPOSITE TUBULAR CONNECTIONS IN OFFSHORE STRUCTURES

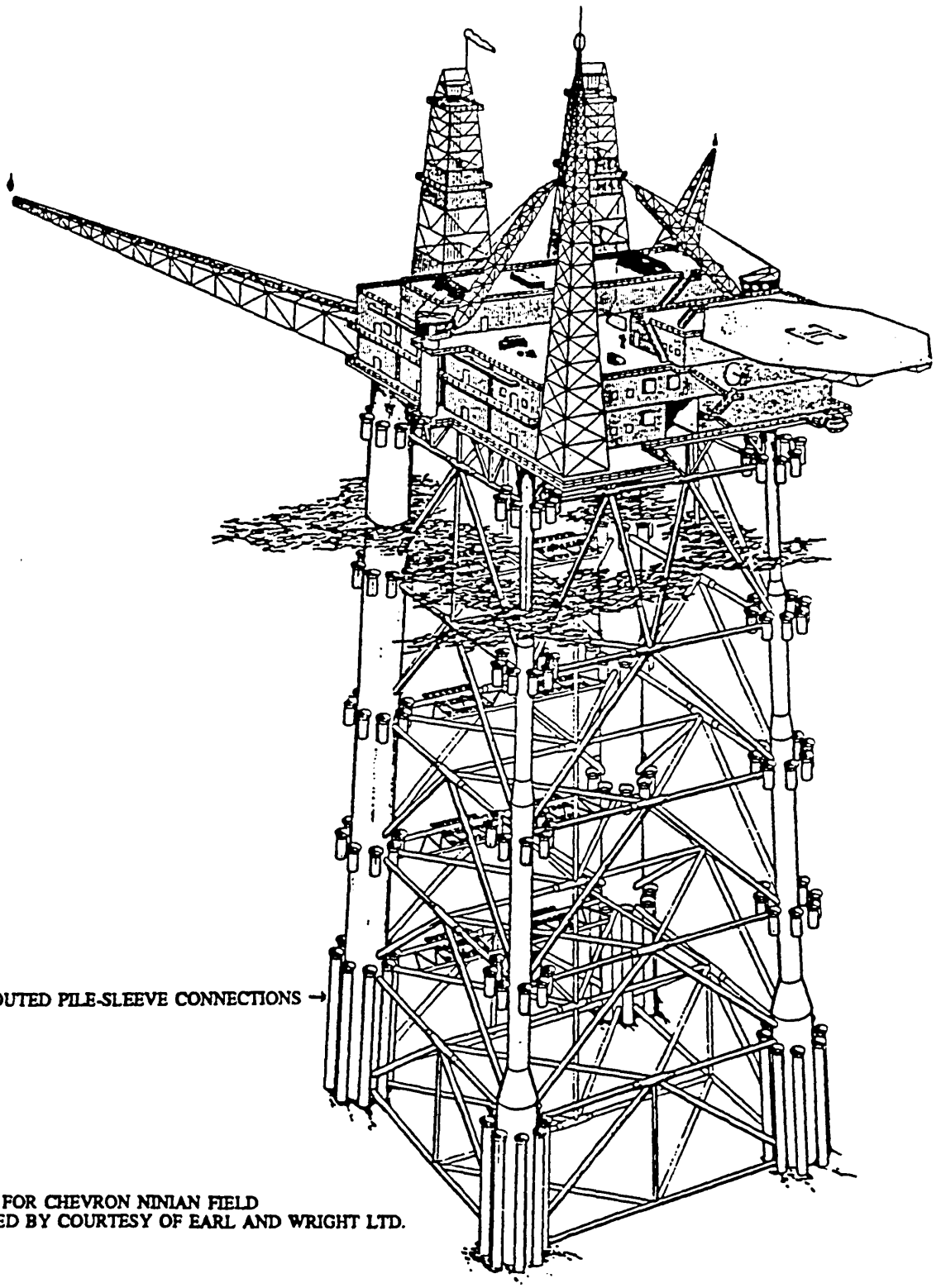
A Thesis submitted for the degree of
Doctor of Philosophy
in the Faculty of Engineering
of the University of London

by

Wendy Aritenang, MSc, DIC

Civil Engineering Department
Imperial College of Science, Technology and Medicine
September 1989

Dedicated to my parents and my wife



PLATFORM FOR CHEVRON NINIAN FIELD
REPRODUCED BY COURTESY OF EARL AND WRIGHT LTD.

ABSTRACT

This thesis deals with the behaviour of grouted pile-sleeve connections with weld-beads, typically used for offshore oil platform foundations. Experimental and analytical investigations are undertaken to shed light on the behaviour patterns, failure modes, post-ultimate response and design considerations.

On the experimental side, small scale weld-beaded connections were tested, with the aim of providing much needed load-slip curves for use in numerical analysis. The tests also provided interesting observations on the post-ultimate behaviour and damage patterns.

A semi-analytical model is presented and shown to include all the phenomena governing the behaviour, as observed in experimental work. The model compares well with available laboratory data. The value of such a model lies in its efficiency and versatility, hence it can be used to conduct extensive parametric studies.

A simplified analytical approach is also presented. Ultimate load estimates obtained from this simple technique exhibit less scatter than existing design expressions. This model can be used for the rapid assessment of obtainable strength from a given design, and to investigate the effect of varying key parameters in a design situation.

Finally, repair techniques using two half-sleeves are reviewed and a method of analysis is developed. Based on the above comprehensive study of weld-beaded grouted connections, design recommendations are made and areas worthy of further studies are identified.

ACKNOWLEDGEMENTS

I would like to express my deep gratitude to my supervisors, Professor Patrick J Dowling, Head of Civil Engineering Department, and Dr Amr S Elnashai, Lecturer in Dynamics and Numerical Methods. Professor Dowling gave me the opportunity to carry out the research work soon after I finished my MSc. Without his encouragement and patience in giving guidance, combined with the 'highly pressured' supervision from Dr Elnashai, this thesis would have taken much longer to finish. To Dr Elnashai, I am really thankful for his expertise in day-to-day supervision throughout my studies.

My gratitude also goes to the following :

- Dr Brian Carroll for his help in conducting the experimental work and many useful discussion,
- Mr Jack Neale and his colleagues, who helped me during the experimental work,
- Mr Richard Parker for the photographs of the experiments,
- Dr Wardiman Djojonegoro, Deputy Chairman of The Agency for the Assessment and Application of Technology - Republic of Indonesia, and Mr Suhairy Jusuf, former Head of Finance and Facilities Bureau in the same institution, for giving me the opportunity to persue my study in United Kingdom through the Overseas Fellowship Programme.

I also have to thank my colleagues and friends for many things :

- Mr Vangelis Vassilikos, for many useful discussions throughout my research since we were in the same MSc course.
- Mr Bambang Pratomosunu, who helped me to get started with the word processor, and also for taking some of the photographs.
- Dr Bassam Burgan and Dr Marios Chryssantoupoulous, my senior room mates, who helped me to get started with the finite element program FINAS and the graphics package.
- Mr Hassan Lamiri, Mr Pedro Vellasco, Mr Ellisiu Netto, Mr Joao Bento, Dr Ioannis Kountouris, Dr Paul Duxbury, Miss Helen Bolt, Dr Toula

Onoufriou and Dr Luis da Silva, with whom I shared and enjoyed the life in room 424 during my three years research study.

No word could express my gratitude to my parents who have worked so hard to provide a good education for me. My thanks also go to my parents-in-law who gave me support during my study.

Lastly, my study would not have been possible without enormous encouragement and support from my wife, Tjut Wanda, to whom I am really thankful.

NOTATIONS AND ABBREVIATIONS

A : cross section area

API : American Petroleum Institute

C_g : grout strength parameter

C_h : weld-bead height parameter

C_k : radial stiffness parameter

C_L : L/D_p parameter

C_s : surface roughness parameter

D : outer diameter

D' : inner diameter

DEn : Department of Energy UK

δ_a : axial relative displacement between the pile-grout

E_c : modulus of elasticity of concrete

E_g : modulus of elasticity of grout

E_s : modulus of elasticity of steel

ε_a : axial strain

ε_h : hoop strain

f_{bu} : average bond strength

F_{bu} : bond strength parameter

f_{cu} : uniaxial strength of grout

f_{cc} : confined strength of grout

h : weld-bead height

K : radial stiffness parameter according to the DEn

K_m : modified K (due to the used of longitudinal stiffener)

L : connection length

m : E_s / E_g

R : radius

S : weld-bead spacing

σ_b : bearing stress of the grout beneath the weld-bead

σ_h : hoop stress

σ_o : normal octahedral stress

: $1/3\ (\sigma_1 + \sigma_2 + \sigma_3)$

σ_r : radial stress

σ_n : transverse stress

t : thickness

τ_o : shear octahedral stress

: $1/3 \sqrt{(\sigma_1-\sigma_2)^2 + (\sigma_2-\sigma_3)^2 + (\sigma_3-\sigma_1)^2}$

τ_u : shear strength

μ : Poisson's ratio

SUBSCRIPTS

g : grout

p : pile

s : sleeve

o : outer wall

i : inner wall

TABLE OF CONTENTS

page

ABSTRACT i
ACKNOWLEDGEMENTS ii
NOTATIONS AND ABBREVIATIONS iv

CHAPTER 1 : INTRODUCTION

1.1 Background 1
1.2 Research Objectives 2
1.3 Organisation of the Thesis 3

CHAPTER 2 : REVIEW OF PREVIOUS WORK

2.1 Introduction 5
2.2 Friction 5
2.2.1 Interacting Surfaces 5
2.2.2 Friction Mechanisms 6
2.2.3 Wear 7
2.3 Concrete and Grout Strength 8
2.3.1 Uniaxial Strength 8
2.3.2 Strength of Confined Concrete 10
2.3.3 Strength of Cement Mortar and Grout 14
2.4 Bond between Concrete and Steel 15
2.5 Background to Existing Design Approaches 17
2.5.1 Introduction 17
2.5.2 API Design Formula 18
2.5.2.1 Derivation of the formula 18
2.5.2.2 Discussion 22
2.5.3 DEn Design Formula 22
2.5.3.1 Derivation of the formula 22
2.5.3.2 Discussion 28
2.6 Extension of DEn Test Programme 34

2.6.1 Early Age Cyclic Loading 34
2.6.1.1 Experimental programme 34
2.6.1.2 Discussion 35
2.6.2 Long Term Tests 36
2.6.2.1 Experimental programme 36
2.6.2.2 Discussion 37
2.6.3 Sleeve Buckling Tests 37
2.6.4 Length, Longitudinal Stiffeners and Size Effect Tests 38
2.6.4.1 Experimental programme 38
2.6.4.2 Discussion 38
2.7 Conclusion 39
Figures 41

CHAPTER 3 : EXPERIMENTAL PROGRAMME

3.1 General 57
3.2 Description of Models 57
3.3 Grouting 59
3.4 Instrumentation 59
3.5 Test Rig and Procedure 60
3.6 Test Result 61
3.6.1 General 61
3.6.2 Load-displacement relationship 61
3.6.3 Strain Gauge Results 64
3.6.3.1 Uncoupled readings 64
3.6.3.2 Average axial strain 67
3.7 Examination of Grout Annulus 67
3.7.1 General 67
3.7.2 Individual Results 69
3.7.3 End Effects 70
3.8 Discussion of Results 71
3.9 Conclusions 73
Figures 75

CHAPTER 4 : NUMERICAL ANALYSIS

4.1 Introduction 108
4.2 Bond Spring Element 108
4.3 Finite Element Formulation 109
4.4 Bond Slip Properties in Plain Connections 111
4.5 Load Transfer Mechanisms in Weld-beaded Connections 112
4.6 Bond Slip Properties in Weld-beaded Connections 113
4.7 Confined Grout Strength 115
4.8 Hoop Stress 116
4.9 Iterative Procedure 118
4.10 Finite Element Model 119
4.11 Comparison of Results 120
4.11.1 Comparison with the present tests 120
4.11.2 Comparison with the Wimpey tests 121
4.12 Long Connections 128
4.13 Scaling Effects 130
4.14 Conclusions 132
Figures 134

CHAPTER 5 : ANALYTICAL APPROACH AND DESIGN FORMULA

5.1 Simplified Analytical Approach 152
5.1.1 Simplified Model 152
5.1.2 Weld-bead Bearing Component 152
5.1.3 Friction Component 154
5.1.4 Correction due to Hoop Strain 155
5.1.5 Friction Strength 158
5.1.6 Comparison of Results 160
5.1.7 Discussion 161
5.2 Derivation of Design Equation 162
5.2.1 Basic Assumptions 162
5.2.2 Relation between Hoop and Radial Stress Components 162
5.2.3 Grout Strength at Weld-bead 163
5.2.4 Failure Modes 164

5.2.5 Effect of Bottom Weld-bead 166
5.2.6 Effect of Weld-bead Height 166
5.2.7 Effect of Length to Diameter Ratio 168
5.2.8 Summary 171
5.2.8.1 Weld-beaded connections 171
5.2.8.2 Plain connections 172
5.2.9 Discussion 173
Figures 179

CHAPTER 6 : GROUTED CONNECTIONS IN REPAIRS

6.1 Causes of Defects 193
6.2 Methods of Repairs 194
6.2.1 Welding 194
6.2.2 Grout Filling 194
6.2.3 Clamping 194
6.2.3.1 Friction clamp 195
6.2.3.2 Grouted clamp 195
6.2.3.2.1 Plain connections 196
6.2.3.2.2 Prestressed connections 196
6.2.3.2.3 Weld-beaded connections 197
6.3 Analytical Study 198
6.3.1 Assumptions 198
6.3.2 Analysis 200
6.3.2.1 Theory of cylindrical shell 200
6.3.2.2 Idealisation of the problem 200
6.3.2.3 Solution of the differential equations 201
6.3.2.4 Strength of grout beneath the weld-bead 203
6.4 Case Study 204
6.5 Discussion 205
Figures 207

CHAPTER 7 : CONCLUSIONS AND SUGGESTIONS FOR FURTHER RESEARCH

7.1 Summary and Conclusions 215
7.2 Suggestions for Further Research 218

APPENDICES 220

REFERENCES 232

CHAPTER ONE
INTRODUCTION

1.1 Background

Fixed steel jacket offshore oil platforms are typically fabricated from tubular members and supported on pile foundations. The super-structure is fabricated onshore and towed to its location. In shallow water, tubular piles are driven through the legs and the annuli between the pile and the legs are then filled with cement grout. The top ends of the piles are directly welded to the topside. For this type of structure, the grouted connection thus formed is not responsible for carrying any vertical load since the load is directly transmitted into the pile. The grout connection only contributes to increasing the stiffness of the pile in the lateral direction.

In deeper water, however, the piles are not extended up to the platform deck, but terminated at some distance above the mud line. The lower end of main legs are provided with tubular sleeves, through which the piles are driven. The annulus between pile and sleeve is filled with grout. In this case, the strength of the connection depends on the bond strength of the pile-grout-sleeve interface, which in turn is responsible for transmitting the total axial load from topside to the foundation sub-strata.

In first generation offshore oil platform, grouted connections were usually in pipe-to-pipe assemblies, in which the strength of the connection rely on friction between the grout and the steel surfaces. The strength of a plain connection is sensitive to shrinkage and geometric imperfection, hence long connection length were required, leading to substantial increase in the weight of the structure.

To improve the strength of grouted connections, there are two alternatives. One is providing shear connectors on the steel surface, and the other is prestressing the connection. Shear connectors are usually in the form of weld deposits, acting as shear-keys. This type of connection is termed 'weld-bead' connection. By providing shear connectors, a bearing mechanism is introduced by the grout beneath the shear connectors, therefore enhancing the overall strength of the connection.

Depending on the geometry, the strength of a weld-beaded connection can be up to three times that of a plain connection.

Prestressed connections can be produced by two ways, either using an expansive grout, or an active prestressing technique. Although prestressing has been shown to increase the bond strength up to seven times that of plain connections, this alternative has not been used in industry due to practical difficulties. On the other hand, weld-beaded connections are the usual option for increasing the strength of grouted pile/sleeve assemblies, despite the fact that their strength is below that of the prestressing option.

Another application of a grouted connection is in repair of damaged tubular members. Fatigue-cracked or impact-damaged tubular members can be effectively repaired by providing two half-sleeves surrounding the damaged part and filling the annulus with cement grout. The two half sleeves are connected by either short or long bolts. For the former, the grout is continuous, whilst in the latter the grout is normally discontinuous. The demand for repair of tubular members is likely to increase in the future. This is mainly due to two reasons, firstly because more offshore platforms will be built and secondly because many members of platforms have reached, or exceeded, their design life and have consequently suffered significant damage.

1.2 Research Objectives

The objective of this thesis is to propose design and analysis procedures for weld-beaded grouted connections typical of pile/sleeve offshore assemblies. Furthermore, this treatment is envisaged to cover construction of platform foundation as well as repair schemes, based on split-sleeve grouted solutions. Towards these ends, a carefully designed experimental programme is used to obtained the local stress-slip relations at the weld-bead location for use in numerical analysis calibration. This is in contrast to all previous studies that focused attention at the overall behaviour of model connections.

The relationships obtained above are used to develop and enhance a

numerical model based on finite element idealization. This model is then used to evaluate the strength of previously tested specimens. An analytical treatment is also developed and shown to yield results in good agreement with the existing population of test results. Finally, necessary adjustments are made to the developed methodology to include split-sleeve repair clamps, and results are shown to agree with experiments.

1.3 Organisation of the Thesis

In the first chapter a brief introduction of the background to the research programme and its use and applicability to existing offshore practices and future needs, is presented.

A review of the previous research in the area is given in chapter two and related to the present programme. The review is basically concerned with three main areas: bond and friction, concrete and grout strength, and a review of experimental programmes on grouted connections. This chapter also includes a theoretical treatment of the weld-bead connection problem based on previous experimental results. The stress state at the weld-bead is discussed as well as the factors governing its behaviour and strength. A suitable failure criterion for the weld-bead is chosen.

The experimental work of the present programme is given in chapter three. This consists of details of the specimens and their fabrication, test procedures and the experimental results.

In chapter four the finite element analysis is given. The constitutive relation of the weld-bead is derived from a calibration procedure, and used throughout the analysis. The results are compared with existing experimental results.

The derivation of a proposed design formula for weld-beaded connections is given in chapter five. A comparison with the existing design formulae is given for any variation of the governing factors.

Another possible application of grouted connections to the repair of tubular members for offshore structures is studied in chapter seven, and a simplified analytical approach is introduced and shown to give results in good agreement with experimental investigations.

Finally, the summary and conclusions of the whole programme are given in chapter seven. This also includes suggestions for future studies in this field, where a sparcity of results is observed or where significant economy and safety in design may result.

CHAPTER TWO
REVIEW OF PREVIOUS WORK

2.1 Introduction

Weld-beaded connections derive their strength from two components, the bond strength between the steel-grout interface and the bearing strength of the grout beneath the weld-bead. Depending on the geometric and material properties of the connection, the bond strength can be developed by adhesion, friction or wear. The bearing strength is enhanced by the increase of weld-bead height. Unless the radial stiffness is very small, the failure of the connection is normally due to grout crushing. Because of the radial confinement, the bearing strength of the grout beneath the weld-bead is much higher than its uniaxial strength. Some of the related previous work dealing with the behaviour of the two components, namely friction and bearing, is reviewed hereafter.

2.2 Friction

2.2.1 Interacting Surfaces

If two different solid materials are in contact, the actual contact surface area is much less than the total area. This is shown in figure (2.1). To calculate the contact area, Bouden and Tabor (1) introduced the following formula.

$$A_r = C/P_h \qquad (2.1)$$

where,

A_r : real contact area.

C : compression force applied to the area

P_h : penetration hardness (the maximum compressive stress that can be carried by such area without experiencing plastic yielding)

When the surface is very smooth (i.e the surface asperities are very small), there is a possibility that when two surfaces are in contact, there will be no plastic deformation. For this problems A_r become much higher than that from equation

(2.1) above. Therefore, A_r should be calculated by Hertz's equation for elastic deformation as :

$$A_r = 2.9 \left[C\, r \left(1/E_1 + 1/E_2 \right) \right]^{2/3} \qquad (2.2)$$

where,

E_1 : modulus of elasticity of material 1

E_2 : modulus of elasticity of material 2

r : radius of the contact surface

2.2.2 Friction Mechanisms

Friction can be defined as the resistance to a motion in the direction of the contact surface between two bodies. It is well known that the force required to initiate motion is greater than that required to maintain the movement. Consequently, there are two different kinds of friction, namely static and kinetic friction. The static friction is defined as the resistance developed by the contact surface when a material starts to move, while the kinetic friction is defined as the resistance of a moving material. The kinetic friction is dependent on the velocity of the motion. A typical curve showing the relationship between velocity and kinetic friction is given in figure (2.5). A friction coefficient μ is defined as the ratio of the load acting at the material interface (normal to the contact surface) to the friction force required to produce motion. According to adhesion theory, the friction is equal to the ratio of the strength of the weakest material and the penetration hardness (S/P_h). If the shear strength of the contact surface is greater than the shear strength of the weakest material (material 2 in figure (2.6)), failure will occur on path 2. In this case, the shear strength of the joint becomes equal to the shear strength of material 2.

The value of the friction coefficient is normally much higher than that given by the above definition. According to Rabinowicz (2) this is mainly :

- Adhesion theory assumes that friction is independent of the surface roughness, while being dependent upon the real contact area, which is in turn dependent on surface roughness.
- Under a normal load, the contact area deforms elastically and plastically.

- No correlation is assumed between the normal stress and the shear strength, which is contrary to observed behaviour.

Therefore, Rabinowicz introduced an improvement over the simple ratio discussed above. Hence μ is given as,

$$\mu = \frac{S}{P_h \left(1 - 2 W \cos\theta / r P_h \right)} \tag{2.3}$$

where,

P_h : penetration hardness

W : surface energy of adhesion

θ : angle of surface roughness

2.2.3 Wear

Wear is considered as the removal of a material due to mechanical abrasion between two different materials. Wear happens if, due to motion, the strength of the contact surface is greater than the shear strength of the weakest material, as illustrated in figure (2.6). Three main features of wear mechanism are:

- increases with the increase of normal stress.
- increases with the increase of distance of sliding.
- reduces with the increase in surface hardness.

The wear coefficient is defined in the following equation,

$$K = \frac{z \; 3 \; A_a}{x \;\; A_r} \tag{2.4}$$

where,

x : the distance of sliding

A_a : apparant contact surface

A_r : real contact surface

z : depth of wear

2.3 Grout Strength

2.3.1 Uniaxial Strength

The strength of weld-beaded connections is dependent on the three strength properties of the grout, i.e. the compression, tension and shear strength. The former is important in developing the bearing strength of weld-beads, the tensile and shear strength determine the maximum lateral stress which can be sustained due to Poisson's ratio effect. Additionally, in the case of connections using very low grout strength the friction strength of the grout-steel interface is also determined from the latter two strength values. Since analysis and test results using grout are sparse, the theory of concrete strength will be studied here first, and will be compared with grout where appropriate.

The strength of concrete is influenced by;

1. Water/cement to water
2. Ratio of cement to aggregate
3. Size, shape and the strength of the aggregate
4. Curing method and time

Grout does not contain aggregate, therefore points 2 and 3 do not apply. For a specific grout mix only the curing method and curing time will affect the grout strength. The increase in concrete strength with age before 28 days is difficult to predict. This is because the rate of increase in strength is dependent upon the intrinsic hardening of the cement and the water-cement ratio of the concrete mix. For an ordinary Portland Cement, Neville (3) gave the variation of strength with age below 28 days for different water-cement ratios as in figure (2.7). In grout, Billington and Lewis (4), tested four different types of grout mix using different cements; the results are presented in figure (2.8). Regarding the geometry of specimens and loading arrangement, the uniaxial strength of concrete is affected by the loaded and footing area, the depth of specimens, and the eccentricity of the loading (5, 6, 7, and 8).

The most widely accepted basic theory of concrete fracture is due to Griffith (9 and 10), who stated that all brittle materials contain flaws. Because of these flaws, under loading there will be a stress concentration at the tip of the

flaws. The stress concentration at the tips of the flaws can be very high although the nominal average stress of the material is still very low. Therefore, fracture can happen and start to propagate from these points. The derivation was originally concerned with brittle material under tension. However, it was later found to apply to fracture under a compressive stress state. This is because even under biaxial compression, the stress along the edge of the flaws at some points is in tension. Sack (11) extended the theory into three dimensional problems, whilst Clintock and Walsh (12) studied the friction effect on the Griffith's crack criterion for rocks under pressure.

Because it is important to determine the tensile strength, several authors have tried to relate the tensile strength to its uniaxial compressive strength. The typical suggested formula is ,

$$f_t = \alpha f_{cu}^{n} \qquad (2.5)$$

where,

f_{cu} : grout compressive strength

α and n are constants which determined empirically based on experimental results.

Some difficulties in determining the above relationships are because it depends on the following parameters,

- properties of the aggregate (13, and 14),
- age of concrete (15),
- concrete void ratio (16).

Some proposed values for α and n are given in table 2.1.

Table 2.1 Parameters for tensile and compressive strength relationship

α	n	Author
6.2 to 10.4	1/2	Teychenne (17)
8.3	3/4	Gardner (18)
$f_t = \frac{3000}{4 + 12000/f_c}$		Sozen (19)

(all the above values are for equation 2.6, in psi)

Because of the difficulties of testing concrete in direct tension, there are two different types of testing to determine the tensile strength. One is a flexural test and the other is a splitting test. It is widely accepted that the splitting test gives more realistic results of tensile strength than the flexural test. Neville collected some test results as shown in figure (2.9). From the figure it can be seen that the tensile strength of concrete varies between 17% to 7% of its uniaxial compression strength. This percentage decreases as the compressive strength increases.

2.3.2 Strength of Confined Concrete

The effect of confining stress in increasing the strength of concrete has been recognised for quite a long time. One of the earliest publications was due to Brandtzaegt et al (20). The authors used cylindrical concrete specimens loaded under axial compression. The confining stress was applied through hydraulic pressure around the concrete. The test results could be represented as,

$$f_{cc} = f_{cu} + 4.1\, f_3 \qquad (2.6)$$

where,

f_{cc} : concrete confined strength

f_3 : confining pressure

Since then, a number of researchers have attempted to formulate expressions for the confined concrete strength, both in biaxial and triaxial stress states, some of

which are mentioned hereafter.

Bellamy (21) conducted a test series using hollow cylinders subjected to axial load and confining stress. Based on the test results he suggested the following relationship,

$$f_{cc} = f_{cu} + 3\ f_3 \qquad (2.7)$$

Iyengar et al published a series of papers (22, 23, and 24) concerned with the biaxial stress state for concrete and mortar. The authors proposed a failure criterion under biaxial stress states as,

$$\tau_o/\sigma_c = 0.949\ (\sigma_o/\sigma_c)^{0.682} \qquad \text{for concrete,} \qquad (2.8.a)$$

and

$$\tau_o/\sigma_c = 0.550\ (\sigma_o/\sigma_c) + 0.288 \qquad \text{for mortar} \qquad (2.8.b)$$

where,

τ_o : shear octahedral stress

σ_o : normal octahedral stress

σ_c : uniaxial compressive strength

Gerstle (25,26) also formulated a relationship for both biaxial and triaxial stress states as follows.

$$\tau_o = \tau_{ou}\ (\ 1 - e^{(-2G_o/\tau_{ou})Y_o}) \qquad (2.9.a)$$

where,

Y_o : deviatoric strain

G_o : initial shear modulus

It was concluded that concrete strength is highly dependent on loading and boundary conditions (friction between loading platen and specimen) as well as loading path. The proposed formulae for the shear octahedral strength were,

a) For triaxial compression:

$$\tau_{ou} = 6.165 + 0.783\ \sigma_o - 0.00234\ \sigma_o^2 \qquad (2.10.a)$$

b) For compression-tension:

$$\tau_{ou} = -2.13 + 1.044\ \sigma_o - 0.00642\ \sigma_o^2 \qquad (2.10.b)$$

c) For triaxial extension:

$$\tau_{ou} = 1.754 + 0.644\ \sigma_o - 0.00161\ \sigma_o^2 \qquad (2.10.c)$$

Kupfer et al (27) conducted a series of tests using concrete cubes subjected to biaxial stress combinations, namely biaxial compression, biaxial tension and compression-tension. To minimize the effect of restraint from the loading plate, a brush bearing plate was used. The findings of the above work can be summarised as follows.

- The strength of concrete under biaxial compressionan can be up to 16% greater than that under uniaxial loading.
- The variation of water-cement ratio of the concrete did not affect the biaxial strength.
- Under biaxial tension and compression-tension, the relative strength (biaxial divided by uniaxial strength) decreased as the uniaxial strength increased.
- The strength of concrete under biaxial tension was almost equal to its uniaxial tensile strength.

Wang Chuan-Zhi et al (28) tested 170 concrete cubes in biaxial compression, and 40 cubes in triaxial compression. In biaxial tests they found that the compressive strength varied from 1.385 to 1.622 of the uniaxial strength according to the stress ratio. They suggested the following formula for biaxial compression.

$$\sigma_{bc} = (1 + \alpha^{0.3}/e^{0.8\alpha}) \sigma_c \qquad (2.11.a)$$

where,

σ_{bc} : biaxial strength

$\alpha = \sigma_2/\sigma_1$

In triaxial compression, for $\sigma_2=\sigma_3$, their proposed formula was,

$$\sigma/\sigma_o = 1 + 3.7\ (\sigma_3/\sigma_o)^{0.86} \qquad (2.11.b)$$

Hobbs et al (29) proposed design strengths for concrete subjected to multiaxial stresses. They suggested different formulae for each loading condition for different concrete types. The design stress for serviceability limit state was presented as well as the design strength for ultimate limit state.

Two of the more recent studies in this area are due to Ottosen and Kotsovos. Ottosen (30) proposed general failure criteria for concrete which was demonstrated to give a good agreement with experimental results. The formula was

given as follows.

$$f = A\ J_2 / \sigma_c^2 + \alpha \sqrt{J_2} / \sigma_c + B\ I_1 / \sigma_c - 1 \qquad (2.12)$$

where,

$I_1 = \sigma_1 + \sigma_2 + \sigma_3$

$J_2 = 1/2\ (S_1^2 + S_2^2 + S_3^2)$

and,

σ_1, σ_2, σ_3 : principal stresses

S_1, S_2, S_3 : principal stress deviators

A, B, and α are parameters which have to be determined.

Kotsovos published a series of papers dealing with the behaviour of concrete under multiaxial stress-states based on an extensive test series conducted at Imperial College (31, 32, 33, 34, 35, 36, 37, and 38). He studied many aspects of concrete behaviour under general stress states, including the effect of loading path and boundary conditions. An octahedral failure surface was suggested. Although his model includes empirical considerations and simplifications in order to arrive at an 'applicable' mathematical description, it is more comprehensive than the above descriptions. In brief, the proposed general expressions are as follow:

If σ_1, σ_2, σ_3 are the three principal stresses, than in cylindrical coordinates the stress can be expressed as :

$$\sigma_o = 1/3\ (\sigma_1 + \sigma_2 + \sigma_3) \qquad (2.13.a)$$

$$\tau_o = 1/3\ \sqrt{(\sigma_1-\sigma_2)^2+(\sigma_2-\sigma_3)^2+(\sigma_1-\sigma_3)^2} \qquad (2.13.b)$$

and if;

τ_{oe} : the value of τ_o at $\theta = 0°$

τ_{oc} : the value of τ_o at $\theta = 60°$

then τ_{ou}, the ultimate shear octahedral stress is given by:

$$\tau_{ou} = \frac{2\tau_{oc}(\tau_{oc}^2-\tau_{oe}^2)\cos\theta+\tau_{oc}(2\tau_{oe}-\tau_{oc})\sqrt{4(\tau_{oc}^2-\tau_{oe}^2)\cos^2\theta+5\tau_{oe}^2-4\tau_{oc}\tau_{oe}}}{4(\tau_{oc}^2-\tau_{oe}^2)\cos^2\theta+(\tau_{oc}-2\tau_{oc})^2} \qquad (2.14)$$

where

σ_o : normal octahedral stress

τ_o : shear octahedral stress

cos θ : direction of deviatoric component

The values of τ_{oc} and $\tau_{o\infty}$ were found by curve fitting to experimental data. The values are:

$$\tau_{oc} = [\ 0.940\ (\sigma_o/f_{cu} + 0.05)^{0.724}\ ]\ f_{cu} \quad (2.15)$$

$$\tau_{o\infty} = [\ 0.633\ (\sigma_o/f_{cu} + 0.05)^{0.854}\ ]\ f_{cu} \quad (2.16)$$

Full details of these expressions are given in reference (31). The schematic representation of the ultimate strength surface is given in figure (2.9). The model leads to the conclusion that the failure envelope of a triaxial stress state is open ended in stress space. In other words any applied axial stress can always be sustained provided a sufficient confining stress is applied. Since then, many researchers have made use of Kotsovos' model and have observed that it yields results in very good agreement with experimental results from a wide range of plain and reinforced concrete specimens (39 and 40). Although the model is based on testing of concrete, it is reasonable to assume that the above argument also applies to cementitious materials in general, and hence also to cement grout of the type used in offshore practice. This argument is discussed below.

2.3.3 Strength of Cement Mortar and Grout

To the best of the author's knowledge, there are no analytical failure surfaces for grout. The only option remaining is to use surfaces derived for other cementitious materials, such as concrete and mortar. Since the pre-failure behaviour of the grout is only considered through the definition of an appropriate value for Young's modulus, the above approximation does not affect the displacement history. The approximation involved in using a concrete failure criterion for grouts maybe overcome if and when appropriate grout criteria are available. Since there is insufficient data available for the typical grout mix used in offshore grout connections, the experimental data for cement mortar will be examined here. Although their material components differ slightly (grout has no sand), their overall behaviour is likely to be very similar. Only a small number of experiments have

been carried out to study the failure of mortar under a multiaxial stress state. Two of these were due to Bellamy (21) and Niwa et all (41). According to Bellamy the increase in ultimate axial strength can be related to the applied confining stress for both cases as in equation (2.7) before. Niwa conducted tests using a mortar with the proportions by weight of 1: 0.6 : 2 of cement, water and sand respectively. He compared the results with other experiments which used concrete, and in triaxial compression tests he obtained good agreement with the results given by Brantdzaegt (20) and Balmer (42). However, in extension tests more scatter was observed. In figure (2.10) the results from this mortar experiment from Niwa (41) and the triaxial concrete tests by Kotsovos (31) are compared and very good agreement is observed. The small discrepancies between mortar and concrete test results are likely to be due to differences in testing apparatus and the loading technique, rather than behaviour of the material. Thus, a comparison of the results from concrete which has been tested under different procedures often leads to significant variations, although the material components may be the same. Based on this observation, for the purpose of the present programme, it is reasonable to conclude that the failure criterion which was derived for concrete may be applicable to mortar. If there is a discrepancy due to material properties, it must be very small, and should mainly be due to the difference in modulus of elasticity and the uniaxial strength of the material. These two factors, however, are taken into account in the failure criterion and included as parameters in the formulae.

2.4 Bond between Concrete and Steel

Most of the work on bond between concrete and steel dealt with steel bars embedded in concrete (43, 44, 45, 46, 47, 48, 49, and 50), some of which are discussed hereafter. To study the bond-slip for both plain and deformed steel bars embedded in concrete, Edwards and Yaounoupolous (46) tested a number of concrete specimens with embedded reinforcing bars. They found a large scatter in the results, and concluded the following:

- The maximum bond stress increased with increasing concrete cover.
- The maximum bond stress for plain bars was about 1/2 to 1/3 of that of deformed bar, and had smaller slip.
- The initial slope of bond-slip curves was independent of the direction of loading relative to the direction of concrete settlement.

Mirza and Houde (47) performed tension tests on 62 specimens of deformed steel bar embedded in concrete blocks. The aim was to develop a constitutive relationship for the bond stress-slip, and hence to formulate the stiffness matrices in finite element analysis for linking concrete and steel elements. They obtained the following expression.

$$U = 1.95\times10^{6}\, d - 2.35\times10^{9}\, d^{2} + 139\times10^{12}\, d^{3} - 0.33\times10^{15}\, d^{4} \qquad (2.17)$$

where,

U : Bond stress

d : slip displacement

They concluded that the slip was due to a gradual deterioration of the concrete in front of the rib (lug) as a result of very high bearing and shear stresses.

Somayaji and Shah (48) concluded that, based on their experimental results, the bond stress-slip relationship for steel embedded in concrete was not unique, but varies with the distance from the end loading. Untrauer and Henry (49) tested 37 pull out specimens of deformed bars embedded in concrete with the normal stress varying from zero to 2370 psi. Some of their conclusions were as follows:

- The bond strength increases with the increase of normal stress.
- The average bond strength was greater for larger diameter of steel bar.
- The effect of normal pressure was less at smaller slips.

The suggested formula was,

$$f_{bu} = (18 + 0.45 \sqrt{\sigma_n}) \sqrt{f_{cu}} \qquad (2.18)$$

where,

f_{bu} : ultimate bond strength

σ_n : normal stress

Robbins and Standish (50) used concrete specimens with lightweight aggregate. The main conclusions from this reasearch programme were :

- Normal stress could increase pull-out strength by up to 200% for plain bars, and up to 110% for deformed bars.
- For plain bars, this increase was due to the increase of the frictional strength caused by the presence of normal stress.
- For deformed bars, there were 2 possible mechanisms. Under a low normal stress, a bursting failure was predominant. For high normal stress, shear failure could occur. For the latter failure mode, there was no advantage in

increasing the normal stress.

The bond strength of concrete encased in steel cylinders was studied at Imperial College by Virdi and Dowling in 1975 (51). Their main conclusions were as follows:

- The bond strength is mainly due to the surface roughness and the imperfections of the steel cylinder.
- The characteristic bond strength of 1 N/mm^2 was recommended for design, and in the range of tested specimens, no significant effect due to the length, diameter and the thickness of the cylinder was observed.

2.5 Background to Existing Design Approaches

2.5.1 Introduction

The first available design guidance for grouted connections was due to the American Petroleum Institute (API). The API specification RP2A 1977 (52) gives guidance for bond strength prediction of plain pipe connections. The derivation of the design formula was based on a relatively small number of tests. The guidance was soon realised to be inadequate. In the UK, the requirement of the Offshore Industry to have a more efficient and reliable approach led to an extensive test programme at Wimpey Laboratories (53, 54, 55, and 56) for The Department of Energy and Oil companies such as British Petroleum, Union Oil and Chevron Petroleum. This resulted in the formulation of design guidance for plain and weld-beaded connections which was incorporated in the DEn guidance in 1984 (57). In parallel with this programme, in Norway, experimental research on grouted connection was conducted for Det norske Veritas (58). In Japan a series of tests on grouted connections was carried out for Kawasaki Steel Corp. (59). The DEn programme was subsequently extended to investigate other uncertainties such as the effect of cyclic loading and the buckling sensitivity of the sleeve. Studies to extend the range of validity of some parameters such as weld-bead to spacing ratio and grout strength were also undertaken.

In 1984 the API introduced new design guidance as an improvement of its previous design formula (57). This was based on a study of all the available test

data, including those carried out in UK and Norway. The formula includes the provision for plain and weld-beaded connections. In addition to the above, experimental and analytical research on grouted connections has been ongoing for the last ten years at Imperial College (60,61). The current thesis is an extension of the earlier work by Elnashai (62) and Carroll (63) who investigated the behaviour of plain and prestressed connections. The latter technique was introduced as an alternative to weld-beading, and was shown to give very high increase in average bond strength. An analytical and experimental study has also been carried out at the City University (64).

2.5.2 API Design Formula

2.5.2.1 Derivation of the formula

In 1982 the American Petroleum Institute (API) formed a committee on grouted connections. The main task of the committee was to study the possibility of improvement on the existing design formula, both for plain and mechanical shear-key connections. The committee studied all the available test data, including test results carried out in the UK and Norway. In 1984 the committee published its proposed formula (65, and 66). The basic assumptions in deriving the formula were :

1. The failure mode of the connection involves bond failure at the pile-grout interface and crushing of the grout beneath the shear-keys.
2. For connections with mechanical shear-keys, diagonal cracks across the grout annulus appear during the failure process. If the distance between the shear connectors are relatively large compared with the width of the annulus, the crack will only involve one shear connector. However, if the distances are relatively small, the crack will involve two shear connectors (one on the pile and one on the sleeve).
3. The test results from Brandtzaegt (20), which stated that a confining pressure of 1 psi on a concrete cylinder adds 4.1 psi to the axial strength, was assumed to be directly apply to the grouted connection problem.
4. Radial stress acts over an axial distance four times the height of the shear connector.

Following from the above assumptions, the maximum value of load which can be carried by a connection was defined by :

$$P_u = f_{pu}\ \pi\ D_p\ L + n\ f_{cc}\ \pi\ (D_p + h)\ h \qquad (2.19)$$

where,

P_u : maximum load at failure

f_{pu} : value of average bond stress due to friction (and adhesion) at failure

D_p : outer diamter of pile

L : connection length

n : number of shear connectors

f_{cc} : grout confined strength

h : height of shear connector

The average bond stress at ultimate load becomes,

$$f_{bu} = \frac{P_u}{\pi\ D_p\ L} \qquad (2.20)$$

and by defining $C_f = f_{cc}/f_{cu}$, and assuming h/D relatively small, the equation becomes,

$$f_{bu} = f_{pu} + C_f\ f_{cu}\ h/s \qquad (2.21)$$

The factor C_f was derived as follows,

a.According to assumption 3) : $f_{cc} = f_{cu} + 4.1\ f_{conf}$ (2.22)

b.According to assumption 4) : $F_3 = 4h\ f_{conf}$ (2.23)

where,

F_3 : radial stress

F_1 : axial stress at the pile weld-bead

Therefore, from the force equilibrium in figure (2.12),

$$\frac{F_3}{F_1} = \frac{4h\ f_{conf}}{h\ f_{cc}} = \frac{4\ f_{conf}}{f_{cu} + 4.1\ f_{conf}} = R \qquad (2.24)$$

so that,

$$f_{conf} = \frac{R}{4 - 4.1\ R}\ f_{cu} \qquad (2.25)$$

also,

$$C_f = \frac{f_{cu} + 4.1\ f_{conf}}{f_{cu}} \qquad (2.26)$$

$$= 1 + 4.1 \frac{f_{conf}}{f_{cu}}$$

therefore,

$$C_f = \frac{4}{4 - 4.1\ R} \qquad (2.27)$$

The value of R depends on the form of the diagonal cracks.

For the case involving one shear connector,

$$R_A = \frac{F_3}{F_1} = \frac{(D_p + h)(t_g - h)}{D_p\ (S/2 - 4h - \mu\ t_g)} \qquad (2.28)$$

For the case of two shear connectors,

$$R_B = \frac{F_3}{F_1} = \frac{(D_p + h)(t_g - h)}{D_p\ (3S/2 - 4h - \mu\ t_g)} \qquad (2.29)$$

In order to obtain a universal values of C_f, Karsan and Krahl calculated and compared the values from the available test data, assuming the value of μ (coefficient of friction between the pile and the grout) of 0.7. They concluded that a constant value of 1.73 is acceptable. Therefore, equation (2.21) becomes :

$$f_{bu} = f_{pu} + 1.72\ f_c\ h/s \qquad (2.30)$$

The friction contribution f_{pu} was set to an empirical value of 1.15 N/mm^2, thus the final form of the equation becomes,

$$f_{bu} = 1.15 + 1.72\ f_c\ h/s \qquad (2.31)$$

For design purposes, the authors used a statistical examination of the data, and proposed an allowable stress formula for design as,

$$f_{ba} = 0.138 + 0.5\ f_{cu}\ h/s \qquad (2.32)$$

where,

f_{ba} : allowable bond stress in N/mm^2

The limitations of the equation based on the available test results are as follows,

$$2.22 < f_{cu} < 110.42$$
$$0.0 < h/s < 0.0364$$

Furthermore they also presented an analytical prediction of the limitation of h/s as follows. The maximum value of h/s is reached when the shear failure and the grout crushing occur simultaniously, so that,

$$h\ f_{cc}\ \pi\ (D_p + h) = f_{shu}\ \pi\ (D_p + 2h)s \qquad (2.33)$$

$$h/s = \frac{f_{shu}}{1.72}\ \frac{D_p + 2h}{D_p + h} \simeq \frac{f_{shu}}{1.72\ f_{cu}} \qquad (2.34)$$

Substituting $f_{cc} = 1.72\ f_{cu}$ into equation (2.21) above, and re-arranging,

$$f_{conf} = 0.1756\ f_{cu}$$

and by assuming $\mu = 1.4$ (ACI 318-77, for a coeficient of friction of shear through concrete), then,

$$f_{shu} = 1.4\ (0.1756\ f_{cu})$$
$$= 0.246\ f_{cu} \qquad (2.35)$$

substituting this into equation (2.34) above,

$$h/s = f_{shu} / (1.72\ f_{cu})$$
$$= 0.246\ f_{cu} / (1.72\ f_{cu})$$
$$= 0.14 \qquad (2.36)$$

2.5.2.2 Discussion

By following the above derivation of the API design formula, there are several factors adversely affecting the accuracy of the strength prediction using this equation.

- The simplification of the relationship between uniaxial and confined strength of the grout, as assumed in (3) above, is inaccurate since the value of C in the relation $f_{cc} = f_{cu} + C\ f_{conf}$, is not constant, but varies according to the magnitude of the uniaxial strength, confining stress and the geometry of the connection.
- The formula gives non-uniform safety factors which could have a very wide variation. A comparison with the test results showed that for plain connections the safety factor could vary from 8.25 to 2.44, and for connections with shear-keys from 5.05 to 2.

2.5.3 DEn Design Formula

2.5.3.1 Derivation of the formula

As a result of earlier studies (53, and 54), the parameters governing the behaviour and strength of grouted connections were identified to be :

- Grout strength
- Hoop and axial stiffness of the sleeve and pile
- Surface condition of tubulars
- Length to diameter ratio
- Shrinkage and expansion properties of the grout
- Imperfection of the tubulars
- The use of mechanical shear-keys

Based on these considerations, it was decided by the Department of Energy that it would be necessary to carry out some parametric studies (4, 55, and 56) to provide more information essential for the derivation of a design formula. The main findings were :

1.Surface condition effect :

Four types of surface conditions were examined,

- Shot blasted according to Class 2 BS 4243
- Shot blasted as 1), and coated with coal tar epoxy
- As 2), but rolled in grade IOG sand to provide an even sand coating
- New steel pipes.

The results showed a significant variation of bond strength with surface condition, as shown in figure (2.12).

2.Effect of grout properties :

The relationship between grout strength and bond strength from 30 tests was found to be parabolic, and can be expressed as :

$$f_{bn} = A\ f_{cu}^{0.5} \qquad (2.37)$$

where A is a constant. The constant A depends on the volume change behaviour of the grout. The effect of the shrinkage was to reduce the bond strength in the long term. The tests showed that, although the grout strength increases as the age of the grout increases from 3 to 31 days, the bond strength decreases. These results are illustrated in figure (2.14).

3.Effect of geometry :

The effect of geometry on the bond strength is very significant. The increase of radial stiffness results in a significant increase in the bond strength. A stiffness factor for a connection was introduced (55) as the sum of radial stiffnesses of the pile, sleeve and grout.

$$K = S_{grout} + \left(\frac{1}{S_{pile}} + \frac{1}{S_{sleeve}} \right)^{-1} \qquad (2.38)$$

where,

$$S = F/_{\Delta} = E\ (t/D) \qquad (2.39)$$

Δ : radial displacement

t : thickness of tubular

D : diameter of tubular

4.Effect of length to diameter ratio :

A series of specimens with L/D_p from 1 to 8 were tested, and the results showed that the bond strength decreased with the increase in specimen length.

The above results were based on plain connections tests. In tests on specimens with mechanical shear-keys, the following governing factors were studied.

1.Effect of grout strength :

Three types of grout were used,

- Oil Well-B cement grout
- High Alumina cement grout
- A proprietary post setting expansive grout

The important findings were :

- Weld-bead connections have no long-term reduction in strength due to shrinkage.
- For the 3 types of grout, there was no significant difference in the relationship between the bond strength and grout strength.

The results are given in figure (2.16).

2.Effect of radial stress :

A linear relationship between the radial stiffness K and the bond strength was found using 3 different values of radial stiffness.

3.Effect of length to diameter ratio :

In real applications the range of L/D_p could be up to 30. However, it is not possible to test connections with such geometry. This is because for long specimens it is not possible to reach the ultimate bond strength of the connection without yielding of the steel tubulars. Therefore, longitudinal stiffeners were provided on the sleeve. By this way, it was expected to increase the cross sectional area of the steel without increasing the radial stiffness, so that the sleeve could be prevented from yielding without affecting the bond strength of the connections. The results showed the maximum value of bond strength was for L/D_p of 2, and a gradual reduction of bond strength up to 26% at L/D_p of 12.

4.Mode of failure :

Failure of the connection was due to grout crushing beneath the weld-bead, and took place either in the pile-grout or the sleeve-grout interfaces. At the ends of the connections, diagonal cracks formed across the grout annulus.

Based on the above findings, Billington and Lewis (55) proposed a design formula. By substituting equation (2.39) into equation (2.38), the radial stiffness for grouted connections is exppressed as :

$$K = (E_g/E_s)(t/D)_g + [\ (D/t)_s + (D/t)_p\ ]^{-1} \qquad (2.40)$$

where,

E_g : modulus of elasticity of grout

Subscripts g,s,p refer to grout, sleeve, and pile respectively.

By plotting the K factor against the ultimate bond strength and considering the grout strength effect as in equation (2.37), a relationship between bond strength and the two main parameters for plain connections is obtained as :

$$f_b = B\ K\ f_{cu}^{0.5} \qquad (2.41)$$

where, B is a constant dependent on the surface roughness and L/D_p ratio.

In connections with mechanical shear-keys, by assuming a linear relationship between bond strength and h/s (shear-key height to spacing ratio), the equation of bond strength is written as :

$$f_b = C\ K\ (h/s)\ f_{cu}^{0.5} \qquad (2.42)$$

where

C is a factor dependent on the L/D_p ratio.

The B and C constants were derived from curve fitting of the test results, and, after allowing some reduction due to the L/D_p effect, the final bond strength formulae are,

$$f_b = 95\ K\ f_{cu}^{0.5} \qquad (2.43.a)$$

(for plain connections)

$f_b = 15200\ K\ (h/s)\ f_{cu}^{0.5}$ (2.43.b)

(for connections with mechanical shear-keys)

In a later publication, Billington and Tebbett (56), based on the parabolic assumption of relation between bond strength and the grout strength, introduced a 'bond strength parameter', which is a non-dimensional ultimate bond strength used for normalising test results by the grout strength. This is given as :

$$F_{bu} = \frac{f_{bu}}{1.105}\left(\frac{50}{f_{cu}}\right)^{0.5} \quad (2.44)$$

where,

F_{bu} : bond strength parameter

f_{bu} : ultimate bond strength from test result

The factor 1.105 is six times the API RP2A (52) recommended design bond stress for extreme conditions.

After considering the test results and combining the above equations, the proposed general formula for a normalised bond strength is,

$F_{bu} = K\ C_L\ (\ A\ C_s + B\ h/s\ )$ (2.45)

where,

K : radial stiffness

C_L : L/D_p parameter

C_s : surface condition factor

h/s : shear-key height to spacing ratio

A and B are constants which have to be determined from curve fitting of the test results, and have a mean value of A = 76 and B = 9468.

For design purposes, characteristic values are needed. Because a normal distribution of test results showed that a 5% fractile of the test results was found with A and B of 75% of the mean value, the characteristic strength equation is given by :

$F_{buc} = K\ C_L\ (\ 57\ C_s + 7100\ h/s\ )$ (2.46)

By substituting F_{bu} into equation (2.41), the characteristic value of the ultimate bond strength, $f_{bu,}$ becomes,

$$f_{buc} = K\ C_L\ (\ 9\ C_s + 1100\ h/s\ )\ f_{cu}^{0.5} \qquad (2.47)$$

In this formula the contribution for plain connections and connections with mechanical shear-keys are included in one equation. The authors reported that if the plain connection test results were considered separately, a large standard deviation was observed, although the authors also pointed out that this could be justified due to the variation in surface roughness (C_s). The suggested values for C_s are given in table 2.1.

Table 2.1 Surface condition factors

C_s	Surface Conditions
1	Connection with mechanical shear-keys
0.8	Plain connection, shot blasted or lightly rusted
0.6	Plain connection, with mill scale
0.3	Plain connection, with painted or epoxy coated

Recommended values for the L/D_p factor (C_L) are given in table (2.2) below.

Table 2.2 L/D_p factors

C_L	L/D_p
1.0	2 to 4
0.9	4 to 8
0.8	8 to 12
0.7	12 to 20
0.6	> 20

Safety Factors:

In assessing the safety factor of six, as widely used at the present time in offshore structures, Billington and Lewis identified partial safety factors which could affect the safety factor of the connection, categorised as follows.

- Safety factor for loading : Φ_f = 1.2 to 1.6
- Safety factor for material : Φ_m = 1.5
- The difference between the characteristic and mean values : Φ_{b1} = 1.33
- Allowance for effect of Cyclic loading during grouting and curing : Φ_{b2} = 1.20
- Allowance for the effect of incomplete grouting : Φ_{b3} = 1.15
- Allowance for the effect of intermixing with seawater : Φ_{b4} = 1.15
- Allowance for any difference in results between grout cubes prepared onshore and offshore : Φ_{b5} = 1.0 or 1.2
- Allowance for co-existent shear and moment : Φ_{b6} = 1.2
- Allowance for redistribution of load within the pile group : Φ_{b7} : 1.0

Based on these values, and assuming there is no interdependency between the partial values, the required safety factor, taken as a product of all Φ values, is between 4.6 and 7.4. They, therefore, concluded that the safety factor of six is reasonable. For a characteristic value, taken as 75% of mean value, the safety factor should be taken as 4.5. Therefore, the allowable bond stress is defined as,

$$f_{bp} = f_{buc}/4.5 \qquad (2.48)$$

where,

f_{bp} : allowable bond stress

f_{buc} : charateristic bond strength

The bond strength equation as in equation (2.47) was then implemented in the new DEn design guidance as well as the C_L and the safety factors. One of the first applications of the above design equation was in designing BP Magnus platform (67).

2.5.3.2 Discussion

As shown by equation (2.47) above, the mechanisms of weld-beaded connections are governed by radial stiffness, weld-bead height, weld-bead spacing,

grout strength and length of the connections. This in turn is discussed as below.

i. Radial stiffness

Although the parameter K has been shown by previous experiments to have a significant effect on the connection strength, there are some difficulties in formulating a procedure for calculating this effect. Whilst the API (68) does not recognise the effect of radial stiffness, the formula from DEn (57) does not always accurately represent this effect. In the tests report by Wimpey (56), whilst the geometry of the specimens was in the range of the DEn recommendations, some results violated the DEn formula. This can be shown as follows. In the formula of K from the DEn, the effect of variation of pile and sleeve thickness are considered to be the same. However, some test result were in contradiction with this assumption. The K values of models P13 & P14, P7 & P8, P1 & P2, were changed by varying the pile thickness. Whereas, in P1 & P2, P3 & P4, P5 & P6 the K values were changed by varying the sleeve thickness. The curves plotted by the present author show that the effect of the variation of pile thickness is not always the same with varying the sleeve thickness. Moreover, the curves do not show the linear relation between K and bond strength, as depicted by the code, and shown in figures (2.17) and (2.18).

ii. Weld-bead height and spacing

The effects of weld-bead height (h) and spacing (s) are usually combined into one parameter, namely the h/s factor. In some cases the h and s cannot be considered as one parameter since the h/s factor can be either varied by varying the height alone, or varying the spacing alone, or by varying both at the same time. For example, increasing the h/s by doubling the height could give different result than by halving the spacing, although in both cases the h/s is the same. It is evident that the higher the weld-bead height is, the greater the bearing load that may be sustained. However, the bearing capacity might not increase linearly with the increase in weld-bead height, since the average bearing strength of the weld-bead tends to decrease as the height of the weld-bead increases, especially if the the weld-bead height is comparable to the thickness of the tubular.

Specimens R1 up to R10 from test series R (56) and R11 to R16 (71), exhibit a different h/s effect than the results from series Q (56). This is because in series R the spacings were kept constant (and relatively large), whilst in series Q the h was kept constant but the spacing was reduced. Although the test results from series R showed an almost linear increase of the connection strength with the increase of h, these results may need careful condsideration. Assuming a linear relation, with a straight line passing through the values of h/s = 0 and h/s = 0.006, R9 & R10 should have given higher values than those observed in the experiment, as shown in figure (2.19).

Based on the above observations, it seems that at h/s = 0.018, the test results fall below the predicted value from the linear assumption. Furthermore, if the results from series R1 to R16 are plotted on one curve, the linear relation, taken from those results, does not follow the same line. It is therefore believed that, as the weld-bead height increases, the bending moment caused by the eccentricity of the bearing stress increases. This bending moment affects the confinement, therefore reduces the bearing strength of the grout beneath the weld-bead. This is the likely cause for the reduction of the average bearing strength with the increase in weld-bead height. The effect will be significant for connections with small thickness pile. It is noted, however, that due to very little weld-bead height variation in all the test data, the variation of the strength may not be significant. Moreover, in many cases the variation of strength was within the range attributable to approximations due to using the bond strength parameter in comparing the results.

The lateral displacement of the steel cylinder produced by the radial stress as described above diminished rapidly with the distance from the weld-bead in the axial direction. If the spacing between the weld-beads is sufficiently large, the radial displacement produced by one weld-bead will not affect the next. However, if the spacing is relatively small, the transverse displacement of one weld-bead will be superimposed over that of the adjacent weld-beads. In this case the hoop strain becomes higher, thus weakening the confinement. In extreme cases, if the weld-bead spacing is very small, the shear strength of the grout in front of the weld-bead faces could be less than the bearing strength of the weld-bead, thus causing failure of the connection by shear rather than grout crushing. The strength will be

then governed by grout/grout friction of an 'equivalent' cylinder. A series of tests using closely spaced weld-beads have recently been carried out for the Department of Energy (69).

iii. Effect of grout strength

Test results from the work of Billington and Lewis (5) on the relation between the average bond strength and the grout strength in weld-beaded connections are presented in figures (2.15). It was concluded that the relationship was parabolic. As mentioned previously, this assumption may be inaccurate in the region of low grout strength, as can be seen from the above mentioned figure. In plain connections, the test results also show that the relationship was not parabolic. This is because for grout strength above 35 N/mm^2 there was no effect on the bond strength as can be seen in figure (2.14). Moreover, for the long term specimen test, reduction of bond strength was observed.

iv. L/D_p effect

The Department of Energy guidance notes (57) use certain factors to take into account the effect of variation of length to diameter ratio (C_L), as given in the following table.

Table 2.3 Parameter C_L according to DEn

L/D_p	C_L
1	(not considered)
2	1.0
4	0.9
8	0.8
12	0.7

Previous experiments have shown that the L/D_p effect did exist. However, the findings varied from one test programme to anothers (4, 56, and 70). The tests carried out for the Department of Energy (56) gave a parabolic relationship with a peak value corresponding to L/D_p of 4. Although other test by Wimpey (70) also showed the peak value at L/D_p of 4, the curves from the two programmes are quite different, since the latter gave a sharp reduction of strength at L/D_p of 8. Earlier tests by Billington and Lewis (4) resulted in significant differences in strength for L/D_p greater than 2. After reaching the peak at L/D_p of 2, the C_L decreased considerably for L/D_p of 4. However, for L/D_p of 8 it showed an increase again. For comparison, all the curves from the above-mentioned test programmes are plotted in figure (2.20).

Reassessment of the available test data highlighted two aspects of the behaviour requiring further consideration. One is the applicability of the 'bond strength parameter' and the other is the effect of elastic elongation of the steel. These two aspects are discussed below.

a) Bond strength parameter

The bond strength parameter was introduced to normalise the bond strength with respect to the grout strength, hence to allow direct comparison between various test programmes making use of different grouts. The C_L factor from the DEn was derived based on the test results due to Billington and Lewis (4), which showed a parabolic relationship between bond strength and grout strength.

Unfortunately, the above experimental results did not cover the lower range of grout strength adequately. For grout strength less than 10 N/mm^2 there was no evidence of a parabolic relationship. The data for low grout strength was insufficient, and therefore the parabolic extrapolation which was used to extend the curve to the lower range is controversial. Although the discrepancies between the values given by the parabolic relationship and the actual values in this range are small (between 10% to 20%), such errors may be quite significant when the values of bond strength are transformed to value of bond strength parameters. For example, at grout strength f_{cu} = 5 N/mm^2 the f_{bu} will be multiplied by 2.86 to evaluate the corresponding F_{bu}; whereas at f_{cu} = 40 N/mm^2 it will be multiplied only by 1.01.

Therefore, any discrepancies in f_{bu} will be magnified by 2.86 times for f_{cu} of 5 N/mm^2, whilst for f_{cu} of 40 N/mm^2 by only 1.01 times.

The significant discrepancies in the bond strength parameter have also been shown in calculating the predicted bond strength parameter for experimental results given by Billington and Lewis. From a total of 22 specimens the bond strength parameter varied between 2.33 to 1.63 with a mean value of 1.79. If the data fitted with the parabolic assumption, all the results should give the same (or almost the same) bond strength parameter value. This very significant discrepancy (i.e. 2.33 compared with the mean value 1.799) given by f_{cu} = 8.68 N/mm^2 renders the validity of the formula for low grout strength questionable. Moreover, although the results supplied by the British Petroleum showed a better value for f_{cu} = 4.66 N/mm^2 (F_{bu} of 4.85 compared with the mean of 4.79), for f_{cu} = 7.46 N/mm^2 it gave very significant discrepancies (F_{bu} of 4.18 compared with the above mean F_{bu} of 4.79).

It may therefore be concluded that if the bond strength parameter formula is to yield reliable result, the grout strength should not be very low. The closer the grout strength to the value of 50 N/mm^2, the more reliable is the obtained bond strength parameter. However, in studying L/D_p effect, it is not possible to carry out an experiment with high L/D_p values while using normal grout strength, due to test rig capacity limitations. Wimpey Laboratories (56) used f_{cu} between 2.22 N/mm^2 and 8.26 N/mm^2 to study the L/D_p effect from 1 to 12. In another programme (4) f_{cu} between 6.6 to 10.1 N/mm^2 was used to investigate L/D_p effect from 1 to 8. These series of tests employed very low grout strength which, as explained above, could lead to misleading results.

b) Pile elongation

The relative displacement between pile and grout consists of two components. The first is due to the slip movement of the pile under the effect of the applied load, and the second is due to elongation of the pile. If the length of the pile is considerably short and/or the applied load is considerably small, then the elongation of the pile can be neglected. This is the case for typical connections with L/D_p of 1 to 2. However, for a long specimen the elongation will be

significant. Neglecting the pile elongation is equivalent to assuming that the pile is infinitely stiff, hence a constant relative displacement along the length of the pile.

Since the stress-displacement relationship is the same in any weld-bead, it follows that the stress at weld-bead positions will always be the same. Therefore, regardless of the end effect, if the elongation of the pile can be neglected then the average bond strength of the connection must always be the same no matter what the value of L/D_p is. However, previous experimental results did not show this because the elongation did exist and had a significant effect on long connections. The longer the specimen, the greater the difference in total relative displacement between the top and the bottom weld-beads, thus the greater variation of bearing stresses along the length, leading to a lower average bond stress.

2.6 Extension of DEn Test Programme

In an attempt to provide more experimental data on areas of uncertainties and also to study the validity of the design formula beyond the existing range of geometric and strength parameters, the Department of Energy funded further works (69, 70, 71 and 72). The programme included studies of early age cyclic loading, long term effects, sleeve buckling, longitudinal stiffener and size effect. A summary of the test results is given and discussed below.

2.6.1 Early Age Cyclic Loading

2.6.1.1 Experimental programme

A total of eight specimens were tested (71). The geometry was chosen to represent about 1/5 of typical geometries. Two different types of grout were used, oil-well B and high alumina cement (HAC). The applied cyclic loading was designed to represent the effect of typical North Sea wave loading conditions. The typical platform has relative movement about 0.25 inch (6.35 mm) which is equivalent to 8 psi (0.06 N/mm^2) of bond stress when the grout is set. This represents 0.35% of pile diameter of 1829 mm, typically used in offshore practice. For this reason the tests were carried out under cyclic displacements of about 1.2

mm, with a frequency was 1 Hz. The main conclusions from the above programme were:

- The ultimate strength from 'early age cyclic testing' was similar to the specimen cured without movement.
- Connections with Oil-well grout showed a residual displacement about 10% of initial input displacement, while the HAC grout connection gave 50%.
- The reduction in stiffness for these tests was very significant. The relative displacement at ultimate strength was more than two times of the static test. At ultimate load the weld-bead connections gave relative displacement between 15 to 18 mm (compared with 6 to 8 mm for typical static specimens). The plain connections had a relative displacement between 30 to 45 mm. The reduction in stiffness was more significant under working loads (1/6 of the ultimate load). Relative displacements at working loads had a mean value of 1.7 mm, which is about 0.0055 D_p (compared with 0.0005 D_p typically observed in the static tests).
- The reduction in stiffness was not observed during the earlier small scale test. Therefore, there should be a scale effect particularly with regard to scalling input motion.

2.6.1.2 Discussion

By studying the test result in detail, the following interesting observations are made :

- By scaling down the actual displacement to the input displacement in the test according to the d/D_p, the percentage of residual displacement from these tests could not represent the actual behaviour properly. This is because the smaller input displacement gives smaller percentage of residual displacement as confirmed by comparing the result from models W1, W2 and W8. The former two models with input 1.12 mm, gave a residual displacement of about 10%. However, W8, which had an input displacement of 0.56 mm, gave only 5% residual displacement. Therefore, it is likely that at full scale, the residual displacement due to an early age cyclic loading is higher than that predicted by these tests.

- For connections with weld-beads, the residual displacement can be regarded as the formation of voids around the weld-bead. In fatigue tests these voids will result in impact loads exerted on the grout at the weld-bead locations, thus reducing the fatigue life of the specimen. Unfortunately, the fatigue tests were not performed on the specimens with early age cyclic loading history.
- The significant reduction in stiffness needs more attention since it could affect the serviceability of fixed offshore structure.

2.6.2 Long Term Tests

2.6.2.1 Experimental programme

A total of thirteen specimens were used, all with the same geometry as the specimens for the 'early age cyclic tests', and consisted of 3 plain and 10 weld-beaded connections. Only one plain connection specimen was tested under cyclic loading. There was no deterioration up to about 80% of predicted ultimate load. In weld-bead specimen the loading was varied from 0.27 to 0.78 of the predicted ultimate strength, whilst the frquency was set to 0.1 and 3 Hz. The main conclusions were :

- For specimens with weld-beads subjected to reversible loading the endurance limit was about 40% of the predicted bond strength. Considering a safety factor of six, the DEn design equation still has safety factor against fatigue of 2.
- Connections subjected to unidirectional loading were less susceptible to fatigue damage.
- Plain connections are less susceptible to fatigue failure.
- In practice, pile/sleeve connections are much longer than those tested. Therefore, the elastic stress distribution will be non-uniform along the connection. For long specimens, higher stress concentrations may result, leading to local fatigue failure, which will in turn affect the achievable ultimate strength.

2.6.2.2 Discussion

From the present author's point of view there are two matters that should be considered in studying the above test results :

- All specimens tested had the same geometry, thus the same radial stiffness (K about 0.012). If their stiffness was less, their relative displacements would be higher, so that there would be larger voids in the vicinity of the weld-beads, thus increasing the effect of impact on the grout. It is therefore concluded that fatigue of specimens with low radial stiffness may be critical, a factor not studied above.
- The weld-bead outstand is likely to have a significant effect on the fatigue strength. For low weld-bead outstands, friction assumes a more significant role, thus reducing the effect of impact. This is the likely caused for the observation that the plain connections are less susceptible to fatigue in this test series. For higher weld-bead outstands, the effect of impact will be higher. Therefore, there will be a lower fatigue strength. Since all specimens of this test series had the same geometry, the effect of varying the weld-bead height has also not been studied.

2.6.3 Sleeve Buckling Test

Typically a grouted connection has a sleeve of a lower thickness than the pile. If the sleeve is very thin there is a possiblity that failure of the connection will be governed by yielding or buckling of the sleeve. This possibility was studied by Wimpey (72) for the Department of Energy. The models were tested under compressive stress states applied by one of the following loading configurations.

- Compression on sleeve from both ends.
- Compression on the sleeve from one end and the pile from the other end.
- Compression on the sleeve from one end and tension on the pile from the other end.

The test series comprised both plain and shear-key connections. The test results showed that the compressive strength of the sleeves in grouted connections were significantly higher than that predicted by buckling theory of cylindrical shells (73 and 74). Under all studied conditions of loading, buckling always occured at a stress

above the yield strength of the sleeve. Therefore, for design purposes the sleeve can be adequately designed for its full plastic capacity.

2.6.4 Length, Stiffener and Size effect Test

2.6.4.1 Experimental programme

More recently, Wimpey Laboratories performed tests to investigate the length, longitudinal stiffening and size effect (70). The aim of the investigation was to study any possible effect of longitudinal stiffeners on the bond strength of the connection. This was because most of the specimens tested in previous studies were provided with longitudinal stiffeners to ensure no longitudinal buckling or yielding of the sleeve would take place prior to grout crushing. The length and scaling effects were included in order to study the validity of the previous findings from small scaled tests. The following conclusions were drawn :

- Longitudinal stiffeners had no effect on the bond strength.
- The length did have an effect in reducing the bond strength, although the results gave different values of L/D_p factors compared with other previous tests.
- No conclusion could be drawn from the test results on scaling effects. This was due to the inconsistency of the test results and also due to the fact that very few specimens were used.

The test results are presented in figure (2.21).

2.6.4.2 Discussion

The first conclusion requires careful consideration. While the use of longitudinal stiffeners may be necessary to prevent premature failure of the connections, the first conclusion stated that longitudinal stifeners did not affect the bond strength. It is the present author's opinion that for short specimens the longitudinal stiffeners do not have a significant effect on the bond strength. This is because the failure of such connections will always be due to grout crushing. However, for long specimens the failure (by yielding or buckling) of the sleeve could take place before the grout crushing, i.e the average bond strength for long

specimens could be much less than that for short specimens.

If longitudinal stiffeners are provided, the failure mode is 'forced' to be by grout crushing since the axial strength of the sleeve becomes larger than the grout bearing strength. Therefore, it is believed that since in the actual application the sleeve normally does not have any stiffeners, comparison of test results with and without stiffeners is suspect.

2.7 Conclusion

From re-assessment of existing experimental data, the following conclusions are drawn.

- The bond strength increases with the increase of grout strength. However, the effect is reduces as the grout strength increases. For grout strength above 35 N/mm^2, the effect of grout strength on bond strength is negligible.

- If the grout strength is very low, the bond component is likely to be governed by wear rather than friction mechanism.

- The grout beneath the weld-bead is under a triaxial stress state, consisting of bearing, radial and hoop stress components.

- The radial and hoop stresses are produced by the confinement. These two components of confining stress cause a significant increase in the bearing strength of the grout beneath the weld-bead over the uniaxial strength.

- The strength of a weld-bead is significantly affected by the radial stiffness.

- The effect of variation of the pile thickness is not the same as the effect of variation of the sleeve thickness, although both may lead to the same increase in radial stiffness.

- The buckling strength of the sleeve is increased by the restraint from the

grout and the pile. Therefore, the sleeve can be designed up to its yield stress.

- The effect of variation of the weld-bead height and spacing should not be considered as one parameter h/s, but has to be considered individually. Increasing h/s by increasing weld-bead height could have a different effect to increasing h/s by decreasing the spacing.

- The elongation effect is negligible for short connections, but the effect increases as the length of the specimen increases.

- The use of bond strength parameter for comparing experimental results is not always reliable, especially for specimens with low grout strength.

The survey presented above clearly indicates that there are many areas requiring further research, to develop a full understanding of the load-transfer and failure mechanisms of grouted connections, leading to more effective design procedures. In this context, the current project was initiated with the objective of identifying the possible failure mechanisms and arriving at a quantitative treatment of the ultimate strength. The experimental and analytical investigation presented hereafter attempts to compliment the existing-of-the-art.

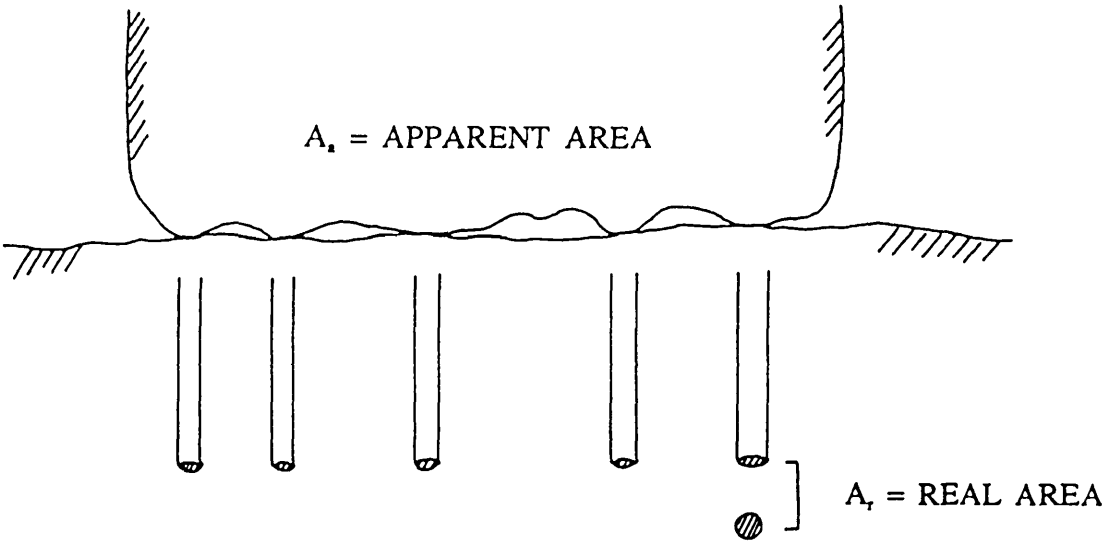
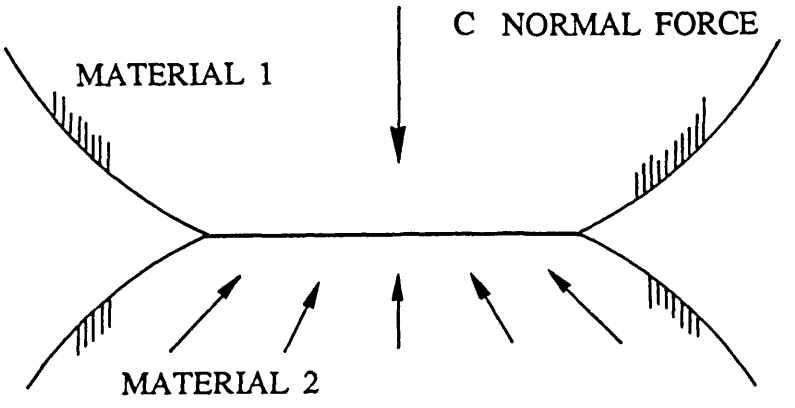


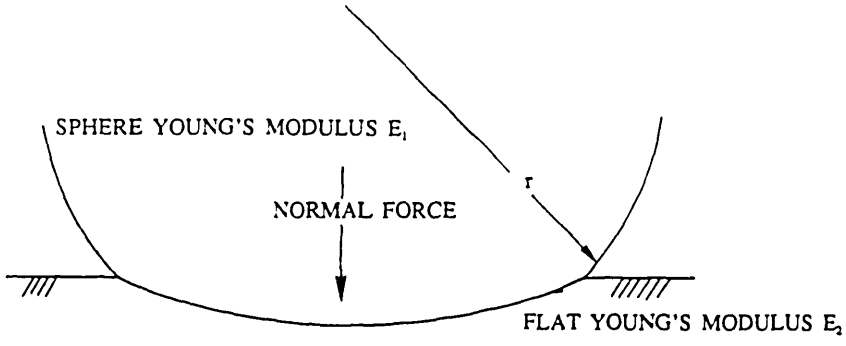
ILLUSTRATION OF A CONTACT SURFACE (RABINOWICZ-2)

FIG 2.1



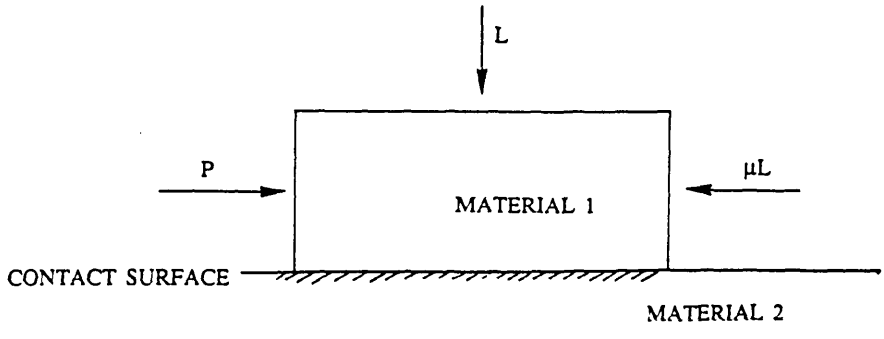
CONTACT AREA DUE TO PLASTIC DEFORMATION
(BOUDEN & TABOR-1)

FIG 2.2



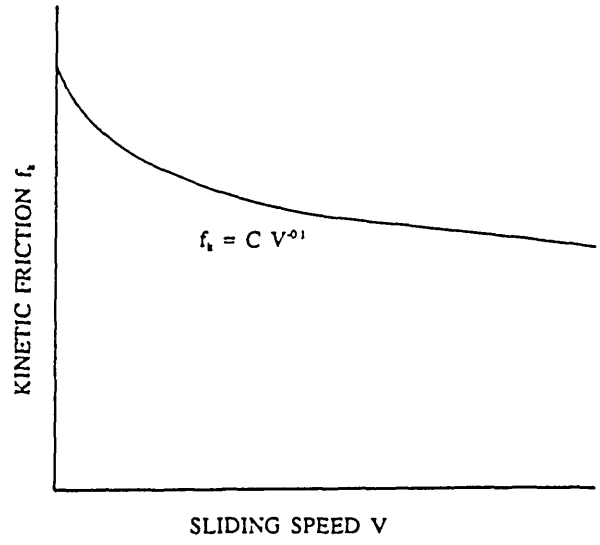
CONTACT AREA DUE TO ELASTIC DEFORMATION
(RABINOWICZ-2)

FIG 2.3



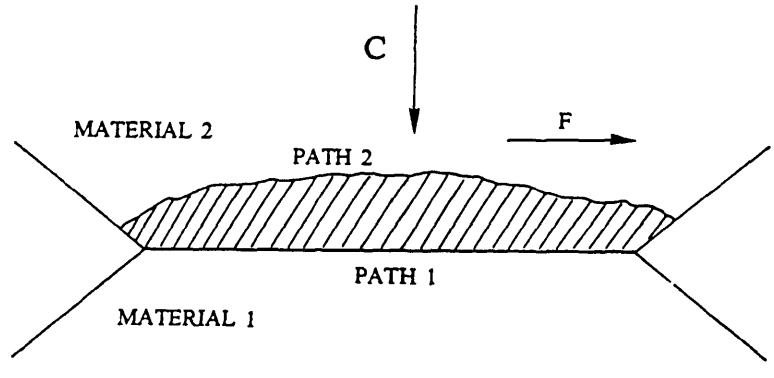
SCHEMATIC ILLUSTRATION FOR NORLMAL LOAD L,
HORIZONTAL FORCE P, AND FRICTION FORCE μL

FIG 2.4



TYPICAL RELATIONSHIP OF KINETIC FRICTION AND SLIDING SPEED

FIG 2.5

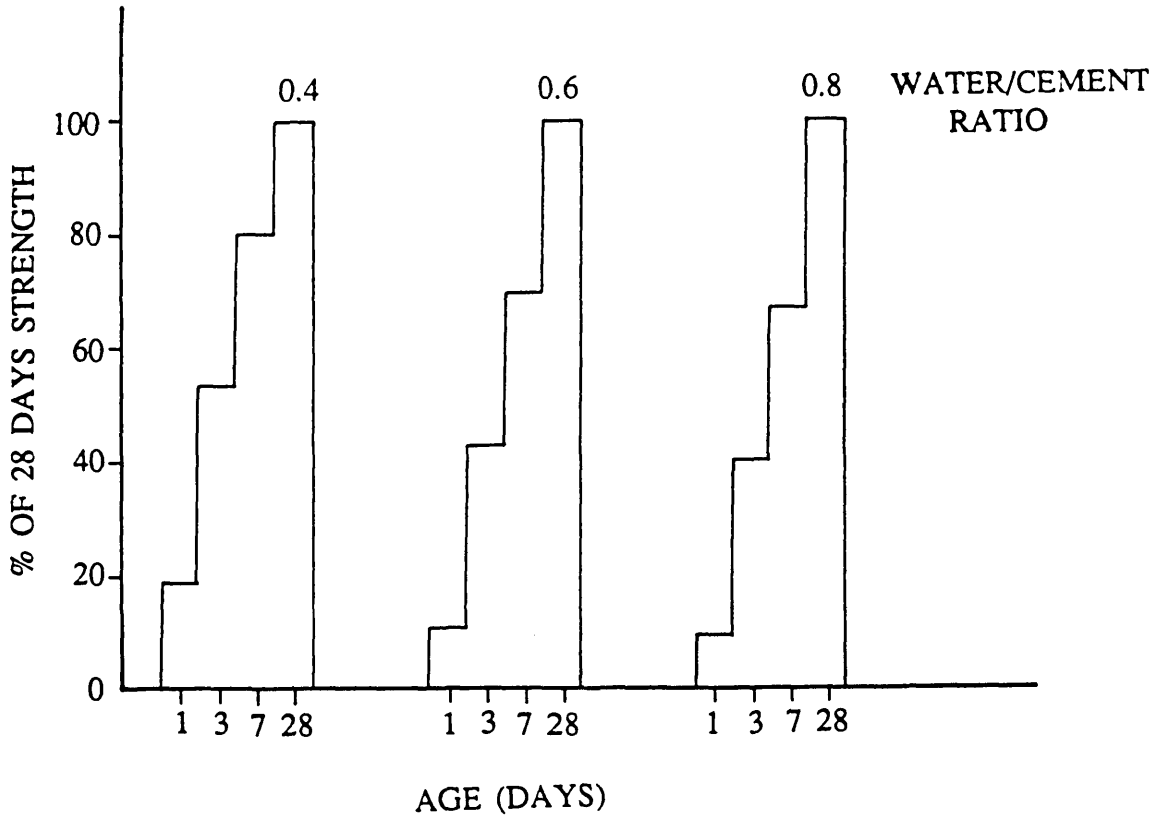


SHEARING ACTION BETWEEN TWO MATERIAL

IF THE SHEARING STRENGTH OF THE CONTACT SURFACE IS BIGGER THAN SHEARING STRENGTH OF MATERIAL 2, SHEARING FAILURE WILL TAKE PLACE ALONG PATH 2

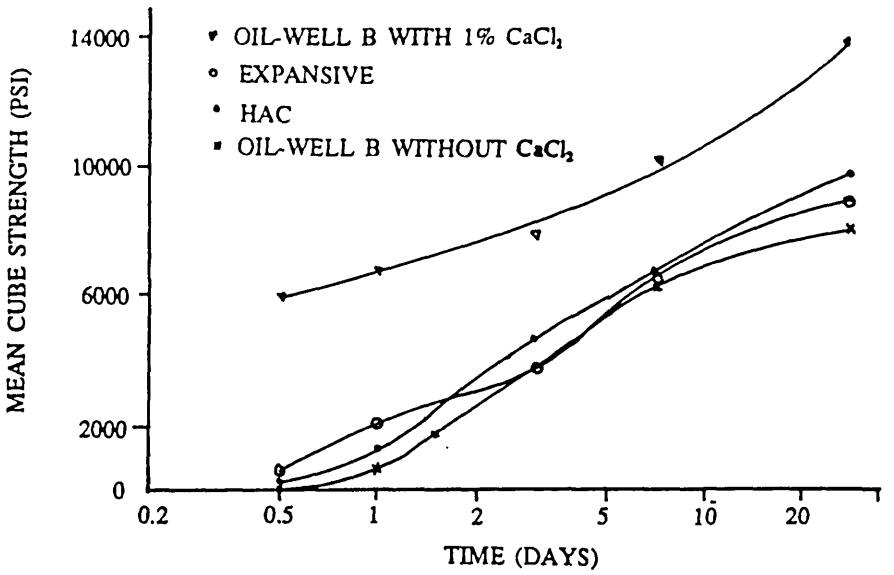
(RABINOWICZ-2)

FIG 2.6

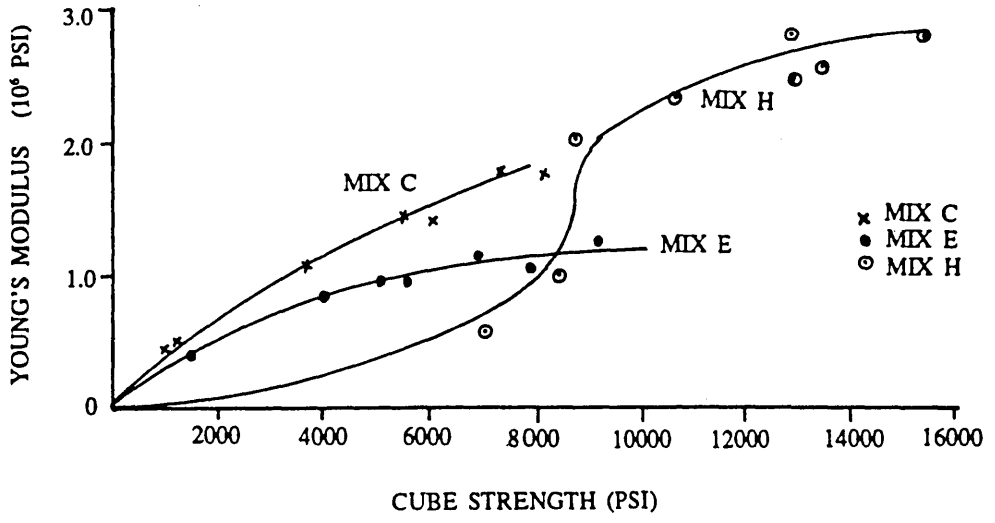


RELATIVE GAIN IN STRENGTH WITH TIME FOR CONCRETE WITH DIFFERENT WATER/CEMENT RATIO (NEVILLE-3)

FIG 2.7

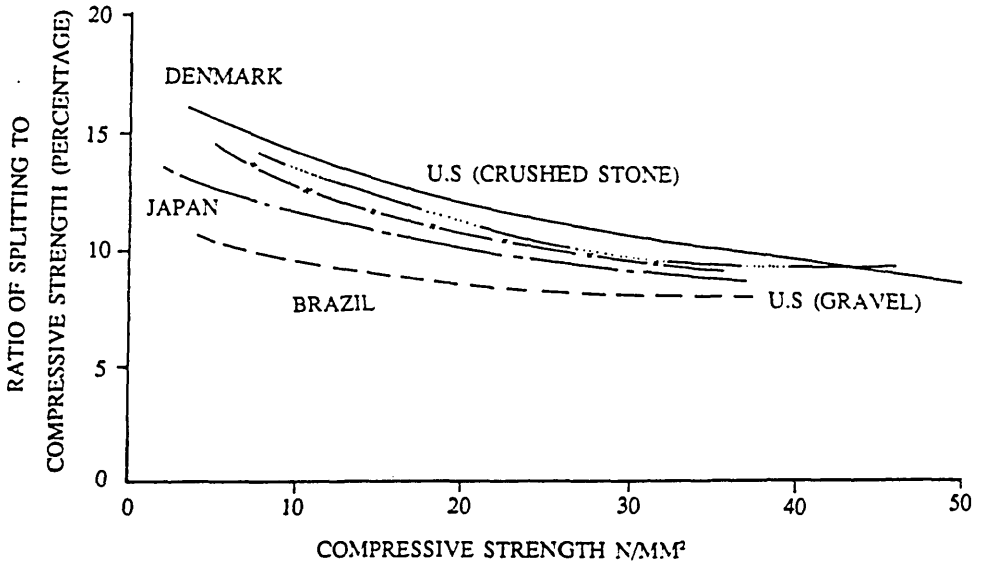


(a) VARIATION OF CUBE STRENGTH WITH TIME FOR FOUR GROUTS (BILLINGTON&LEWIS-4)



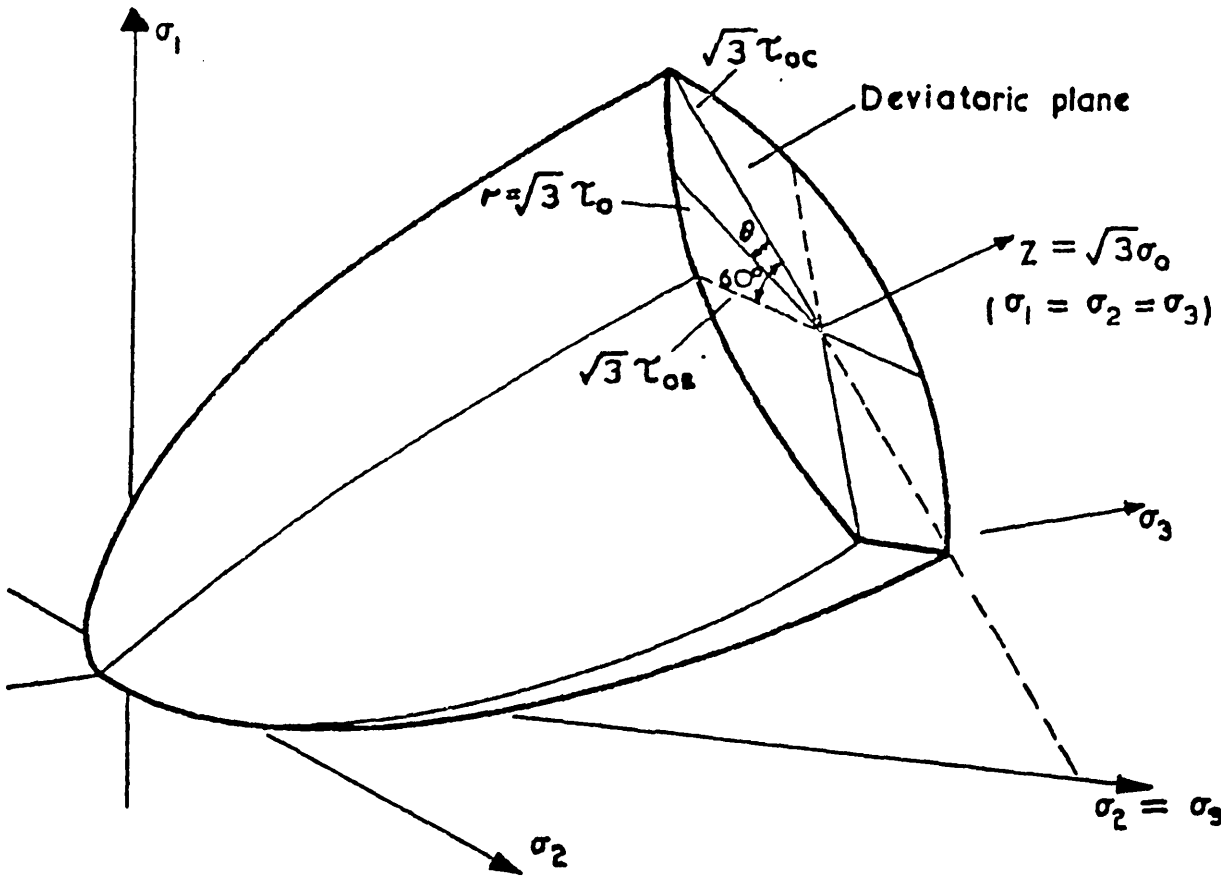
(b) VARIATION OF ELASTIC MODULUS WITH COMPRESSIVE STRENGTH FOR THREE GROUTS (BILLINGTON&LEWIS)

FIG 2.8

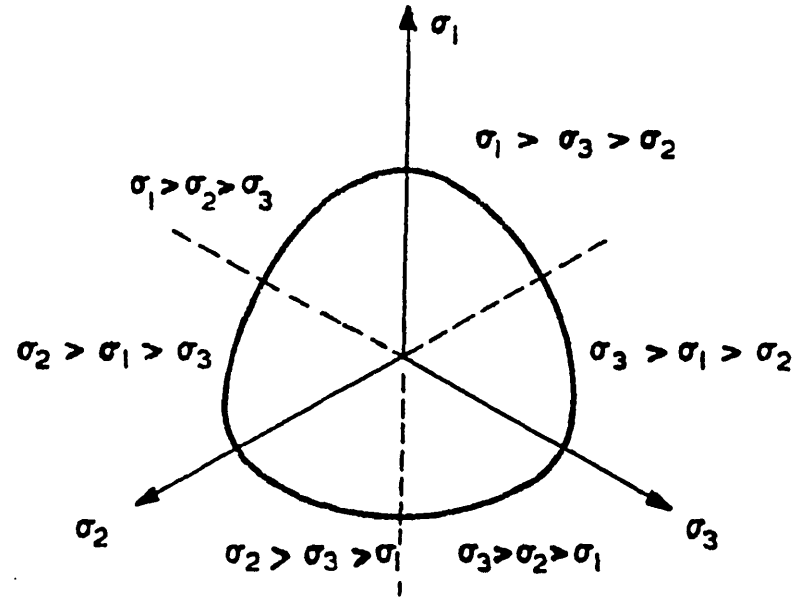


TENSILE SPLITTING STRENGTH OF CONCRETE CYLINDERS OF VARYING COMPRESSIVE STRENGTH
(NEVILLE-3)

FIG 2.9



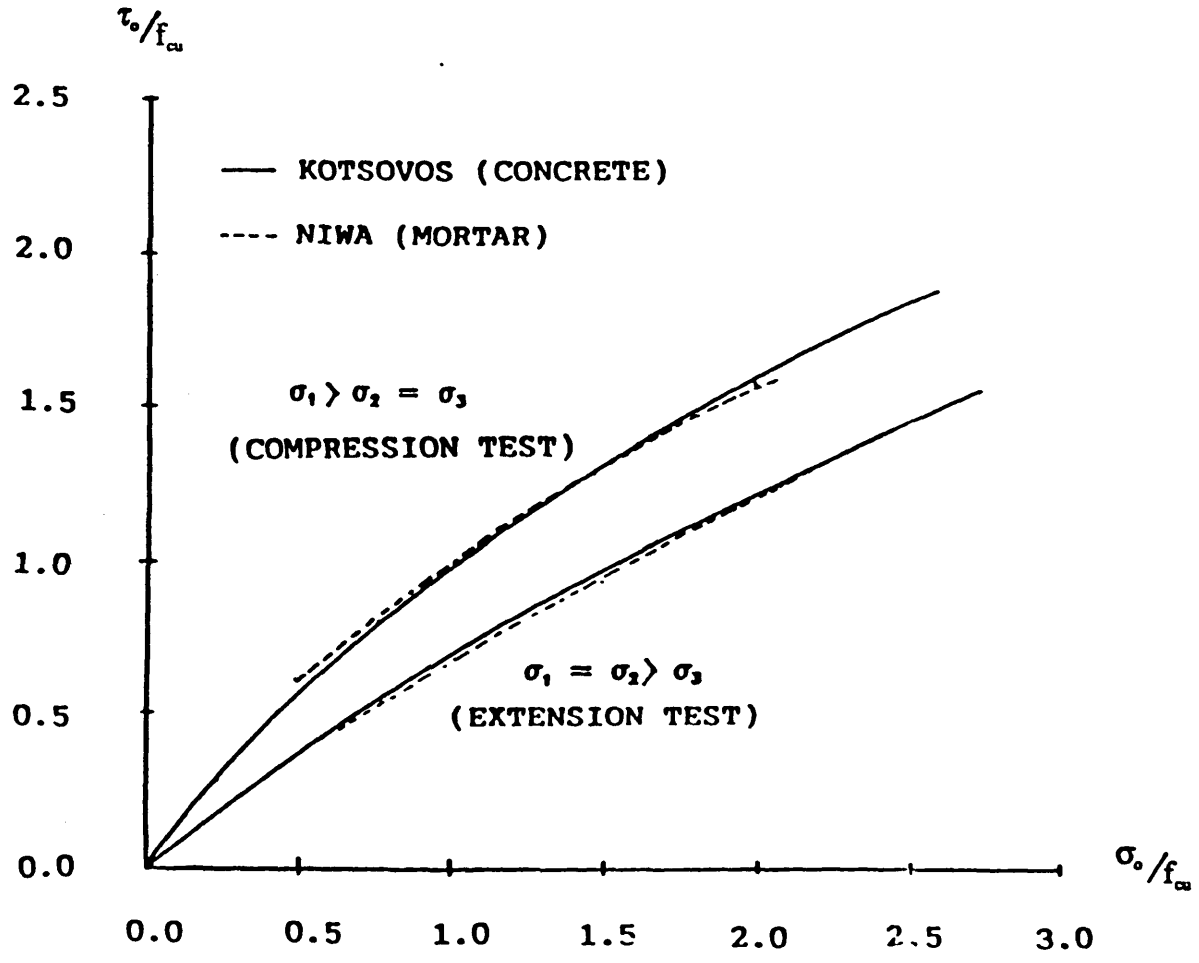
(a) Three-dimensional representation



(b) Deviatoric plane

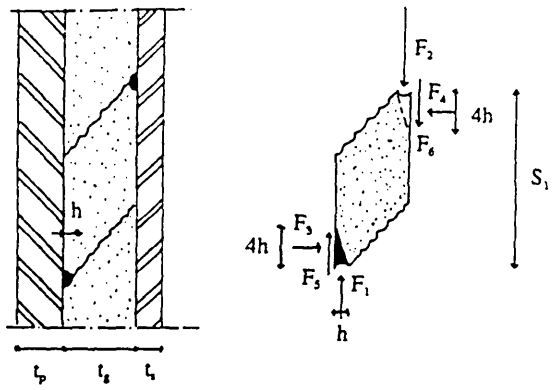
REPRESENTATION OF YIELD SURFACE FOR CONCRETE.
(KOTSOVOS-31)

FIG 2.10

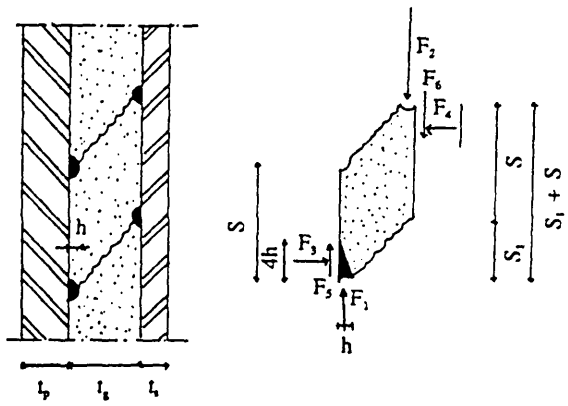


COMPARISON BETWEEN TEST RESULTS OF CONCRETE AND MORTAR

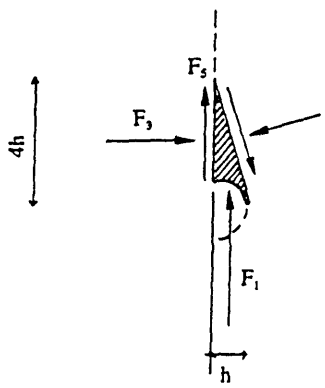
FIG 2.11



(a) FREE-BODY DIAGRAM OF CRACKED ANNULAR GROUT
CASE A (KRAHL&KARSAN)



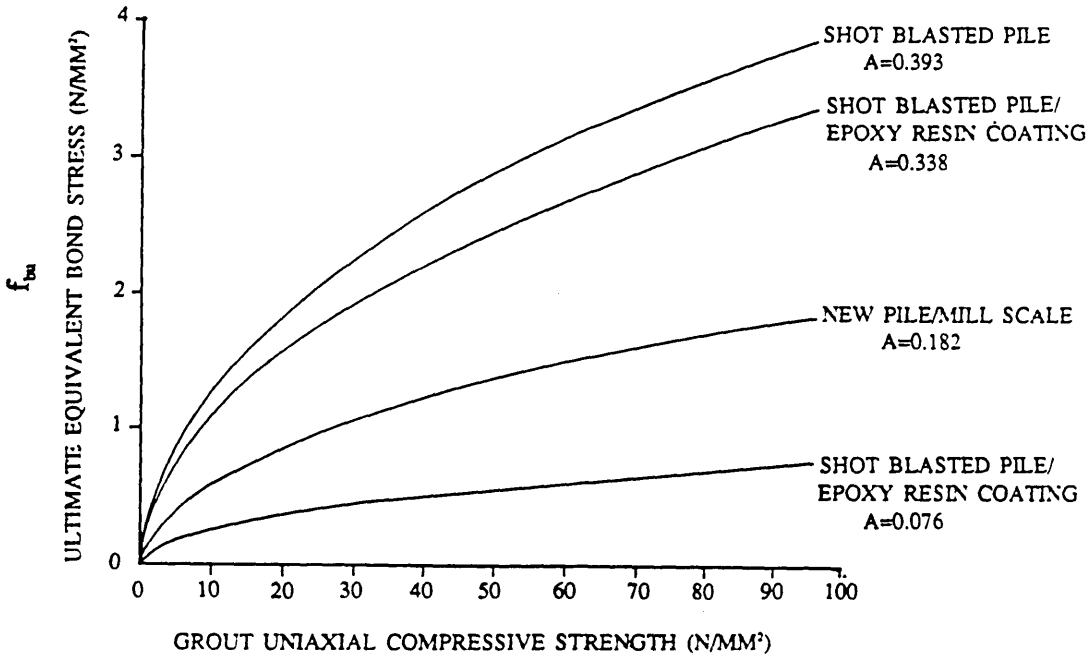
(b) FREE-BODY DIAGRAM OF CRACKED ANNULAR GROUT
CASE B



(KRAHL&KARSAN-65)

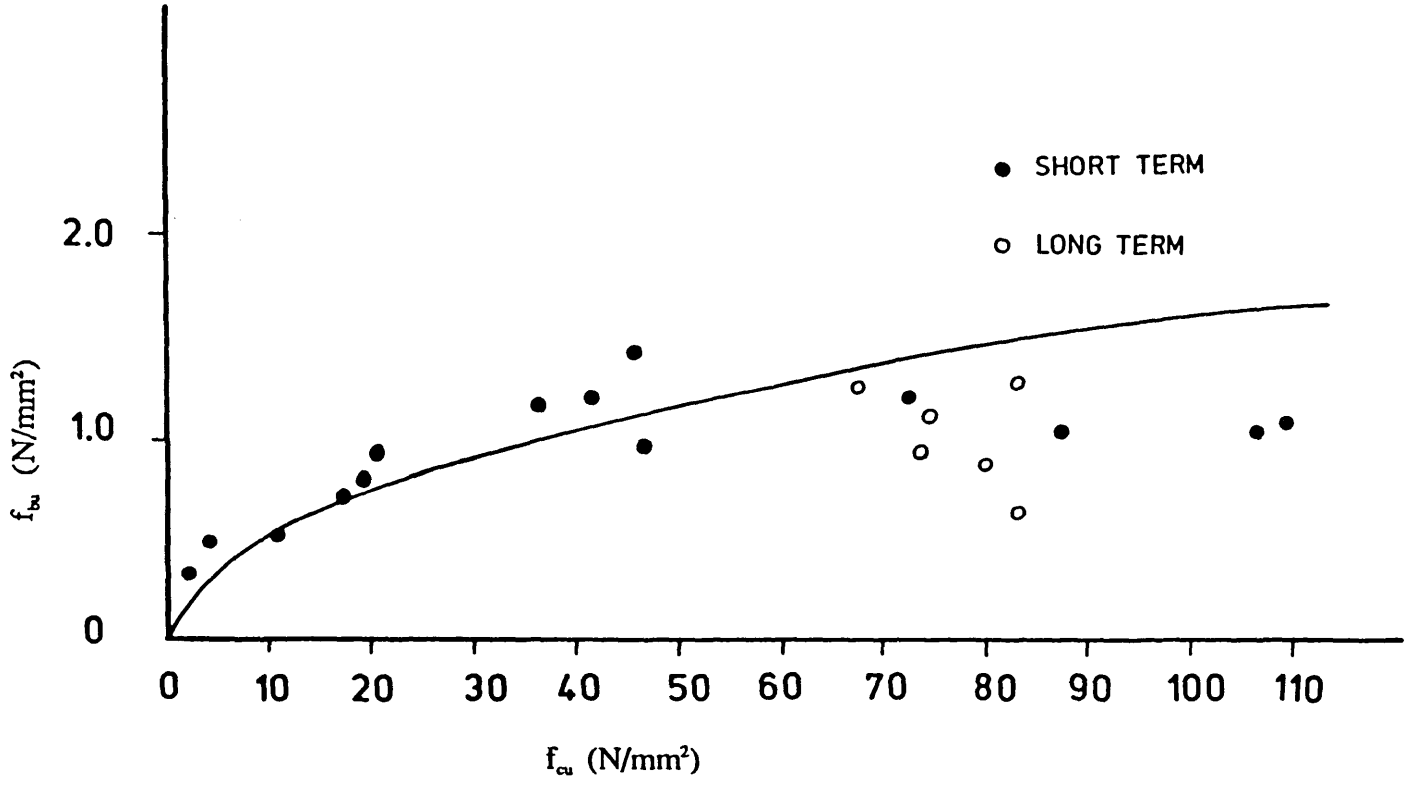
(c) CRUSHING FORCES IN GROUT AT SHEAR CONNECTOR ON PILE

FIG 2.12



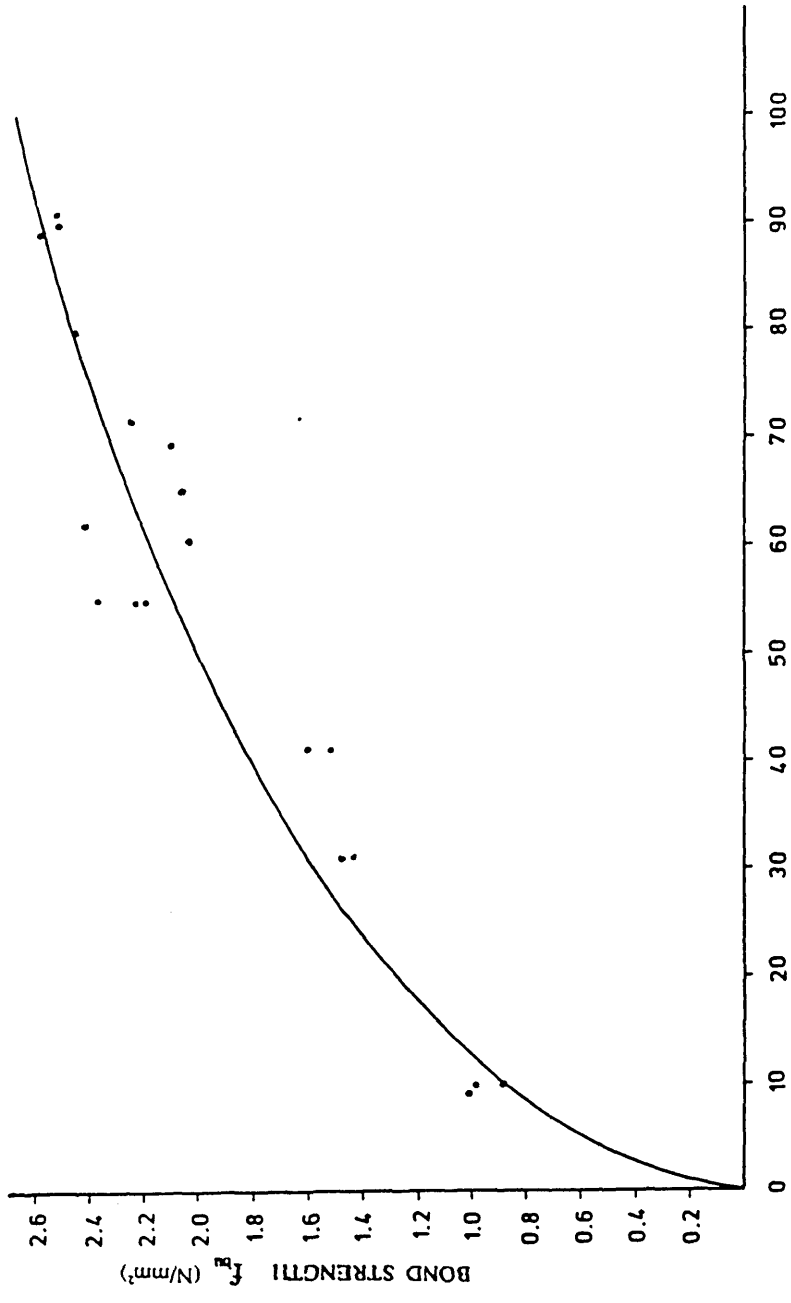
EFFECT OF SURFACE ROUGHNESS ON BOND STRENGTH
(BILLINGTON&LEWIS-4)

FIG 2.13



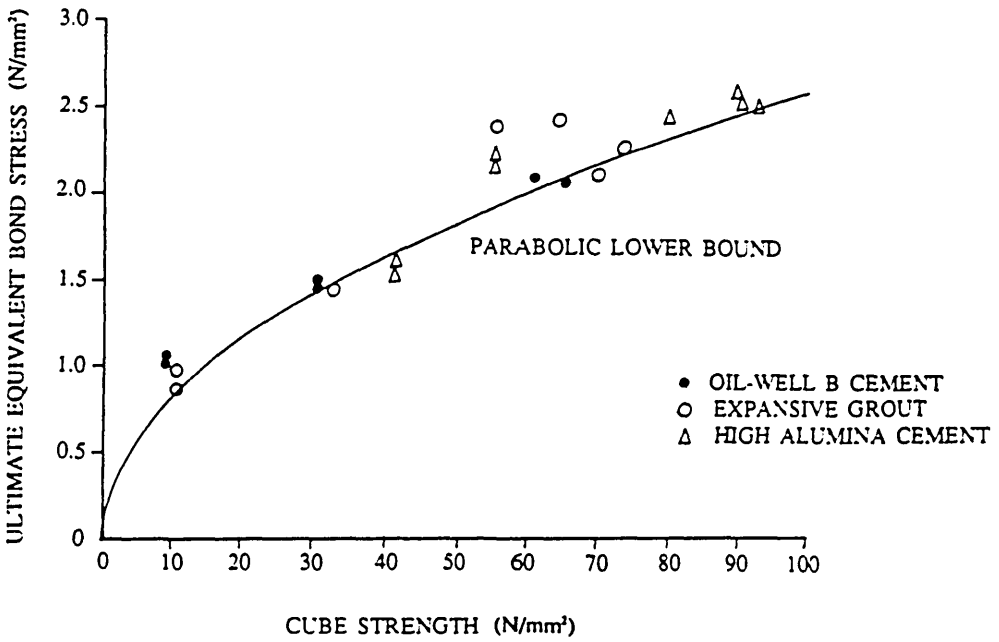
EFFECT OF GROUT STRENGTH ON BOND STRENGTH FOR PLAIN CONNECTIONS
(OTP-11,-56)

FIG 2.14



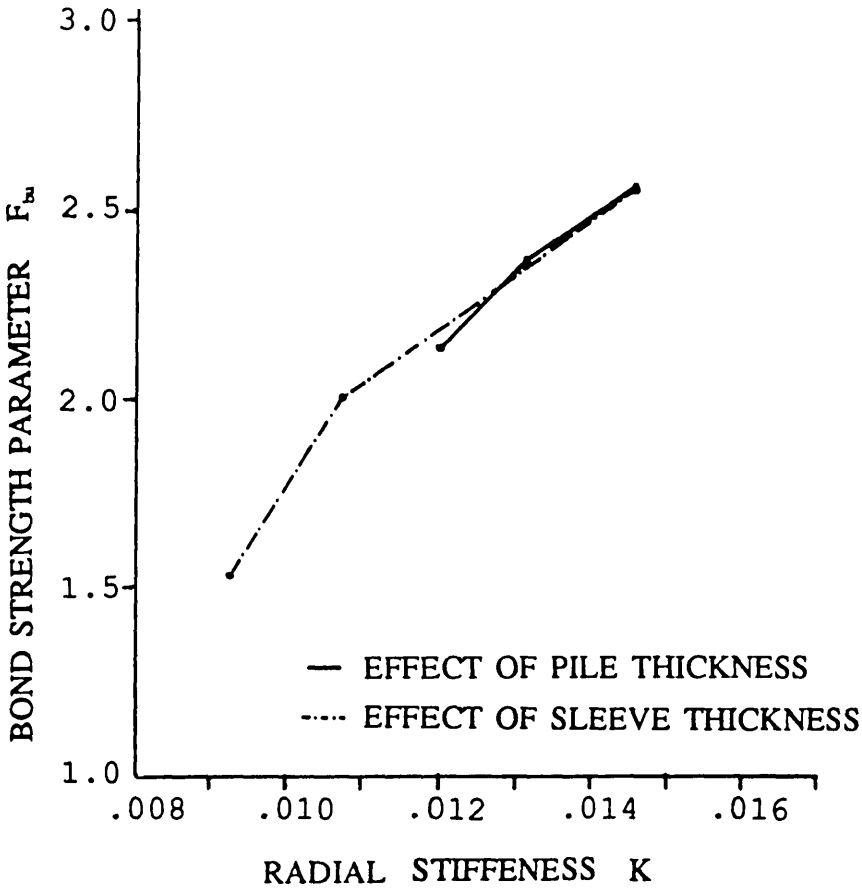
EFFECT OF GROUT STRENGTH ON BOND STRENGTH FOR WELD- BEADED CONNECTIONS (OTP-11,-56)

FIG 2.15



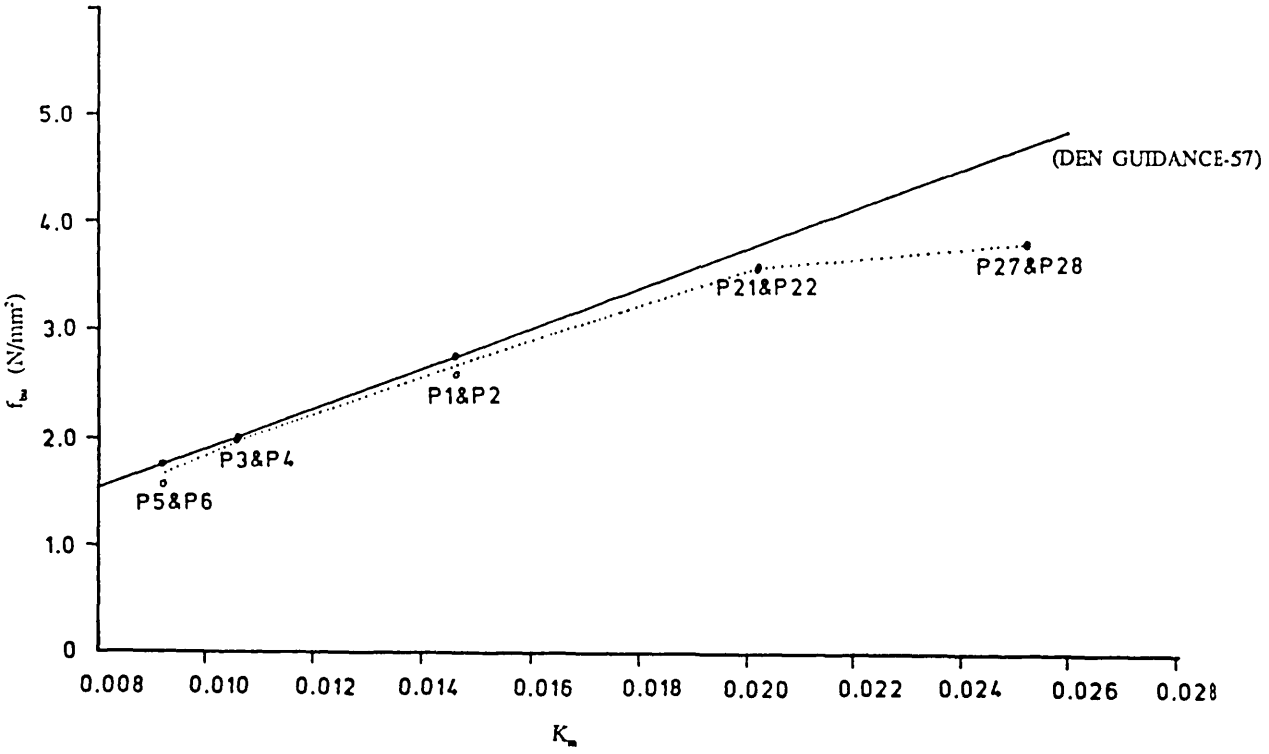
EFFECT OF GROUT TYPE ON BOND STRENGTH
WHEN USING MECHANICAL SHEAR-KEYS
(BILLINGTON&LEWIS-4)

FIG 2.16



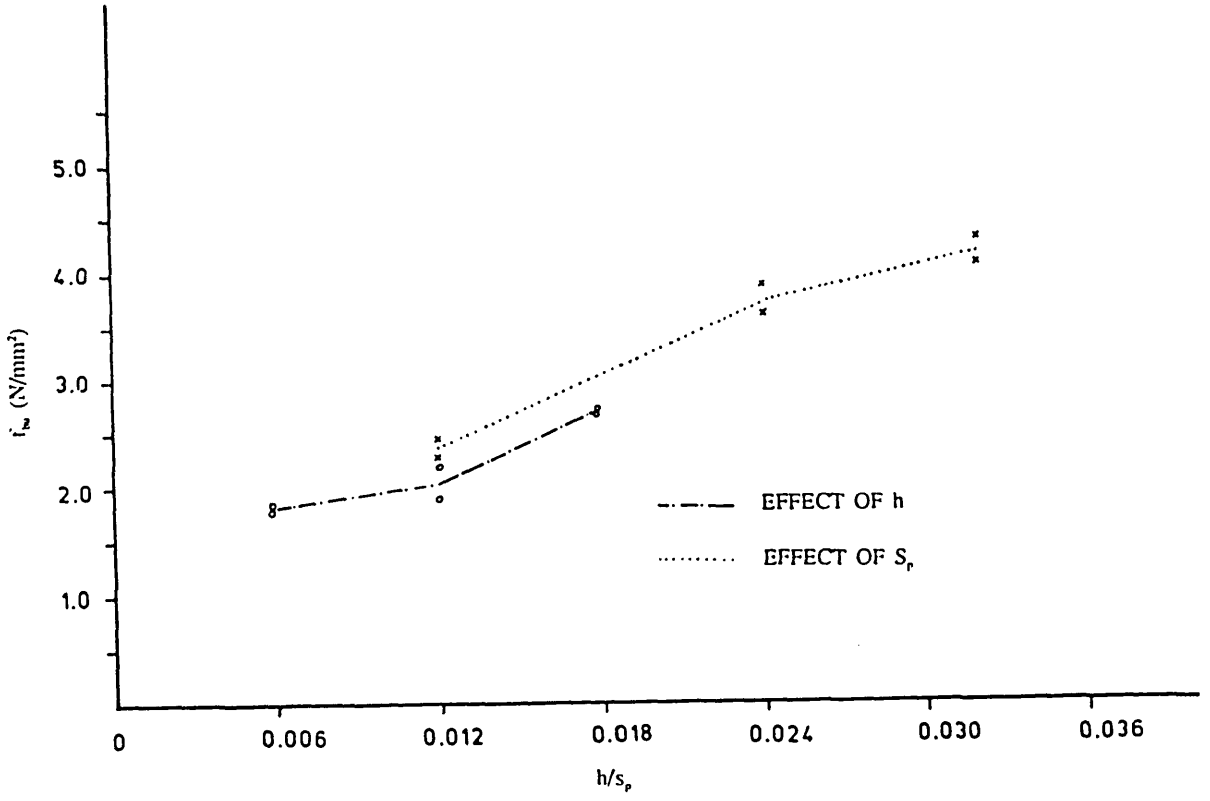
EFFECT OF PILE & SLEEVE THICKNESS
ON BOND STRENGTH PARAMETER

FIG 2.17



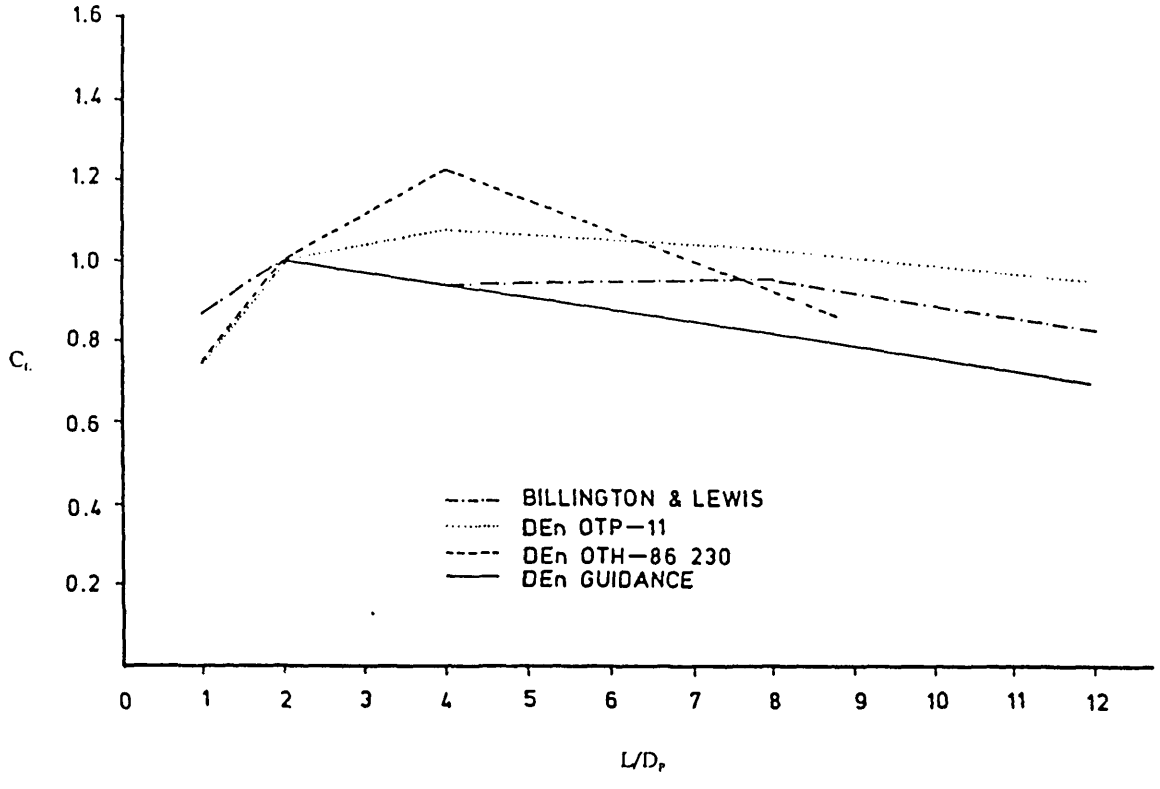
EFFECT OF RADIAL STIFFNESS K ON BOND STRENGTH (BY VARYING SLEEVE THICKNESS t_s)

FIG 2.18



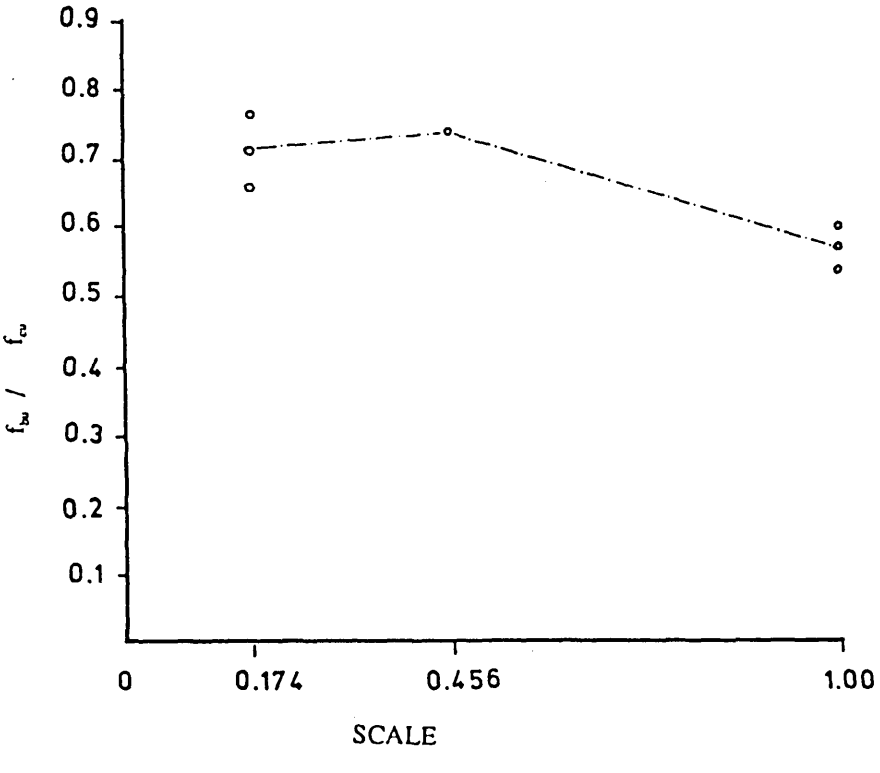
EFFECT OF WELD-BEAD HEIGHT TO SPACING RATIO

FIG 2.19



COMPARISON OF L/D_F EFFECT FROM VARIOUS TEST PROGRAMMES

FIG 2.20



EFFECT OF SCALING (OTH 86230,-70)

FIG 2.21

CHAPTER THREE
EXPERIMENTAL PROGRAMME

3.1 General

The objective of the test programme was to investigate failure mechanisms at the weld-bead, and to provide experimental data for the calibration of the numerical model. Towards this end, fundamental information on the stress-slip relationship and the stress transfer of the weld-beads was required, and therefore transducers measuring slip at each weld-bead, and strain gauges to give variation of axial and hoop strain across the weld-bead were used. Furthermore, it was the intention to examine the failure mechanisms by cutting open the grout annulus after testing.

The scope of the experimental programme was limited, and a necessary criterion for the experimental models was that they had a geometry and expected failure load suitable for testing in the loading rig available in the Imperial College laboratories. The range of parameters was restricted to variations in the pile stiffness and weld-bead height. An important feature of the models was the need to ensure that end effects from loading were minimized, as it was realised from previous work that these could influence the confinement at the loaded end.

3.2 Description of Models

The test programme consisted of six models with variations in principal geometric dimensions as shown in table (3.1). A cross section through the specimen is given in figure (3.1). The sleeve was 360 mm outside diameter and 5 mm wall thickness, while the pile had an outside diameter of 300 mm and a wall thickness which varied as shown in the schedule. The grout annulus remained 25 mm in all specimens. A weld-bead spacing of 70 mm was used on both pile and sleeve with the weld-bead height varying from 1.2 to 1.8 mm. The connection length of the specimen was 315 mm, giving a length to diameter $(L/D)_p$ ratio just over 1.0. Compared with typical North Sea pile/sleeve arrangements the cross section represents a model with a scale of about 1:4 to 1:5 .

Both pile and sleeve were fabricated from steel plate grade 50 to BS 4360, which was rolled and welded along a longitudinal seam, typically the method used for the fabrication of tubulars in the offshore industry. Weld-beads of a semi circular cross section were applied to the outer walls of the piles and inner walls of the sleeves by the 'metal-inert-gas' (MIG) process using a purpose made welding rig. The weld-beads were staggered so that the pile weld-beads were positioned mid-way between the opposite sleeve weld-beads.

The connection was designed for a "push-pull" loading arrangement in which the pile is pulled through the connection by loading on the bottom while the sleeve rests on a bottom reaction plate. Thus the pile is in axial tension while the sleeve is in compression, and the Poisson effect leads to dilation across the grout annulus, minimising any secondary confining effect. To apply this push-out load a thick walled cylindrical ram sitting on a heavy loading plate welded to the bottom of the pile was used at about one diameter away from the bottom end of the grout connection. The effects of secondary bending stresses and radial displacement due to the applied load were thus minimal. Furthermore, the radial stiffness of the connection was not affected by the loading platen. Views of the pile showing weld-beads on the outer wall and instrumentation on the inner wall are given in figure (3.2).

Table 3.1 Properties of the experimental models

Model	L	Dp	Tp	Tg	Ts	h	S
W1	315	300	8	25	5	1.2	70
W2	315	300	8	25	5	1.8	70
W3	315	300	10	25	5	1.2	70
W4	315	300	10	25	5	1.8	70
W5	315	300	15	25	5	1.2	70
W6	315	300	15	25	5	1.8	70

note:
(dimensions in mm)

3.3 Grouting

An "Oil-Well 'B'" grout was used with the proportions shown in table (3.2). The grout was mixed in a small paddle-type electric mixer, for about ten minutes and the mix was then poured into the grout annulus which was set-up in an inverted position. This was to ensure that no voids existed due to the immediate settlement which occurred below the weld-beads, in the direction of the subsequently applied load. The arrangement for casting is shown in figure (3.3.a). After pouring, the specimen was covered with a polythene sheet to prevent drying. The specimens were usually prepared for push-out testing at about three to seven days after casting; settlement of the grout due to bleeding or initial shrinkage was found to be of the order of about 35 mm, or 10% of the initial poured depth. This was confirmed by measuring the settlement of the grout in a small diameter PVC cylinder which gave almost the same amount. Two cubes 100mm by 100mm were cast for each specimen to check the development of grout strength and the strength at push out. The curve showing relationship of the grout strength and age for the present grout mix is given in figure (3.3.b).

Table 3.2 Grout composition

Material	Proportion by weight
Oil Well 'B' cement	100
Water	35
Plasticiser (Cormix)	2

3.4 Instrumentation

The instrumentation consisted of transducers and strain gauges for two models (W1 and W2), and transducers alone for the remaining four models. The transducers were used to measure the relative displacement between the pile weld-beads and the grout. Above each pile weld-bead, a threaded steel pin was cast into the grout and projected through a slotted hole in the pile wall. A transducer, which was attached to the pile wall by an aluminium channel bracket, measured the

movement as the pile slipped past the grouted pin. Using this system relative movement could be measured with an accuracy of 0.01 mm. Each specimen was provided with three pairs of transducers to measure the displacement under each pile weld-bead, the transducers in a pair being positioned at opposite ends of a diameter, thus giving a check on the circumferential variation in slip.

Both foil and wire strain gauges were used for measuring strain. The gauges were applied prior to casting. On the pile-grout interface, the gauges were protected by water-proofing and covered by a triangular shaped steel or plastic section. On the pile, a total of fourteen pairs of strain gauges on the inner wall and eight pairs on the outer wall were used. Each pair consisted of gauges aligned in the axial and circumferential direction. On the inner wall of the pile, the gauges were positioned both at the weld-bead positions and mid-way between the beads. On the outer wall the gauges were positioned only between the weld-bead positions. The strain gauge and transducer arrangement is shown in figure (3.4).

3.5 Test Rig and Procedure

A rig of capacity 300 tonnes was used to apply the push-out load as shown in figures (3.5 and 3.6), using a loading piston as described previously. To ensure concentric loading, the loading piston was attached to a spreading plate, which was embedded in an epoxy grout in the bottom of the pile and aligned using a centre hole in the pile bearing plate, by means of a guide rod. The loading was applied in increments of 45 KN, and at each load level the relative displacements, strains and the total displacement were recorded. The relative displacement and strain were measured using a SOLARTRON data acquisition system, using both paper output and disk storage. The load versus total displacement curve was obtained using an X-Y HP plotter. At ultimate load the relative displacement increased rapidly and the applied load dropped. When this behaviour was observed, the load was then gradually reduced to zero. In some models, the loading and unloading process was repeated using the same procedure. To examine the failure mode, the specimens were cut after testing. The two grout cubes which had been cast for each specimen, were crushed after load testing.

3.6 Test Results

3.6.1 General

The overall test results are given in table (3.3). Column (3) gives the radial stiffness calculated according to the DEn guidance (4) using a modular ratio (m) of 16.0. Column (5) gives the corresponding compressive cube strength, whilst column (6) gives the total ultimate loads. The average bond strengths taken as the ultimate load divided by the total area of pile/grout interface is given in column (7). It can be seen that there is an increase in the average bond strength as the stiffness and the weld-bead height increases. However, it appears that the increase due to weld-bead high is less then might be expected using the DEn method. On re-loading after failure, there is a drop in load which varied from 15% to 35%.

Table 3.3 Overall test results

Model	D/t			K	h/s	f_{cu}	P_{ult}	f_{bu}
	P	S	G			(N/mm^2)	(KN)	(N/mm^2)
W1	37.5	72.0	14.0	0.0136	0.017	50.0	675	2.274
W2	37.5	72.0	14.0	0.0136	0.025	60.5	720	2.425
W3	30.0	72.0	14.0	0.0143	0.017	51.5	585	1.971
W4	30.0	72.0	14.0	0.0143	0.025	50.2	760	2.561
W5	20.0	72.0	14.0	0.0153	0.017	63.0	620	2.080
W6	20.0	72.0	14.0	0.0153	0.025	63.9	819	2.759

3.6.2 Load-Displacement Relationships

Curves showing the load displacement relationship at each transducer position along one of the longitudinal monitoring sections are plotted for each model in figures (3.7,3.8 and 3.9). Each transducer effectively measures the relative displacement between grout and the immediately adjacent weld-bead, and the curves

are therefore described as displacement at the top, middle or bottom weld-bead, as appropriate. Generally, the curves for the positions diametrically opposite were almost identical and thus only one set of curves is presented.

It is immediately obvious that the relationship for the upper two weld beads are very similar, consisting of an initial stiff response followed by a gradual softening of the curves, with failure at a displacement generally of between 1.5 mm and 4.5 mm. In contrast, the response at the bottom weld-bead is initially very stiff, then either relative displacement ceases or a small displacement continues to failure. This behaviour, as confirmed by strain gauge results and by inspection of the failure pattern, was caused by splitting of the grout across the annulus at the bottom and a complete loss in load capacity below the weld-bead. On reloading, after initial failure, the displacement response was much stiffer, and failure was more sudden at a reduced load. The response of each model is considered in more detail below.

Model W1

The load-displacement curves gave almost exactly the same relationship for the top and the middle transducers up to ultimate load level. At post ultimate stage the top transducer relationship was slightly softer, giving a larger increment of relative displacement compared with the middle transducers. The curve for the bottom transducers was similar to the top and middle curves only up to an applied load of about 580 KN; thereafter it recorded significantly less relative displacement. The unloading and reloading process showed a high reserve of strength existed in the post ultimate stage, even at very large displacements. Ultimate load was reached at a slip of about 4 mm, while at a slip of about 12 mm the connection still sustained more than 70% of the ultimate strength. The measurements for the transducers placed 180 degree apart gave similar results for the top weld-beads; at the bottom weld-bead agreement existed up to the ultimate strength. The comparison could not be made for the middle transducers since one of the transducers seized to function properly.

Model W2

The general shape of the curves is similar to model W1. At the bottom weld-bead the transducer could not record any relative displacement after the weld-bead failed at 450 KN applied load (which is about 62% of the ultimate load). The middle and the top weld-bead continued slipping until the maximum load of 720 KN, and the corresponding relative displacement was 3.2 mm. For this specimen no unloading-reloading was performed. Instead, the load was removed immediately after the ultimate load was reached. This was in order to examine the crack pattern at first failure load. By comparing with the top weld-bead it can be seen that the middle weld-bead was somewhat less stiff immediately after the ultimate load was reached.

Model W3

In test W3 the bottom transducer failed at an applied load of less than 360 KN (about 60% of the maximum load). The corresponding relative displacement at this stage was very small, about 0.29 mm, compared with the corresponding relative displacement at the ultimate load of 3.0 mm. The unloading - reloading process shows that at post ultimate the connection still had more than 75% of the ultimate strength. As in the previous test, the stiffness of the middle weld-bead in the post ultimate stage was also less than the top weld-bead.

Model W4

In testing model W4, the failure of the bottom weld-bead occurred at an applied load of about 600 KN, which is almost 80% of the ultimate strength. The post ultimate strength was about 82% of the ultimate strength.

Model W5

In this test the bottom weld-bead failed at a relatively high load, i.e 540 KN, which is over 82% of the ultimate load of 620 KN. The corresponding relative displacement was 0.28 mm compared with 1.44 mm, the corresponding relative displacement at ultimate load. The post ultimate strength was greater than 80% of the ultimate strength.

Model W6

Here the unloading and reloading process was repeated several times. It appears that the post strength ultimate was almost constant, and was more than 80% of the initial ultimate strength. The bottom weld-bead failed at load 585 KN, this is about 71% of the 819 KN ultimate load. The corresponding relative displacement was, 0.34 mm, compared with 2.129 mm relative displacement at ultimate load.

3.6.3 Strain Gauge Results

For a number of reasons, including a breakdown of the waterproof protection, the strain gauges reading were not fully reliable, particularly on the outer wall of the pile (at the grout interface). The results were, nevertheless, sufficient to provide adequate information on the behaviour of the connections, including bending and radial confinement and stress transfer across the weld-beads. Initially the reading were processed as described below to provide data which could be readily interpreted.

3.6.3.1 Uncoupled Readings

The readings from each gauge comprise primary effects from actions in the principal direction of the gauge and Poisson effects from the orthogonal direction. These effects were un-coupled using the following basic relationships, so that resulting strains provided a measure of the forces acting in the principal direction of the gauge:

$$\varepsilon_h' = \frac{(\varepsilon_h + \mu\varepsilon_a)}{(1-\mu^2)} \qquad (3.1)$$

$$\varepsilon_a' = \frac{(\varepsilon_a + \varepsilon_h)}{(1-\mu^2)} \qquad (3.2)$$

where,

ε_h : hoop strain from reading

ε_a : axial strain from reading

ε_h' : uncouple hoop strain

ε_a' : uncouple axial strain

It is assumed in the above derivation that the Poisson effect of strains caused by stress in the radial direction was negligible. In the present case this assumption is valid, since at the surfaces of both the inner wall of the pile and the outer wall, where the gauges were protected from the grout by the isolating strips, there were no radial stresses.

Model W1

Variation of hoop and axial strains on inner and outer walls are shown in figures (3.10 and 3.11). At positions A, C, and E, (between the weld-beads) the axial strain differed between inner and outer wall, due to bending stresses caused by the eccentricity of the bearing load at the weld bead. The largest difference occurred at the upper position (B), indicating maximum load transfer at this weld-bead. A change in shape of these axial strain curves occurred from the lower to the upper positions. Near the load application, there was a strain response from initial loading and almost linear variation with load. Towards the upper positions, the curves became bi-linear, with an initial stiff response followed by a softening at a load level of some 450 KN. At the top weld-bead no significant strain response took place until this load.

Hoop strains on the inner wall at the weld-bead were compressive over the load range with response from initial loading. At the bottom weld-bead there was a sudden reversal in the strain at about 600 KN, possibly indicating cracking of the grout below the weld-bead. A continuous increase in compressive hoop strain was present at the other two weld-beads until failure. At the top weld-bead the strain was about 2000 microstrain, which for this material is in the non-linear zone of the stress-strain diagram and probably yield. Between the weld-beads, the hoop strain was of a magnitude similar to the adjacent lower weld-bead position.

On the outer wall of the pile, between the weld-beads, the hoop strains were tensile at position C and E. This may have been due to bending in the hoop direction caused by the discontinuities in the weld-bead interface with the grout both at the protecting steel strip and at the transducer slots in the wall.

Model W2

The same features which characterised the behaviour of model W1 were present in the load-strain curves for this specimen, as given in figures (3.12 and 3.13). At the bottom gauge positions, on the inner wall, axial strain increases almost linearly with load. Elsewhere, the typical bi-linear behaviour described above occurred. At the middle weld-bead position and above, the change in the curves from a stiff response to a softer response occurs at a load of between 300 KN and 400 KN (42% to 55% of the failure load). On the outer wall the axial strains at the bottom two positions were very erratic after about 50% of failure load. The differences in strain across the wall thickness again indicate bending stress associated with the weld-bead bearing force.

The hoop strain on the inner wall varied in response over the length of the connection. At the bottom weld-bead, there was a marked reversal in the strains at 450 KN which appeared to indicate cracking of the grout at this position. Confirmation of this was provided by a sudden sharp crack during load application, pointing to a release of strain energy in the tubular. At the middle weld-bead, increase of hoop strain with load continued up to the penultimate load step. At the top weld-bead the confinement strain increased to failure load, reaching a magnitude of about 1900 microstrain. At the middle weld-bead the peak value prior to failure was about 600 microstrain. On the outer wall, the hoop strains were less reliable, particularly above a load of some 400 KN, although from the strain difference between the inner and outer walls bending was indicated as in model W1.

3.6.3.2 Average Axial Strain

Using the un-coupled axial strain at positions A,C,E and G, on the inner and outer walls the average axial strains have been calculated and plotted against the load in figure (3.14) for W1 and figure (3.15) for W2. The difference in these strains across successive weld-beads is a measure of the load transfer.

Model W1

At the bottom of the pile, the calculated average magnitude through the thickness varied from 375 to 354 microstrain at the two diametrically opposite positions. Between the two lower weld-beads, the strain varied from 360 to 391 microstrain, while between the middle and top weld-bead, the average strain was between 257 and 243 microstrain. Although the strain below the bottom weld-bead was less than the calculated value (440 microstrain), and an increase in strain occurred across this weld-bead, it appears that the top weld-bead carried more load than that of the middle weld-bead. Furthermore, the bottom weld-bead may have transferred a small load until its failure at about 600 KN.

Model W2

In model W2, the average strains were very erratic, and no information regarding transfer across the lower weld-beads at failure may be deduced. However, the strain between the top and middle positions is very similar to model W1, confirming the high load transfer at this position.

3.7. Examination of Grout Annulus

3.7.1 General

After testing, the sleeves of each specimen were cut through at two ends of a diameter, and each half sleeve carefully removed to expose the failed grout annulus. Whilst each specimen differed in detail there were certain features which were characteristic of the failure patterns.

At the bottom weld-bead a complete separation of the grout had occurred in all cases at a diagonal fracture surface which extended from the sleeve weld-bead to the pile at an angle of about forty five degrees. With the exception of model W2, the annuli were also fractured across the annulus at a similar angle at both middle and top weld-beads. These diagonal cracks extended from the sleeve weld-bead and met the pile grout interface above the pile weld-bead in the groove which remained in its wake. It appeared on close examination that these cracks were wider at the sleeve than at the pile, suggesting that they may have originated at the sleeve. However, the release of locked-in tension strain in the pile and compressive strain in the sleeve as the sleeve was split, may have also caused opening or closing of these cracks. Longitudinal cracks were also present in the annuli, although these may similarly have been due to the release of residual stresses in the sleeve on cutting open.

The grooves, which formed above each weld-bead, varied in length from the top to bottom weld-bead on the pile, with maximum length at the top weld-bead. Where the groove at the bottom weld-bead could be examined, it was much shorter corresponding to the displacement at failure as indicated by the transducer readings. In front of each weld-bead, barrelling (bulging) of the grout occurred over a length of about 10 mm. The grout in this region did not appear loose or powdery, but rather had a fine dense appearance. It may be concluded that this corresponded to a plastic flow caused by ploughing of the grout, similar to that seen in metal deforming operations. The grout was under a tri-axial confinement in this region, and would exhibit high strains both laterally and axially.

The geometry of the grooves is shown in figure (3.16). At the top and bottom the shape is semi-circular corresponding to the weld-bead geometry. Between these positions, the groove is convex, the peak corresponding to maximum lateral displacement of the pile at failure. The peak displacement as measured from the grooves varied from about 0.3 mm to 0.4 mm, with the maximum displacement occurring at the upper weld-bead. The cross sections of the grout after testing for Specimen W1 up to W6 are presented in figures (3.17) to figures (3.22). In figure (3.23) a photograph of the cut section of model W4 shows the typical features of the vertical and diagonal cracks.

3.7.2 Individual Results

Model W1

Diagonal cracks were present at the top and middle weld-bead, extending from sleeve to pile at an angle of about 45°. The crack at the top weld-bead intersected the groove at 11 mm below the top of the groove, which may be compared with the displacement of 5 mm at maximum load. Measurement of the convex profile of the grooves indicated maximum lateral displacement of 0.39 mm at the top weld-bead and 0.2 mm at the middle weld-bead. Vertical cracks existed, which may explain the difference in transducer reading at opposite ends of a diameter.

Model W2

In this specimen the load was removed immediately after the ultimate load was reached, and therefore the observations represent initial failure conditions. Maximum groove length at top and middle weld-bead was 3.5 mm, which agrees with the transducer reading. A diagonal crack existed at the middle weld-bead, at an angle of about 42°, intersecting the groove at about 6 mm. Below the top weld-bead, a fine crack extended only part way through the annulus as shown in figure (3.18). Vertical cracks also existed. Maximum lateral displacement was 0.44 mm at the top weld-bead and 0.32 mm at the middle weld-bead.

Model W3

Diagonal cracks extended across the annulus at the top and middle weld-bead with an angle of about 45°. The bulging grout at the front of the weld-bead was 0.35 mm to 0.30 mm thick. In both the top and middle weld-beads, the angle of diagonal cracks was 45°. The maximum lateral displacement was 0.38 mm at the top weld-bead and 0.31 mm at the middle weld-bead.

Model W4

The angle of the diagonal crack was about 41° for both the top and middle weld-beads. At the top weld-bead, the crack intersected the groove at 5 mm below the top of the groove. Maximum lateral displacement was 0.43 mm at the top weld-bead, and 0.37 mm at the middle one. The thickness of the bulged region appeared to be about 0.2 mm.

Model W5

In this test, loading was maintained until the displacement had reached about half the weld-bead spacing. The crack pattern is shown in figure (3.21). Cracks extended at angles of 70°, 60°, 45°, 0° from sleeve to pile. Some of the cracks did not start at the sleeve weld-bead, as shown. The bottom crack was almost horizontal. Maximum lateral displacement was 0.44 mm at the top weld-bead.

Model W6

The diagonal cracks had an angle of about 45°. At the top weld-bead, the crack intersected the groove at 10 mm from the top of the groove. Maximum lateral displacement were 0.41 and 0.20 mm at the top and middle weld-beads respectively.

3.7.3 End Effect

In the present programme, the bottom weld-bead always failed in the early stage of loading. The failure was manifested as diagonal cracks, extending between the bottom weld-bead of the pile to the bottom weld-bead of the sleeve. This was confirmed by the transducer and strain gauge readings, and also from examination of the opened specimens after testing. This earlier failure of the bottom weld-bead compared with the upper weld-bead is due to a difference in the factors which govern the strength. At the bottom weld-bead, failure is due to tensile cracking across the annulus, whilst in the upper weld-beads failure is by crushing of the

grout beneath the weld-beads.

As the applied load pulls the pile downward, the pile tends to move down the grout which is resisted by bearing and friction. The forces exerted on the grout during downwards movement of the pile are transferred to the sleeve/grout interface and resisted by bearing of the sleeve weld-beads. If the pile and sleeve are sufficiently stiff, high compressive stress can be resisted by the grout beneath the weld-beads. At the bottom weld-beads, however, the force transferred to the sleeve-grout interface is only resisted by friction since there is no lower weld-bead to produce bearing. Therefore earlier tensile failure may occur across the grout annulus. If the arrangement is such that the bottom weld-bead of the pile is lower than the bottom weld-bead of the sleeve, then the crack could run from the bottom weld-bead of the sleeve to the second lowest of the pile weld-beads as described in figure (3.24). In this case, there will be two ineffective pile weld-beads.

Lack of contribution from weld-beads at the loaded end to the total strength may not be significant in full connections. It should be noted that due to the loading arrangement used in some previous tests, failure at the bottom weld-bead might be prevented by prying forces induced at the loading end. This prying force causes the pile to move toward the grout, thus causing stiffening of the bottom weld-bead. The existence of such prying forces, which can cause the strength of the connection to be overestimated, particularly in short connections, has also been reported by Lamport et al (75).

3.8 Discussion of Results

Previous investigations both at Wimpey laboratories and elsewhere used scaled models for testing, and have extrapolated the results to full size connections. The present series of tests have been subject to the same limitation and this should be borne in mind when considering the results. It should be noted that the tests described here were designed to avoid the end effects which were a feature of the DEn test programme, and plain bond was minimised by varnishing of the pile contact surface.

In general the results confirmed the increase in strength with radial stiffness and weld-bead height, although the range of parameters was not sufficient to thoroughly investigate the trends. In spite of this limitation it appears that the increase of strength with weld-bead height is rather less than suggested by the existing design equations. Increasing the weld-bead height by 50% (from 1.2 mm to 1.8 mm), did not lead to a proportional increase in the load capacity. Possible explanations for this may lie in the contribution made by bending moment. The bending moment is resulted from eccentric bearing stresses at the weld-beads, and causing additional radial stresses which weaken the confinement of the steel cylinder. As the weld-bead height increases the bending effect become more significant, thus more reduction in confinement. This in turn decreasing the average bearing strength of the grout beneath the weld-beads.

Displacements at failure did not follow any definite pattern, ranging from 1.8 mm to about 3.5 mm. After the ultimate load was reached, the displacements were affected by cracking, and thus led to a reduced displacement at the middle weld-bead relative to the top weld-bead. At the bottom of the connection, the grout slipped with the weld-bead until final failure and separation.

The main crack direction was at about 45° to the vertical, which is orthogonal to the angle of principal diagonal tension in the grout annulus. Examination of model W2, in which post ultimate displacement were avoided, showed a crack commencing at the middle of the annulus. It may be concluded that the crack then spreads to the tip of the weld-beads, after further displacement; the exact path being dictated by the state of confinement local to the weld-beads. Where large displacements were imposed (model W5) and the weld-beads were finally positioned directly opposite, a horizontal crack resulted. The results contradict the assumptions of Krahl and Karsan (65,and 66) regarding the ultimate failure mechanism for these geometries, which is the basis of the API equation.

Strain at the top weld-bead, both in the axial and hoop directions, showed that maximum load transfer took place at that position. The Poisson effect, although small in magnitude, may contribute to the lower bond at the middle weld-bead. In effect, the top weld-bead controlled the displacement and load capacity of the connection. The high strain at the top weld-bead was an important factor in the

failure of the models with 8 mm wall thickness, and could be a governing consideration in the failure of the most heavily loaded weld-bead for the remaining geometries. Further results would be required to confirm this as dilation and confinement in these tubulars are dependant on both radial and bending stiffness (bending stiffness increase more rapidly with wall thickness).

3.9 Conclusions

The main conclusions from the experimental programme may be summarised as follows:

- Load-carrying capacity of the connections increased with radial stiffness, and weld-bead height.

- The increase in strength with weld-bead height was less than given by the DEn equation.

- Maximum stress transfer took place at the upper weld-bead. The bottom weld-bead carried negligible load at failure.

- Diagonal cracking existed between the weld-bead positions on the pile and sleeve. From the specimens this was a post-ultimate observation.

- A region of crushed grout existed beneath the weld-bead. High contact stresses in this area may contribute to significant frictional bond.

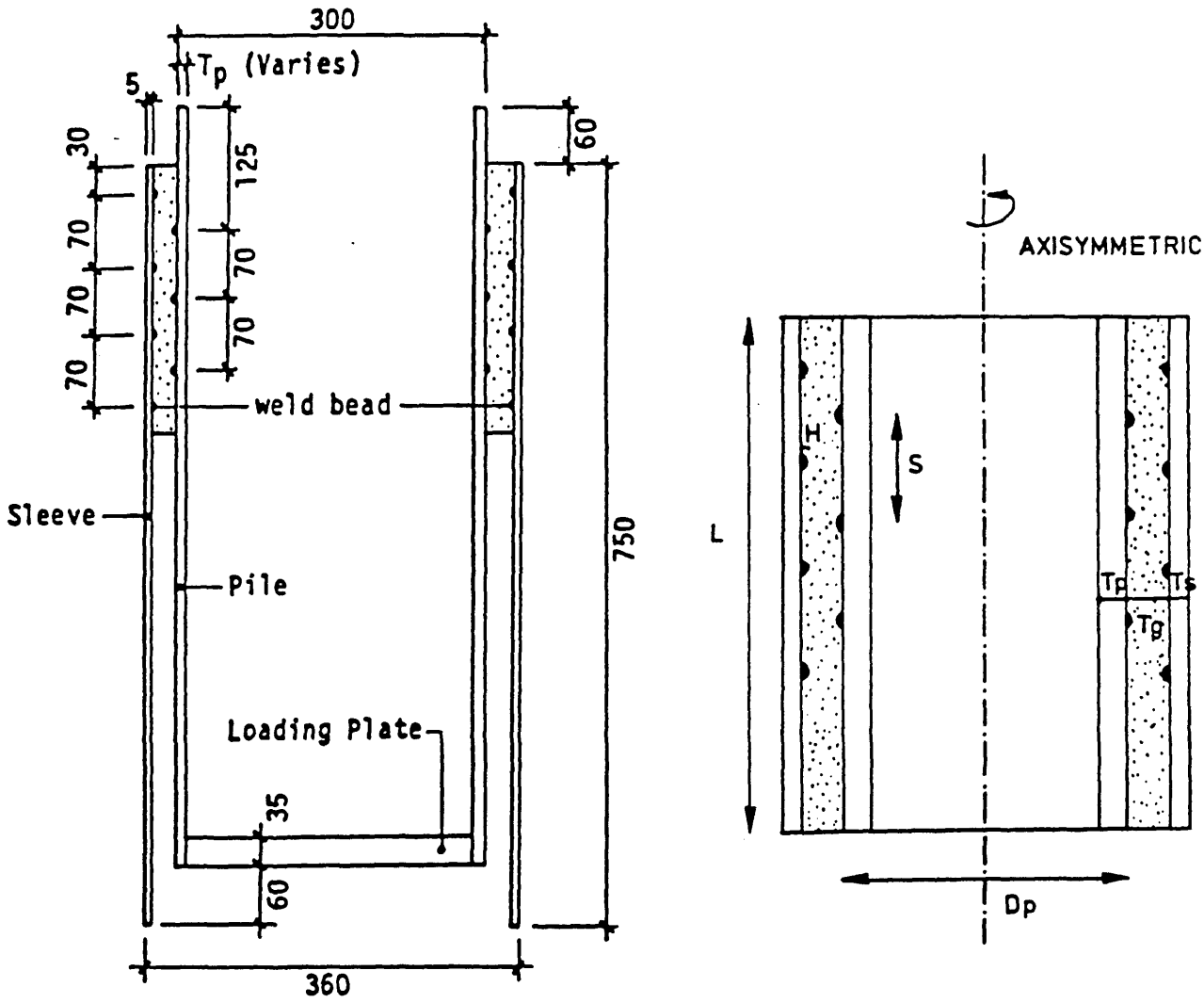
- The bottom weld-bead of the pile did not contribute to the connection strength.

- Non-linear strain in the pile at the top weld-bead preceded failure.

- Displacements at failure varied from 1.8 mm to 3.5 mm. Post ultimate displacements of magnitude equal to the weld-bead spacing could be

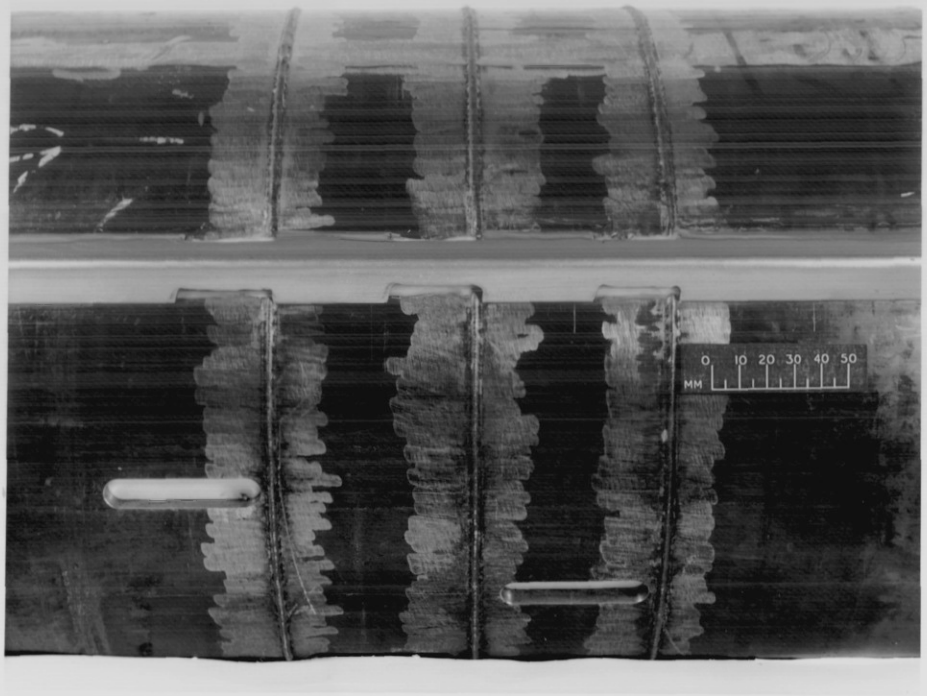
achieved at loads of 80% of ultimate.

These conclusions apply to the geometry of these models, and scaling up to full size may result in some differences, particularly in the confinement strains.



SECTION THROUGH MODEL CONNECTION

FIG 3.1



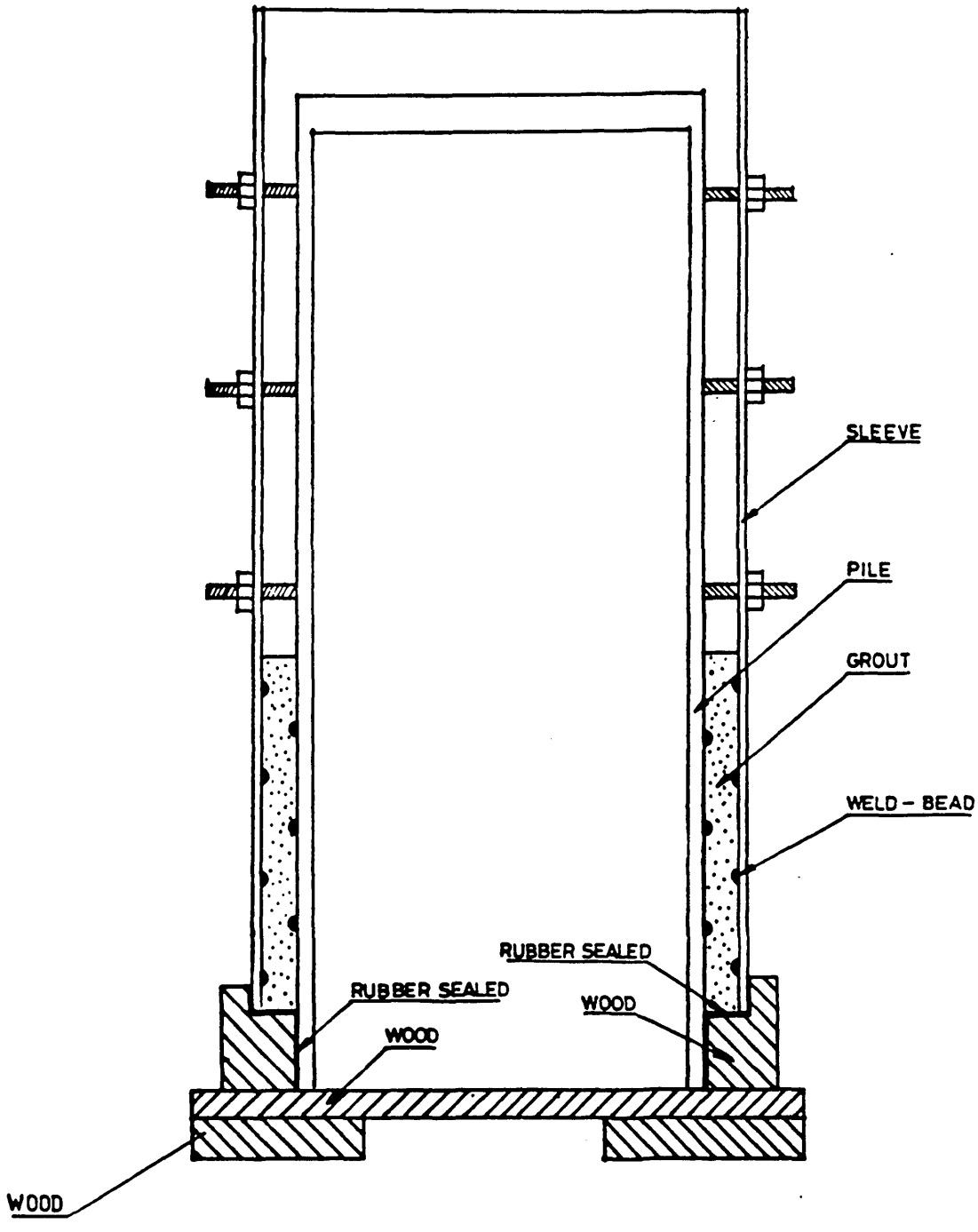
(a) OUTER SURFACE WITH WELD BEADS



(b) INNER SURFACE WITH INSTRUMENTATIONS

PILE TUBULAR

FIG 3.2



ARRANGEMENT FOR CASTING

FIG 3.3(a)

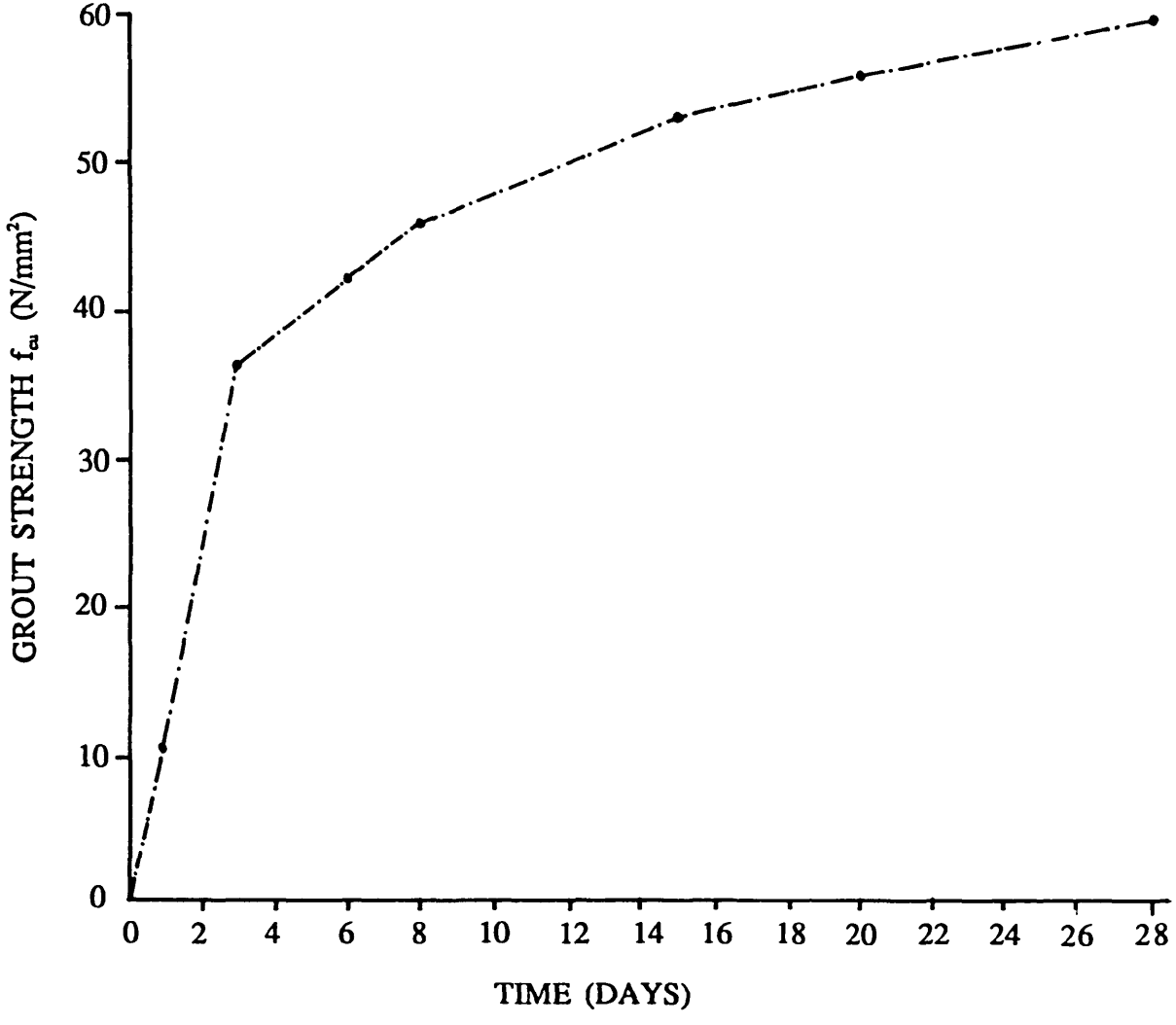


FIG 3.3 (b)

VARIATION OF CUBE STRENGTH WITH TIME FOR GROUT

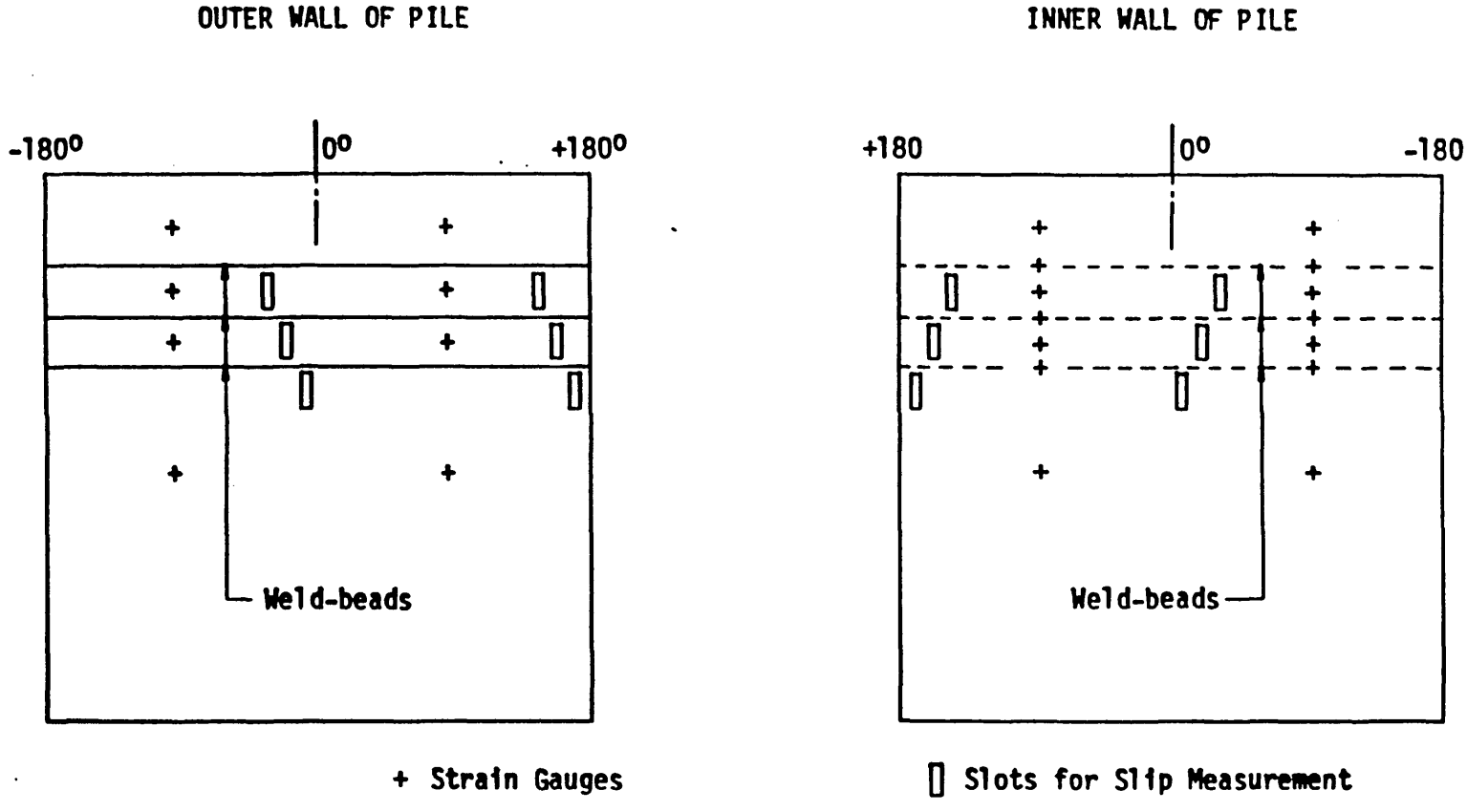
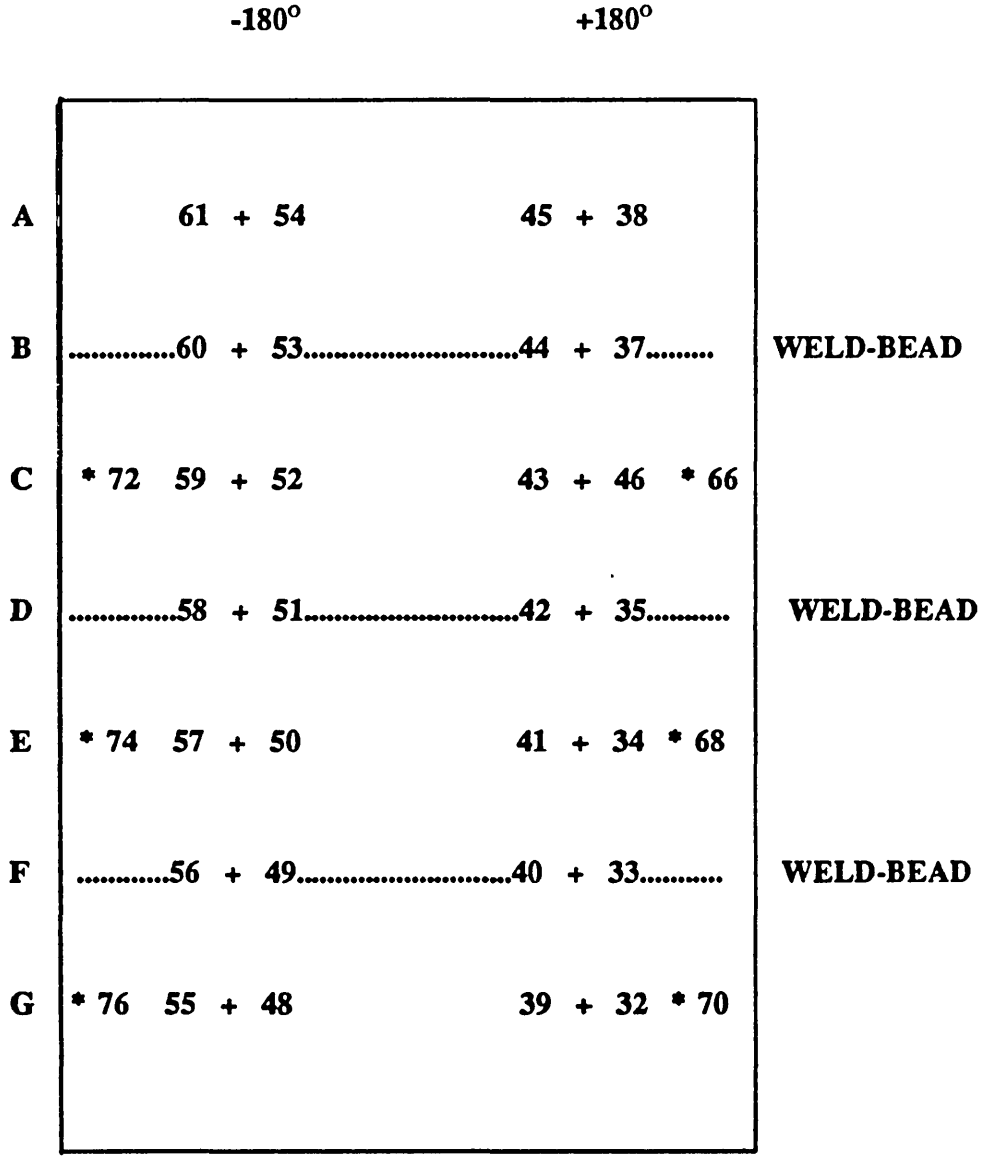


FIG 3.4 (a)

DEVELOPED LAYOUT OF TRANSDUCERS & STRAIN GAUGES

INNER WALL OF PILE



32,33,34,35,36,37,38,48,49,50,51,52,53,54 : AXIAL STRAIN GAUGES

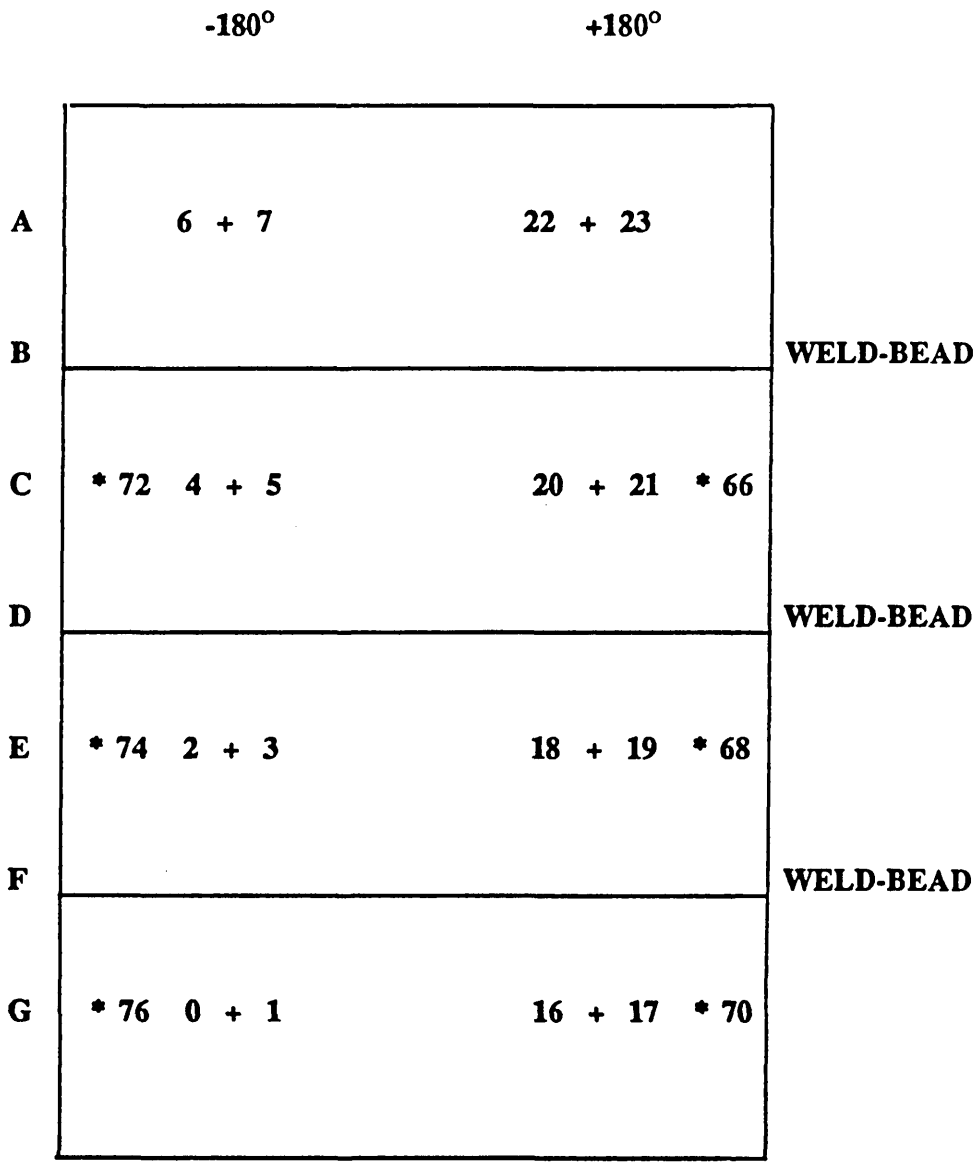
39,40,41,42,43,44,45,55,56,57,58,59,60,61 : HOOP STRAIN GAUGES

66, 68, 70, 72, 74, 76 : TRANSDUCERS

DEVELOPED LAYOUT OF TRANSDUCERS AND STRAIN GAUGES W1

FIG 3.4 (b)

OUTER WALL OF PILE



1, 3, 5, 7, 17, 19, 21, 23 : AXIAL STRAIN GAUGES

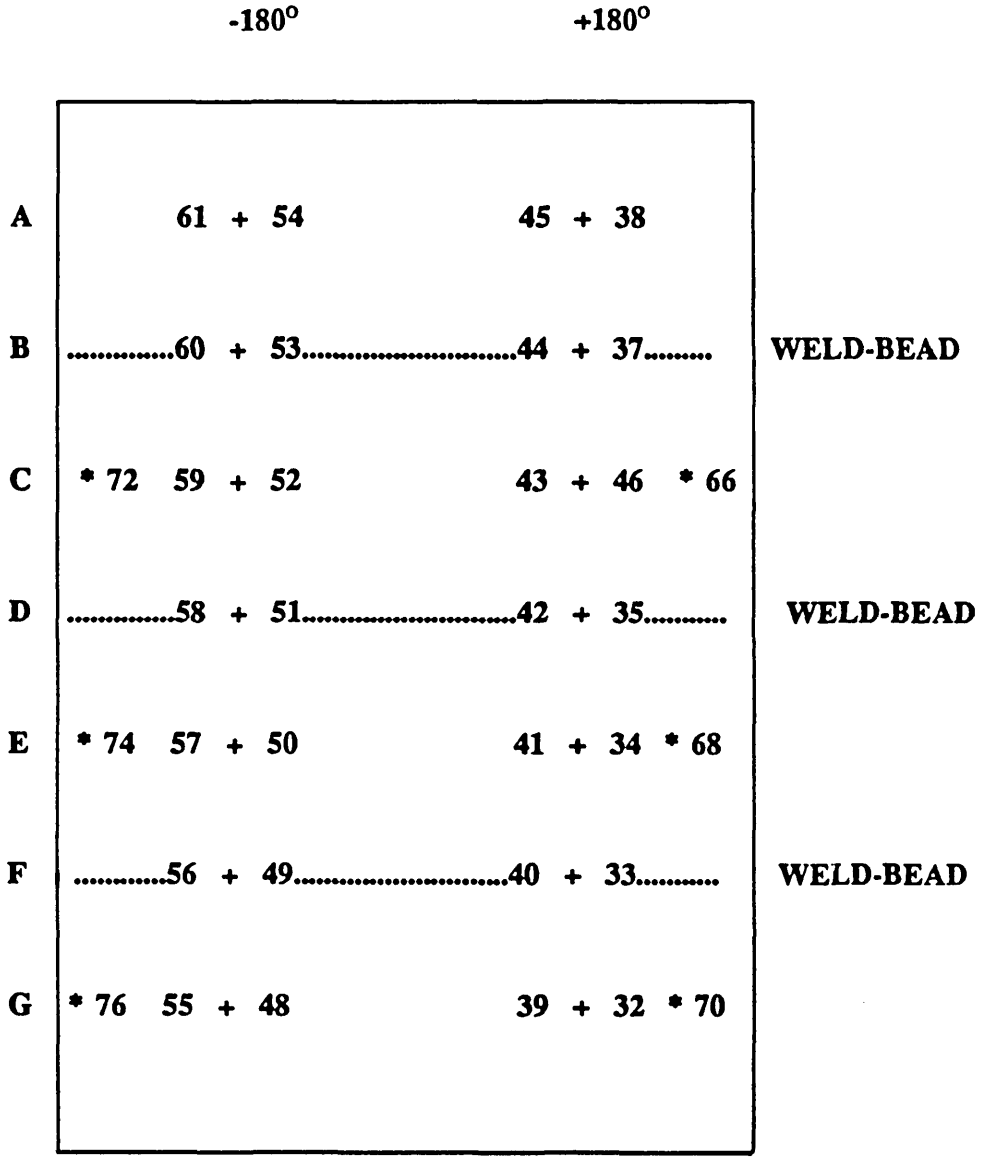
0, 2, 4, 6, 16, 18, 20, 22 : HOOP STRAIN GAUGES

66, 68, 70, 72, 74, 76 : TRANSDUCERS

DEVELOPED LAYOUT OF TRANSDUCERS AND STRAIN GAUGES W1

FIG 3.4 (c)

INNER WALL OF PILE



32,33,34,35,36,37,38,48,49,50,51,52,53,54 : AXIAL STRAIN GAUGES

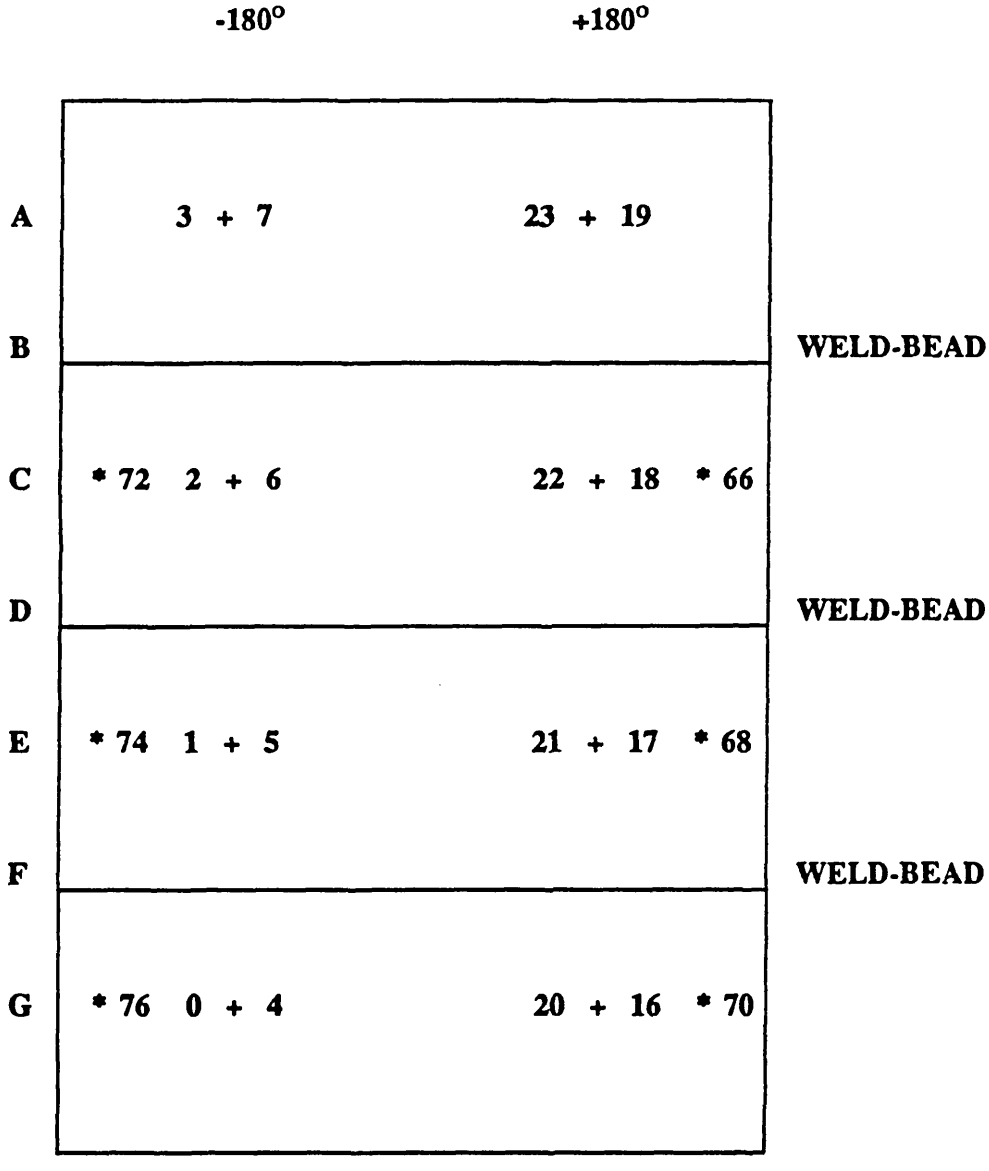
39,40,41,42,43,44,45,55,56,57,58,59,60,61 : HOOP STRAIN GAUGES

66, 68, 70, 72, 74, 76 : TRANSDUCERS

DEVELOPED LAYOUT OF TRANSDUCERS AND STRAIN GAUGES W2

FIG 3.4 (d)

OUTER WALL OF PILE



0, 1, 2, 3, 16, 17, 18, 19 : AXIAL STRAIN GAUGES

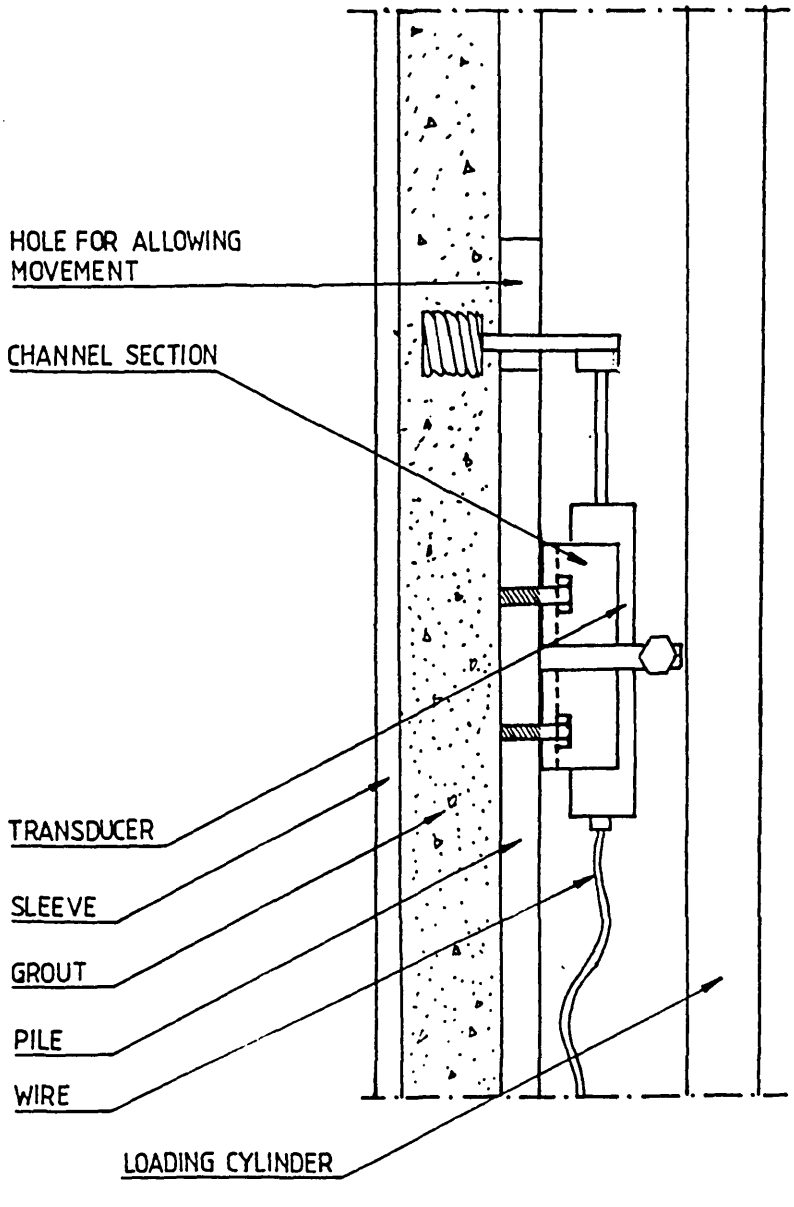
4, 5, 6, 7, 20, 21, 22, 23 : HOOP STRAIN GAUGES

66, 68, 70, 72, 74, 76 : TRANSDUCERS

DEVELOPED LAYOUT OF TRANSDUCERS AND STRAIN GAUGES W2

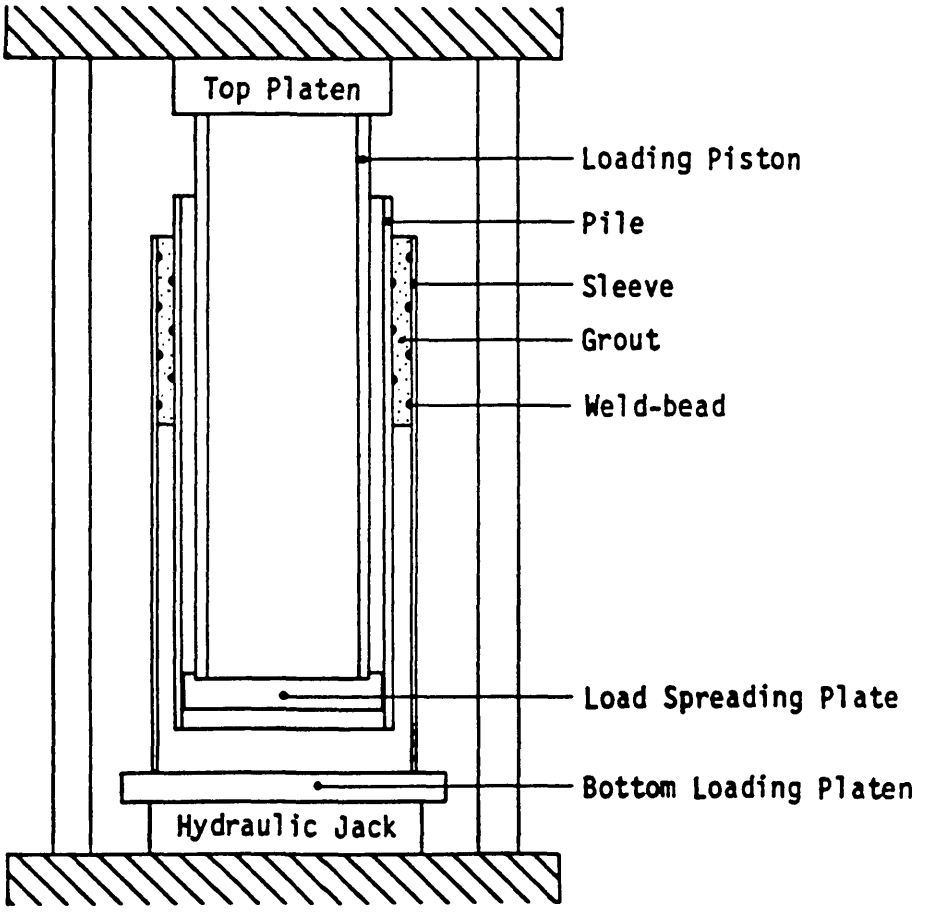
FIG 3.4 (e)

DETAIL POSITION OF TRANSDUCER FITTED



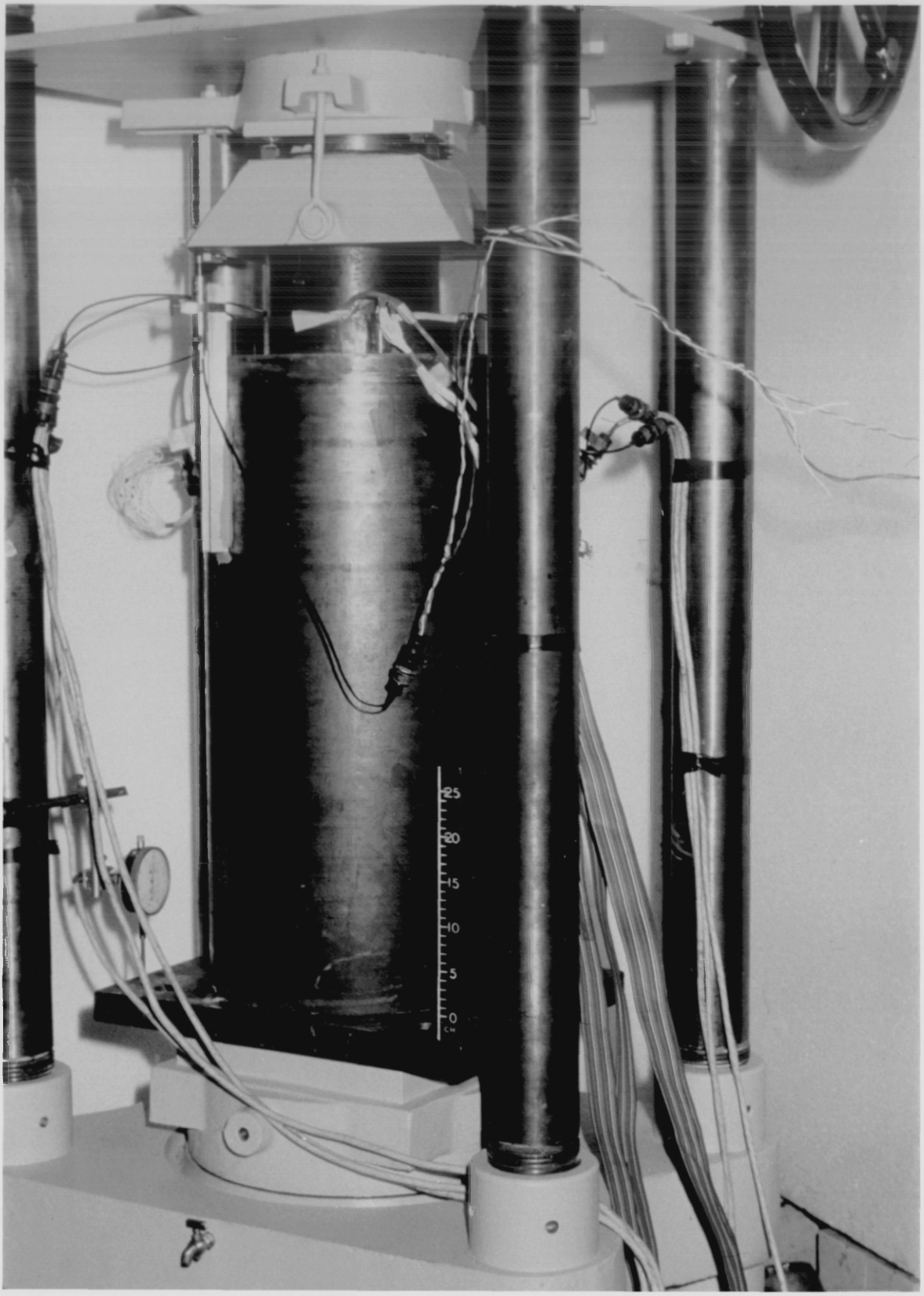
ELEVATION VIEW

FIG 3.4 (f)



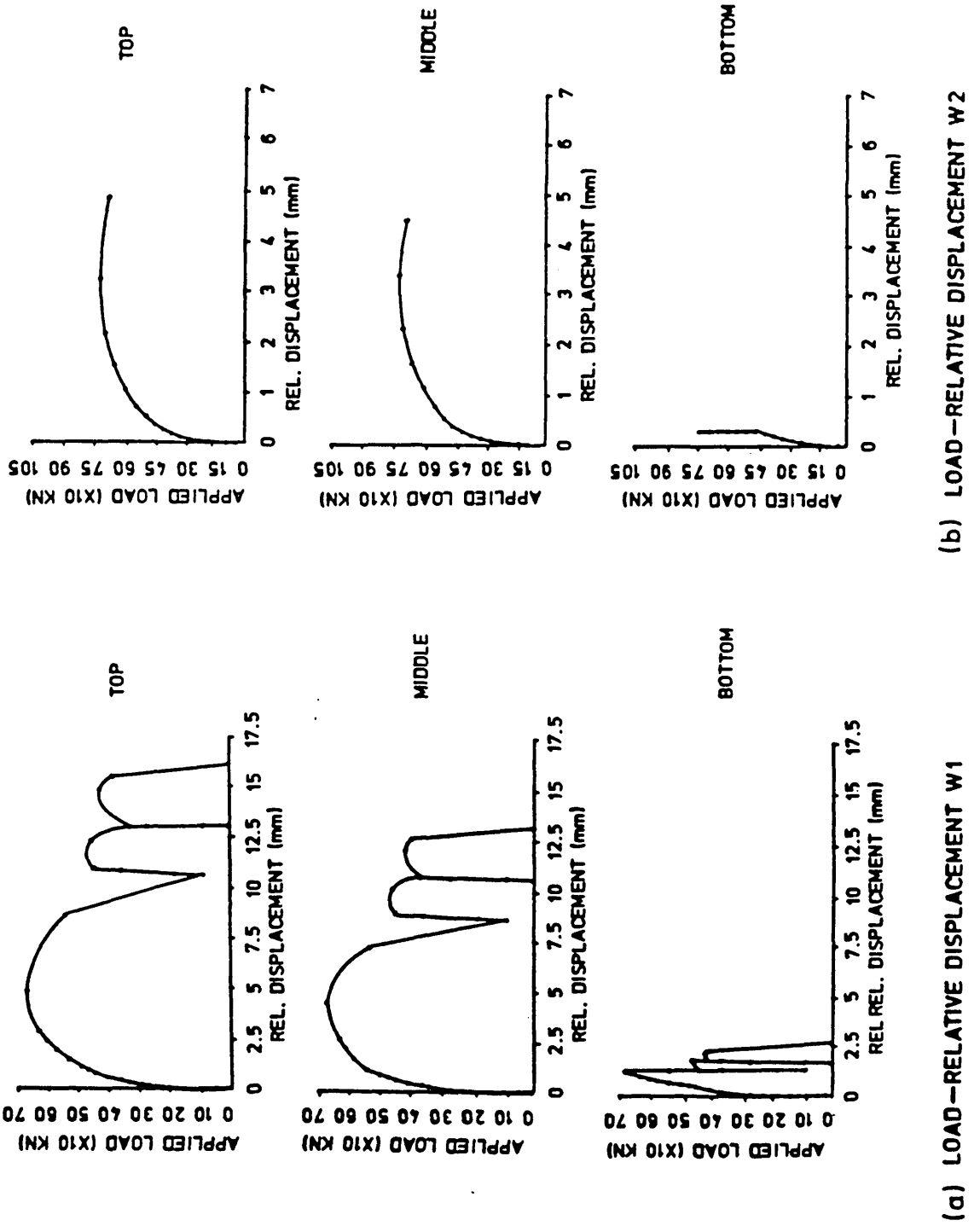
LOADING ARRANGEMENT

FIG 3.5



TEST ARRANGEMENT

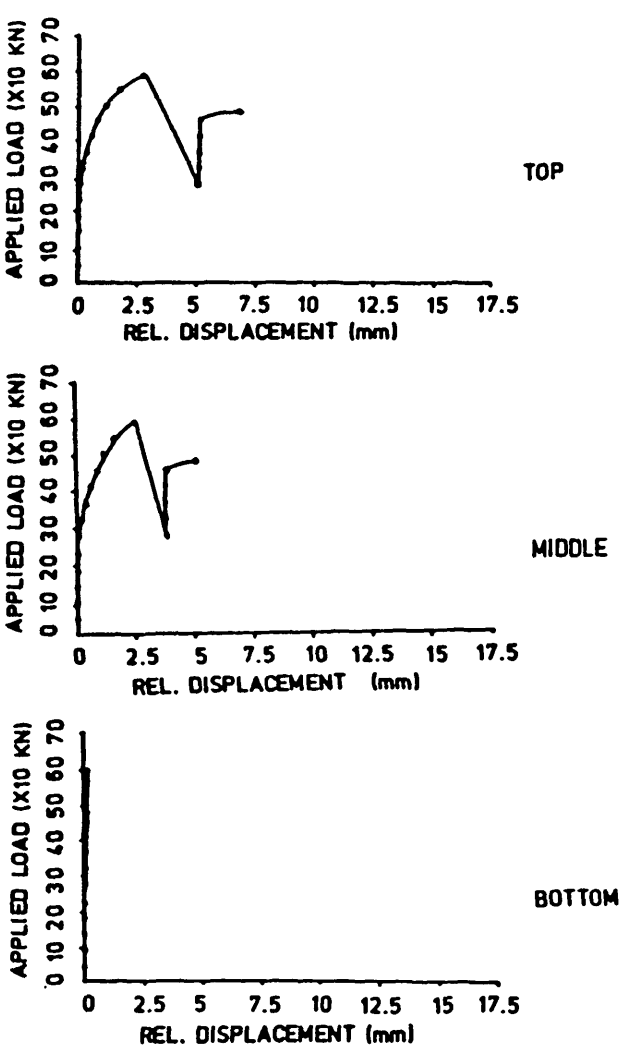
FIG 3.6



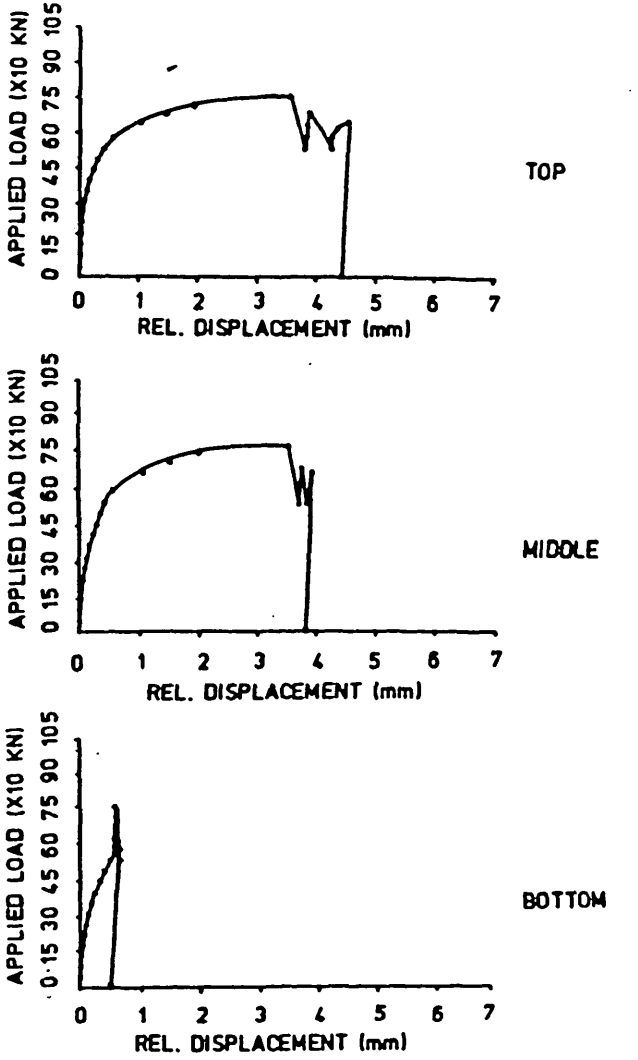
(b) LOAD–RELATIVE DISPLACEMENT W2

(a) LOAD–RELATIVE DISPLACEMENT W1

FIG 3.7



(a) LOAD–RELATIVE DISPLACEMENT W3



(b) LOAD–RELATIVE DISPLACEMENT W4

FIG 3.8

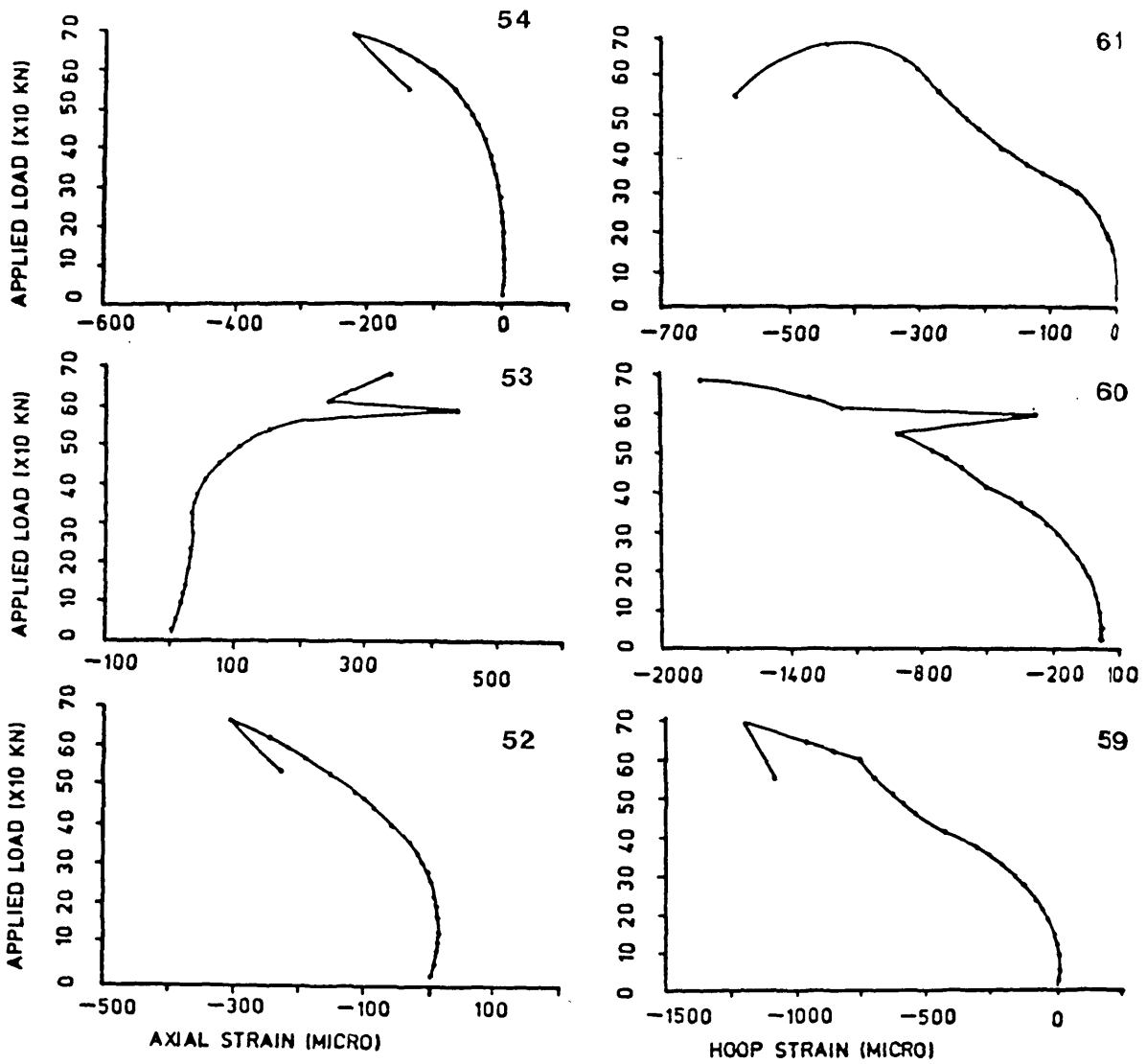
(a) LOAD–RELATIVE DISPLACEMENT W5

(b) LOAD–RELATIVE DISPLACEMENT W6

FIG 3.9

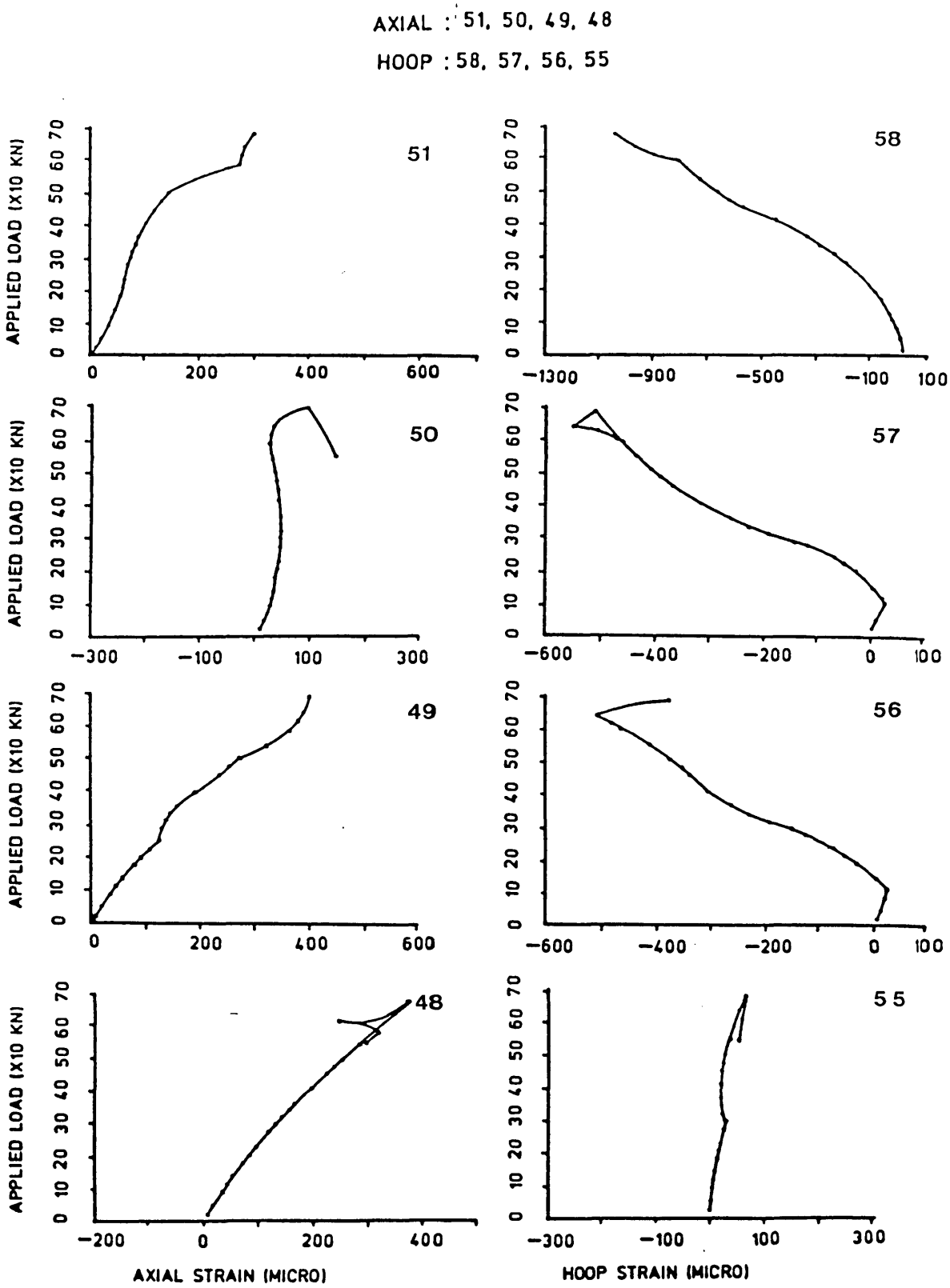
AXIAL : 54, 53, 52

HOOP : 61, 60, 59



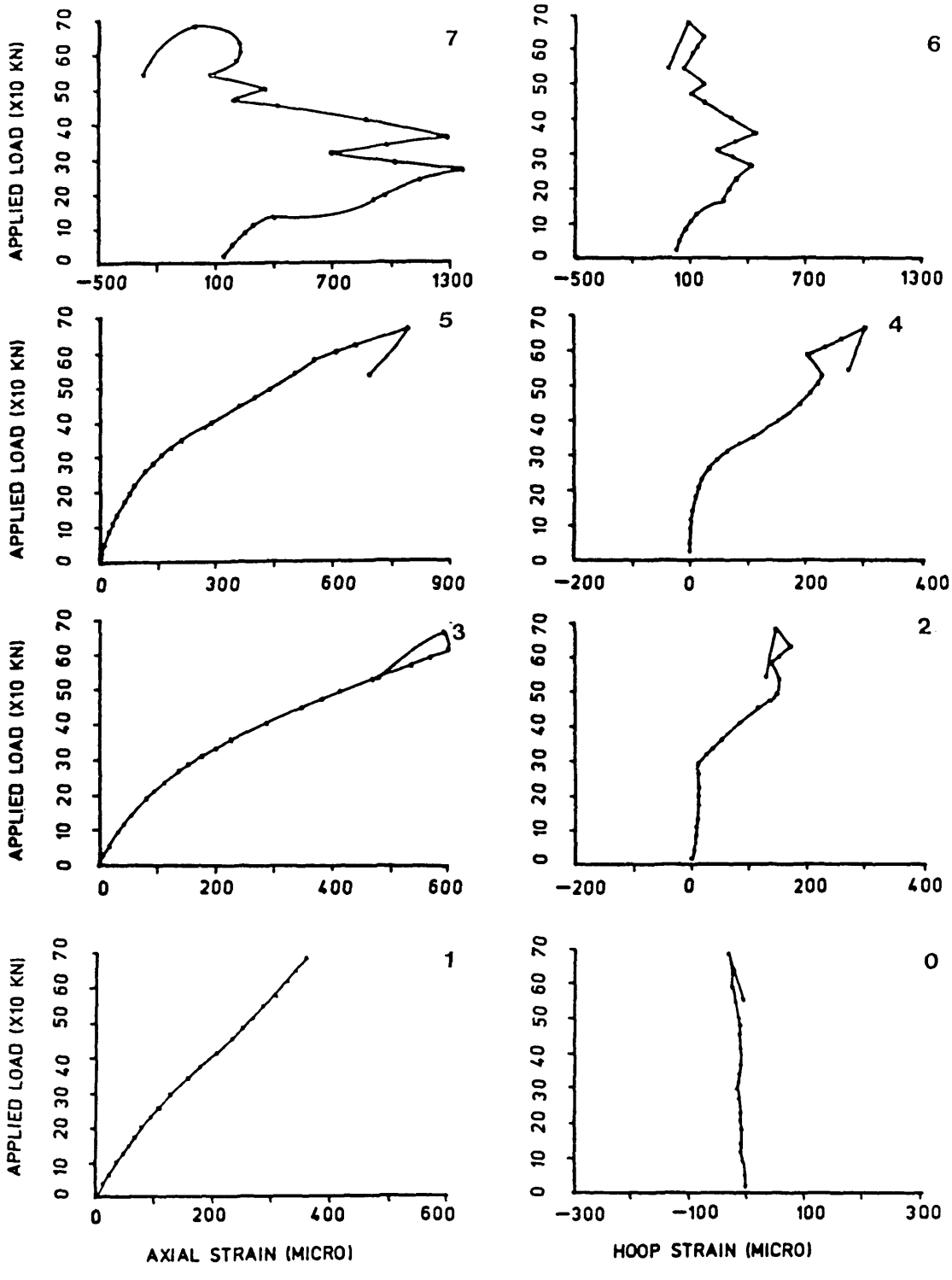
STRAIN GAUGE READING FROM THE INNER WALL OF PILE W1

FIG 3.10(a)



STRAIN GAUGE READING FROM THE INNER WALL OF PILE W1

FIG 3.10 (b)



STRAIN GAUGES READING FROM THE OUTER WALL OF PILE W1

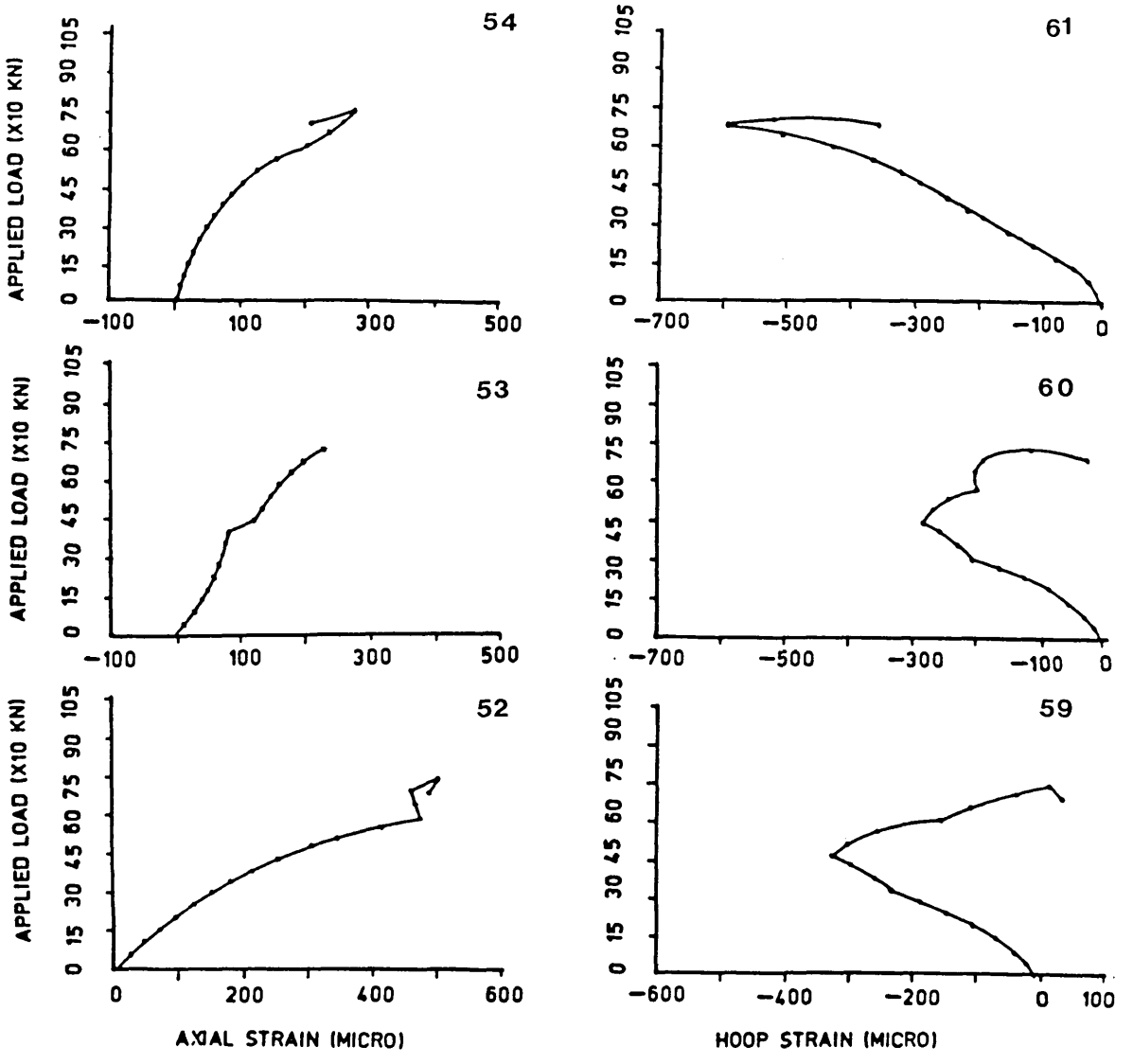
AXIAL : 7, 5, 3 1

HOOP : 6, 4, 2 0

FIG 3.11

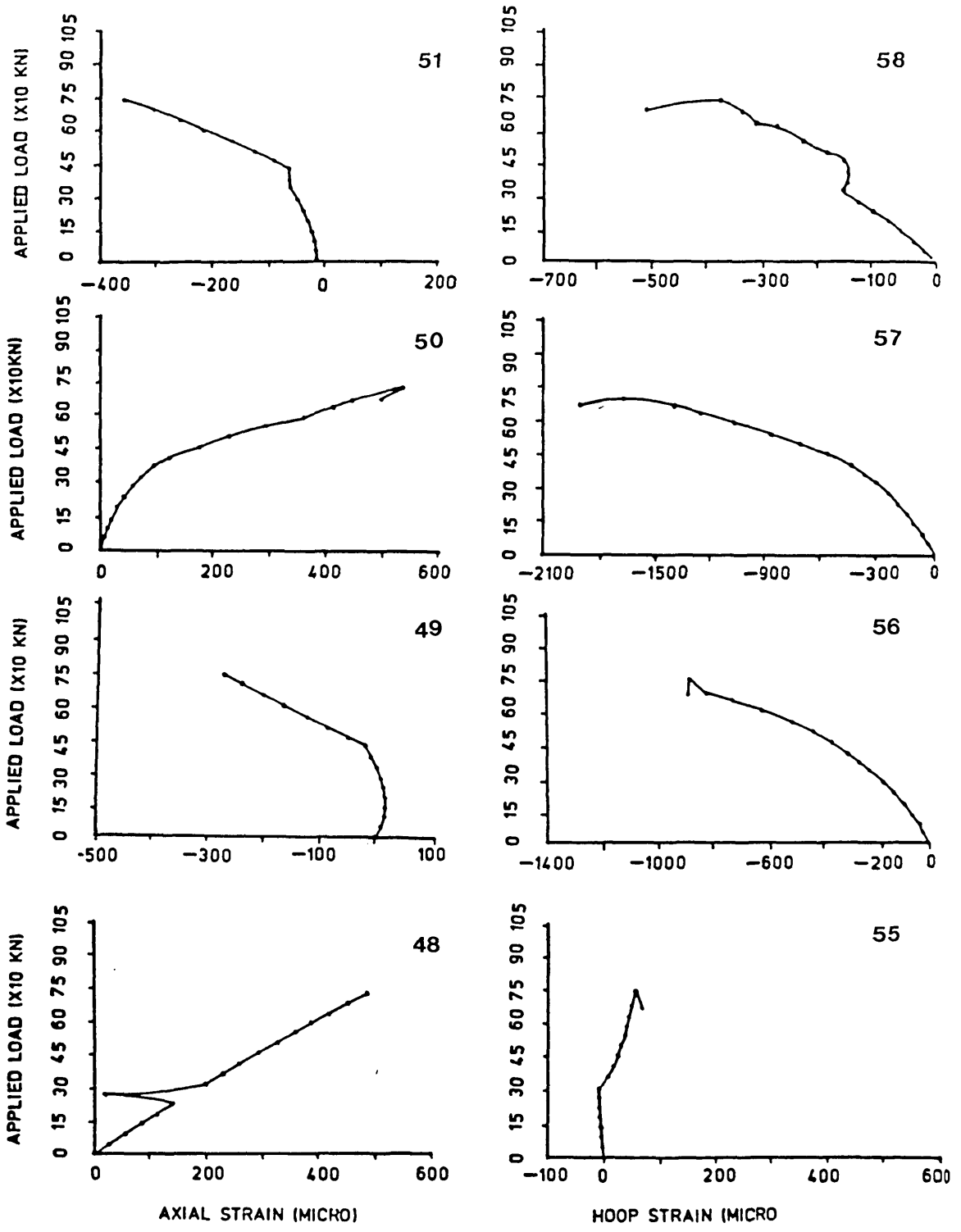
AXIAL : 54, 53, 52

HOOP : 61, 60, 59



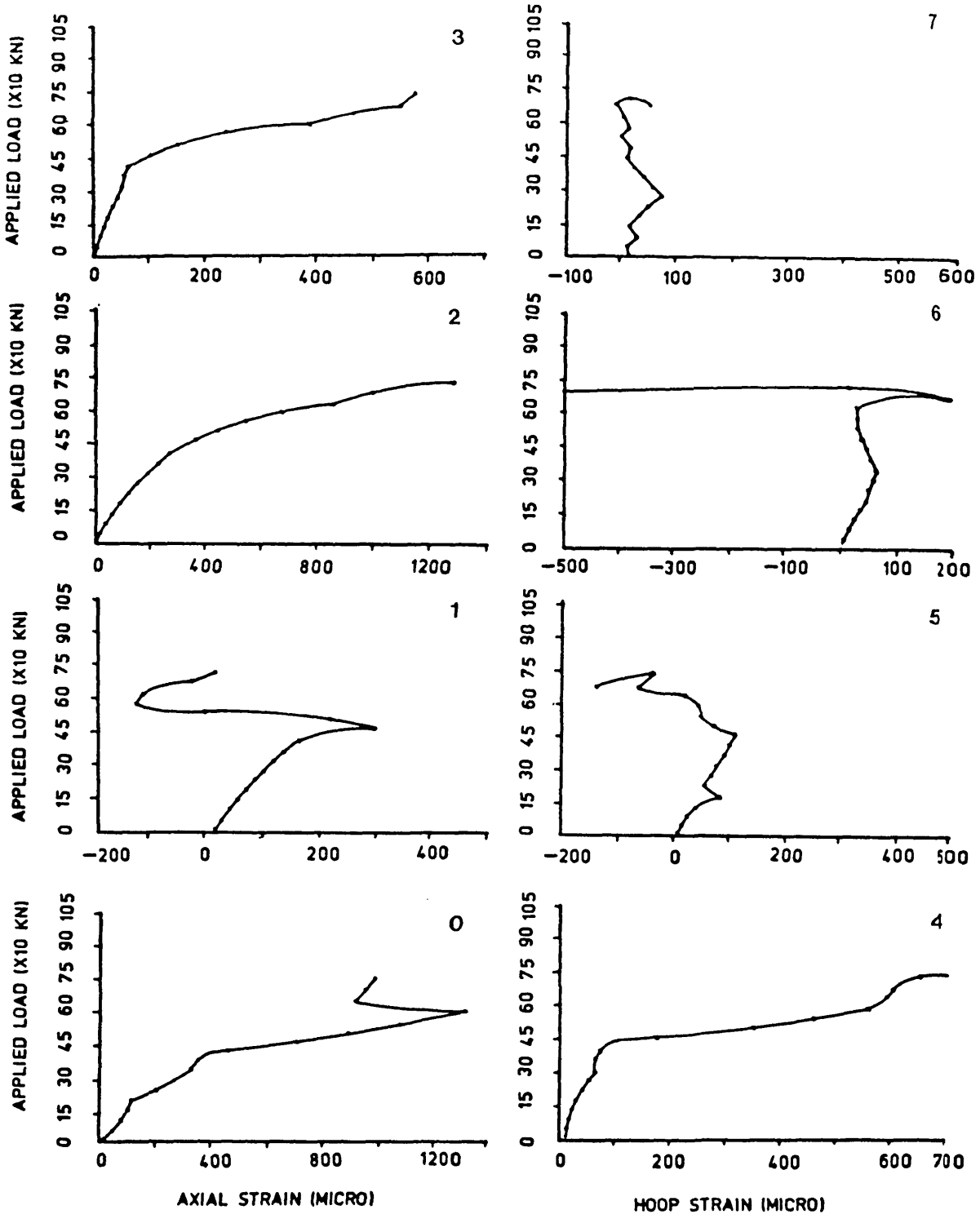
STRAIN GAUGES READING FROM THE INNER WALL OF PILE W2

FIG 3.12 (a)



STRAIN GAUGES READING FROM THE INNER WALL OF PILE W2

FIG 3.12 (b)

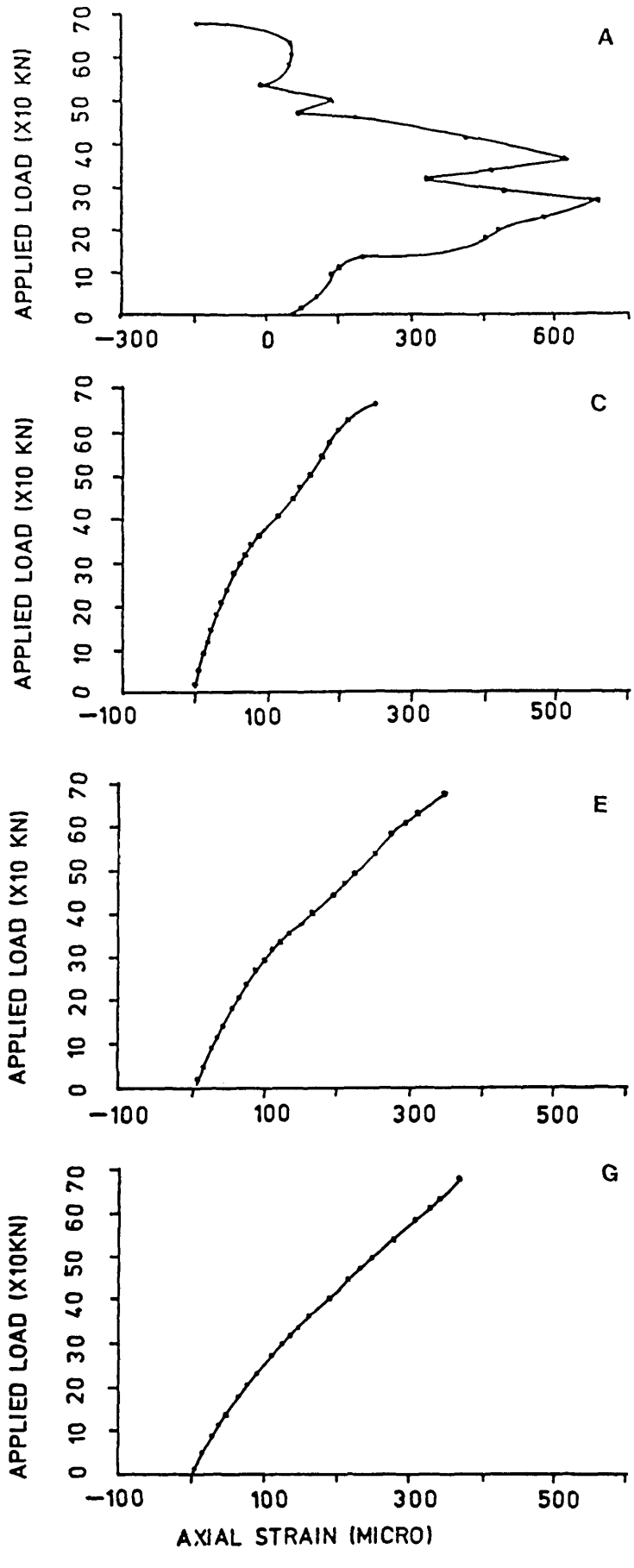


STRAIN GAUGES READING FROM THE OUTER WALL OF PILE W2

AXIAL : 3, 2, 1 , 0

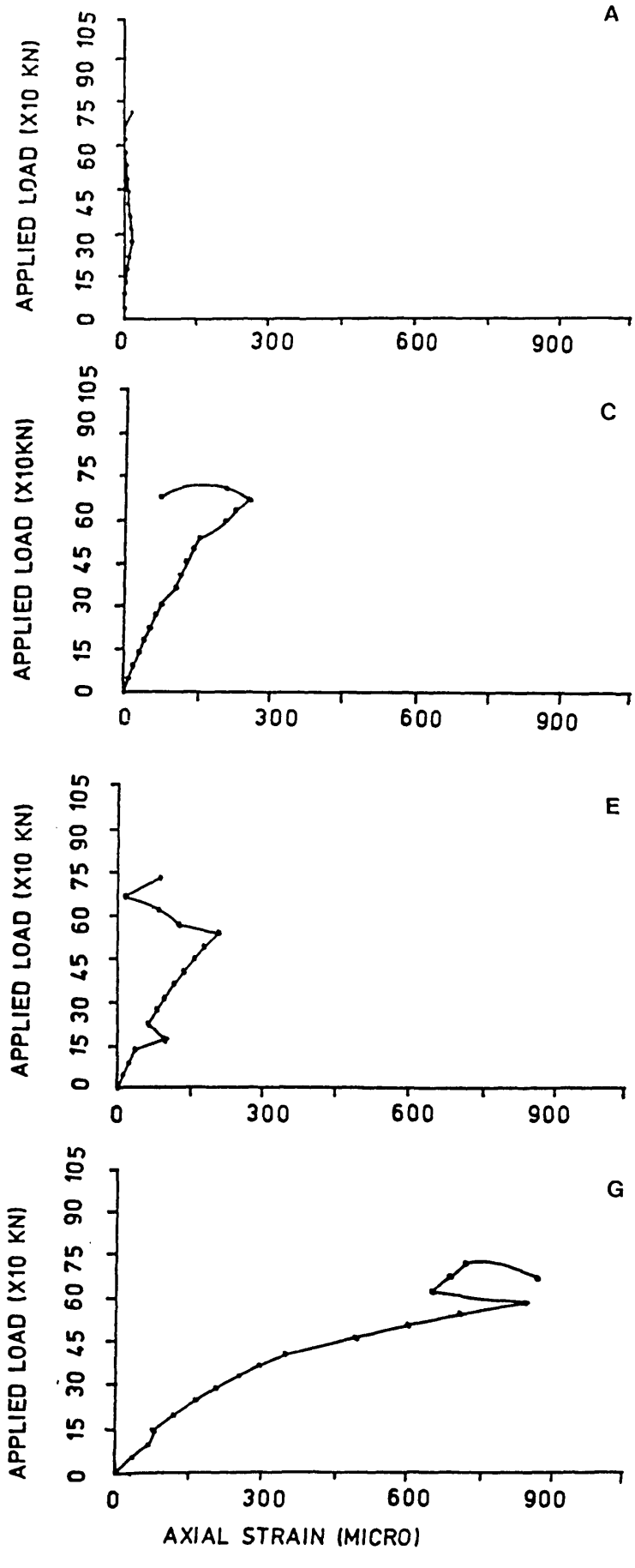
HOOP : 7, 6, 5, 4

FIG 3.13



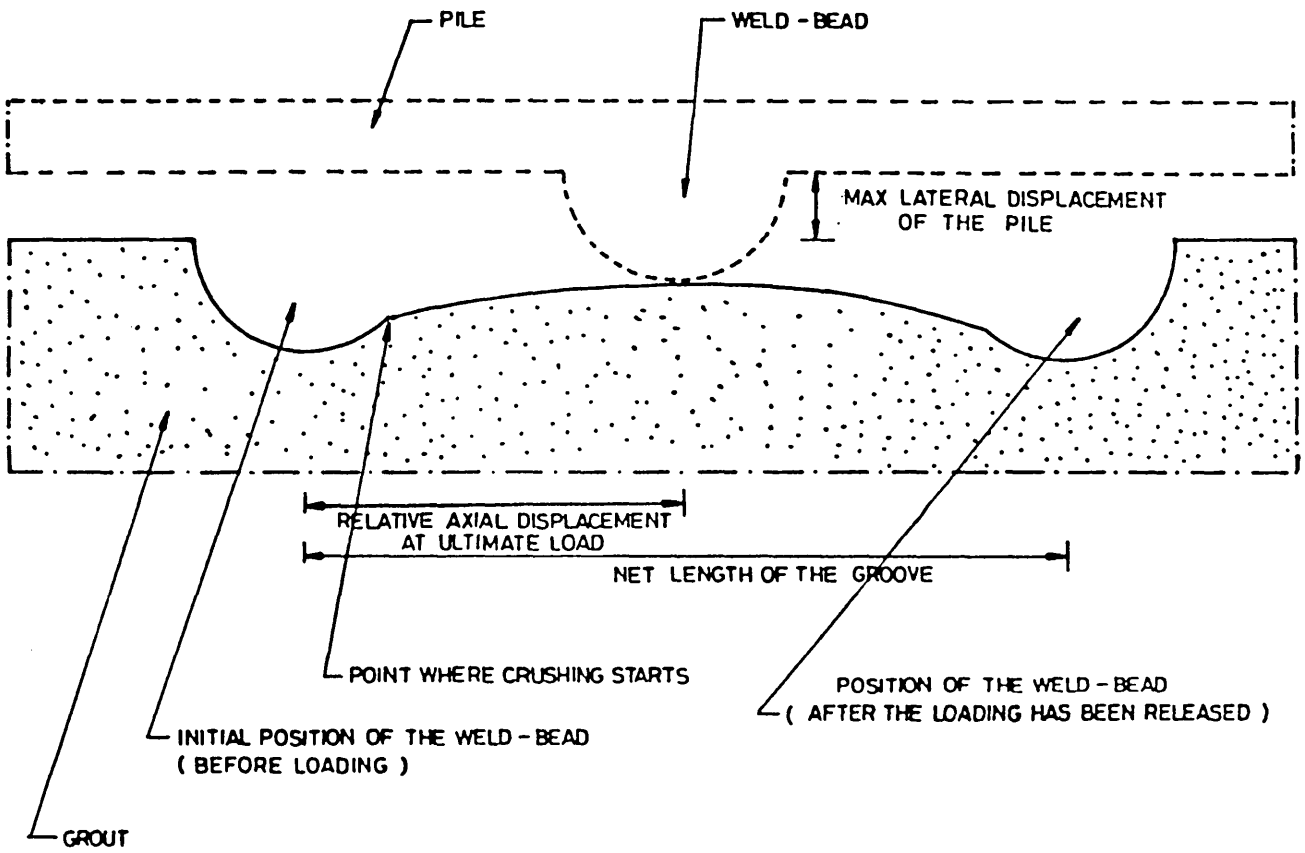
AVERAGE AXIAL STRAIN W1

FIG 3.14



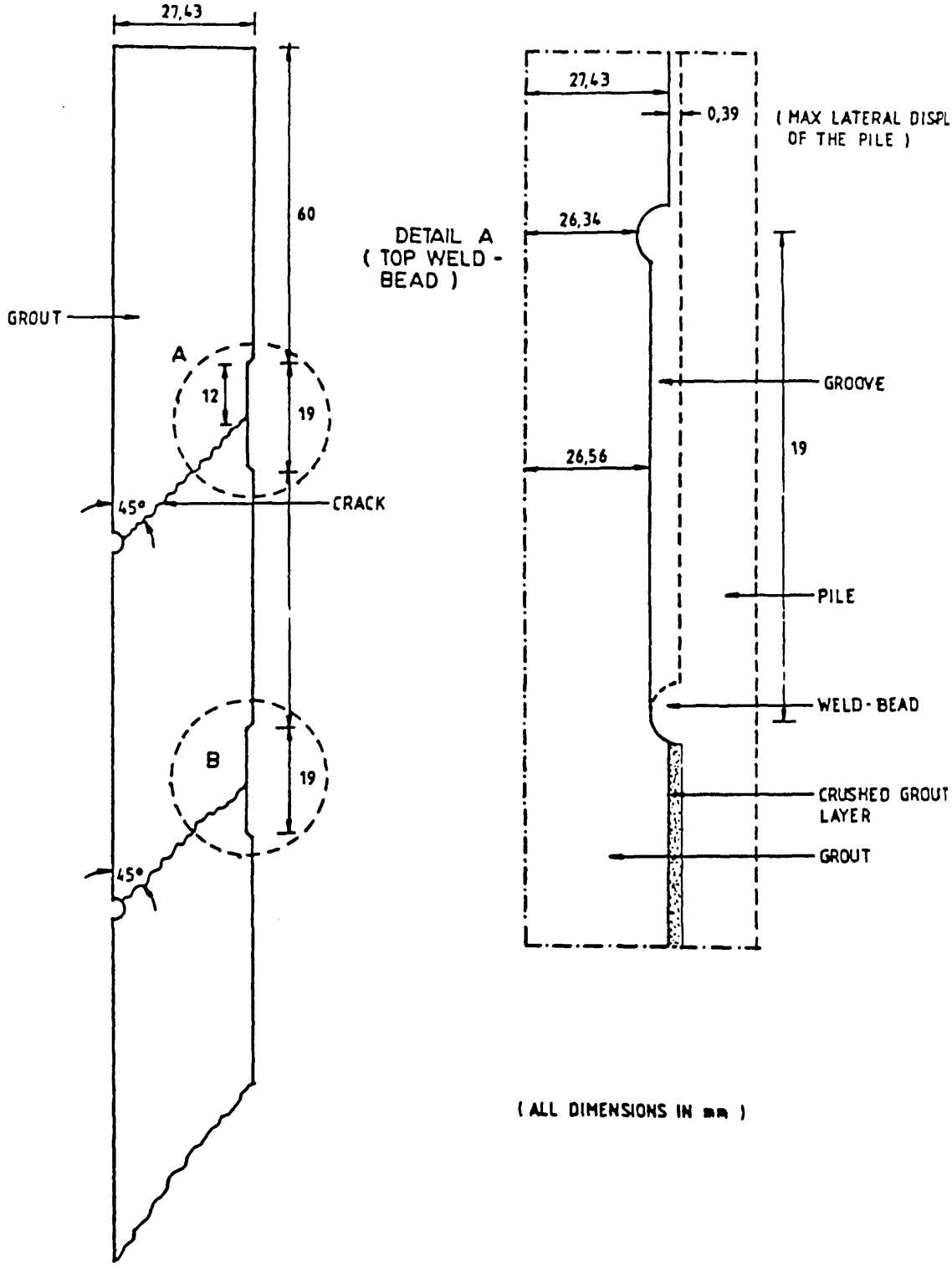
AVERAGE AXIAL STRAIN W2

FIG 3.15



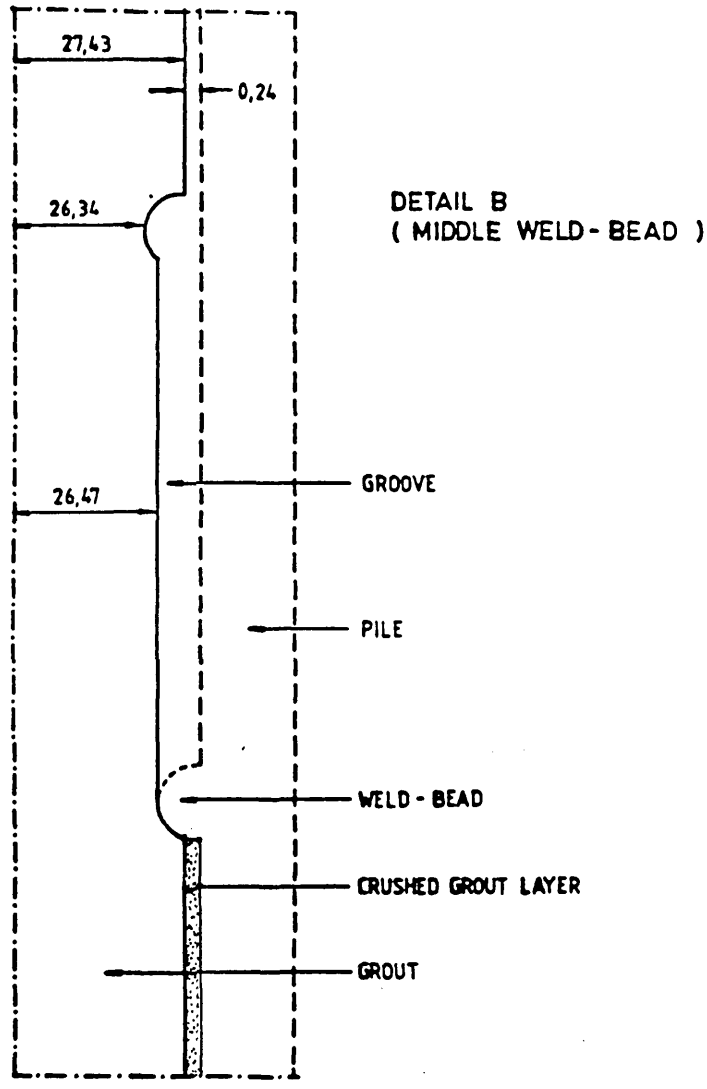
GENERAL FEATURES OF THE GROOVES

FIG 3.16



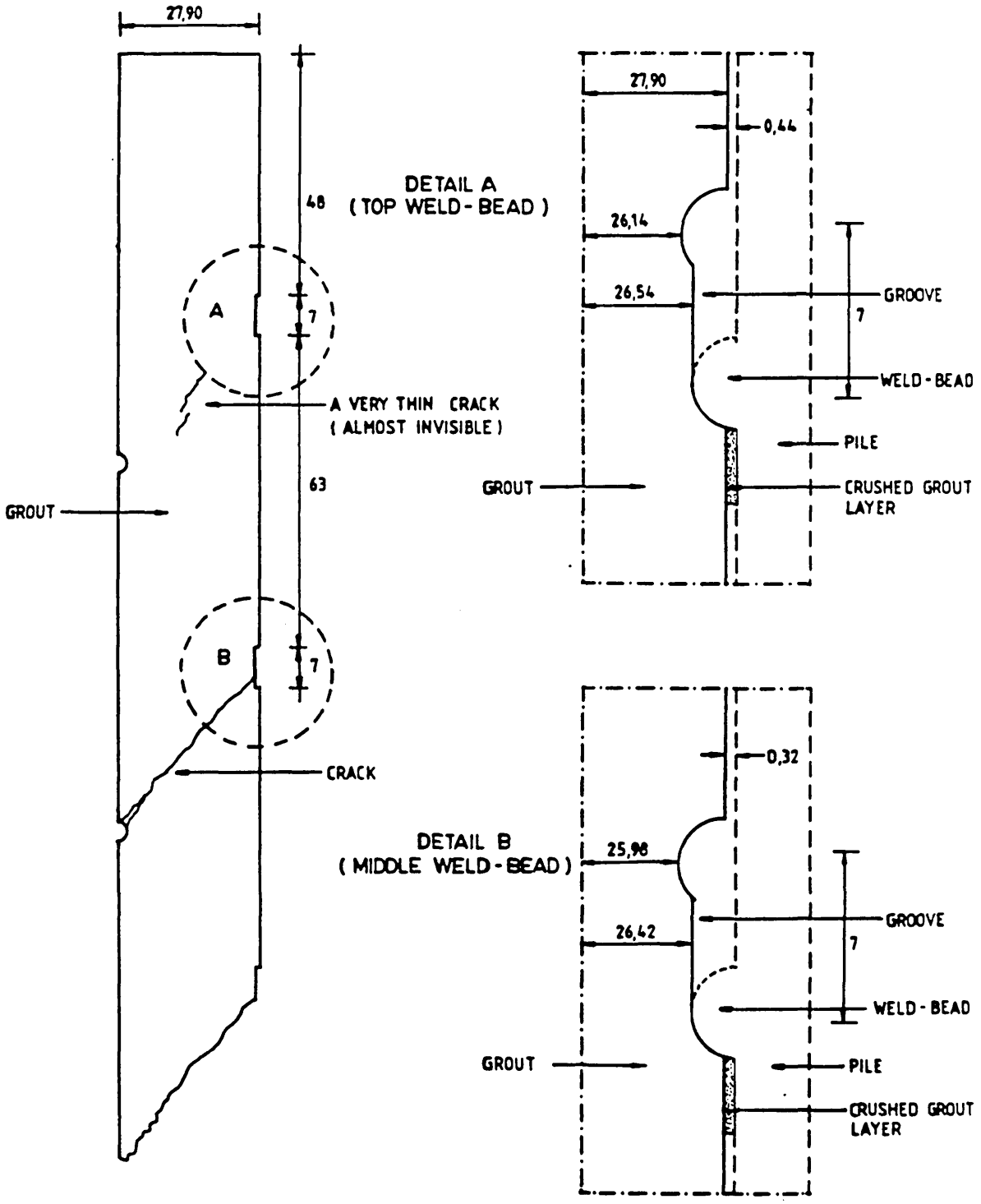
OPENED SPECIMEN AFTER TESTING W1

FIG 3.17 (a)



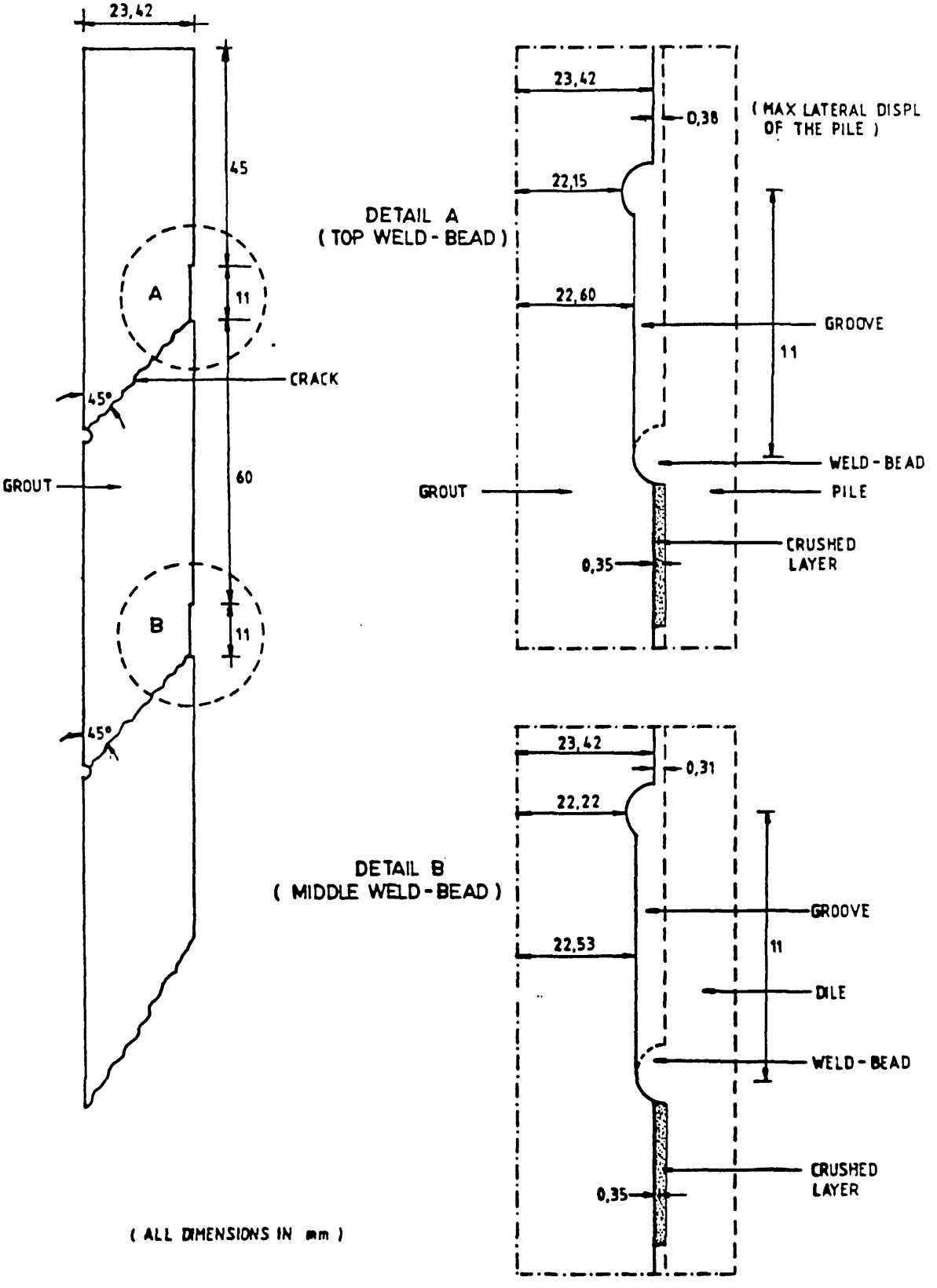
OPENED SPECIMEN AFTER TESTING W1

FIG 3.17(b)



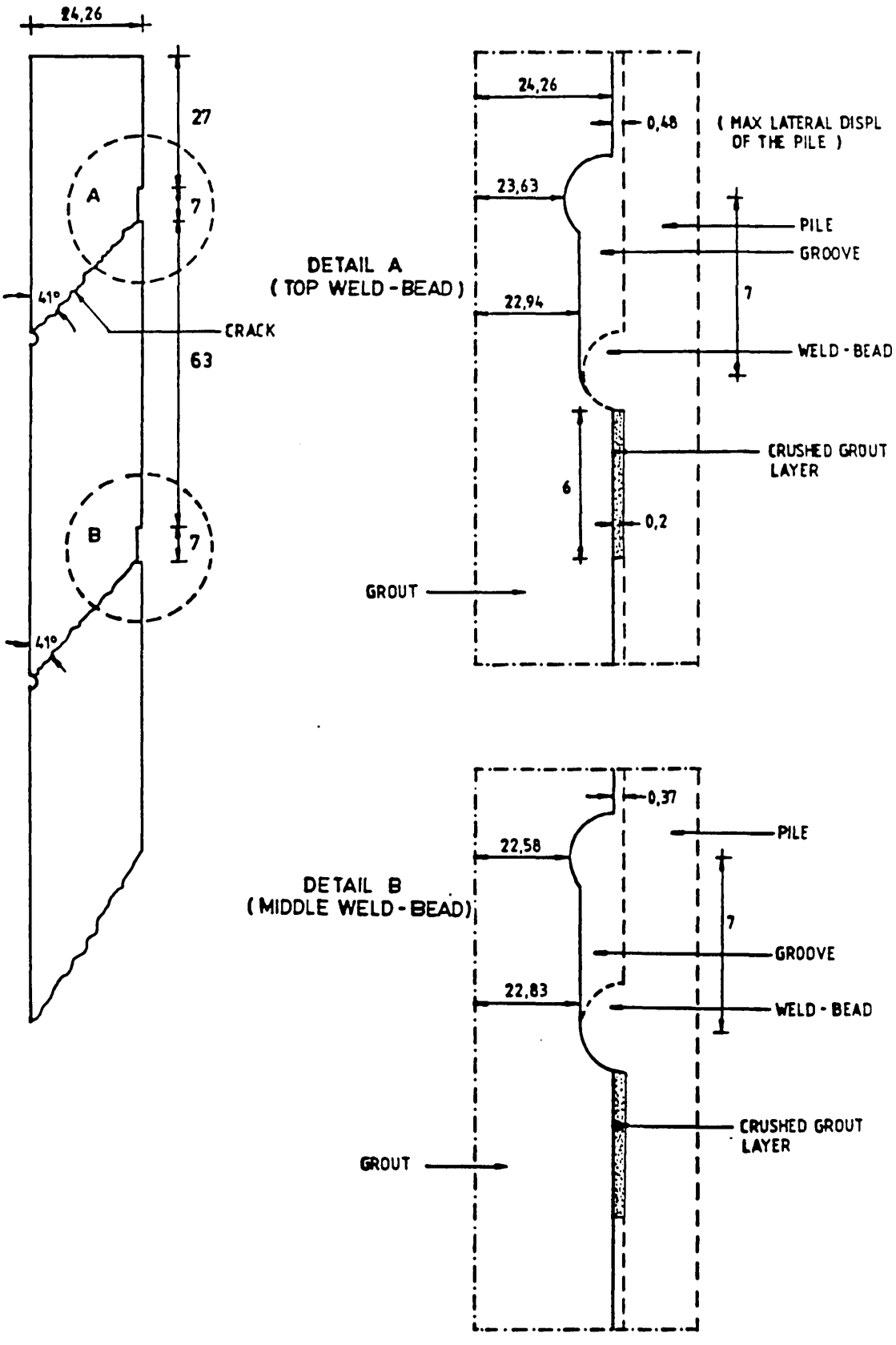
OPENED SPECIMEN AFTER TESTING W2

FIG 3.18



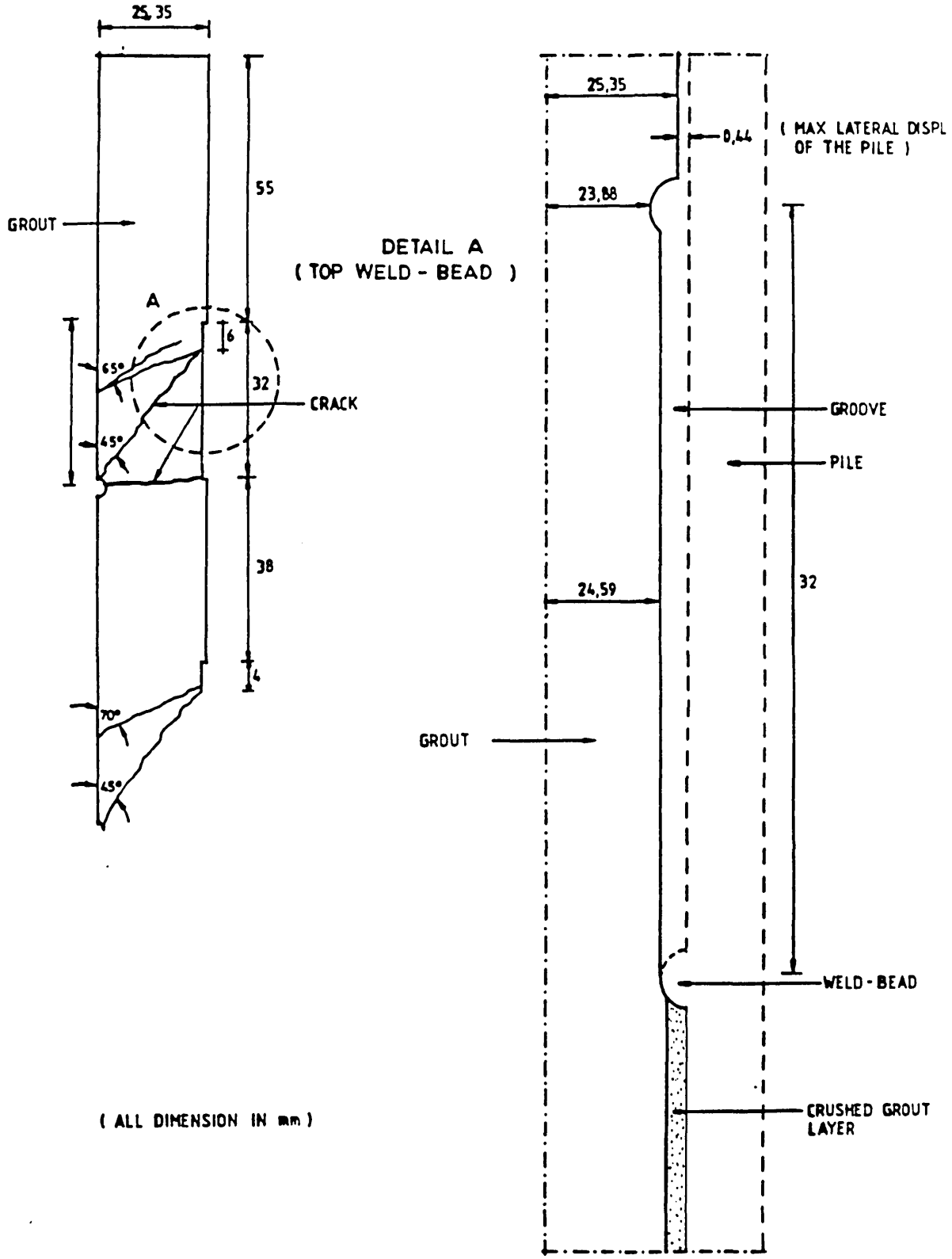
OPENED SPECIMEN AFTER TESTING W3

FIG 3.19



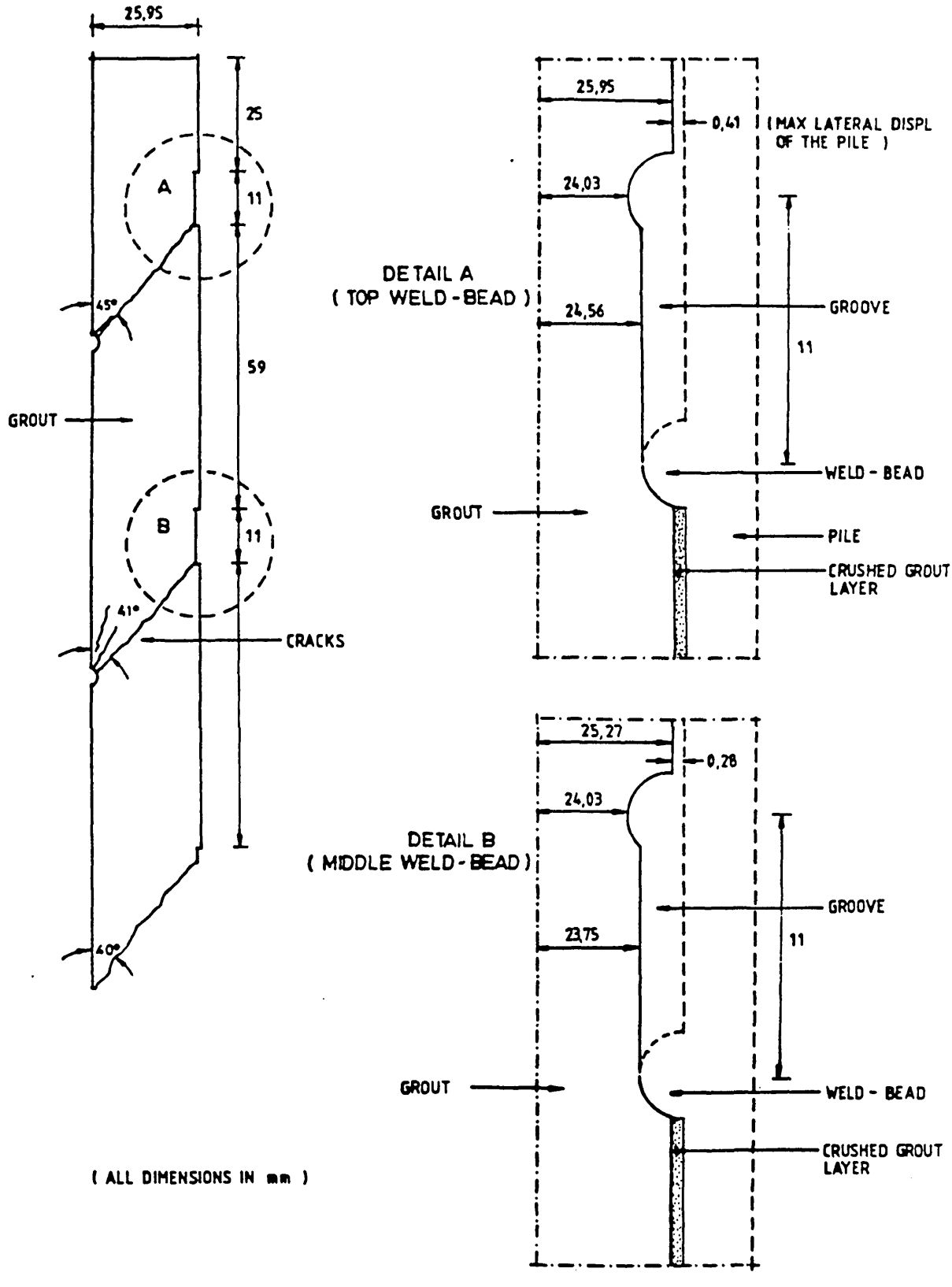
OPENED SPECIMEN AFTER TESTING W4

FIG 3.20



OPENED SPECIMEN AFTER TESTING W5

FIG 3.21



OPENED SPECIMEN AFTER TESTING W6

FIG 3.22



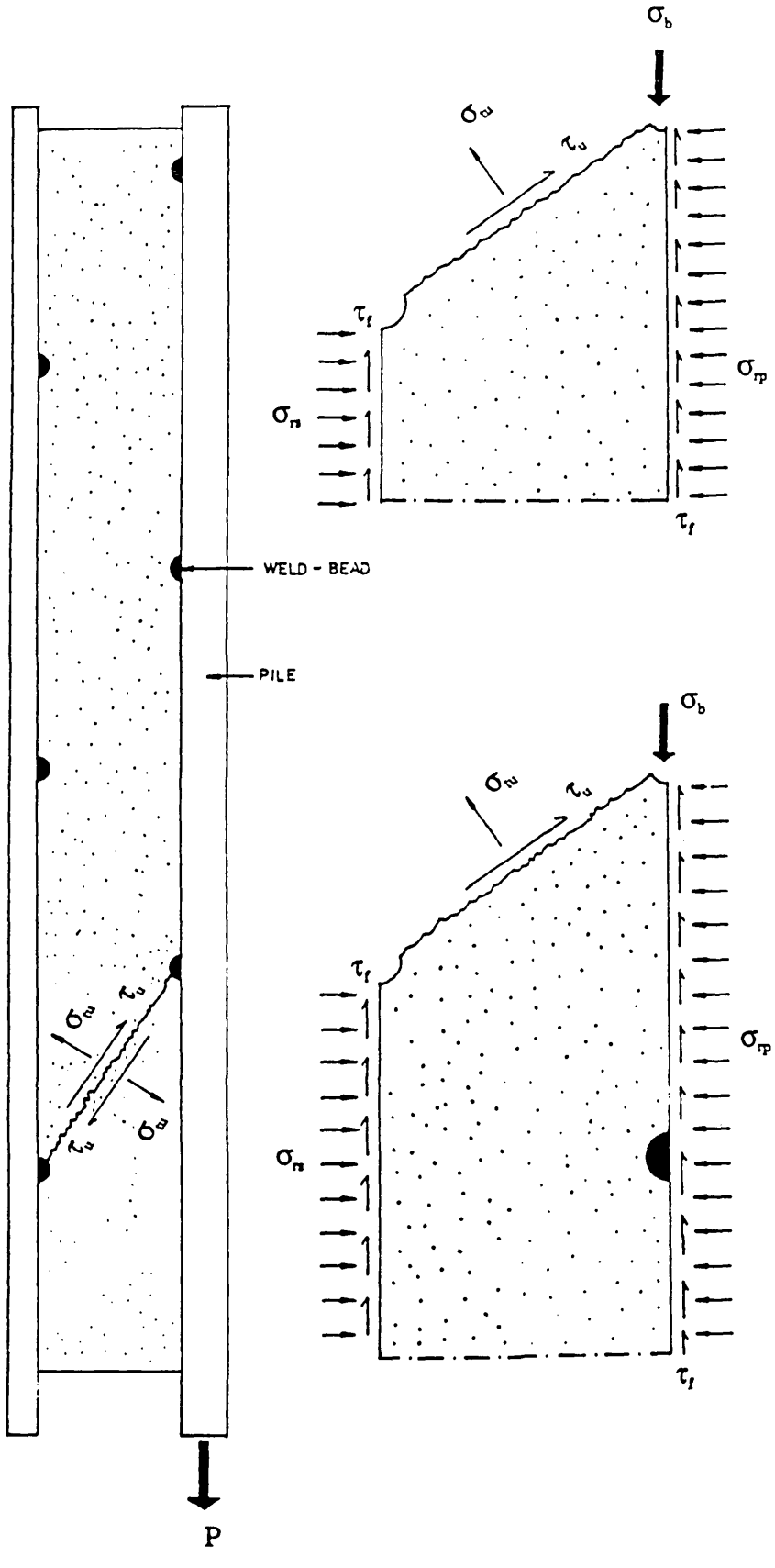
(a) VERTICAL CRACKS IN GROUT ANNULUS



(b) DIAGONAL CRACKS IN GROUT ANNULUS

CRACKS IN GROUT ANNULUS AFTER TESTING

FIG 3.23



(a) CASE 1 :
BOTTOM WELD-BEAD OF PILE IS IN HIGHER POSITION THAN BOTTOM WELD-BEAD OF THE SLEEVE.
FAILURE ONLY INVOLVING 1 WELD-BEAD OF PILE

(b) CASE 2 :
BOTTOM WELD-BEAD OF PILE IS IN LOWER POSTION THAN BOTTOM WELD-BEAD OF SLEEVE.
FAILURE INVOLVING 2 WELD-BEADS OF PILE.

FAILURE OF BOTTOM WELD-BEADS

FIG 3.24

CHAPTER FOUR
NUMERICAL ANALYSIS

4.1 Introduction

Whereas experimental testing remains the most realistic means of studying the behaviour of structural components, the need of accurate analytical procedures can not be over emphasized. This is due to the followings :

- From a practical point of view, the range of geometric configuration of the connections is too wide to be fully covered by experiments.

- Full scale tests are difficult to conduct and are capital intensive. On the other hand, reduced scale testing suffers from scale effects and does not provide sufficient proof of full-scale performance.

- Due to material variability, repetition of tests using the same 'target' properties are essential, thus increasing the cost and rendering accurate comparisons more difficult.

To compliment experiments and to overcome some of the above problems, numerical analysis procedures, such as the finite element method may be used. For this purpose, the connection is modelled by an axisymmetric continuum membrane element to represent the steel tubular and the grout annulus, and spring elements to represent the bond action between the steel and the grout.

4.2 Bond Spring Element

For contact problems involving two different materials, it is necessary to derive an element which can represent the incompatibility of displacements between the two materials. Amongst others working in the fields of reinforced concrete and rock mechanics, Elnashai (62) derived a spring element to represent the bond-slip action in grouted connections. The spring is an axisymmetric element with two degrees of freedom at each node, and is used to link two different materials.

Physically, the spring element is fictitious since it does not have any geometric dimensions. The material properties of the spring can be linear or non linear, since this is a 'user defined' parameter.

In the above reference, Elnashai used the spring element to analyse the bond strength of plain and prestressed grouted connections. In conjunction with the spring element, a semi-empirical material model was formulated. The behaviour pattern and failure modes observed in practice were used to derive a parametric representation, and calibration to existing data was performed. The full details of the derivation of the element are given in reference (62). However, a brief description is given below.

4.3 Finite Element Formulation

Referring to figure (4.1), the displacements between joint i and j are

$$\Delta r = r_j - r_i \tag{4.1.a}$$

$$\Delta s = s_j - s_i \tag{4.1.b}$$

If the strain vector is expressed in term of joint displacement, then :

$$\begin{bmatrix} \varepsilon_r \\ \\ \varepsilon_s \end{bmatrix} = 1/t \begin{bmatrix} -1 & 0 & 1 & 0 \\ \\ 0 & -1 & 0 & 1 \end{bmatrix} \begin{bmatrix} r_i \\ s_i \\ \\ r_j \\ s_j \end{bmatrix} \tag{4.2}$$

where;

t : thickness

This can be written as:

$$\underline{\varepsilon} = \underline{B}\ \underline{\delta} \tag{4.3}$$

The stress strain relation is given by

$$\begin{bmatrix} \sigma_r \\ \sigma_s \end{bmatrix} = \begin{bmatrix} d_{rr} & d_{rs} \\ d_{sr} & d_{ss} \end{bmatrix} \begin{bmatrix} \varepsilon_r \\ \varepsilon_s \end{bmatrix} \tag{4.4}$$

or,

$$\underline{\sigma} = \underline{D}\ \underline{\varepsilon} \tag{4.5}$$

In general, the stiffness matrix is given by:

$$K_{rs} = \int_v \underline{B}^T\ \underline{D}\ \underline{B}\ dv \tag{4.6}$$

Substituting in (4.6) yields :

$$K_{rs} = A/t^2 \begin{bmatrix} d_{rr} & d_{rs} & -d_{rr} & -d_{rs} \\ d_{sr} & d_{ss} & -d_{sr} & -d_{ss} \\ -d_{rr} & d_{rs} & d_{rr} & d_{rs} \\ -d_{sr} & -d_{ss} & d_{sr} & d_{ss} \end{bmatrix} \tag{4.7}$$

where A is the area covered by the spring.

To avoid the problem of defining an initial fictitious thickness t, the elements of the matrix are multiplied by t. Therefore, the stiffness is directly related to displacements instead of strains.

$$K_{rs} = A \begin{bmatrix} d_{rr} & d_{rs} & -d_{rr} & -d_{rs} \\ d_{sr} & d_{ss} & -d_{sr} & -d_{ss} \\ -d_{rr} & -d_{rs} & d_{rr} & d_{rs} \\ -d_{sr} & -d_{ss} & d_{sr} & d_{ss} \end{bmatrix} \tag{4.8}$$

For steel /grout interface problems the non dilatant joint formulation has been found to agree well with experimental results (76, 77 and 78), and therefore all the

coupling terms have been neglected in element matrices. By referring to the geometry of the connection, the transformation from local to the global axes systems produces an identical matrix in X-Y axes. The final form of the stiffness matrix can be written as:

$$K_{xy} = 2\pi RL \begin{bmatrix} C_{xx} & 0 & -C_{xx} & 0 \\ 0 & C_{yy} & 0 & -C_{yy} \\ -C_{xx} & 0 & C_{xx} & 0 \\ 0 & -C_{yy} & 0 & C_{yy} \end{bmatrix} \quad (4.9)$$

Where L is the spacing between the springs.

This stiffness matrix represents the bond-slip behaviour of the connection. Although the stiffness matrix does not include mixed terms, the coupling effect is taken into account by the intrinsic shear strength used in the pseudo-material model given hereinafter.

4.4 Bond Slip Properties in Plain Connections

In general the procedure of defining the biaxial stress-slip formulation of the plain connection is as follows:

1. Under the given load, longitudinal and transverse displacements exist between the steel and the grout. The transverse displacement is then used to calculate the transverse stress σ_n

2. To calculate the shear strength τ_{max} of the interface under the given normal stress σ_n, a Mohr-Coulomb failure envelope is used.
   $\tau_{max} = C - f(\sigma_n)\ \sigma_n$ (4.10)
   where C is termed, 'intrinsic shear strength', the value of which depends on the geometry of the connection. From the calibration procedure Elnashai used the value given below :
   $C = 5.65 \sqrt{K}$ (4.11)
   where K is the radial stiffness according to the DEn (57).

3. After defining the shear strength τ_{max} and the corresponding axial relative displacement δ_{cr}, a polynomial function relating the axial relative displacement and the shear stress can be established. This passes through the origin and the peak point (τ_{max},δ_{cr}). The polynomial was derived from a parabolic fit of the available test results, as illustated in figure (4.2).

4. Using this stress-displacement curve, the actual shear stress from the corresponding relative displacement δ_s and the equivalent nodal loads can be calculated.

5. The out-of-balance load vector can be calculated and applied in the following iteration.

The final form of stress-slip curve is given in appendix I.

4.5 Load-transfer Mechanisms in Weld-beaded Connections

For a weld-beaded connection, the stress-slip relationship can be described using two components. The first is due to friction as described above, and the second is due to the presence of bearing stress at the weld-bead. The mechanism of the bearing component is governed by the radial stiffness, weld-bead height, and confined grout strength. If the radial stiffness is very low, the relative lateral displacement will be high, resulting in a by-passing of the shearkey without grout crushing. The weld-bead reaction causes bending moments, which increase with weld-bead height and weaken the confinement. Although the effect of the weld-bead shape (whether rectangular or circular) has not been investigated, relevant studies were carried out by Lutz (43), who examined failure modes of a ribbed reinforcement bar, embedded in concrete. Two failure modes were observed, namely a wedging action and crushing action. If the rib had an angle less than 30°, the total bearing strength developed by the front rib (together with the friction between the rib face and the concrete) were not sufficient to prevent the relative movement between concrete and steel along the interface. Therefore, no concrete crushing occurred. However, when the angle of the rib was greater than 40°, crushing took

place. For a typical offshore grouted connection, the weld-bead has a semi-circular section. Therefore, provided that the radial relative movement is less than half the weld-bead height (which can be achieved if the steel tubular has a sufficient radial stiffness), the angle of the weld-bead face is always greater than 45°. Hence, if Lutz's conclusions are adopted, the failure mode of a typical weld-bead connection is always a crushing mode.

4.6 Bond-Slip Properties in Weld-Beaded Connections

Although the mechanism is different from the plain problem discussed before, the spring element can still be used with some modifications in the material properties. The modified spring element for a weld-bead connection problem can be regarded as having a two phase constitutive model. The first represents friction, and the second is the bearing component. The friction contribution generally follows the above description for the plain bond problem. The difference between the friction properties of a weld-bead connection and a plain bond is that the distribution of lateral stress in a weld-bead connection is less uniform. In the area below the weld bead, the lateral stress could be very high, i.e about 20 to 35 N/mm^2, depending on the stiffness of the steel tubulars. This high lateral stress can increase the friction strength considerably. On the other hand, some parts of the connection could dilate and lose their frictional strength. The groove behind the weld bead (a void formed as the weld bead moves), and near the loaded end (due to Poisson effect), are the two areas which lose their friction strength. As a result of numerical studies, the value shown below was chosen for the 'intrinsic shear strength' (τ_{max}).

$$C = 9 \sqrt{K} \qquad (4.12)$$

instead of $5.65 \sqrt{K}$ as used for plain connections in reference (62).

In a weld-bead connection, as the pile is loaded, relative displacement occurs between the pile and the grout as well as between the grout and the sleeve. The latter, however, is relatively small. Movement is resisted by the friction strength along the interface and the bearing strength (which is given by the weld-bead). It was observed that the bearing strength of the grout beneath the weld-bead

can be much higher than the uniaxial strength. The previous test results (56) and the present programme have showed that the strength of weld-beads are significantly affected by the radial stiffness, weld-bead height and spacing, and the grout strength. These governing factors determine the confining stress which can be imposed by the steel tubulars on the grout. The mechanism and the governing factors relating to the behaviour of cementitious materials under generalised stress states have been discussed in the previous chapter.

It is then assumed that the constitutive relations for the bearing mechanisms can be represented as:

$$\sigma_b = C_k \; C_h \; C_g \; f(\delta_a) \tag{4.13}$$

where,

C_k : radial stiffness parameter

C_h : weld-bead height parameter

C_g : grout strength parameter

$f(\delta_a)$: function dependent on relative axial displacement

These parameters are derived empirically by a calibration process, making use of all the available data including the existing experimental results and the test series by Wimpey Laboratories for the Department of Energy (56). The procedure of calibration is as follows:

1. Calculate the friction contribution to the total strength. Since the total strength consists of friction and weld-bead strength, it is necessary to remove the friction contribution in order to study the bearing action. In the present experiments, the friction was reduced to a minimum by varnishing. For all other experimental results, this strength was calculated using the finite element model for plain connection due to Elnashai.

2. By subtracting the friction contribution, the bearing strength of the weld-bead can then be calculated. Furthermore, by removing the friction contribution in the total stress-slip relation, the bearing stress-slip relation can be determined.

3. Using the bearing stress-slip relation, a non-linear stiffness relation for the weld-bead can be formulated.

4. The procedure is then repeated, varying all the governing factors (K,f,h) in order to study the effect of each parameter.

The calibration procedure is illustated in figure (4.7) and the results are given in appendix II, which is refinement from the earlier calibration by the author (79, 80 and 81). The calibration result of the stress-relative displacement relationship is given in figure (4.3), whilst curves showing the effect of the governing parameters are given in figures (4.4), (4.5) and (4.6).

4.7 Confined Grout Strength

As discussed above, the confining stress (radial and hoop stress) increases as the axial stress increases. The two components of the stress state are interrelated, i.e. the higher the confining stress, the higher the axial stress which can be sustained. The relationship is open-ended as long as the surrounding medium is able to provide sufficient confining stress. Once the required confining stress is no longer available, then the limit of axial stress increase is reached and the ultimate strength is obtained. In two of the existing tests (where the specimens were strain gauged) this stage corresponded with the yielding of the steel pile tubular in the hoop direction.

The stress state involved in this weld-bead mechanism includes three components of stress, i.e axial, radial and hoop stress. As considered previously, the failure criterion due to Kotsovos (31) is used herein with some modification. Using the same principle of deriving the triaxial failure criterion, a numerical study of the strength of the grout in weld-beaded connections resulted in a modification which is necesary to render the failure criteria suitable for the existing grouted connection problems. The modified values of τ_{oc} and τ_{oe} (as defined in the above reference) are;

$$\tau_{ocg} = 1.080\ [\ (\sigma_o/f_{cu} + 0.05)^{0.724}\ ]\ f_{cu} \qquad (4.14)$$

$$\tau_{oeg} = 0.685\ [\ (\sigma_o/f_{cu} + 0.05)^{0.857}\ ]\ f_{cu} \qquad (4.15)$$

τ_{ocg} and τ_{oeg} can then be used in calculating the ultimate shear octahedral strength τ_{ou} as has been described in the chapter (2).

To apply the triaxial strength failure criteria, it is necessary to calculate the radial and hoop stress relationship for predicting the confined bearing strength of the weld-bead. The coupling between the axial stress and confining stress is included in the iteration procedure as described in the flow chart in figure (4.9), using an experimentally-derived expression described below.

4.8 Hoop Stress

Since the confinement stress is a passive stress it is very difficult to formulate an analytical relationship for its calculation. Therefore, experimental results have been used for predicting the hoop stress expression by calibration. The result is a polynomial function of axial stress, as follows:

$$\sigma_{hi} = a_0 + a_1\ \sigma_b + a_2\ \sigma^2_b + a_3\ \sigma^3_b + a_4\ \sigma^4_b \qquad (4.16)$$

and the value of the constants are given in appendix III.

Once the hoop stress at the steel tubular is known, the radial and hoop stresses at the grout may be calculated using Lame's equations (82). For a hollow circular ring subjected to radial pressure as shown in figure (4.8), the relationship between the hoop and radial stresses is given by;

$$\sigma_{hr} = \frac{-a^2b^2(p_o-p_i)}{(b^2-a^2)}\ \frac{1}{r^2} + \frac{(p_ia^2-p_{ob}{}^2)}{(b^2-a^2)} \qquad (4.17)$$

where,

a : inside diameter of the hollow cylinder

b : outside diameter of the hollow cylinder

σ_h : hoop stress

r : distance from the centre point

p_i : radial stress acting on inside surface

p_o : radial stress acting on outside surface

This relationship was derived based on the plane stress assumption. Since the problem under consideration is closer to plain strain, the above equations do not apply exactly. However, as shown in numerical analysis and experimental testing, the axial stress is significantly lower than the radial and circumferential components. It is therefore reasonable to use the above relation, neglecting the effect of axial stress.

if $p_i = 0$, at inside face (r = a) the equation become:

$$\sigma_{ha} = -2p_o b^2 / (b^2-a^2) \tag{4.18}$$

or,

$$p_o = -\sigma_{ha}(b^2-a^2) / 2b^2 \tag{4.19}$$

For uniform the notations, the equations is re-written as in the figure (4.8);

$a = R_{ip}$ (inner radius of the pile)

$b = R_{op}$ (outer radius of the pile)

$p_o = \sigma_{rop}$ (radial stress on outer wall of the pile)

$\sigma_{ha} = \sigma_{hip}$ (hoop stress on inner wall of the pile)

The equation then becomes;

$$\sigma_{rop} = -\sigma_{hip}(R_{op}-R_{ip}) / 2R_{ip}^2 \tag{4.20}$$

And the hoop stress at the interface is given by

$$\sigma_{hop} = -\sigma_{rop}(R^2_{ip}+R^2_{op}) / (R^2_{ip}-R^2_{op}) \tag{4.21}$$

4.9 Iterative Procedure

After the radial and hoop stresses have been calculated, the confined grout strength can be determined from the triaxial stress failure criterion. The following procedure summarizes the calculations:

1. Assume an initial load increment (or initial displacement).

2. Calculate the relative displacement between the grout and the steel.

3. Calculate the axial stress at the weld-bead σ_b according to equation (4.13).

4. Calculate the lateral displacement caused by σ_b.

5. From the lateral displacement of the pile, the corresponding hoop and radial stresses of the pile can be calculated using equations (4.16) and (4.20).

6. Using the pile stress, the hoop and radial stress in the grout at the weld-bead can be calculated by assuming hoop strain compatibility on the steel-grout interface.

7. Calculate the confined strength of the grout under the effect of the hoop and radial stresses according to the 'modified triaxial stress failure envelope'.

8. Compare the confined strength of the grout with the axial bearing stress of the weld-bead.

9. If the confined strength is greater than the bearing stress, the process can be repeated from (1) by taking another increment of applied load.

10. If the confined strength is less than or equal to the bearing stress, the grout has reached its ultimate strength.

The calculation of the confined strength in step (7) above, can be briefly described as below;

1. Calculate τ_{ocg} the shear octahedral stress at $\theta = 0°$.

2. Calculate τ_{ocg} the shear octahedral stress at $\theta = 60°$

3. Calculate τ_{ou} the ultimate shear octahedral stress.

4. Calculate τ_o the shear octahedral stress corresponding to the stress state.

5. If $\tau_o < \tau_{ou}$ the grout has not failed, and another load increment can be sustained.

6. If $\tau_o \geq \tau_{ou}$ the grout has failed.

The above procedure is described in figure (4.9).

4.10 Finite Element Model

For models W the connections were modelled using eight noded quadrilateral axisymmetric elements. The pile and the sleeve were divided axially into eight elements. The grout was also divided into eight elements axially, and into two elements in the radial direction. The bond action at the steel-grout interface was represented by the spring bond elements. The load was applied as a distributed load at the bottom of the pile, and at the bottom of the sleeve three nodes were fixed in the axial and radial directions, respectively. The overall layout and node numbering of the mesh is given in figure (4.10). The mesh has a total of 155 nodes, and a number of degrees of freedom of 304.

For analysing models from the Wimpey Laboratories tests (56), specimens P and R were modelled with six elements axially and one element for the steel and two elements for the grout in the radial directions, as shown in figure (4.15). The total number of nodes is 119, with 232 degree of freedoms.

4.11 Comparison of Results

4.11.1 Comparison with the Present Tests

Table (4.1) gives the predicted strength using the numerical method described above for the small experimental models used in the present programme. Comparison with the experimental results shows that apart from test W1, the numerical predictions are consistently about 11% to 18% higher. This is mainly due to the earlier failure of the bottom weld-bead. This end effect, as discussed previously, will diminish as the number of the weld-beads increases. In columns 5 and 6 the mean strength prediction obtained from the DEn guidance (equation (5) in reference (57)) is also presented. This was calculated using the surface condition factor (C_s) of 0.1 and a length to diameter parameter (C_L) of 0.8. The same surface condition factor was used in the numerical analysis. Whilst the strength from numerical analysis provides an overestimates by about the same percentage for each radial stiffness (except for W1), the DEn prediction depends on the weld bead height, with improved correlation for the higher weld bead. For each radial stiffness, the DEn gives better agreement for the 1.8 mm weld bead, whilst overestimating the reduction in strength due to the reduction in weld-bead height to 1.2 mm. This observation lends weight to the conclusions given in chapter three regarding the effect of weld-bead height on the overall strength of grouted connections, and emphasises the significance of a new parameter h/t.

Table 4.1 Comparison with the present test results

Model	f_{bu} Expt (N/mm^2)	Numerical		DEn guidance	
		f_{bu}	Num./Expt	F_{bu}	DEn/Expt
W1	2.274	2.269	0.998	1.463	0.589
W2	2.425	2.733	1.127	2.136	0.881
W3	1.970	2.305	1.170	1.430	0.725
W4	2.561	3.013	1.177	2.046	0.799
W5	2.080	2.342	1.126	1.693	0.814
W6	2.759	3.062	1.110	2.470	0.895

4.11.2 Comparison with the Wimpey Tests

Comparison with the test results from Wimpey Laboratories (56) is shown in table (4.3). The predicted strengths using the DEn and API methods are given in columns 5 and 7 respectively, whilst column 6 gives the ratio of DEn/Experimental results. Since the new API recommendation is given in terms of allowable stresses, it is not included directly in the comparison. Rather, the variation in safety factors i.e. the ratio of API/experimental result is shown. From the table it is observed that the poorest correlation between numerical and experimental results is for model Q1. This may be due to one of the followings :

1. The loading arrangement in the tests, in which the loading plate which was welded to the bottom end of the pile, tends to enhance the confinement of the bottom weld-bead by producing prying forces. This effect will be more significant for short specimens with few weld-beads as in model Q1.

2. As discussed previously, the arrangement of the weld-beads could significantly affect the total strength of the connection. The numerical analysis was performed by assuming that only 2 weld beads on the pile contributed to the strength, and the bottom weld-bead was ignored. However,

if the bottom weld-bead was assumed not to fail at an early stage, the numerical result would be 2.171 N/mm^2, which is very close to the experimental result. The author decided to present the analysis by using this assumption in order to be consistent with the assumption of typical weld-beads arrangement used throughout all models in the series P, R and Q. This assumption was made because more precise data on the geometry for each model for these series is not available to the author.

Table 4.2 Properties of the DEn test

Model	D/t p	D/t s	D/t g	K	h (mm)	s (mm)	h/s	f_{cu} (N/mm²)
Series R :								
R1	32.00	114.24	22.00	0.0105	1.02	169.32	0.006	38.15
R2								45.89
R3	32.00	114.24	22.00	0.0105	3.06	169.32	0.018	35.56
R4								39.35
R5	32.00	109.14	44.00	0.0095	2.03	169.32	0.012	33.94
R6								45.89
R7	32.00	124.45	11.00	0.0125	2.03	169.32	0.012	35.79
R8								44.53
R9	32.00	114.24	22.00	0.0105	2.03	169.32	0.012	46.75
R10								50.83
Series P :								
P1	20.00	72.06	22.00	0.0146	2.03	169.32	0.012	54.21
P2								47.59
P3	20.00	114.24	22.00	0.0106	2.03	169.32	0.012	53.42
P4								50.37
P5	20.00	139.50	22.00	0.0093	2.03	169.32	0.012	59.61
P6								51.27

Table 4.2 Properties of the DEn test (continued)

Model	D/t p	D/t s	D/t g	K	h (mm)	s (mm)	h/s	f_{cu} (N/mm²)
P7	32.00	72.06	22.00	0.0131	2.03	169.32	0.012	53.08
P8								53.26
P9	32.00	114.24	22.00	0.0100	2.03	169.32	0.012	53.57
P10								52.06
P11	32.00	139.50	22.00	0.0088	2.03	169.32	0.012	58.81
P12								55.60
P13	40.00	72.06	22.00	0.0120	2.03	169.32	0.012	49.91
P14								54.37
P15	40.00	114.24	22.00	0.0095	2.03	169.32	0.012	57.47
P16								52.68
P17	40.00	139.50	22.00	0.0085	2.03	169.32	0.012	57.14
P18								53.42
P19	24.00	84.75	25.56	0.0121	1.81	152.40	0.012	51.20
P20								53.08
Series Q :								
Q1	32.00	114.24	22.00	0.0105	2.03	169.32	0.012	31.76
Q2								36.29
Q3	32.00	114.24	22.00	0.0105	2.03	84.66	0.024	30.10
Q4								27.61
Q5	32.00	114.24	22.00	0.0105	2.03	63.50	0.032	36.26
Q6								33.50

Table 4.3 Comparison with the DEn test results

Model	f_{bu} Expt (N/mm²)	Numerical f_{bu}	Num/Exp	DEn f_{bu}	DEn/Exp	API f_{bu}	SF
Series R :							
R1	1.722	1.610	0.935	1.349	0.784	0.337	5.110
R2	1.862						
R3	2.494	2.816	1.129	2.404	0.964	0.613	4.068
R4	2.599						
R5	2.213	2.049	0.926	1.810	0.818	0.457	4.842
R6	2.354						
R7	2.494	2.449	0.982	2.213	0.888	0.472	5.284
R8	2.512						
R9	2.354	2.340	0.994	2.125	0.902	0.560	4.204
R10	2.073						
Series P :							
P1	2.789	2.761	0.990	3.181	1.140	0.620	4.498
P2	2.9331						
P3	2.283	2.693	1.180	2.293	1.004	0.613	3.724
P4	2.213						
P5	1.862	2.097	1.126	2.124	1.140	0.496	3.754
P6	1.700						
P7	No test result available						
P8	2.705	2.626	0.971	2.815	1.040	0.457	5.919

Table 4.3 Comparison with the DEn test results (continued)

Model	f_{bu} Expt (N/mm²)	Numerical f_{bu}	Num/Exp	DEn f_{bu}	DEn/Exp	API f_{bu}	SF
P9	2.072	2.486	1.200	2.157	1.041	0.459	4.514
P10	2.139						
P11	1.792	2.075	1.158	1.987	1.108	0.491	3.650
P12	1.862						
P13	2.422	2.369	0.978	2.499	1.032	0.437	5.542
P14	2.406						
P15	2.143	2.541	1.186	2.111	0.985	0.483	4.437
P16	2.055						
P17	1.774	1.959	1.104	1.901	1.072	0.481	3.688
P18	1.890						
P19	1.802	2.002	1.111	2.512	1.394	0.445	4.049
P20	3.001						
Series Q :							
Q1	2.143	1.714	0.800	1.401	0.636	0.439	4.880
Q2	2.073						
Q3	3.301	3.331	1.009	2.174	0.658	0.668	4.942
Q4	2.915						
Q5	3.814	4.256	1.116	2.981	0.782	0.718	5.312
Q6	3.899						

The ratios of 'predicted to measured' strength from DEn, API and numerical analysis are presented in figure (4.20) in the form of a histogram. From table (4.3) it is observed that the correlation between the experiment and the DEn method improves as the weld bead height increases, for a constant radial stiffness. Thus in models R1, R3, and R9 with h/s ratios of 0.006, 0.012, and 0.018 respectively, the ratio of DEn method to experimental result increases from 0.784 to 0.964. In these models the weld bead height was increased from 1.02 mm to 3.06 mm, whilst the spacing remained unchanged.

When considering the models in series Q, however, there is very little variation in the correlation between the experiment and the DEn method for two model Q1 and Q3, although the h/s ratio increases. This is because in the models the weld-bead spacing was varied, but the height remained constant. It can, therefore, be concluded that the effect of weld bead height is not accurately reflected in the DEn method. An increase in weld-bead height will not necessarily provide the increase in strength which the equation indicates. As discussed previously, this may be in part due to the neglect of the high frictional bond below the weld bead, with the assumption that a 'plain-pipe' component in plain connections is present, and the neglect of the bending effect at the weld bead. The variation in spacing, on the other hand, does not increase the secondary bending or alter the frictional bond, so that the effect is likely to be linear. Hence this parameter should be separated from the height effect. If the spacing becomes too close, interaction between the weld beads may occur.

In column 8 it is observed that the API safety factor is not consistent, varying from 5.1 to 3.7. This observation was discussed by Carroll, Elnashai, and Dowling (83). The significant difference in safety factors for R1 and R3, (5.11 and 4.068 respectively), shows that the API also does not accurately predict the effect of weld-bead height. Another important point is the exclusion of the radial stiffness parameter K in the API recommendations. Since the API equation does not include the K parameter, the method gives almost the same strength for both models P1 and P3, with radial stiffness of 0.0146 and 0.0106 respectively. The same observation is made regarding models R5 and R7.

4.12 Long Connections

In attempting to use the numerical model to predict the effect of L/D_p ratio for L/D_p greater than two, there are several matters that have to be considered carefully, as follows :

- To minimize the error involved in using 'bond strength parameter' (as discussed previously), the model should have a reasonably high grout strength, about 35 to 60 N/mm^2 which is typically used for tests with L/D_p of one or two. However, to use high grout strength causes the failure mode to be governed by sleeve buckling or yielding instead of grout crushing.

- Results of tests using low grout strength are less reliable for general comparison, since the failure mode of immature grout could be different from that of a mature grout.

To conduct a numerical investigation of the L/D_p effect, model P1 from reference (56) was chosen as the basic geometry for a model with L/D_p equal to two. The length of this model was then increased and the effect on the connection strength was monitored.

Geometry of model P1 :

$L/D_p = 2$

$t_s = 8$ mm

$f_{cu} = 54.21$ N/mm^2

fbu = 2.789 N/mm^2

$D_p = 508$ mm

For this model the maximum axial stress at the sleeve (total load divided by the cross sectional area of the sleeve) is 354 N/mm^2, which is near to the yield stress of the steel. If the geometrical and material properties are kept constant, an increase in L/D_p from 2 to 4 will almost double the sleeve axial stress. Clearly, sleeve yielding will take place well before this load is reached. One way out of this difficulty is by studying a model with very large thickness of pile and sleeve, so

that with the range of L/D_p values under consideration (say L/D_p of 2 to 8) the failure of the connection due to the yielding or buckling of the steel tubular is prevented.

As an example, the thickness of the pile and sleeve of specimen P1 was doubled, so that the radial stiffness K became 0.0235. However, it was soon noticed that even for studying L/D equal 4, the required axial load caused yielding in the sleeve. This is because by increasing the radial stiffness K the weld bead and friction strength also increase significantly, so that the total bond strength was more than doubled, hence the failure would be by axial yielding of the sleeve.

It was therefore decided to analyse a model with a thickness of four times that of the pile and sleeve of P1. This gave a radial stiffness K of 0.0414. The bond strength increased by more than two times over P1, i.e. 5.739 N/mm^2. It was soon also realised that if the length of the connection is doubled (so that the L/D_p become 4) failure of the connection will also be due to sleeve yielding. Therefore, it was concluded that long connections tested experimentally or analytically will suffer from yielding and/or buckling of the steel tubulars, unless adequate precautions are taken, such as the provision of stiffness.

In the long specimen test of the DEn test programmes (70), longitudinal stiffeners were provided. The authors argued that these longitudinal stiffeners would not affect the bond strength. It is thought by the present author that providing the pile and the sleeve with longitudinal stiffeners the connection becomes very stiff in the longitudinal direction, so that yielding or buckling of sleeve will not occur. In other words, the failure mode of the connection is forced to be grout crushing. The following provides an explanation of these observations.

In general, failure modes of grouted connection with weld-beads can due to;

1. Bond failure due to slipping ('by-passing').
2. Failure in the grout due to crushing.
3. Pile failure due to buckling or yielding.
4. Sleeve failure due to buckling or yielding.

Mode 3 is unlikely since the thickness of the pile is always greater than the sleeve. Mode 1 is also unlikely, unless the thickness of the sleeve and the pile are very small, so that due to the bearing stress, the weld beads will move laterally, and therefore no bearing strength is developed by the weld beads.

Failure mode 4 can be avoided by using a sufficiently thick sleeve. Therefore, in most cases failure will be due to mode 2. This failure mode is significantly affected by the radial stiffness since it determines the value of the confined grout strength. There is no effect due to the longitudinal stiffness for this mode. Therefore the presence of longitudinal stiffeners will not increase the strength of the connection. This is the case examined in reference (56 and 70). However, if this conclusion is generalised (as assumed by the author of reference (70)), the problem will be misjudged. If failure mode is 4 (sleeve yielding) exist, which is likely to be the failure mode for models with thin sleeves, it is obvious that the governing factors will be the stiffnesss in the longitudinal direction instead of radial stiffness.

In reference (70) above the authors based their argument on particular programme of studying the effect of longitudinal stiffening using short specimens ($L/D_P = 1$). While it is true that the longitudinal stiffening does not affect the grout strength in short connections, in long specimens it significantly increases the connection strength since it prevents the connection failing due to sleeve (or pile) yielding. Moreover, by providing the longitudinal stiffening, the pile and sleeve elongation are also reduced. It was discussed previously that the pile elongation affects the distribution of bearing stress at the weld bead along the length of the connection. Hence, this affects the average bond strength.

4.13 Scaling Effects

Based on the above reasons, it was decided to analyse the scale effect. Here again model P1, from reference (56) was used as a control model. The geometry of the connection was then scaled to half, two, four, and six times of the original dimensions. The results are presented as follows.

Table 4.4 Scaling effects

Scale	L (mm)	R_p (mm)	t_p (mm)	t_t (mm)	t_g (mm)	K	h (mm)	s (mm)	f_{bu} (N/mm^2)	Ratio
0.5	504	114.3	12.7	4.0	12.7	0.0134	1.015	86.66	3.052	1.058
1.0	1008	228.6	25.4	8.0	25.4	0.0134	2.03	169.32	2.884	1.000
2.0	2016	457.2	50.8	16.0	50.8	0.0134	4.06	338.64	2.831	0.982
4.0	4032	914.4	101.6	32.0	101.6	0.0134	8.12	677.28	2.933	1.017
6.0	6048	1371.6	152.4	48.0	152.4	0.0134	12.18	1015.92	2.935	1.018

By increasing the scale, the surface area of the connection increases quadratically. The average friction strength contribution will not be affected by the scaling because the radial stiffness K and the grout strength are constant. The bearing strength contribution will also not be affected, because although the eccentricity of the bearing stress increases as the weld bead height increaes, the effect of the bending stress on the steel confinement does not increase since the thickness of the steel tubular also increases proportionally. Therefore, the confinement stress which can be produced does not change. One factor which could affect the strength of a scaled connection is the elongation. The increase of elongation will cause a greater difference in the relative displacement between the weld-beads. However, since the elongation of the sleeve and the grout also increases, the effect on differential relative displacement of the weld-bead becomes insignificant. Based on this argument, it might be expected that by scaling the specimens there is no significant effect on the average strength of the connection. The finite element analysis give the same conclusion.

4.14 Conclusions

Based on the numerical analysis presented in this chapter and the comparison of experimental and existing design methods, the following conclusions apply:

1. A numerical model for weld bead connections has been introduced, making use of the spring element which has been previously developed.

2. The axial stress and confining stress-relative displacement relationship for the weld-bead was formulated from a calibration process using the available experimental data.

3. The numerical analysis has been shown to agree very well with the experimental results, both for the existing programme and for the previous DEn programmes. The scatter of results from numerical predictions is significantly less than predictions using DEn and API guidance notes when normalised by the corresponding experimental value. This lends weight to the assumptions used in the derivation of the model, and encourages its use as a tool for predicting connection strength.

4. The existing DEn recommendations do not accurately account for the effect of weld bead height on average strength, and could lead to reduced safety margins for large weld-bead outstands.

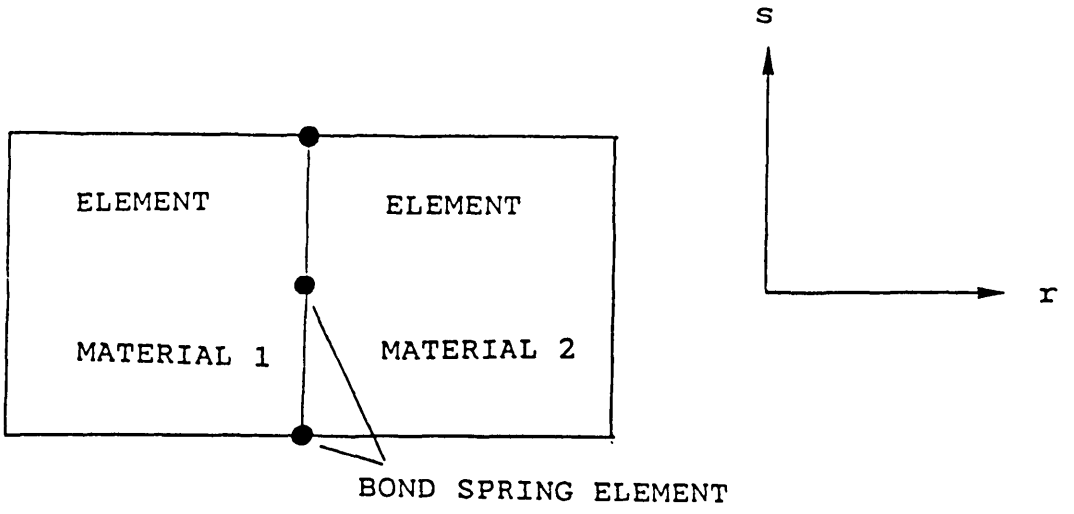
5. Since the effect of varying the weld-bead height is different from varying the spacing, the two should not be included as one composite parameter. Rather, they should be considered as two independent parameters.

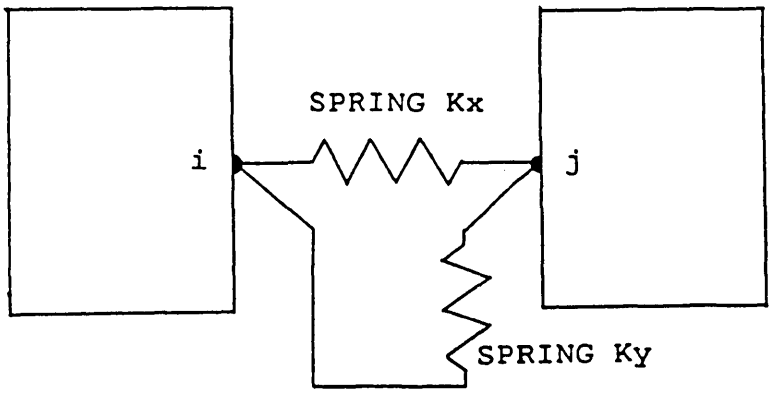
6. The exclusion of the radial stiffness parameter in the API design equation cannot be justified, and has been shown to give inconsistent results.

7. The use of longitudinal stiffeners could affect the connection strength. Therefore, the results of tests using such models should be considered

carefully for comparison with unstiffened models.

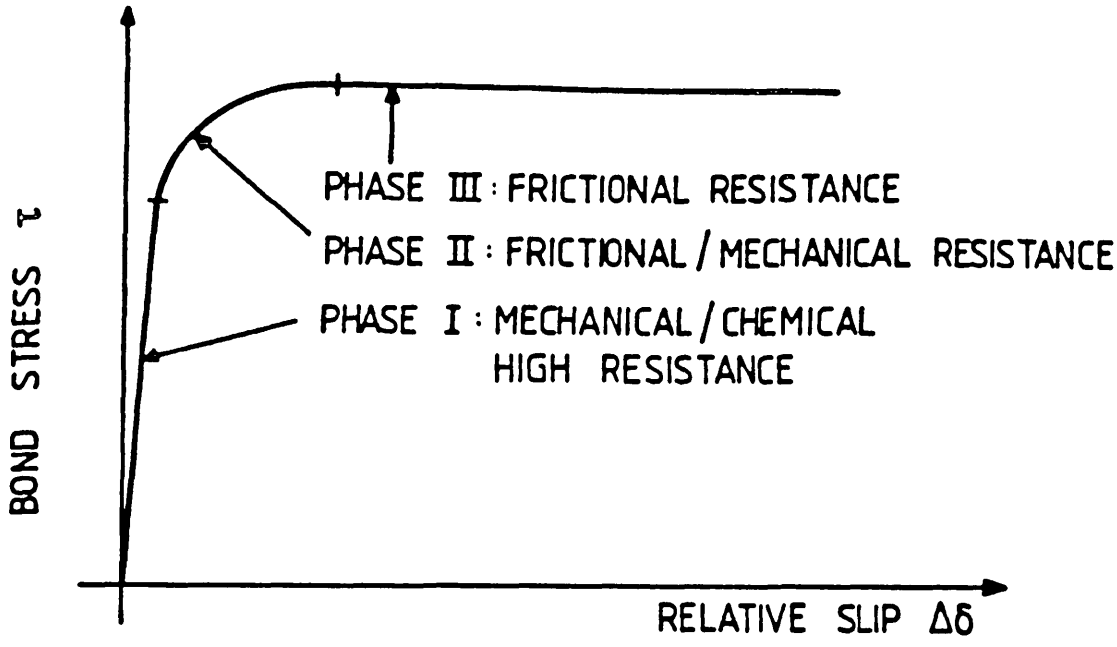
8. From the numerical analysis it can be shown that the effect of scaling the geometry on the average strength of the connection is negligible.



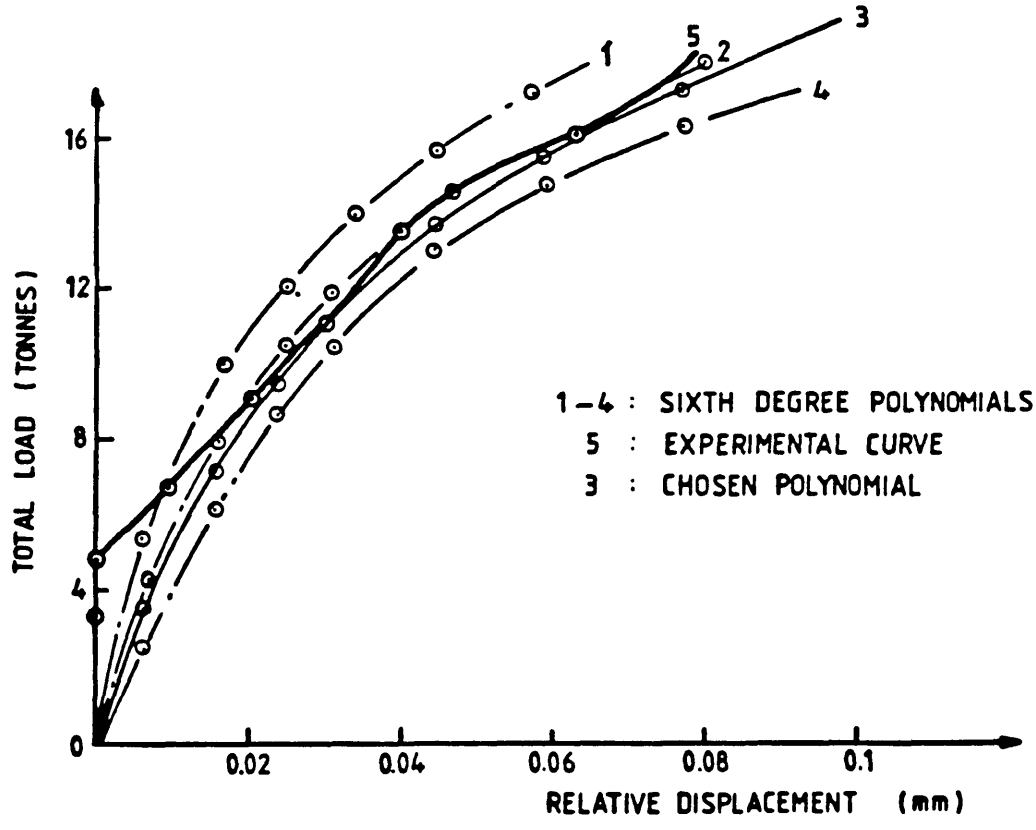


BOND SPRING ELEMENT

FIG 4.1

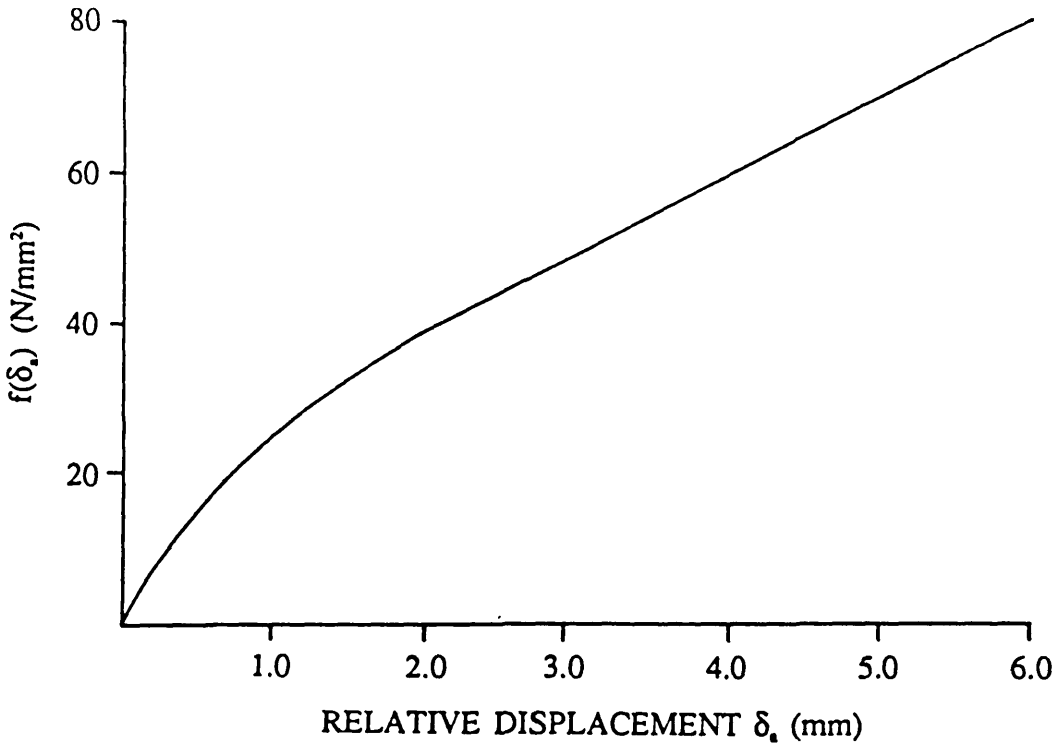


(a) BOND STRESS SLIP CURVE



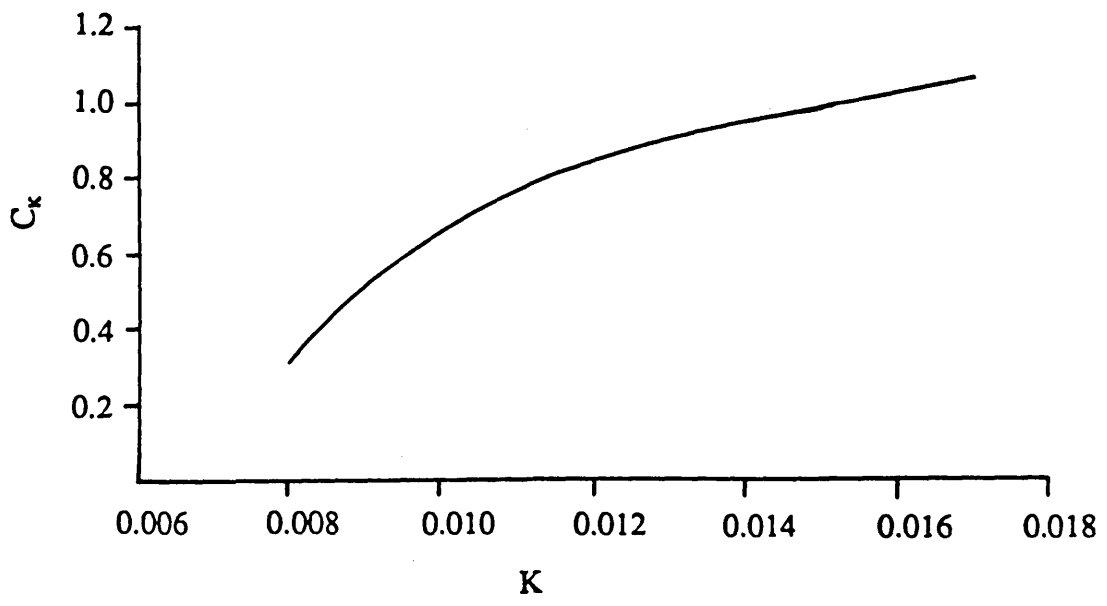
(b) LOAD-RELATIVE DISPLACEMENT RELATIONSHIP FOR PLAIN CONNECTIONS (ELNASHAI-62)

FIG 4.2



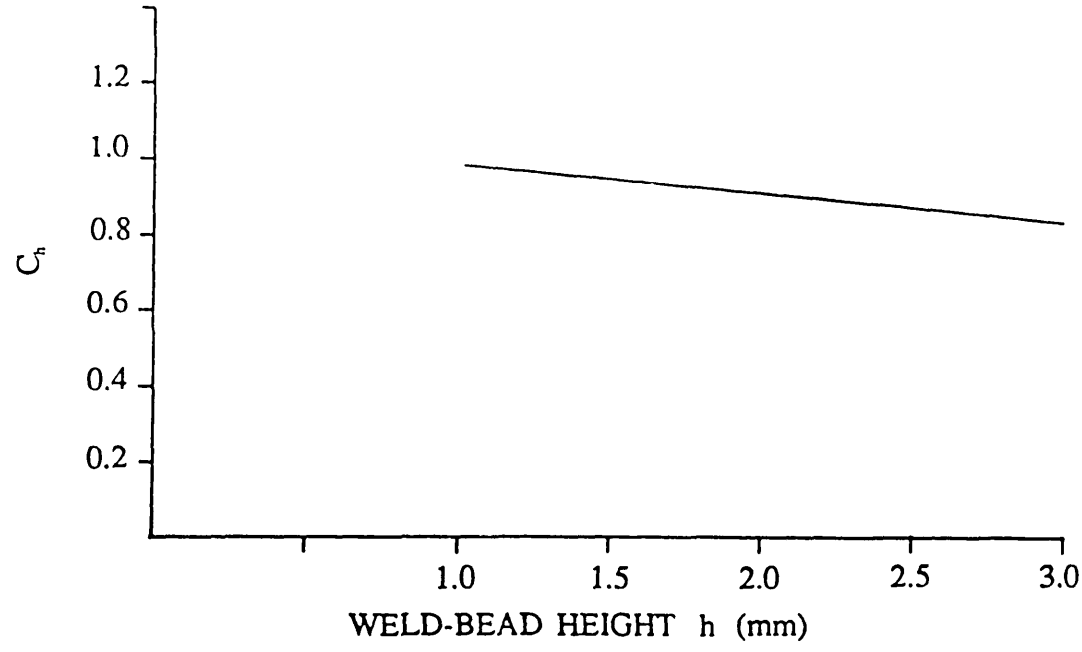
BEARING STRESS-RELATIVE DISPLACEMENT RELATIONSHIP

FIG 4.3



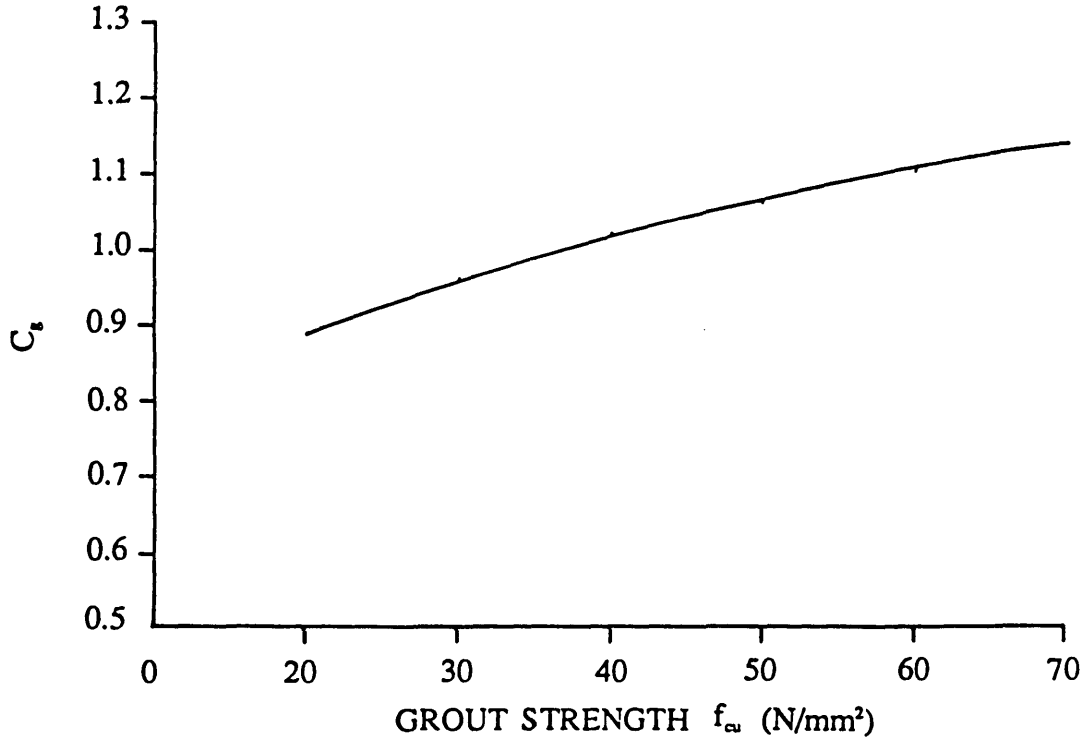
EFFECT OF RADIAL STIFFNESS K

FIG 4.4



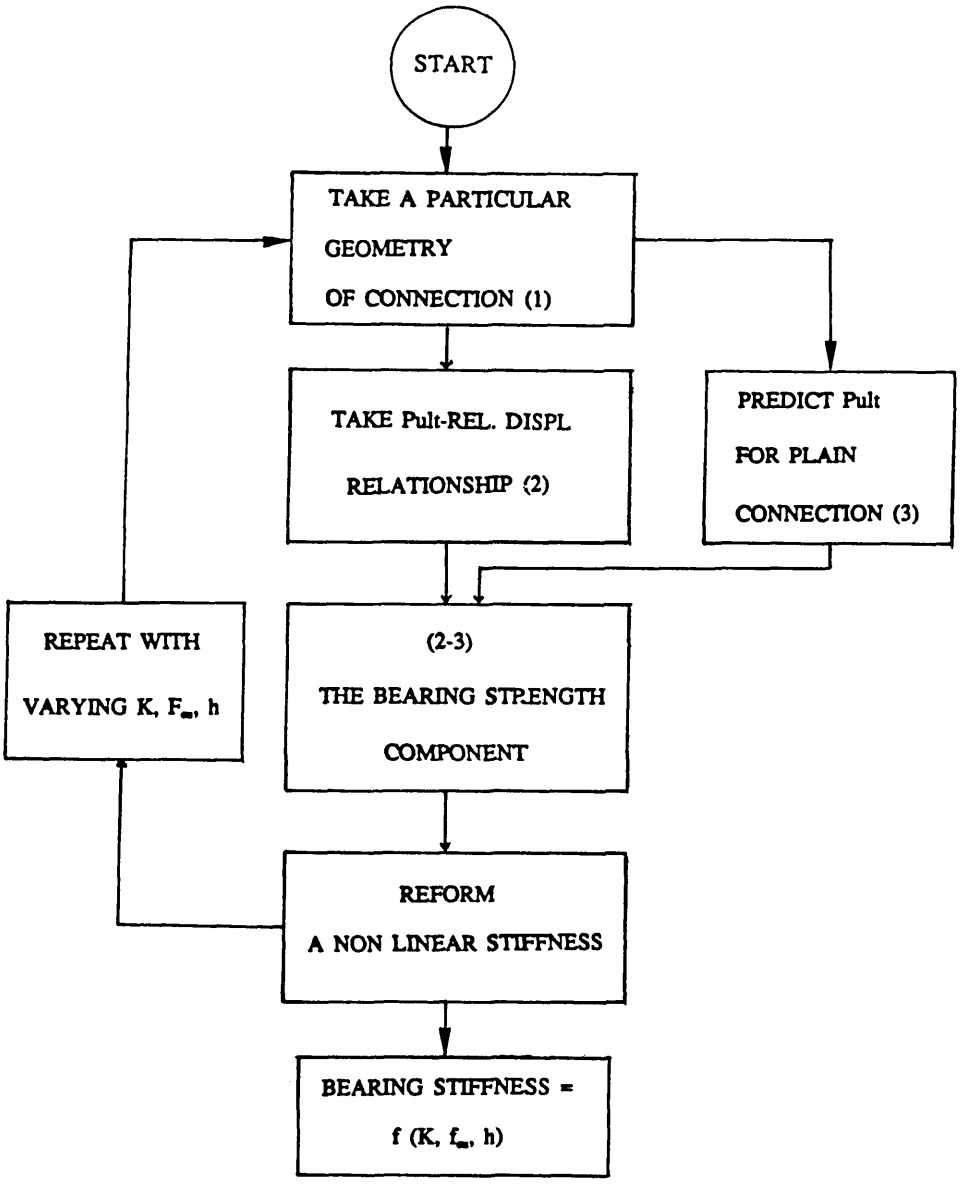
EFFECT OF WELD-BEAD HEIGHT

FIG 4.5



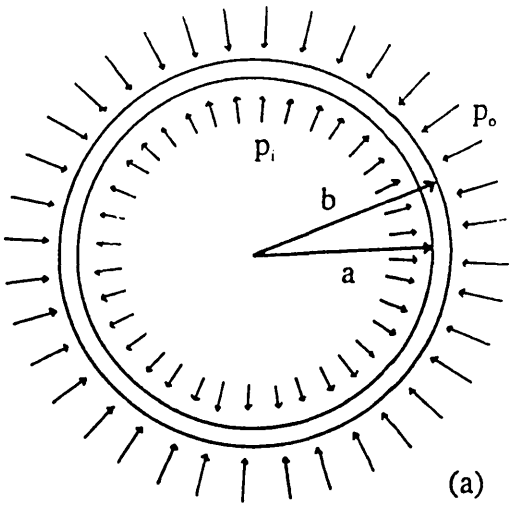
EFFECT OF GROUT STRENGTH

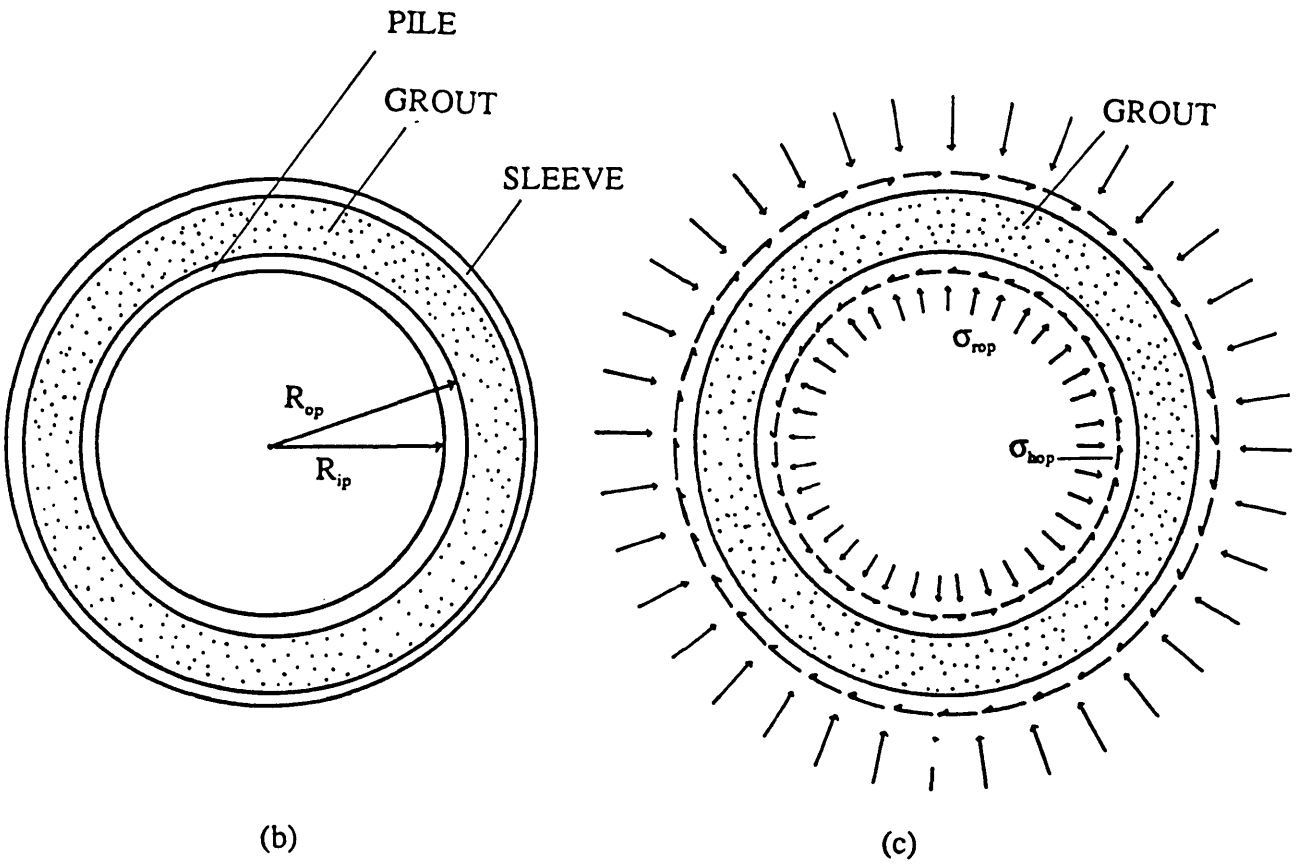
FIG 4.6



ESTIMATION PROCESS FOR WELD-BEAD STIFFNESS

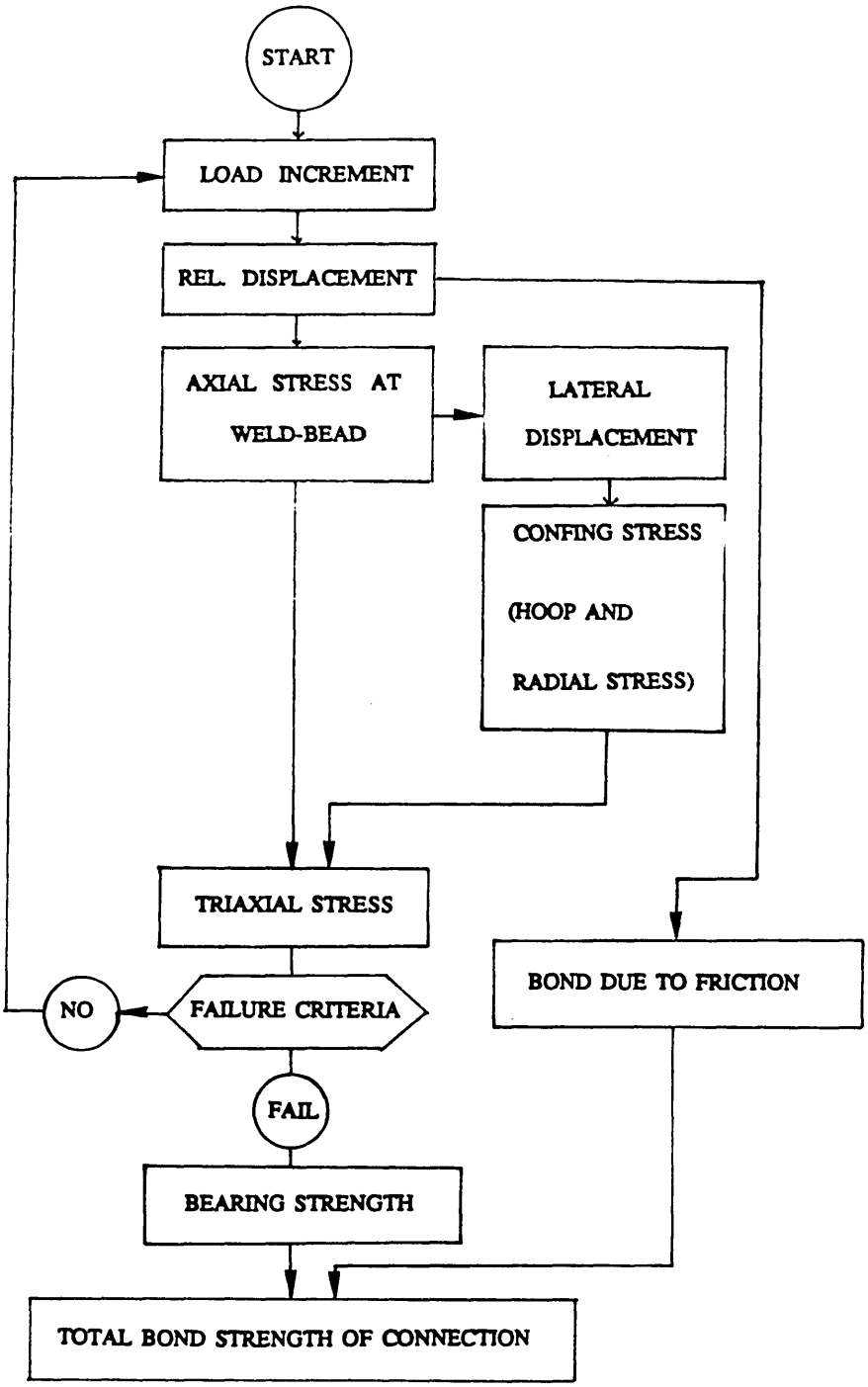
FIG 4.7





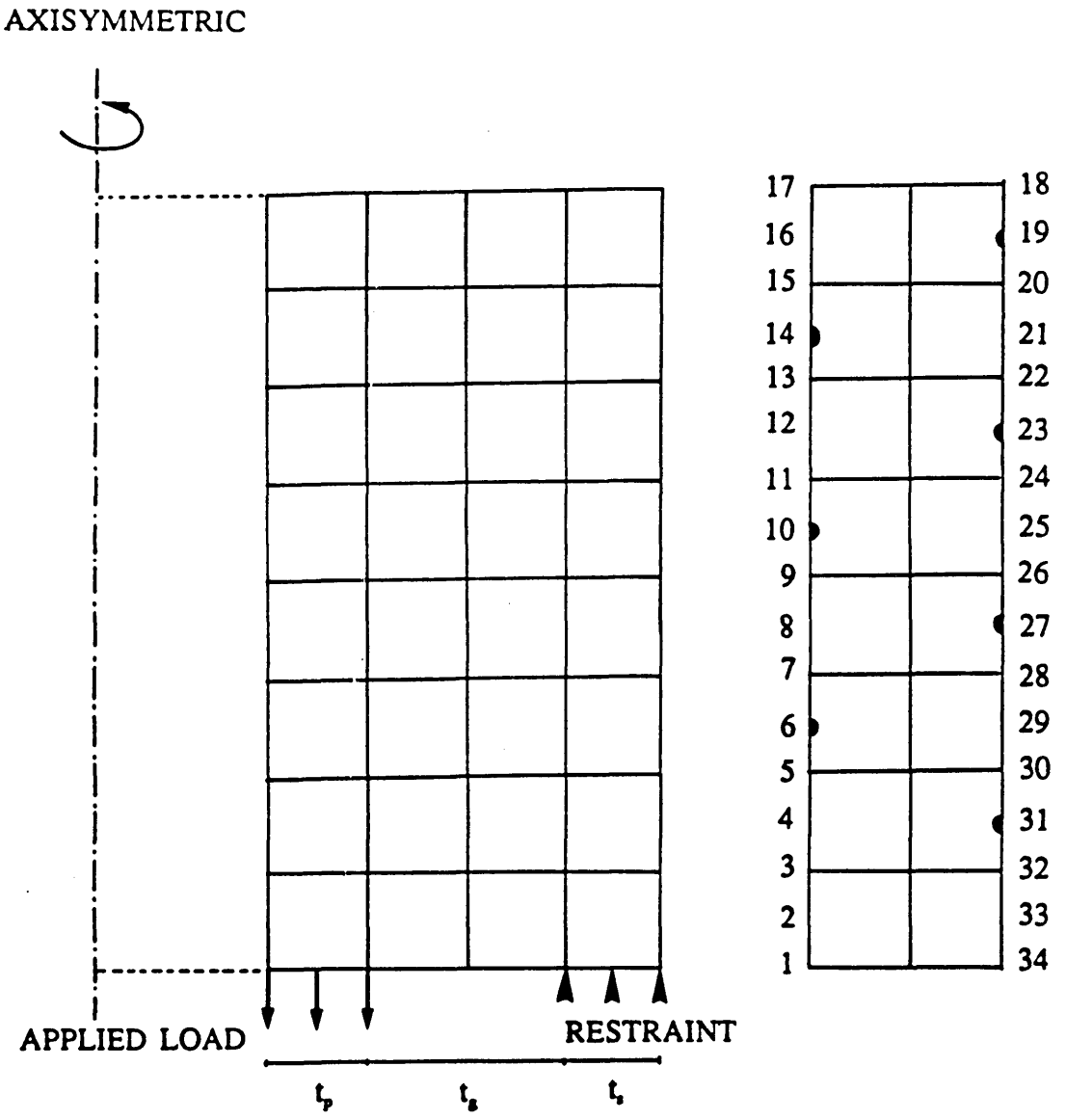
STRESS STATE AT CONTACT SURFACES

FIG 4.8



IMPLEMENTATION OF TRIAXIAL FAILURE CRITERION

FIG 4.9

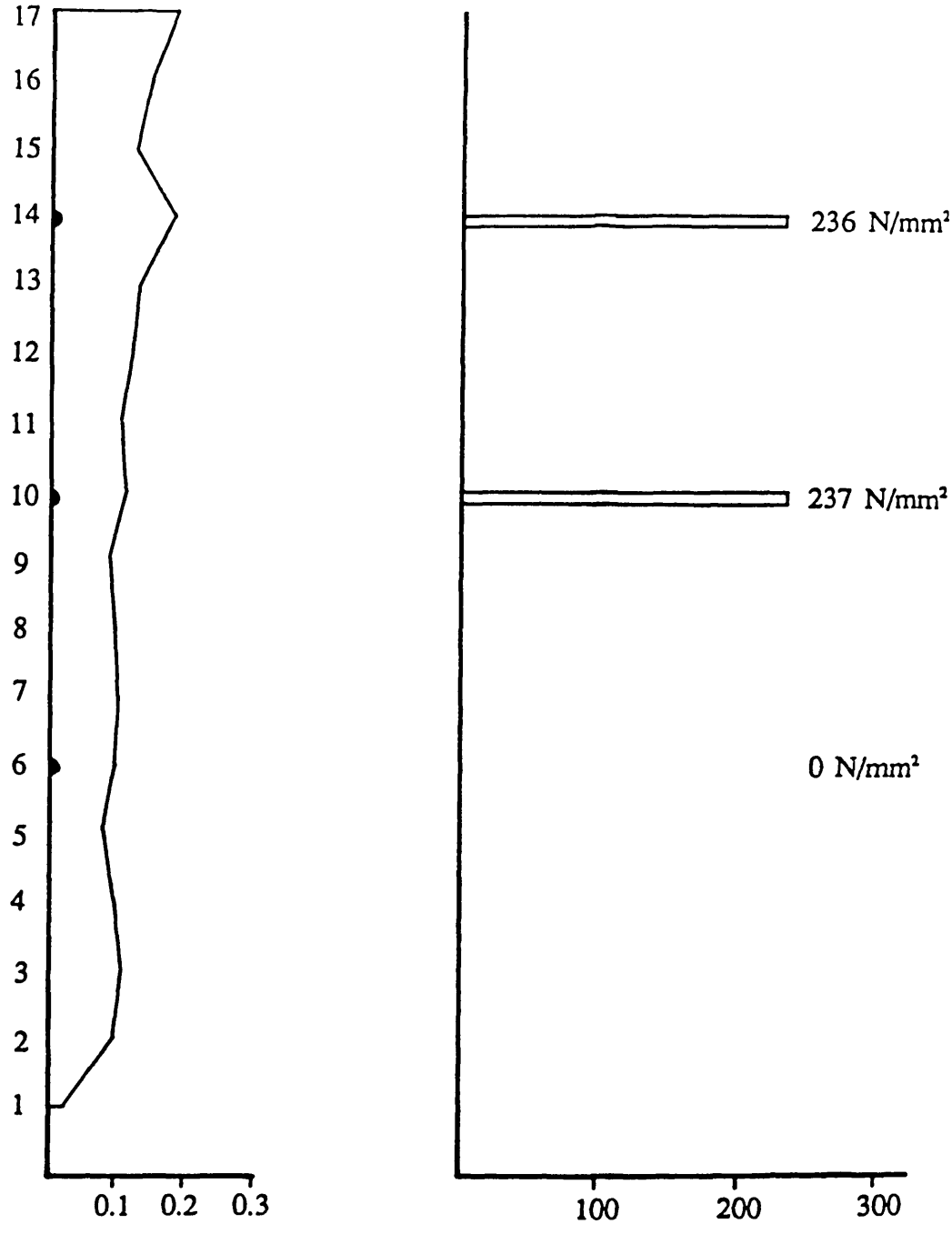


(a) MESH FOR NUMERICAL MODEL

(b) NUMBERING FOR SPRING BOND ELEMENTS

NUMERICAL MODEL FOR TEST SERIES W

FIG 4.10

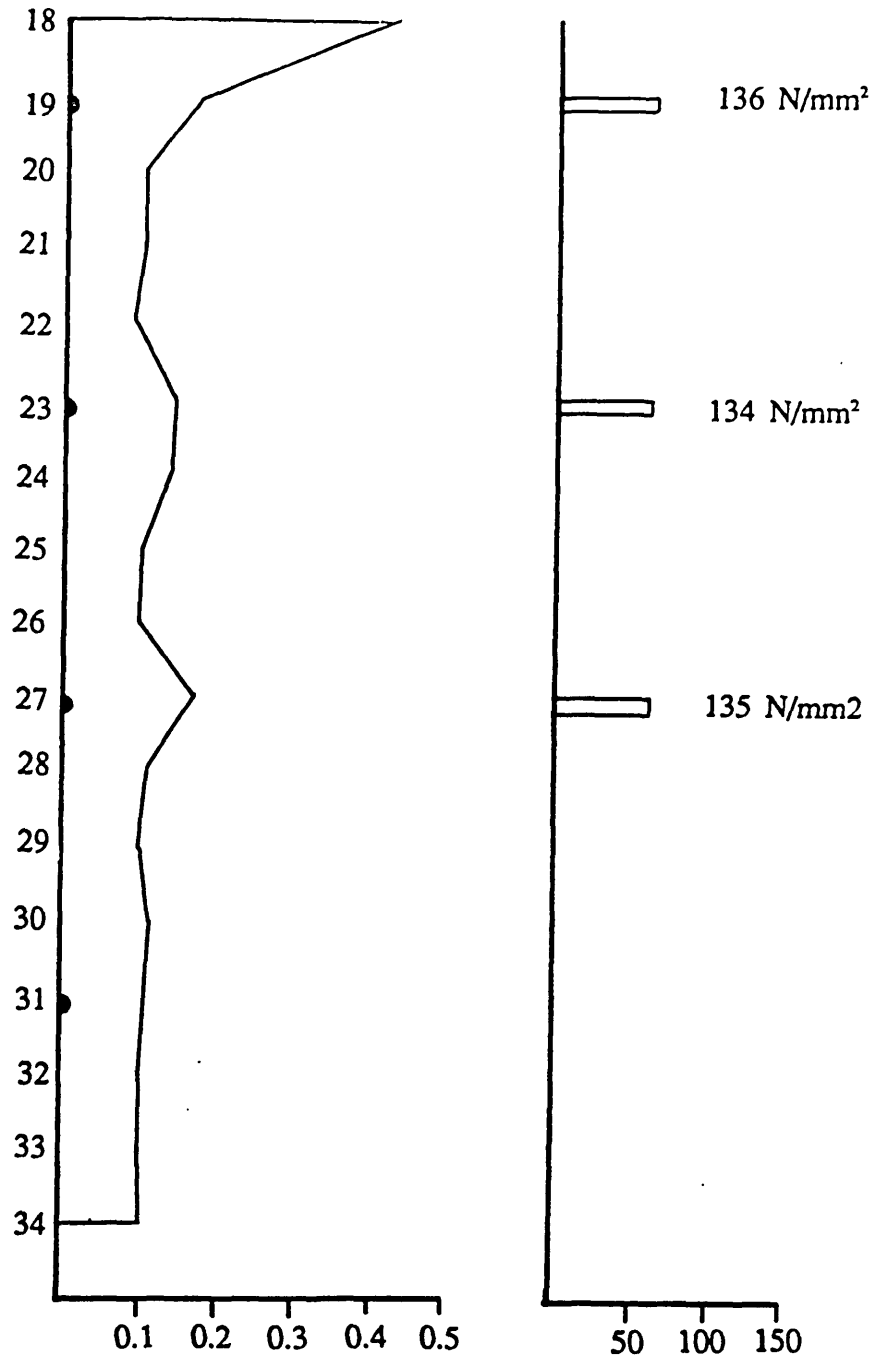


(a) FRICTION STRESS (N/mm²) (b) BEARING STRESS (N/mm²)

STRESS DISTRIBUTION ALONG THE PILE-GROUT INTERFACE AT ULTIMATE LOAD

MODEL W2

FIG 4.11

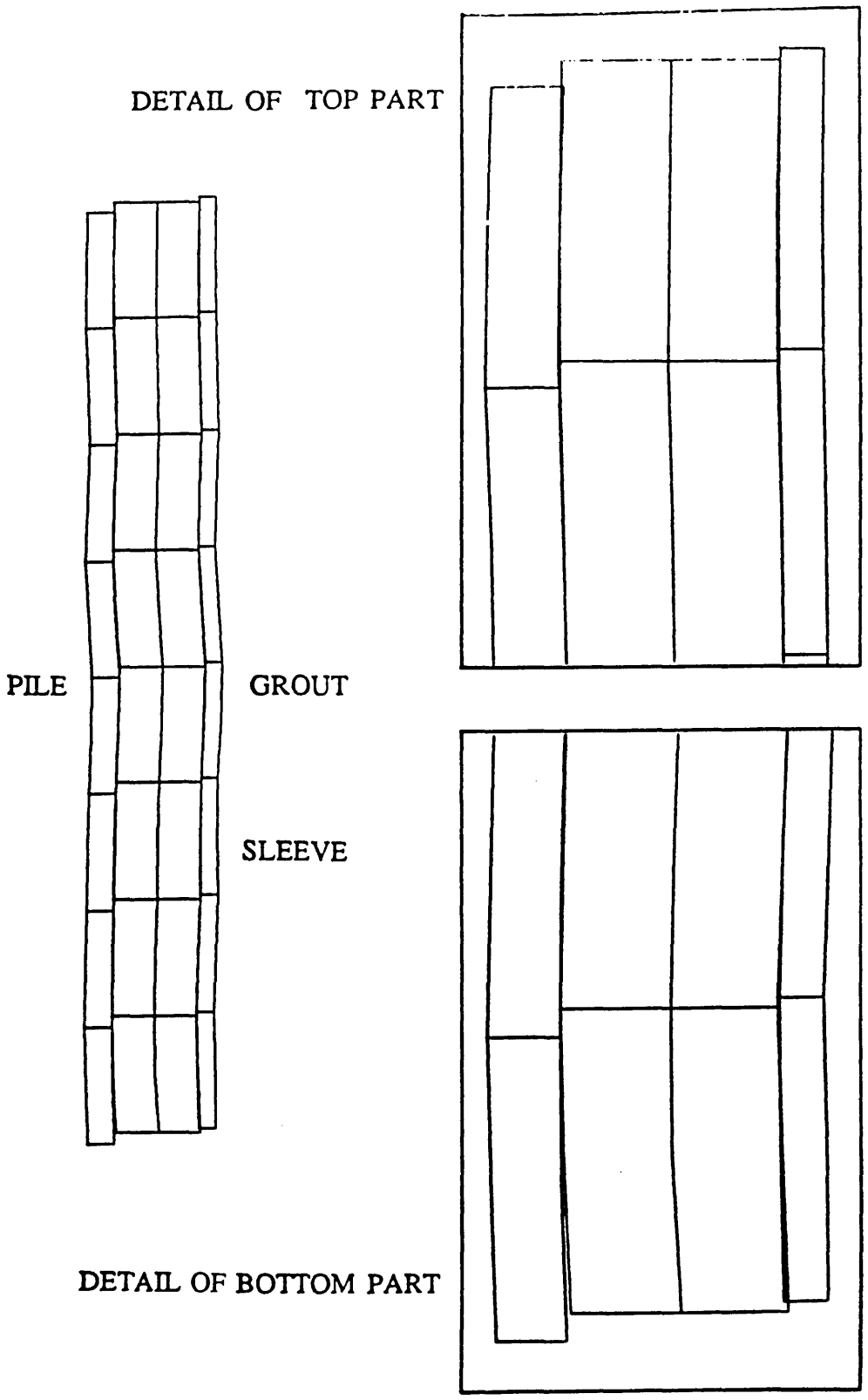


(a) FRICTION STRESS (N/mm²) (b) BEARING STRESS (N/mm²)

STRESS DISTRIBUTION ALONG THE SLEEVE-GROUT INTERFACE AT ULTIMATE LOAD

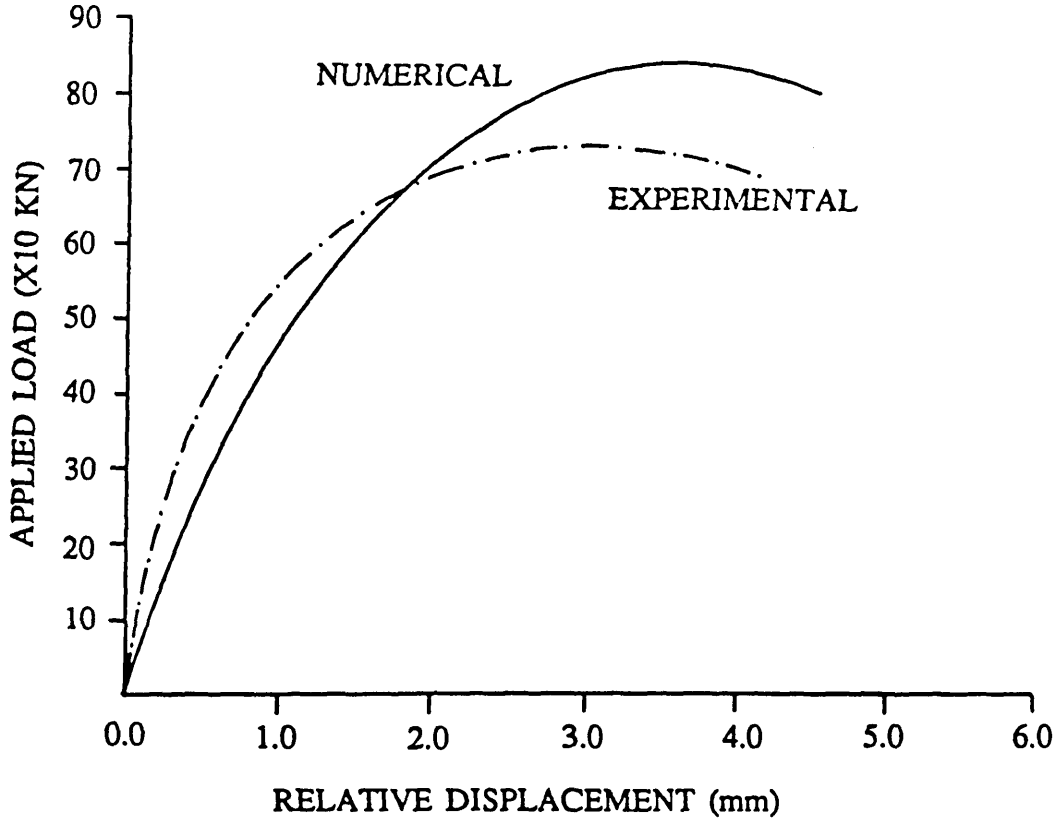
MODEL W2

FIG 4.12



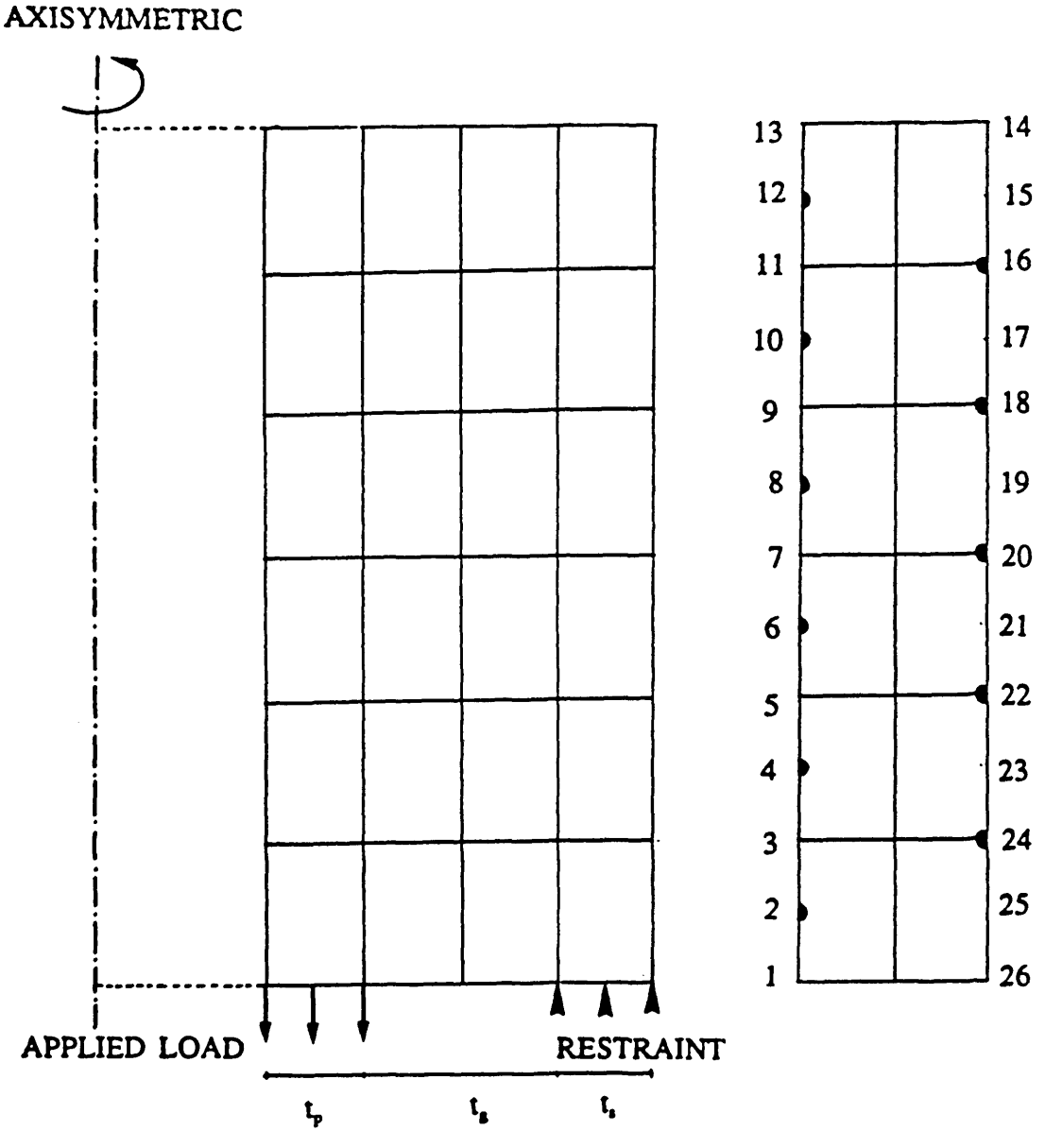
DEFORMED SHAPE AT ULTIMATE LOAD-MODEL W2

FIG 4.13



LOAD-RELATIVE DISPLACEMENT-MODEL W2

FIG 4.14

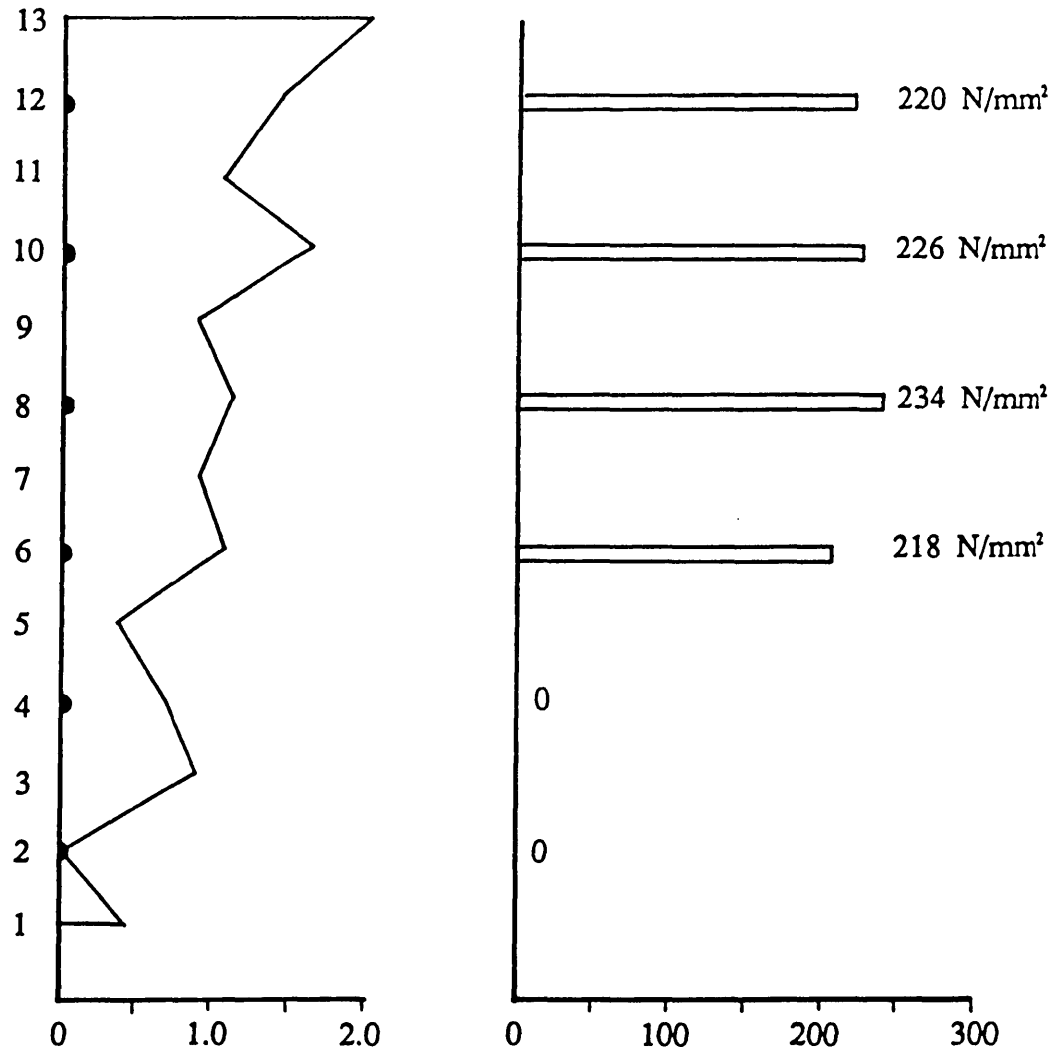


(a) MESH FOR NUMERICAL MODEL

(b) NUMBERING FOR SPRING BOND ELEMENTS

NUMERICAL MODEL FOR TEST SERIES P AND R

FIG 4.15

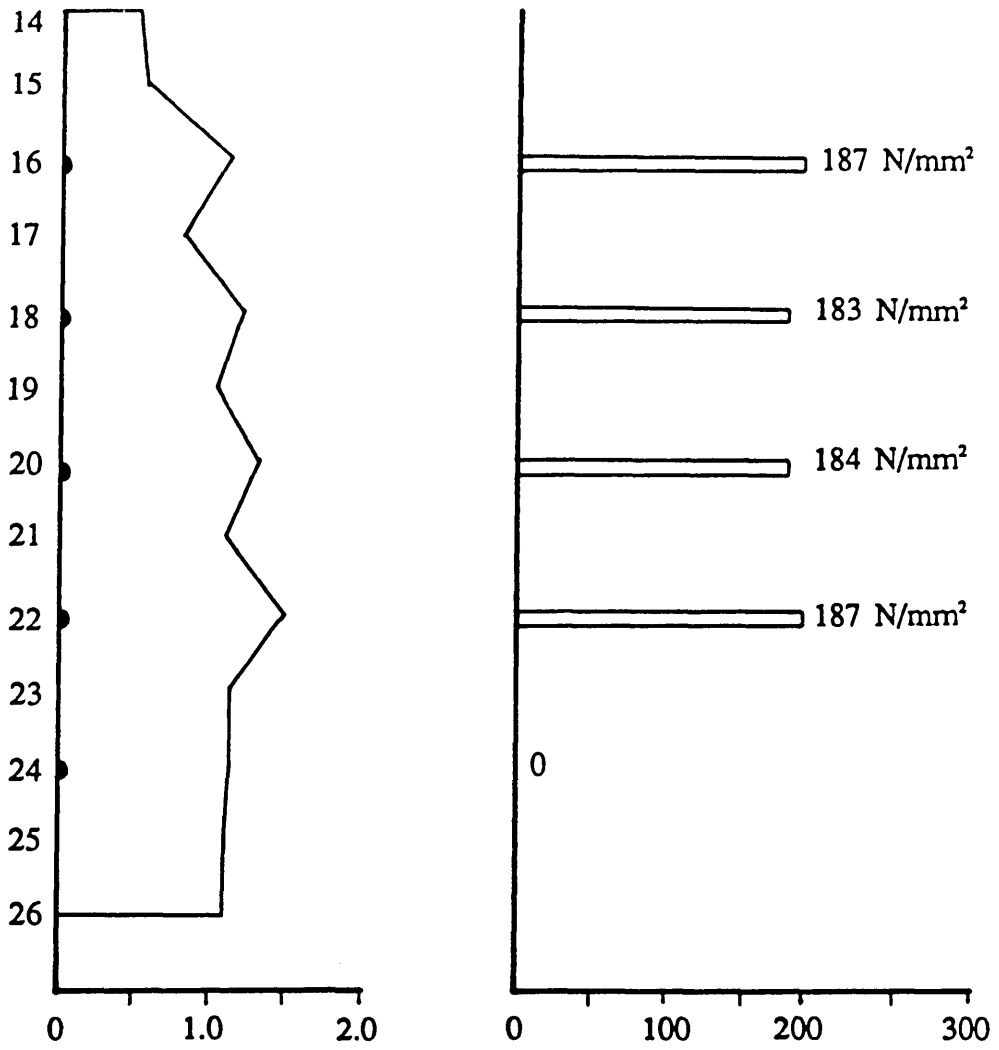


(a) FRICTION STRESS (N/mm²) (b) BEARING STRESS (N/mm²)

STRESS DISTRIBUTION ALONG THE PILE-GROUT INTERFACE AT ULTIMATE LOAD

MODEL P1

FIG 4.16

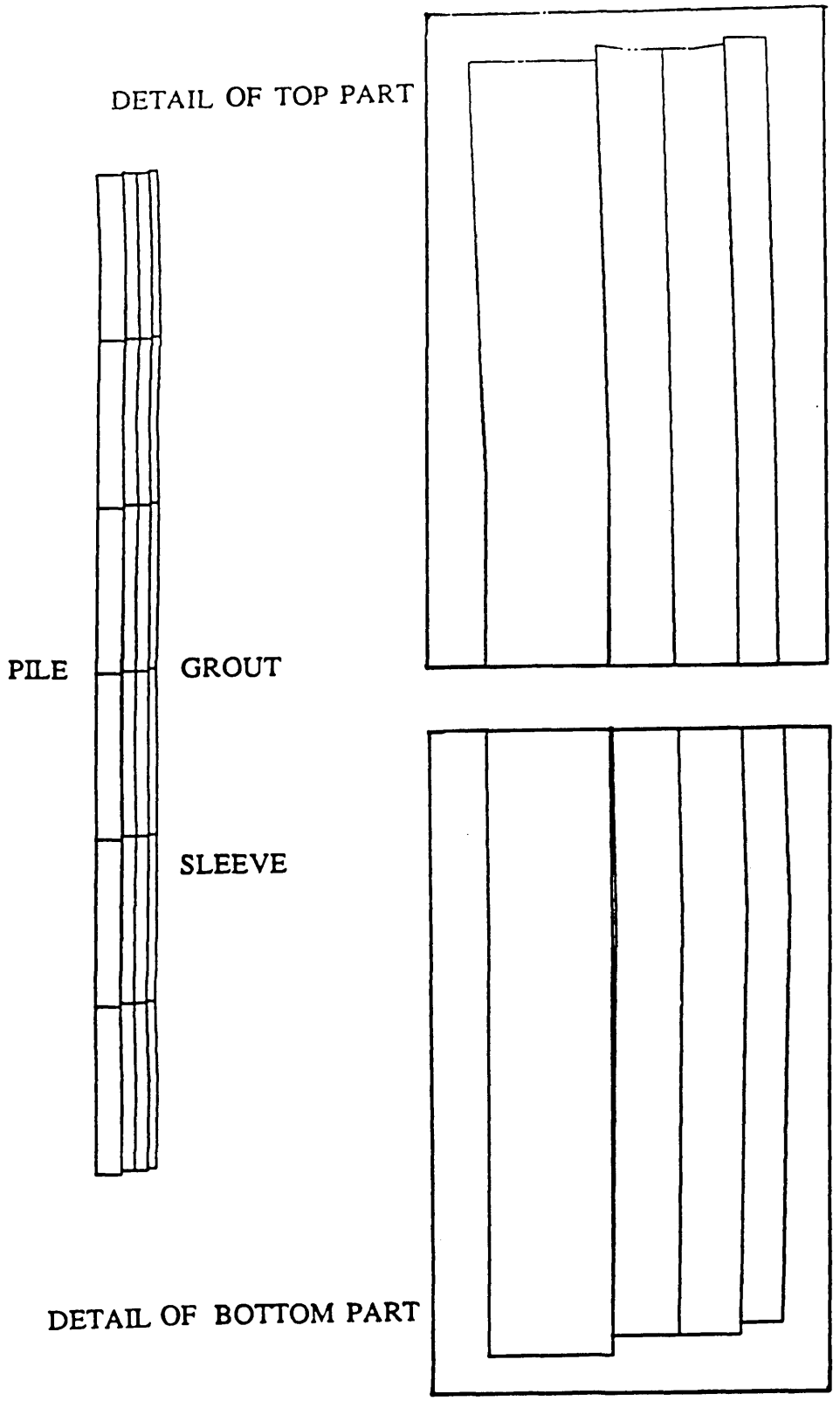


(a) FRICTION STRESS (N/mm²) (b) BEARING STRESS (N/mm²)

STRESS DISTRIBUTION ALONG THE SLEEVE-GROUT INTERFACE AT ULTIMATE LOAD

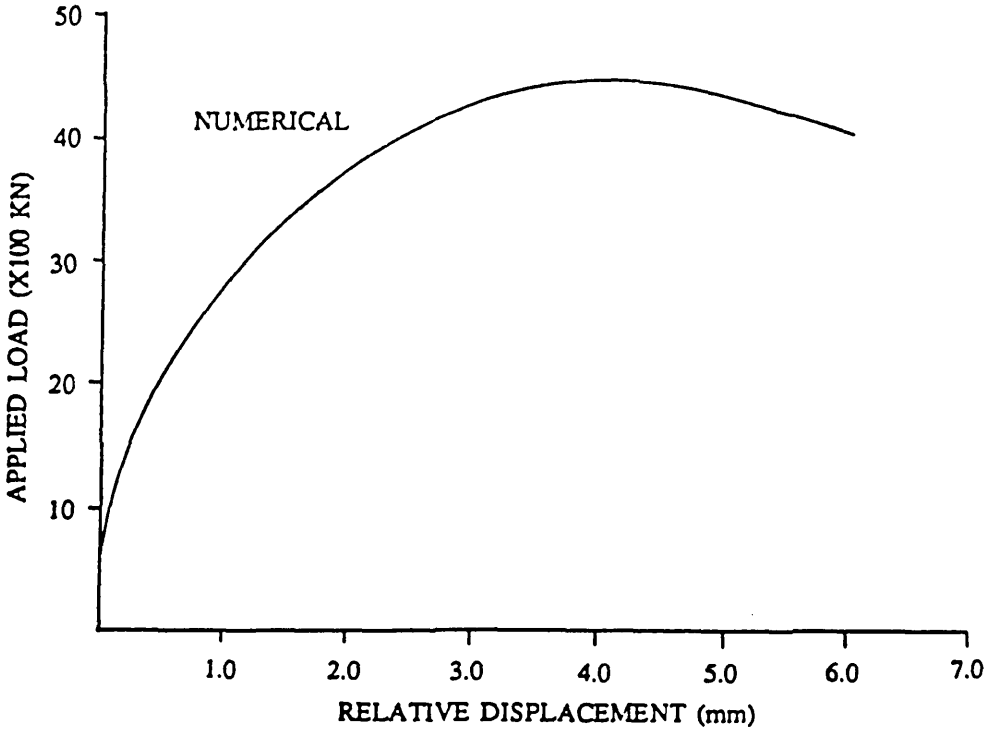
MODEL P1

FIG 4.17

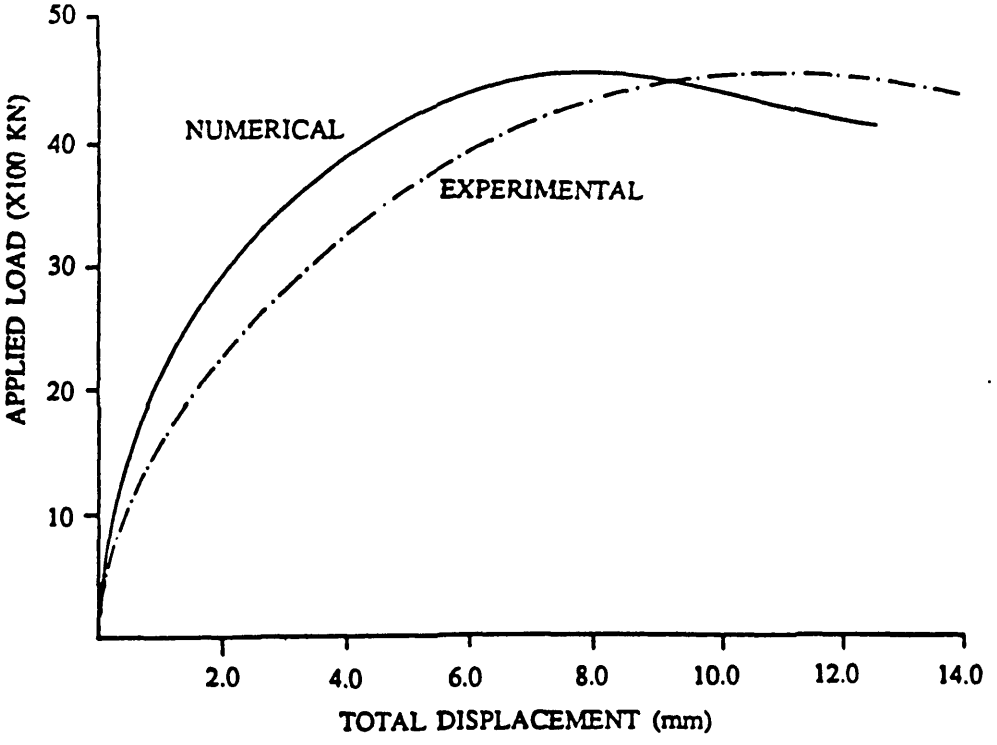


DEFORMED SHAPE AT ULTIMATE LOAD-MODEL P1

FIG 4.18

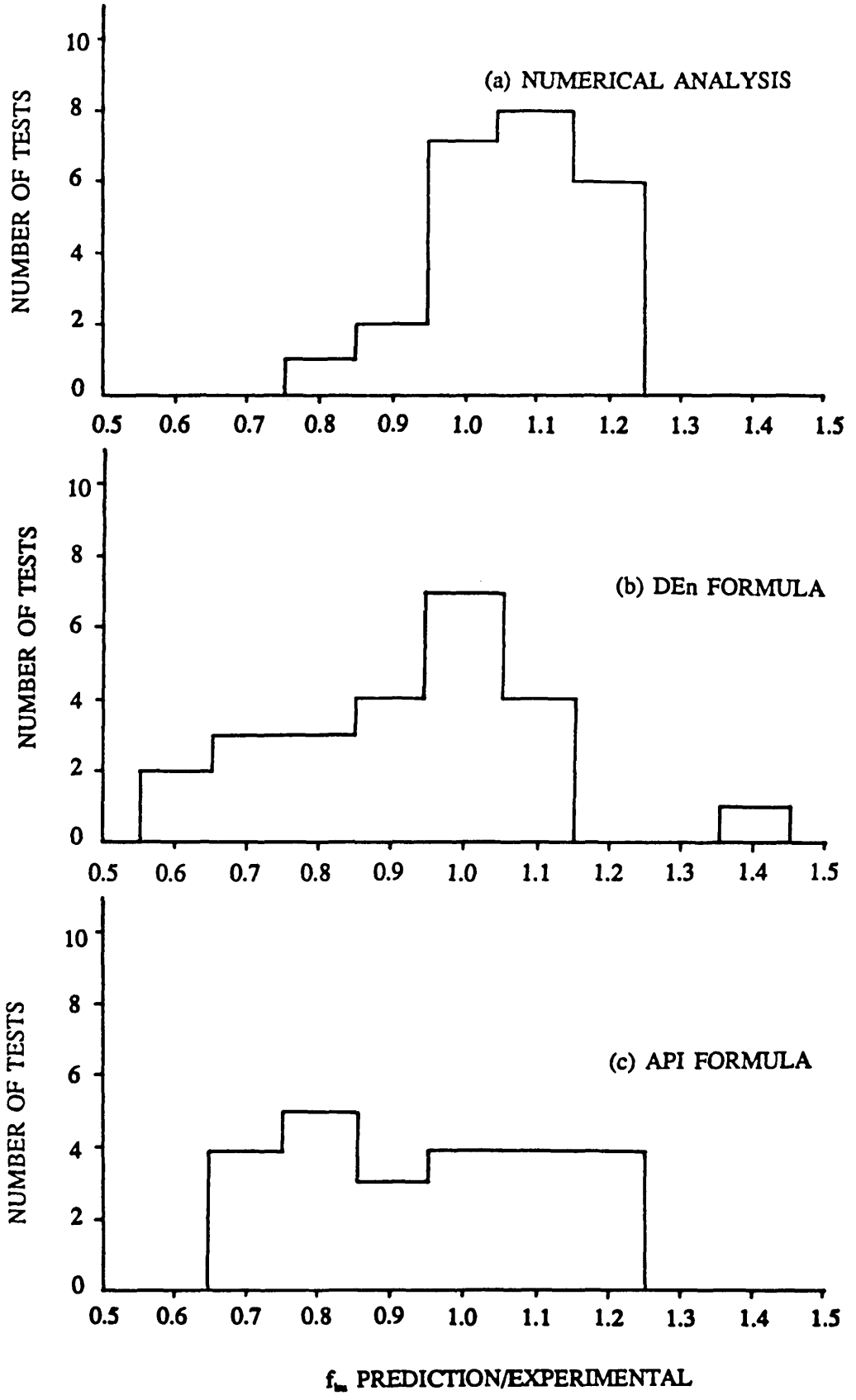


(a) LOAD-RELATIVE DISPLACEMENT-MODEL P1



(b) LOAD-TOTAL DISPLACEMENT -MODEL P1

FIG 4.19



BOND STRENGTH PREDICTION AND EXPERIMENTAL RESULTS

FIG 4.20

CHAPTER FIVE
ANALYTICAL APPROACH AND DESIGN FORMULA

5.1 Simplified Analytical Approach

5.1.1 Simplified Model

In addition to the finite element approach presented in the previous chapter, the strength of the connection is also studied analytically. Simplified analytical treatments may prove useful in assessing the ultimate capacity only. A simple analytical model of the connection as shown in figure (5.1) is examined, where the connection has three weld-beads. The thickness of the tubular is t, and the weld-bead spacing is S_p. Springs K_1, K_2 and K_3 represent the stiffness of the bottom, middle and top weld-bead, respectively. If the elongation of the pile is Δl_i and the displacement of the weld-bead is δ_0, then δ_i, which is the total movement of the weld-bead, is $\delta_0 + \Delta l_i$.

5.1.2 Weld-bead Component

From figure (5.1), the elongation of the tubular can be found using the elastic stress-strain relationship.

$$\varepsilon = \sigma / E_s \tag{5.1}$$

or,

$$\frac{\Delta l_i}{S_p} = \frac{F_i}{E_s \; t}$$

$$\Delta l_i = \frac{F_i}{E_s \; t} S_p \tag{5.2}$$

where F is the force at the weld-bead per unit circumference, and can be defined as

$$F_i = \sigma_i \; h \tag{5.3}$$

where σ_i is the bearing stress on the weld-bead and h is the weld-bead height. σ_i can be calculated from the expression,

$$\sigma_i = K_i \, \delta_i \tag{5.4}$$

where K_i is the secant modulus of the corresponding stress-relative displacement relationship. Substituting these values into equation (5.1),

$$\Delta l_i = h \, (K_i \, \delta_i) \, S_p \, / \, (E_s \, t) \tag{5.5}$$

Referring to figure (5.1), in general form, the above equation can be written as :

$$\Delta l_j = \frac{h \, Sp}{E_s \, t} \sum_{i=1}^{j} K_i \delta_i \tag{5.6}$$

The total displacement is the summation of the displacement δ_0 and the elongation Δl; i.e

$$\delta_j = \delta_0 + \sum_{i=1}^{j} \Delta l_i \tag{5.7}$$

If,

$$E_s' = \frac{E_s \, t}{S_p \, h} \tag{5.8}$$

equation (5.5) becomes,

$$\Delta l_j = \frac{1}{E_s'} \sum_{i=1}^{j} K_i \, \delta_i \tag{5.9}$$

by substituting equation (5.9) into equation (5.7) the following is obtained :

$$\delta_j = \delta_0 + \frac{1}{E_s'} \sum_{i=1}^{j} (K_i \delta_i)(j+1-i) \tag{5.10}$$

equation (5.10) can be re-arranged as;

$$\delta_j = \delta_0 + \frac{1}{E_s'} \sum_{i=1}^{j-1} (K_i\delta_i)(j+1-i) + \frac{1}{E_s'} K_j\delta_j$$

or,

$$\delta_j = \frac{E_s' \delta_0 + \sum_{i=1}^{j-i} K_i\delta_i (j+1-i)}{(E_s' - K_j)} \qquad (5.11)$$

K_i is the secant stiffness of the weld-bead, defined as,

$$K_i = f_b/\delta_i \qquad (5.12)$$

where

f_b : bearing stress at the weld-bead

$= C_K C_h C_g f(\delta_a)$,

as defined by equation (4.13) in chapter 4.

Equation (5.11) yields 'j' simultaneous non-linear equations.

5.1.3 Friction Component

By referring to figure (5.1.b), the elongation due to friction is,

$$\Delta l_f = \int_0^{s_p} \frac{\tau\, y}{E_s\, t}\, dy \qquad (5.13.a)$$

or,

$$\Delta l_f = \frac{\tau}{E_s\, t}\, 0.5\, S_p^2 \qquad (5.13.b)$$

where,

Δl_f : elongation due to friction

τ : friction

If j is the sequential number of the weld-bead, counted from the top, then the elongation due to the friction (assuming the friction is constant along the length) for each weld-bead becomes,

$$\Delta l_{fj} = \frac{0.5\, \tau}{E_s\, t} (j\, S_p)^2 \qquad (5.14)$$

By adding equations (5.14) and equation (5.11), the total displacement due to the bearing and friction stress is,

$$\delta_j = \frac{E_s'\, \delta_0 + \sum_{i=1}^{j-1} K_i \delta_i (j+1-i) + \dfrac{0.5\, \tau}{E_s\, t} (j\, S_p)^2 (E_s' - K_j)}{(E_s' - K_j)} \qquad (5.15)$$

5.1.4 Correction due to Hoop Strain

To study the effect of hoop strain, the following properties of weld-beaded connections have to be considered.

- The variation of the axial stress along the length of the connection.
- The variation of radial stress along the length.
- Bending moment due to the eccentricity of the bearing stress at weld-beads.

From the experimental investigation it was observed that the hoop strain was related to the bearing stress, as explained below.

- The bearing stress at the weld-bead is significantly affected by the

confinement stress produced by the steel tubular.

- The higher the confining stress, the higher the bearing stress that can be sustained at the weld-bead.
- Since the confining stress is directly related to the hoop strain, it is then considered that the hoop strain is also directly related to the bearing stress.

From the calibration of the strain gauge results from the experiment, an empirical relationship was derived to represent the inter-dependence between the hoop strain and the bearing stress (equation (4.16)). Taking the biaxial stress-strain condition into account, the elongation of the pile becomes,

$$\Delta l' = \frac{(\varepsilon_a + \mu\, \varepsilon_h)}{(1-\mu^2)} S_p \tag{5.16}$$

or,

$$\Delta l' = \frac{\Delta l}{(1-\mu^2)} + \frac{\mu\, \varepsilon_h\, S_p}{(1-\mu^2)} \tag{5.17}$$

where,

$\Delta l'$: elongation of the pile after taking into account the bi-axial state.

ε_h : hoop strain

ε_a : axial strain

Equation (5.17) shows the relationship between the uniaxial and biaxial pile elongation. This relationship can be used to transform equation (5.15) into its biaxial form, resulting in,

$$\delta_j = \frac{\delta_0}{(E_s'-K_j)/E_s'} + \frac{\frac{1}{E_s'}\sum_{i=1}^{j-1} K_i\delta_i(j+1-i) + \frac{0.5\,\tau}{E_s' E_s\, t}(j\, S_p)^2(E_s'-K_j)}{(E_s'-K_j)\,(1-\mu^2)\,/\,E_s'} + \frac{\mu\, \varepsilon_h\, S_p}{(1-\mu^2)} \tag{5.18}$$

or,

$$\delta_j = \frac{E_s' \delta_0(1-\mu^2) + \sum_{i=1}^{j-i} K_i\delta_i(j+1-i) + [(0.5\ \tau\ j^2S_p^2)/(E_s t) + (\mu\varepsilon_h S_p)][E_s' - K_j]}{(E_s' - K_j)\ (1-\mu^2)} \tag{5.19}$$

Since $E_s' = \dfrac{E_s\ t}{S_p\ h}$

Equation (5.19), becomes;

for $j > 1$:

$$\delta_j = \frac{E_s' \delta_0(1-\mu^2) + \sum_{i=1}^{j-1} K_i\delta_i(j+1-i) + [(\tau j^2 S_p)/(2E_s' h) + (\mu\varepsilon_h S_p)](E_s' - K_j)}{(E_s' - K_j)(1-\mu^2)} \tag{5.20}$$

and, for $j = 1$,

$$\delta_j = \frac{E_s' \delta_0(1-\mu^2) + [(\tau\ S_p)/(2E_s\ h) + (\mu\ \varepsilon_h\ S_p)]\ (E_s' - K_j)}{(E_s' - K_j)(1-\mu^2)} \tag{5.21}$$

Equation (5.20) gives the displacement at any weld-bead position δ_j, taking into account the elongation of the tubular as well as the biaxial effect due to hoop strain. Once the displacements have been obtained, the stresses at any weld-bead (j) follow, as the product of the displacement and corresponding secant stiffness K_j.

5.1.5 Friction Strength

The only term which has not been examined so far is the friction strength τ_u. As discussed previously, this is affected by;

- Surface roughness
- Grout strength
- Radial stiffness

The surface roughness is difficult to express in a general format, because the roughness of the pile surface could vary from one pile to another and also along the length of the pile itself. Therefore, due to lack of data, for the present analysis the surface condition factor given by the DEn guidance is adopted.

According to the DEn formula (57) and test results by Wimpey Laboratories (56), the grout strength affects the bond strength of the connections. In the API guidance (68), the friction strength is regarded as independent of the grout strength as long as the latter is within the range 17.25 N/mm^2 to 110 N/mm^2. From the test results carried by Wimpey for the DEn (56), it is observed that for f_{cu} within the range of 30 to 70 N/mm^2, the variation of the bond strength is negligible. The bond strength increases with the grout strength only if the latter is very low. This is justified by the observation that for high grout strength (with the consequential increase in shear capacity), the interface shear resistance becomes the critical factor in the behaviour of the connection. This stage is likely to occur for f_{cu} of about 35 N/mm^2 as can be seen in figure (2.14) and (2.15). The only parameter which affects the friction strength above that value is the radial stiffness and the surface condition of the steel tubulars.

In weld-beaded connections the mechanism of friction is different to plain connections. The lateral pressure beneath the weld-bead may be quite high, and may significantly increase the friction strength in its vicinity. Behind the weld-bead, however, voids are formed due to relative displacement, hence the area behind the weld-bead has no friction strength. Moreover, since weld-bead connections carry higher loads than friction-only connections, the axial stress in the pile and sleeve become much higher, such that the effect of dilation due to Poisson's ratio becomes more apparent. It is believed that as a whole, there is no significant effect of grout strength on the friction strength. However, it should be noted that if the grout

strength is very low, there is a possibility that the bearing stress can exceed the shear strength of the grout. In this case, neither grout crushing nor diagonal cracks will occur. Instead, shear failure occurs, extending from one face of a weld-bead to another.

Based on the above arguments, and after studying all the available data, it was decided to use the following formulae for friction.

a. For plain connections :

$\tau_u = 9 \sqrt{K} (f_{cu}/35)^{0.25}$ for $f_{cu} \leqslant 35$ N/mm^2 (5.22.a)

or,

$\tau_u = 9 \sqrt{K}$ for $f_{cu} > 35$ N/mm^2 (5.22.b)

b. For weld-beaded connections :

$\tau_u = 9 \sqrt{K}$ for any value of f_{cu} (5.23)

These equations are used to calculate the friction contribution in equation (5.20). The total strength of the connection can therefore be calculated from the following equation.

$$P_{max} = 2\pi R \left(\sum_{i=1}^{n} K_j \delta_j + \tau_u L \right) \quad (5.24)$$

where,

L : the total length of the connection

n : total number of weld-beads

δ_j : relative displacement according to equation (5.20)

The average bond strength of the connection is,

$$\tau_{bu} = \frac{1}{L} \sum_{j=1}^{n} K_j \delta_j + \tau_u \quad (5.25)$$

The flow-chart of the program for solving the above equations is illustrated in figure (5.2).

5.1.6 Comparison of Results

This simplified analytical approach has been used to calculate the strength of weld-bead connection models tested for the DEn (56), and the results show good agreement, as shown in table (5.1) below.

Furthermore, the analysis was applied to long specimens. The use of such an analytical approach in long specimens is beneficial since realistic tests are extremely difficult to conduct. The results are presented in table 5.2.

Table 5.1
Comparison of results

Ref.	f_{bu} Analytical (N/mm^2)	f_{bu} Experimental (N/mm^2)	Anal/Expt
P1	2.664	2.790	0.995
P3	2.237	2.283	0.980
R1	1.585	1.722	0.920
R3	2.546	2.494	1.021

(the program and the example are shown in the appendix)

Table 5.2
C_L from simplified analysis

L/D	C_L (Analysis)	C_L (DEn)
1	0.818	-
2	1.000	1.000
4	1.010	0.900
8	0.905	0.800
12	0.886	0.700

(note : The geometry is taken as model P1)

5.1.7 Discussion

A simplified analytical approach has been shown to give very good agreement with the test results. It is based on the observation that because of the difference in the displacements, the bearing stress on the weld-beads is not uniformly distibuted in the axial direction. The weld-beads closer to the loaded end, for a given load, have a higher bearing stress compared with the weld-beads at the opposite end. For a short connection, the difference in bearing stress from one weld-bead to another will not be significant, but as the specimen becomes longer the difference becomes more pronounced.

The effect of radial stress has also been taken into account. This causes the pile to displace inwards, so that its diameter decreases: i.e, the hoop strain in the pile is negative. Due to Poisson's ratio effect, this hoop strain causes an increase in the elongation.

The stiffness of the weld-bead was determined from the previous calibration results. The bearing stress at any weld-bead is taken as its total displacement multiplied by its stiffness. The summation of the bearing stress at ultimate load is the total bearing capacity of the connection. By adding this to the friction strength of the interface, the total strength of the connection is obtained.

The results from this approach agree well with the test results. The approach can be easily used to analyse long specimens without having the difficulty of using very low grout strengths as in experimental testing. However, it should be noted that because this approach does not account for the reduction of bond strength due to dilation between the steel-grout interface, the result for predicting the strength of long connection could be higher than finite element analysis.

5.2 Derivation of Design Equation

5.2.1 Basic Assumptions

In deriving a design formula, three requirements have to be considered. Firstly, the formula has to be consistent with the degree of accuracy used practically. Secondly, it has to be in a simple form for use by practicing engineers. The third consideration is that parameters used have a physical interpretation, as to avoid the use of unrealistic values. These three factors are usually difficult to achieve simultaneously. The following observations of the behaviour of weld-beaded connections are used as the basic assumptions in deriving the required design formula.

- Failure of the connections in most cases is associated with hoop yielding of the steel tubular. However, for very thin sleeves, the failure could be due to axial yielding of the sleeve.

- The bearing strength of a weld-bead is governed by the triaxial strength of the grout, where the confining stress is supplied by the steel tubular.

- The bottom weld-bead of the pile often fails at an earlier stage of loading, therefore it rarely contributes to the maximum strength. If the bottom weld-bead of the pile is above that of the sleeve, only one bottom pile weld-bead will exhibit this effect. Otherwise, two bottom pile weld-beads will be affected.

5.2.2 Relation between Hoop and Radial Stress Components

At failure the steel tubular yields such that, $\sigma_{hult} = \sigma_y$. The relationship between radial stress σ_R and hoop stress σ_h can be expressed by Lame's equation (4.17). Because $p_i = 0$ (radial stress only acting on one side), the equation becomes,

$$\sigma_h = -\frac{a^2\ b^2\ p_o}{(b^2-a^2)}\ \frac{1}{R^2} - \frac{p_o\ b^2}{(b^2-a^2)} \tag{5.26}$$

since t = (b-a), then :

$$\sigma_h = \frac{\sigma_R}{(b+a)t}\ (\frac{a^2\ b^2 + b^2\ R^2}{R^2}) \tag{5.27}$$

where, $\sigma_R = p_o$

In equation (5.27), if the thickness is relatively small, the square of the radius term can be used as an approximate value both for (ab) and (bR) without significant loss of accuracy. Therefore,

$$\sigma_h = \frac{\sigma_R\ 2\ R^4}{2\ R^3\ t}$$

or,

$$\sigma_R = \sigma_h \frac{t}{R} \tag{5.28}$$

5.2.3 Grout Strength at Weld-bead

In a simple form, the confined strength of the grout beneath the weld-bead can be related to its uniaxial strength and confining stress as :

$$\sigma_b = f_{cu} + C\ \sigma_R \tag{5.29}$$

where,

σ_b : bearing strength of weld-bead
(confined strength of grout beneath the weld-bead)

f_{cu} : uniaxial strength of the grout (unconfined strength)

C : a parameter to be determined
(representing the effect of radial stress)

Substituting σ_R from equation (5.28) into equation (5.29),

$$\sigma_b = f_{cu} + C \frac{t}{R}\ \sigma_h \tag{5.30}$$

Since from experimental results the ultimate stress σ_b corresponds to σ_y, the equation becomes,

$$\sigma_b = f_{cu} + C \frac{t}{R} \sigma_y \qquad (5.31)$$

The parameter C has to be determined from the corresponding failure criterion, and is unlikely to be a constant since it depends on the value of f_{cu} and σ_R. However, it was found from numerical studies and experimental observations that in typical grouted connection problems, the parameter C can be assumed to have a constant value of four. Therefore, as an approximation, the equation can be written as :

$$\sigma_b = f_{cu} + 4 \frac{t}{R} \sigma_h \qquad (5.32)$$

The total strength of the connection is the sum of the bearing strength from equation (5.32) and the friction strength from equation (5.23) as shown below.

$$P_{total} = P_{weld\text{-}bead} + P_{friction}$$
$$= [(\sigma_b \, h \, n) + \sigma_f \, L] \, \pi \, D \qquad (5.33)$$

where,

L : total length of the connection

h : weld-bead height

n : total number of weld-beads

Subsituting the corresponding values for σ_b and σ_f,

$$P_t = [(f_{cu} + C \, \sigma_y \, t/R) \, n \, h + 9 \, L \, \sqrt{K}] \, \pi \, D \qquad (5.34)$$

5.2.4 Failure Modes

As mentioned above, the failure of the connection is associated with either of the following mechanisms :

1. Sleeve yielding in axial direction :

If the sleeve (or the pile) is very thin, the axial stress in the sleeve could exceed its yield strength.

$$P_t = \pi D_s t_s \sigma_y \quad (5.35)$$

and,

$$f_{bu} = (\pi D_s t_s \sigma_y) / (\pi D_p L)$$

$$= (\sigma_y t_s D_s) / (D_p L) \quad (5.36)$$

Axial yielding of the pile will not normally occur because the pile is usually significantly thicker than the sleeve. It should be noted here that because of the grout annulus there is no possibility of sleeve buckling taking place before yielding. This has been shown in the tests (72).

2. Sleeve yielding in hoop direction :

In equation (5.34) the parameters t and R correspond to either the t and R of the sleeve or the pile. The P_t should be chosen as the least value of the total strength of the pile-grout or the sleeve-grout interface. Therefore, P_t should be taken as the least of the following values.

$$P_t = [(f_{cu} + C \sigma_y t_p/R_p) n h + 9 L \sqrt{K}] \pi D_p \quad (5.37.a)$$

or,

$$P_t = [(f_{cu} + C \sigma_y t_s/R_s) n h + 9 L \sqrt{K}] \pi D_s \quad (5.37.b)$$

3. Shear failure of the grout :

If the grout strength is very low (eg. in the early stages of curing) or for very small weld-bead spacing, there is a possibility that the bond strength could exceed the shear strength of the grout. Therefore the connection capacity is determined by the shear strength of the grout τ_{cu}, hence,

$$P_t = \tau_{cu} L \pi D_p \quad (5.38)$$

A recent test for the DEn (69) on specimens with closely spaced weld-beads indicated that shear failure in the grout may be a problem in such cases.

5.2.5 Effect of Bottom Weld-bead

Since the bottom weld-bead of the pile always fails first so that it rarely contributes to the strength of the connection, the number of effective weld-beads should be reduced by one or two (depending on the weld-bead arrangement), for use in equation (5.37).

5.2.6 Effect of Weld-bead Height

Bending moments at mid-thickness due to bearing stresses at weld-beads can be estimated as,

$$M = 1/2\ (t + h)\ h\ \sigma_b \tag{5.39}$$

where,

M : bending moment perunit circumference

This moment causes additional axial stress in the tubular, given by :

$$\Delta\sigma_a = \frac{M}{1/6\ t^2}$$

$$= \frac{3\ h\ (t + h)}{t^2}\ \sigma_b \tag{5.40}$$

Due to Poisson's ratio effect, this axial stress increases the existing hoop stress, so that the confined strength of the tubular is reduced. Therefore, the σ_y in equation (5.31) should be corrected by $\mu\ \sigma_a$. Hence equation (5.31) becomes,

$$\sigma_b = f_{cu} + C\ \frac{t}{R}\ (\sigma_y - \mu\ \sigma_a) \tag{5.41}$$

where,

μ : Poisson's ratio

substituting the value of $\Delta\sigma_a$,

$$\sigma_b = f_{cu} + C \frac{t}{R} [\sigma_y - \mu \frac{3(t+h)}{t^2} h \sigma_b]$$

Re-arranging the equation,

$$\sigma_b = \frac{f_{cu} + C (t/R) \sigma_y}{[\ 1 + C \mu (3 h t + h^2)/(t R)\ ]} \tag{5.42}$$

From equation (5.42) it is observed that the numerator is the initial value of σ_b as in equation (5.31) before taking the bending effect into account. Therefore, the denominator represents the effect of bending moment.

$$C_h = \frac{1}{[\ 1 + C \mu (3 h t + h^2)/(t R)\ ]}$$

$$C_h = \frac{t R}{t R + C \mu h (3 t + h)} \tag{5.43}$$

where,

C_h : parameter of weld-bead height effect.

This value of C_h should be used to correct the value of P_t obtained from equations (5.37.a) and (5.37.b) above. The parameters t and R in equation (5.43.a) should be taken as t_p and R_p respectively, and as t_s and R_s for correcting equations (5.37.a) and (5.37.b).

If the parameter C is assumed to be a constant of value 4 as in (5.32), equation (5.43) becomes,

$$C_h = \frac{t R}{t R + 4 \mu h (3 t + h)} \tag{5.44}$$

5.2.7 Effect of Length to Diameter Ratio

The effect of the length to diameter ratio C_L (as defined by DEn), cannot be easily formulated in a simplified form since it involves almost all of the important parameters. The use of a simplified analytical approach as presented above has shown this inter-dependence of the parameters. Different geometric or material properties of the models will give different values of C_L for each corresponding length to diameter ratio.

As a study case, a test model P1 from reference (56) was used as a basic geometry for L/D=2. The length of the connection was then varied to obtain models with L/D_p of 1, 4, 8, and 12. The analysis was performed using the finite element and simplified analytical approach as derived before, by assuming that no axial sleeve or pile yielding will occur prior to grout failure. The results of this analysis are presented in the following table.

Table 5.3
Comparison of C_L from finite element and simplified analysis
(assuming no 'bottom weld-bead effect')

L/D_p	Finite Element	Simplified Approach
1	1.050	1.020
2	1.000	1.000
4	0.902	0.927
8	0.675	0.793
12	0.567	0.720

The above values were calculated based on the assumption that due to the loading arrangement, the bottom weld-bead does not fail. If the bottom weld-bead is assumed ineffective, the results presented in table (5.3) above are changed, as given in table (5.4).

Table 5.4

Comparison of C_L from finite element and simplified approach (assuming the bottom weld-bead is in-effective)

L/D_p	Finite Element	Simplified Approach
1	0.850	0.818
2	1.000	1.000
4	1.050	1.016
8	0.831	0.905
12	0.720	0.885

The difference in C_L values from table (5.3) and (5.4) is attributed to the relative importance of the bottom weld-bead in short connections. This causes a significant reduction in the average bond strength for models with small L/D_p, but the effect is much less as the L/D_p increases. As a result, the C_L which is defined as a normalized value for the strength of $L/D_p = 2$, becomes higher. In most cases, the earlier failure of the bottom weld-bead is very likely to exist. Therefore, the C_L factors from table (5.4) are more realistic.

The comparison between all available experimental and analytical results is presented in table (5.5) below.

Table 5.5

Comparison of C_L from various tests and analytical results

L/D_p	Bill&Lewis	Wimpey	Series O	Finite El.	Analytical	Chilvers	DEn
1	0.816	0.732	0.754	0.850	0.818	1.200	--
2	1.000	1.000	1.000	1.000	1.000	1.000	1.000
4	0.877	1.193	1.088	1.050	1.016	0.920	0.900
8	0.947	0.974	1.035	0.831	0.905	--	0.800
12	0.840	--	0.947	0.720	0.885	--	0.700

(It should be noted that the C_L values from test Series O above cannot be used for comparison since they are based on plain connection tests.)

Based on the above table, it is concluded that the present C_L factors from DEn guidance notes are reasonable for the range of geometries studied herein (model P1). Some remarks can be given as follows:

- For connections with $L/D_p = 1$, C_L can be assumed as equal to 0.8.
- For long connections with $L/D_p = 4$ and more, the C_L parameter can be adequately taken according to the DEn as long as the earlier failure of the bottom weld-bead exists. However, if there is no ealier failure of the bottom weld-bead, the C_L factors for specimens with $L/D_p = 8$ and 12 should be taken as;

  $C_L = 0.675$ for $L/D_p = 8$, and

  $C_L = 0.567$ for $L/D_p = 12$.

These values of C_L are valid provided there is no axial yielding in either the sleeve or the pile, and also that the grout strength is reasonably high so that no shear failure occurs.

5.2.8 Summary

5.2.8.1 Weld-beaded Connections

After including the most important parameters, the final form of the equation for calculating the total strength of the connection will be the lowest value from the following equations.

$$P_t = [\ (f_{cu} + C\ \sigma_y\ t_s / R_s)\ n\ h\ C_{hs} + 9\ L\ \sqrt{K}\ ]\ \pi\ D_g\ C_L \qquad (5.45)$$

where,

$$C_{hs} = \frac{t_s\ R_s}{t_s\ R_s + C\ \mu\ h\ (3\ t_s + h)}$$

or,

$$P_t = [\ (f_{cu} + C\ \sigma_y\ t_p / R_p)\ n'\ h\ C_{hp} + 9\ L\ \sqrt{K}\ ]\ \pi\ D_p\ C_L \qquad (5.46)$$

where,

$$C_{hp} = \frac{t_p\ R_p}{t_p\ R_p + C\ \mu\ h\ (3\ t_p + h)}$$

The average bond strength f_{bu}, which is defined as the total load capacity P_t divided by the outer surface of the pile, becomes,

$$f_{bu} = P_t / (2\pi\ D_p\ L) \qquad (5.47)$$

To simplify the calculation, the value of C has been calculated according to the triaxial failure theory, and the value of ($f_{cu} + C\ \sigma_y\ t/R$) which is the confined strength of the grout, are presented in figures (5.3) , so that part of the equation can be replaced by,

$$f_{cc} = (f_{cu} + C\ \sigma_y\ t/R) \qquad (5.48).$$

Hence the final form of the total strength equations becomes,

$$P_t = [\ f_{cc}\ n\ h\ C_{hs} + 9\ L\ \sqrt{K}\ ]\ \pi\ D_g\ C_L \qquad (5.49.a)$$

or,

$$P_t = [\ f_{cc}\ n'\ h\ C_{hp} + 9\ L\ \sqrt{K}\ ]\ \pi\ D_p\ C_L \qquad (5.49.b)$$

with the following limitations :

a. $P_t < \sigma_y\ A_s$ (no earlier failure due to axial yielding of the sleeve or pile)
where A_s is the cross section area of the pile or sleeve.

b. $f_{bu} < \tau_{cu}$ (no earlier failure due to shear)

The above design equations were used to calculate the strength of some connection models tested elsewhere (56, 71 and 75), and the results are presented in table (5.7) and figure (5.4.a). A comparison with the results from other design equations are also given in figure (5.4.b) and (5.4.c).

5.2.8.2 Plain Connections

The friction strength of plain connection has already been given as in equation (5.22). Therefore the total strength of the connection is,

$$P = [\ 9\ \sqrt{K}\ (f_{cu}/35)^{0.25}\ ]\ \pi\ D_p\ L \qquad \text{for } f_{cu} < 35\ N/mm^2 \qquad (5.50.a)$$

and,

$$P = [\ 9\ \sqrt{K}\ ]\ \pi\ D_p\ L \qquad \text{for } f_{cu} > 35\ N/mm^2 \qquad (5.50.b)$$

The comparison of the above formula with the DEn approach is presented in figures (5.5.a) and (5.5.b).

In comparing the effects of other parameters it is necessary to eliminate the effect of f_{cu}. However, this is not possible since the grout strength f_{cu} always

varies from one specimen to another. To overcome this problem, the DEn introduced a 'bond strength parameter' as in equation (2.44). The bond strength parameter is used to normalise the bond strength f_{bu} from test results. It has been found that this formula only gives very good agreement for grout strength of about 50 N/mm^2. The use of bond strength parameter becomes very important since any discrepancies in transferring the bond strength into the bond strength parameter will cause inaccuracy in the test results. Based on the above proposed equation, it is believed that the bond strength parameter is better expressed as :

$$F_{bu} = f_{bu}\ (35/f_{cu})^{0.25} \qquad \text{for } f_{cu} < 35 \text{ N/mm}^2 \qquad (5.51)$$

and there is no need for a bond strength parameter for f_{cu} greater than 35 N/mm^2 since above that value the increase in grout strength does not have a noticeable effect on the bond strength. Figure (5.6) shows the comparison of bond strength parameters using equation (2.44) and (5.51).

5.2.9 Discussion

The overall comparison of the bond strength prediction using the proposed equations and the existing design formulae are given in figures (5.5.a) to (5.5.c). The results are presented in terms of f_{bu} prediction divided by the corresponding experimental values, and the number of occurrences in certain intervals. The figures show that the proposed equation is slightly better than the DEn formula, and far better than that proposed by the API. The proposed formula reduces the scatter in f_{bu} from 0.7 to 1.4 in the DEn prediction to 0.8 to 1.3, whilst the API formula exhibits more scatter, i.e between 0.4 and 1.6. More models for comparison are not available, since some of the published results do not provide sufficient information on the geometry of the specimens.

In comparing the radial stiffness effects, the present author considered more specific factors, i.e the effect of varying the pile thickness and the sleeve thickness. It is clear from figures (5.7) and (5.8) that the effect of these variations could be different. In figure (5.7) it is observed that the increase in the pile thickness t_p from 15.88 mm to 25.4 mm did not result in any difference in the bond strength.

On the other hand, the increase in sleeve thickness t_s had a significant effect on bond strength. Comparison between the predictions show that the proposed formula agrees better with the experimental results, except when the thickness of the sleeve t_s is very small. This could be due to sleeve yielding in the axial direction. As can be seen, for t_s = 4 mm, the increase in pile thickness from 12.5 mm to 15.88 mm and 25.4 mm did not make any difference in the bond strength.

Contrary to the conclusion of Chilvers (64), the sleeve thickness effect is noticeable. From figure (5.8) it is observed that there is a significant increase in bond strength as the sleeve thickness increases. The comparison between the design formulae in predicting the effect of sleeve thickness variation is presented in figures (5.9.a) to (5.9.c), whilst the effect of pile thickness variation is presented in figures (5.10.a) to (5.10.e) The figures show that the proposed equation gives results closer to the test results compared with both the DEn and API design equations. The effect of weld-bead height is also illustrated in figure (5.11). Although experimental results are insufficient, it is clear from the figure that the assumption of linear variation in bond strength with weld-bead height could reduce the safety margin.

Table 5.6

Prediction of Bond strength using the proposed equations

MODEL	K	f_{cu} (N/mm²)	f_{bu} Expt (N/mm²)	f_{bu} Design (N/mm²)	Design/ Expt
Series P : a. (OTP-11)					
P1	0.0146	54.21	2.789	2.673	0.958
P2	0.0146	47.59	2.933	2.570	0.876
P3	0.0106	53.42	2.283	2.314	1.013
P4	0.0106	50.37	2.213	2.262	1.022
P5	0.0093	59.61	1.862	2.274	1.221
P6	0.0093	51.27	1.700	2.146	1.262
P7	0.0131	53.08	-		
P8	0.0131	53.26	2.705	2.597	0.960
P9	0.0100	53.57	2.078	2.284	1.102
P10	0.0100	52.06	2.139	2.259	1.056
P11	0.0088	58.81	1.792	2.213	1.235
P12	0.0088	55.60	1.862	2.184	1.173
P13	0.0120	49.91	2.422	2.497	1.031
P14	0.0120	54.37	2.406	2.561	1.061
P15	0.0095	57.47	2.143	2.311	1.078
P16	0.0095	52.68	2.055	2.247	1.093
P17	0.0085	57.14	1.774	2.193	1.236
P18	0.0085	53.42	1.890	2.107	1.115
P19	0.0121	51.20	1.802	2.259	1.253
P20	0.0121	53.08	3.001	2.293	0.764

Table 5.6 (continued)
Prediction of Bond strength using the proposed equations

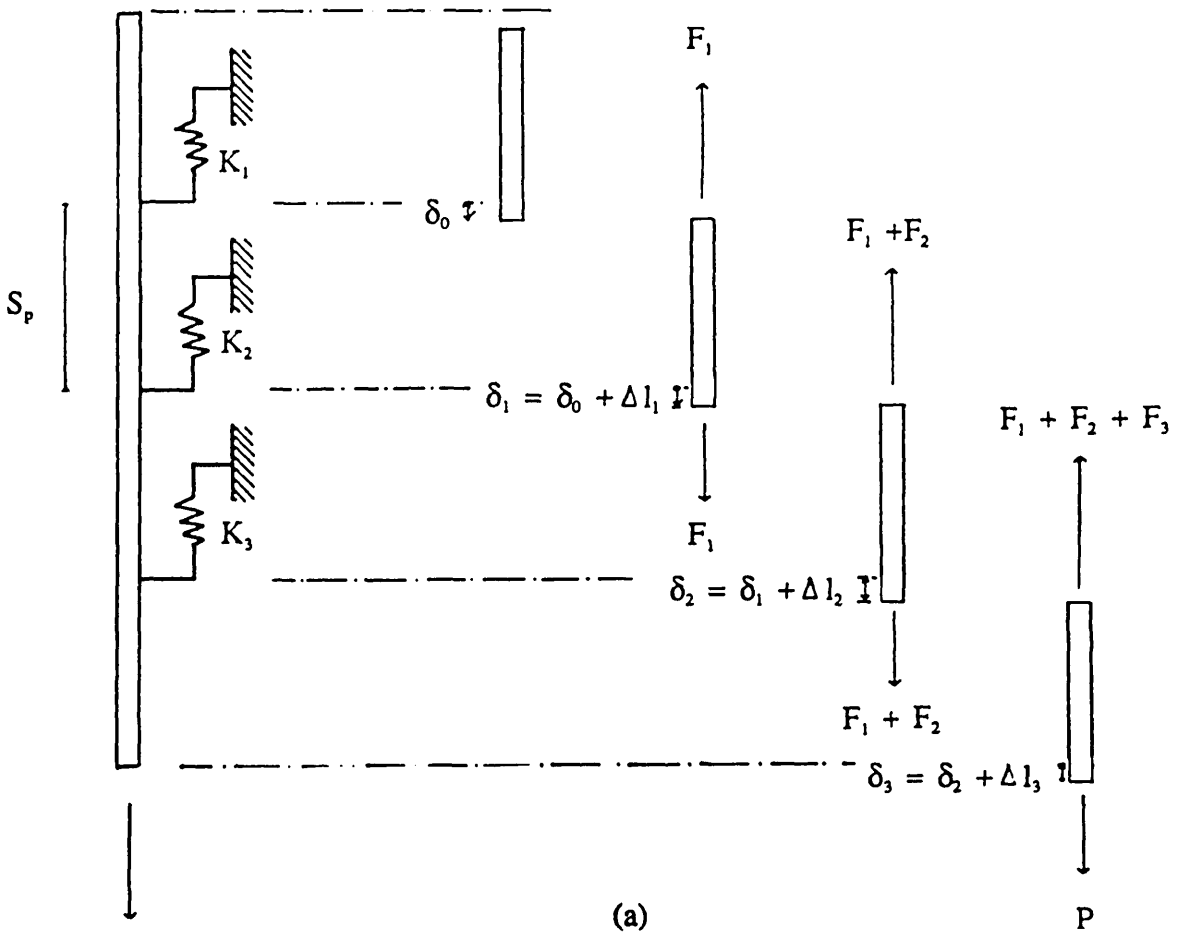
MODEL	K	f_{cu} (N/mm²)	f_{bu} Expt (N/mm²)	f_{bu} Design (N/mm²)	Design/ Expt
b. (OTH 86-210)					
P21	0.0201	21.20	2.377	2.509	1.055
P22	0.0201	18.60	2.582	2.458	0.952
P23	0.0170	20.30	2.746	2.371	0.863
P24	0.0170	23.10	2.664	2.435	0.914
P25	0.0155	31.80	2.786	2.531	0.908
P26	0.0155	18.20	2.131	2.274	1.067
P27	0.0253	22.40	2.664	2.875	1.079
P28	0.0253	19.10	2.786	2.803	1.006
P29	0.0207	20.90	2.664	2.699	1.013
P30	0.0207	23.10	3.360	2.737	0.814
P31	0.0182	20.70	2.791	2.597	0.930
P32	0.0168	26.90	2.569	2.725	1.061
SERIES R					
a. (OTP-11)					
R1	0.0105	38.15	1.732	1.557	0.904
R2	0.0105	45.89	1.862	1.616	0.868
R3	0.0105	35.56	2.494	2.534	1.016
R4	0.0105	39.35	2.599	2.610	1.004
R5	0.0095	33.94	2.213	1.976	0.893
R6	0.0095	45.89	2.354	2.057	0.874
R7	0.0125	35.79	2.494	2.300	0.922
R8	0.0125	44.53	2.512	2.440	0.971

Table 5.6 (continued)
Prediction of Bond strength using the proposed equations

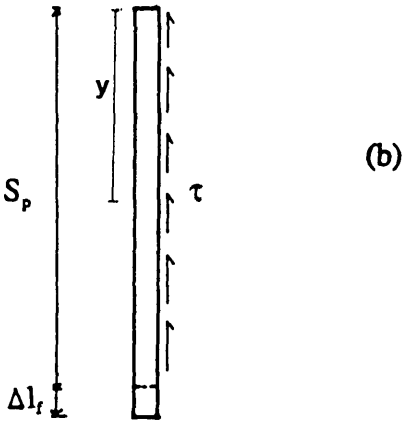
MODEL	K	f_{cu} (N/mm²)	f_{bu} Expt (N/mm²)	f_{bu} Design (N/mm²)	Design/ Expt
R9	0.0105	46.75	2.354	2.207	0.938
R10	0.0105	50.83	2.073	2.271	1.096
b. (OTH-86210)					
R11	0.0108	30.50	2.417	2.838	1.174
R12	0.0108	29.40	2.303	2.808	1.219
R13	0.0108	23.70	3.032	2.969	0.979
R14	0.0108	22.30	2.622	2.908	1.109
R15	0.0108	24.30	3.319	3.345	1.008
R16	0.0108	21.30	3.319	3.315	0.999
SERIES Q (OTP-11)					
Q1	0.0105	31.76	2.143	1.976	0.922
Q2	0.0105	36.29	2.073	2.040	0.984
Q3	0.0105	30.10	3.302	2.886	0.874
Q4	0.0105	27.61	2.916	2.784	0.955
Q5	0.0105	36.26	3.814	3.749	0.983
Q6	0.0105	33.50	3.899	3.646	0.935
SERIES UTA (Univ.Texas)					
UT1	0.0191	27.50	3.591	2.998	0.835
UT2	0.0191	27.78	3.616	2.961	0.818
UT3	0.0179	28.13	3.324	2.932	0.880
UT4	0.0200	46.40	3.514	3.652	1.040
UT5	0.0220	77.80	4.781	4.356	0.911
UT6	0.0220	74.76	4.592	4.290	0.934

Table 5.6 (continued)
Prediction of Bond strength using the proposed equations

MODEL	K	f_{cu} (N/mm²)	f_{bu} Expt (N/mm²)	f_{bu} Design (N/mm²)	Design/ Expt
SERIES W					
W1	0.0136	50.00	2.274	1.650	0.726
W2	0.0136	60.50	2.425	1.908	0.787
W3	0.0146	51.50	1.970	1.474	0.748
W4	0.0146	50.10	2.561	1.895	0.740
W5	0.0153	63.00	2.080	1.993	0.958
W6	0.0153	63.90	2.759	2.833	1.027

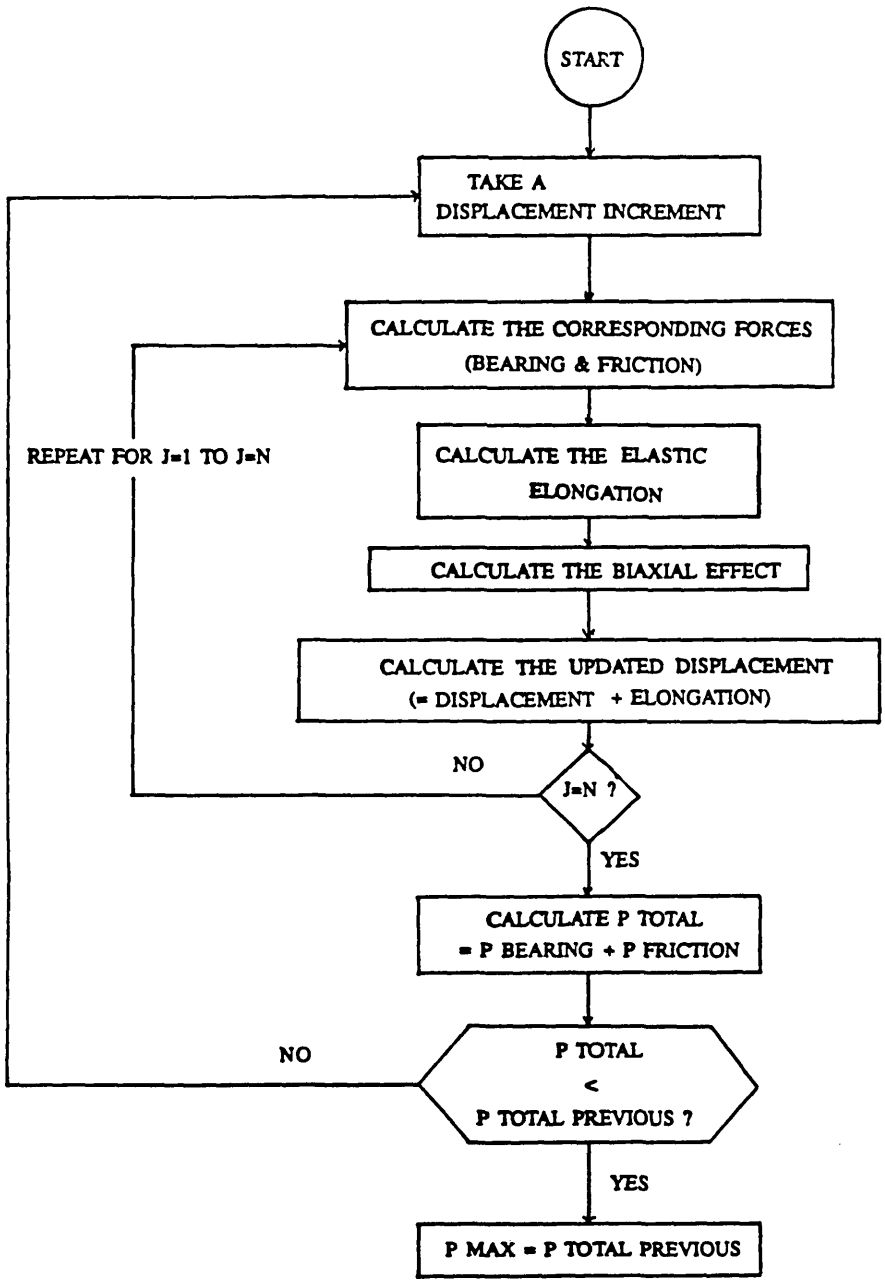


P BEARING



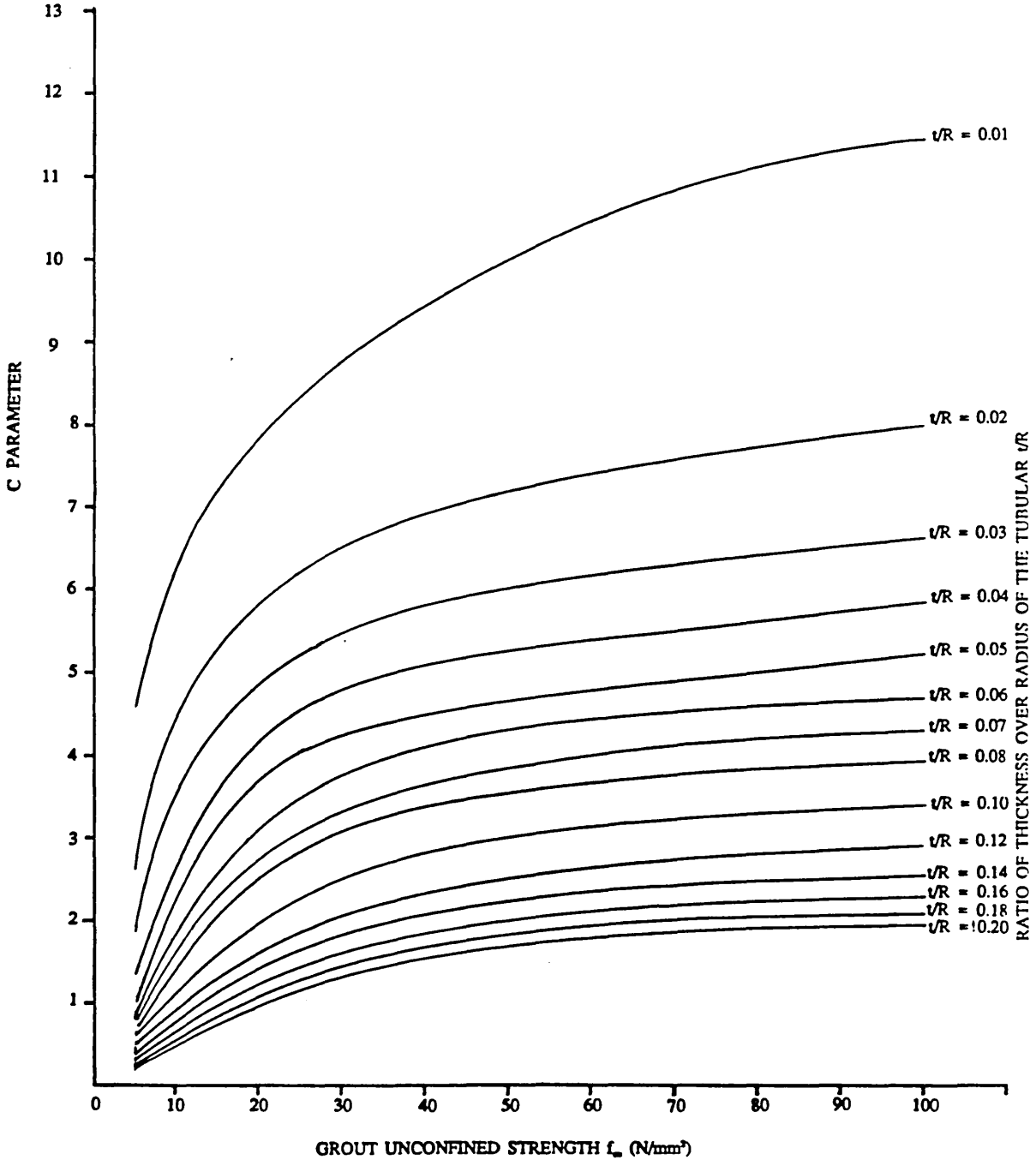
P FRICTION

ELONGATION DUE TO BEARING AND FRICTION STRESSES FIG 5.1



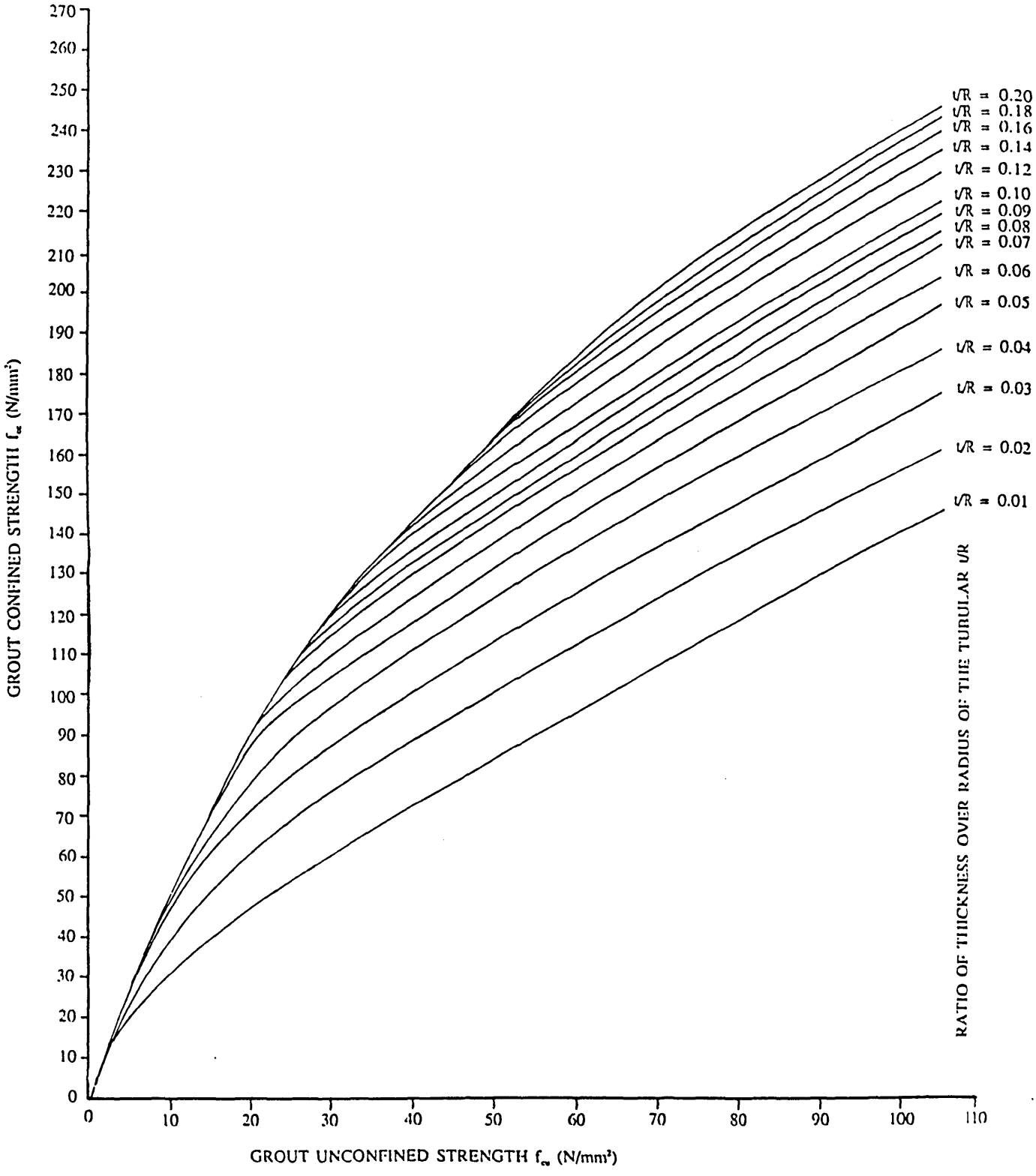
FLOW CHART OF THE SIMPLIFIED ANALYTICAL APPROACH

FIG 5.2



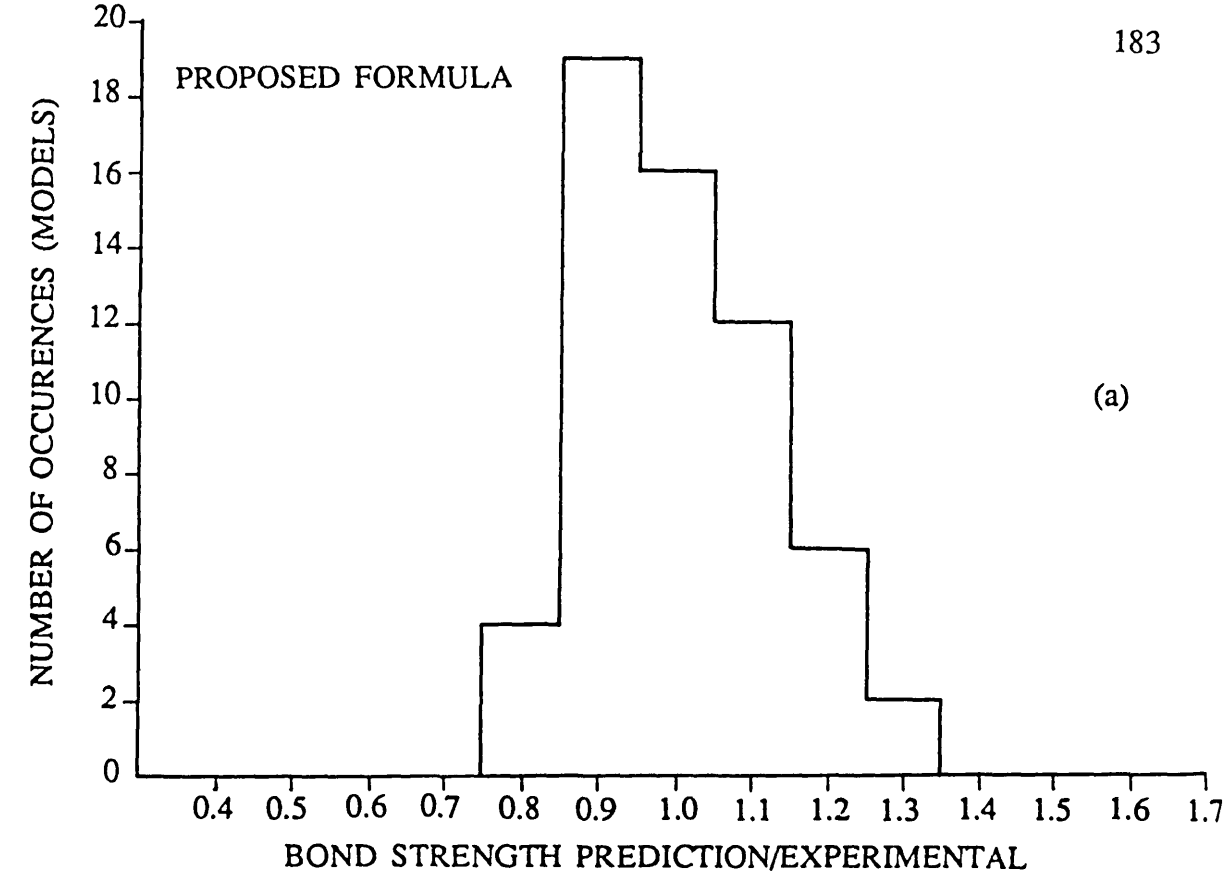
UNCONFINED STRENGTH VS C PARAMETER OF GROUT FOR DIFFERENT VALUES OF t/R

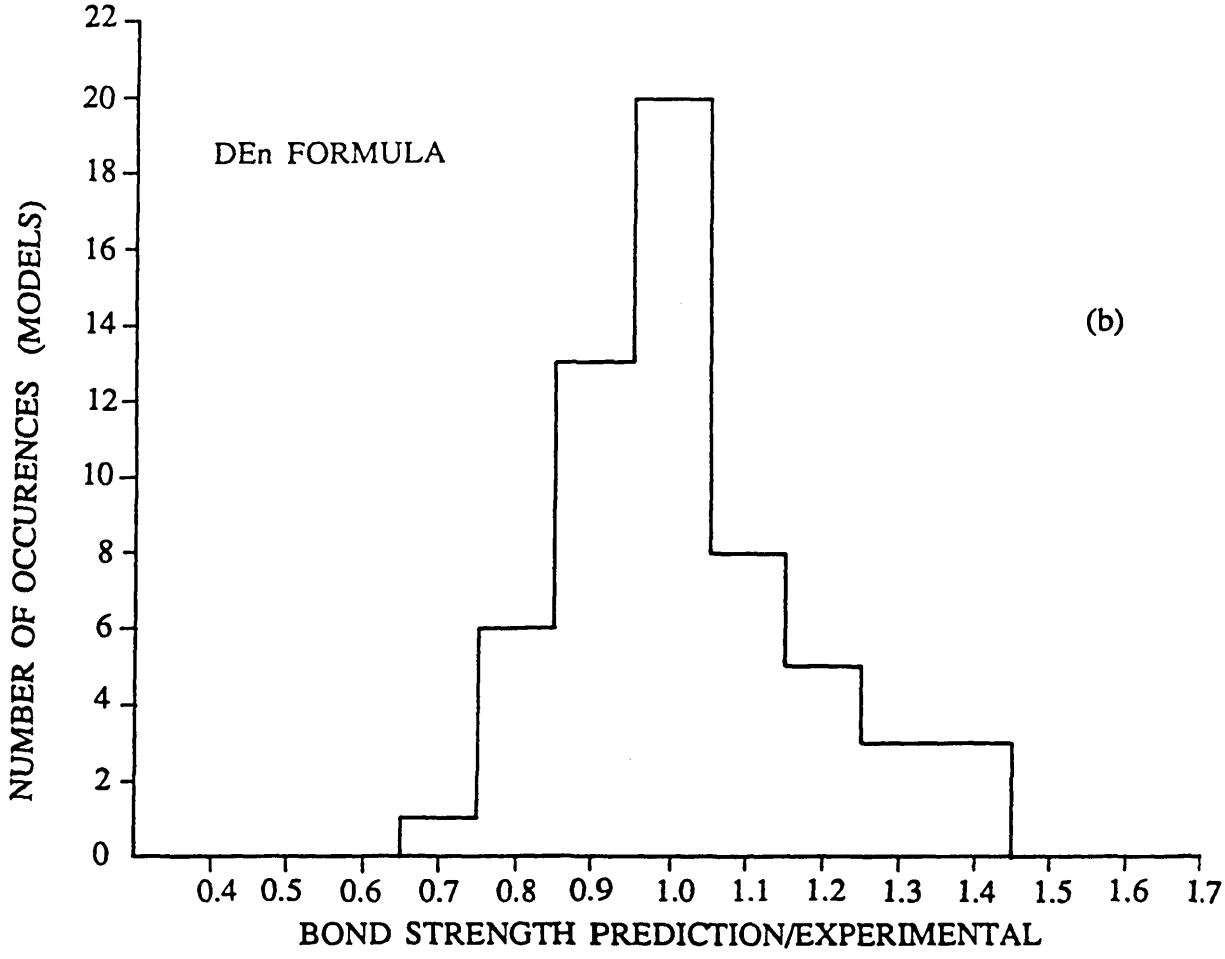
FIG 5.3 (a)



UNCONFINED STRENGTH VS CONFINED STRENGTH OF GROUT FOR DIFFERENT VALUES OF t/R

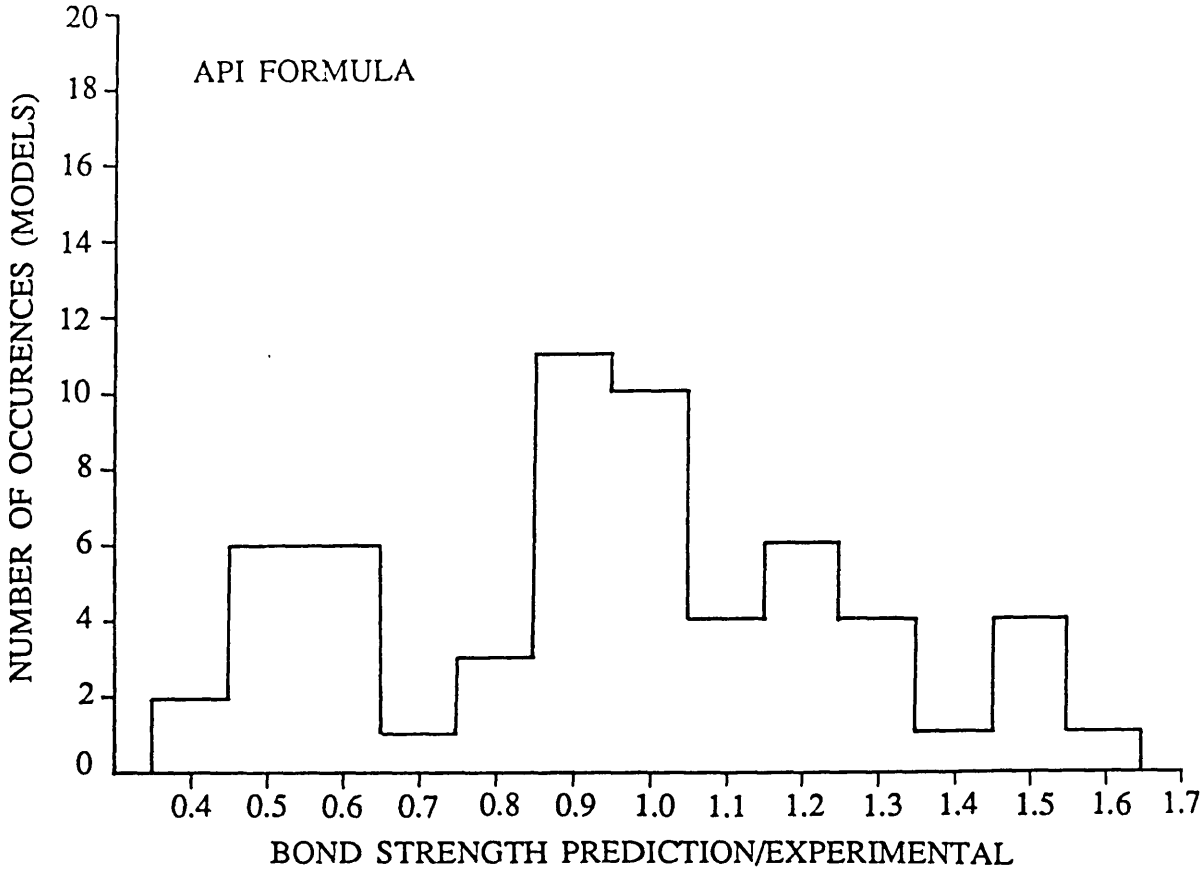
FIG 5.3(b)





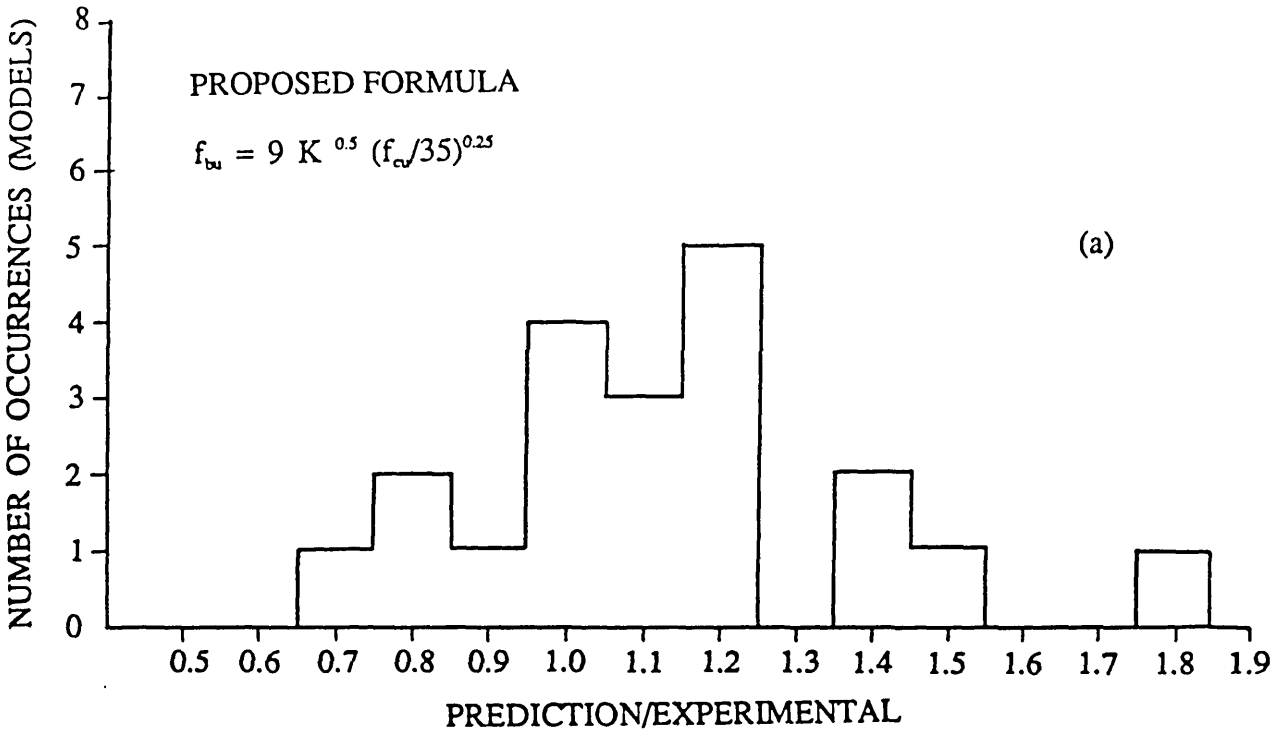
COMPARISON OF PREDICTION/EXPERIMENTAL RESULTS
FOR WELD-BEADED CONNECTIONS

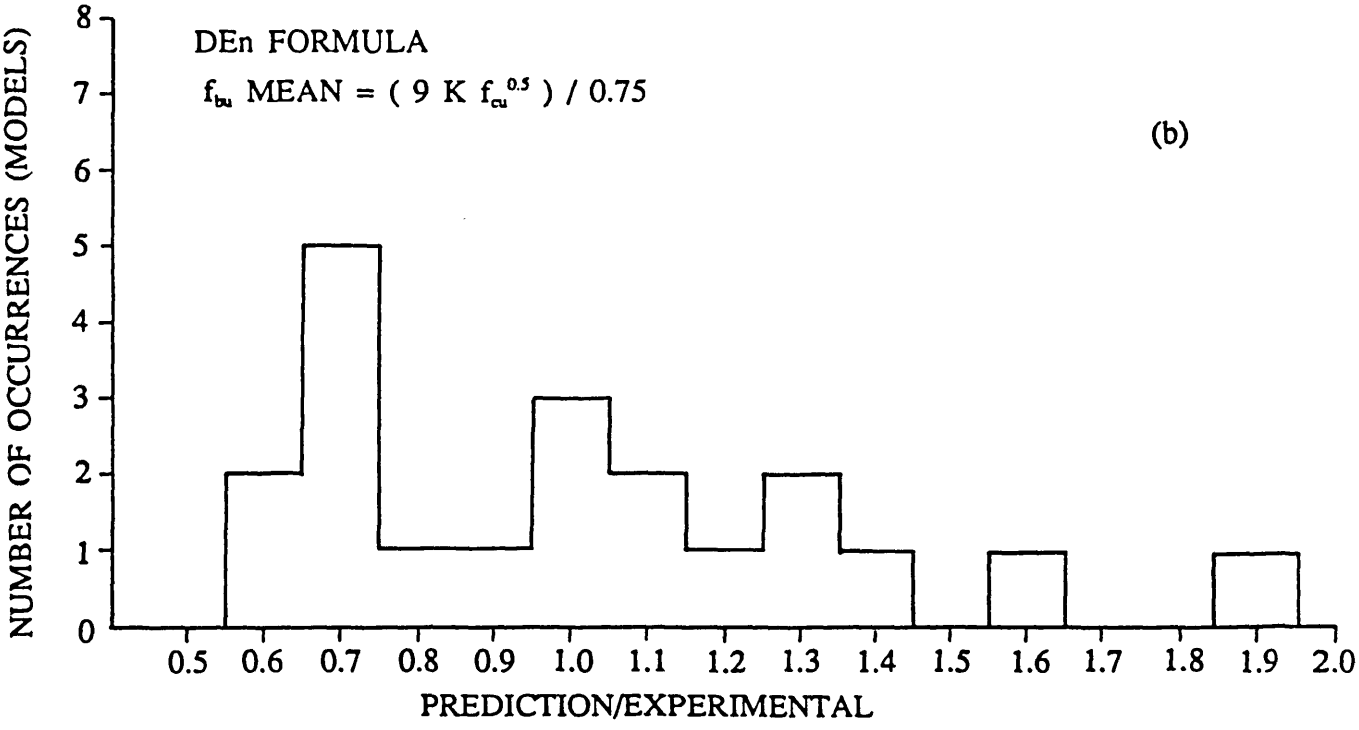
FIG 5.4



COMPARISON OF PREDICTION/EXPERIMENTAL RESULTS
FOR WELD-BEADED CONNECTIONS

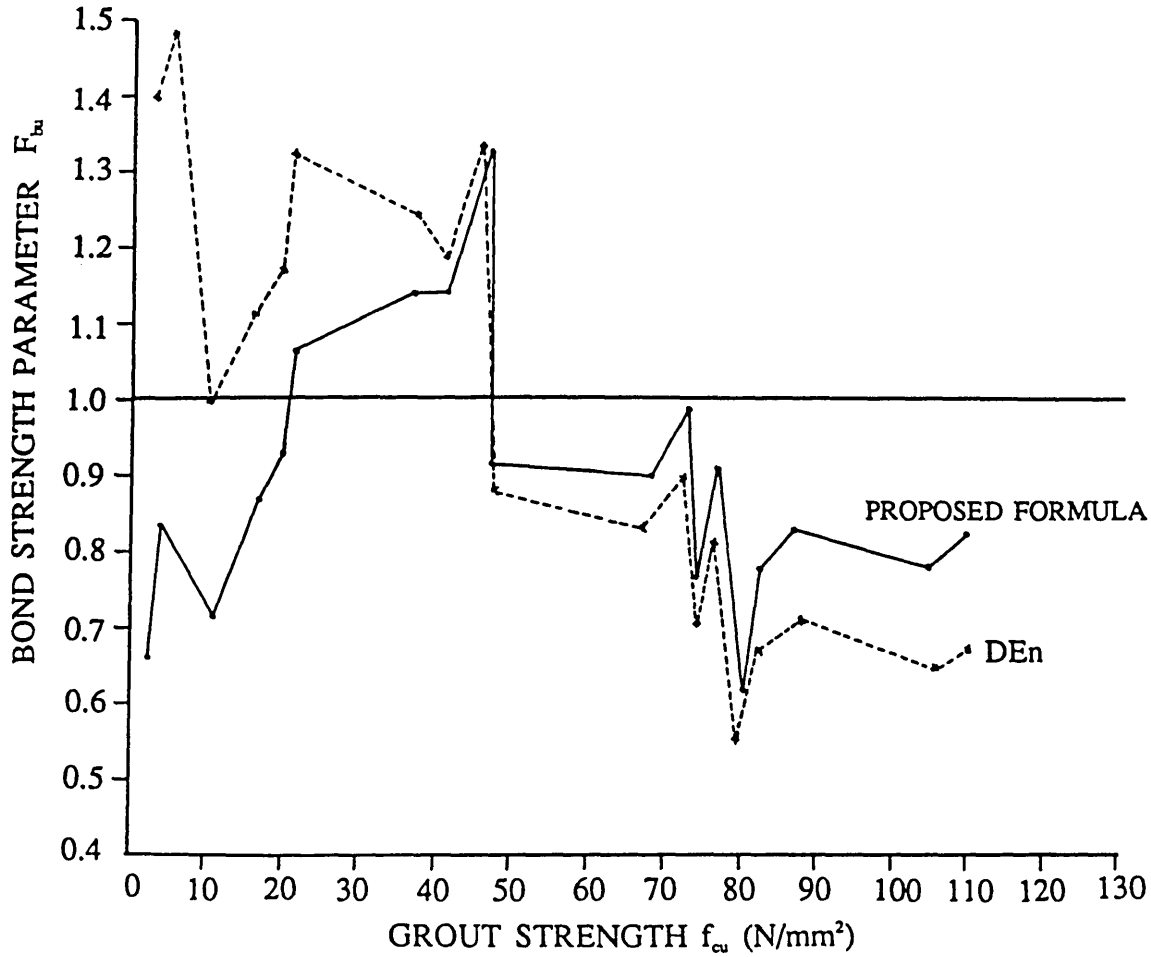
FIG 5.4(c)





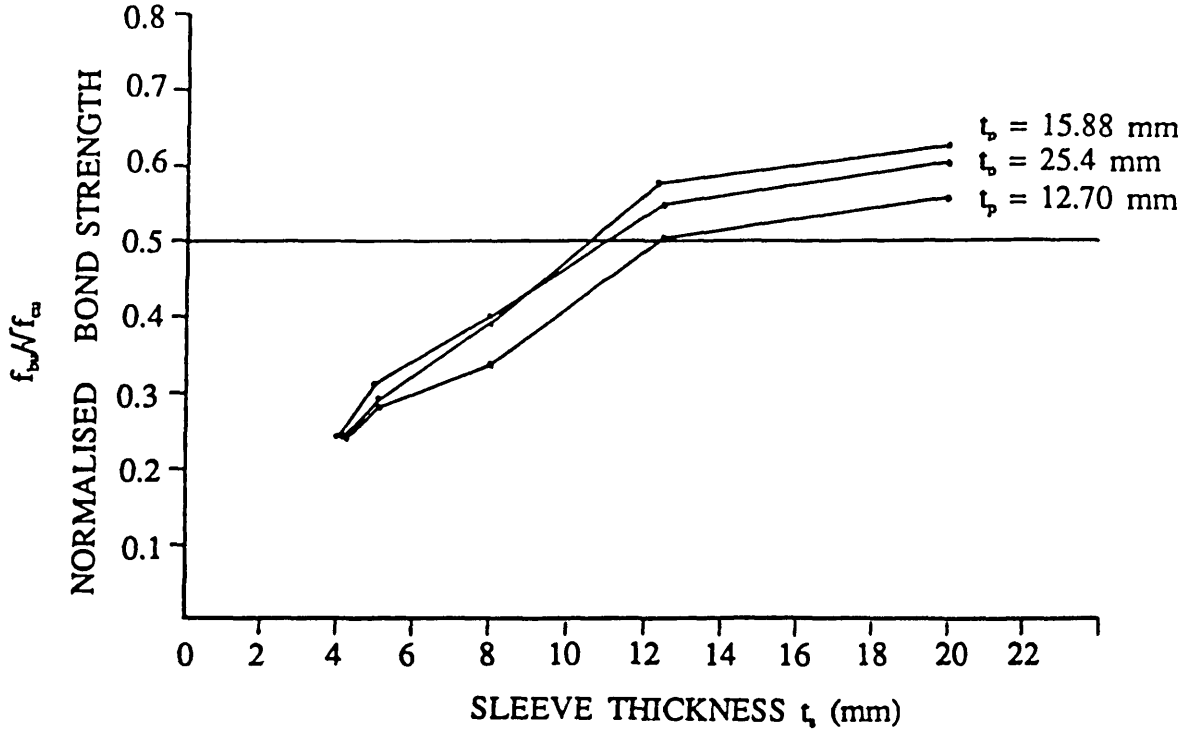
BOND STRENGTH PREDICTION FOR PLAIN CONNECTIONS

FIG 5.5



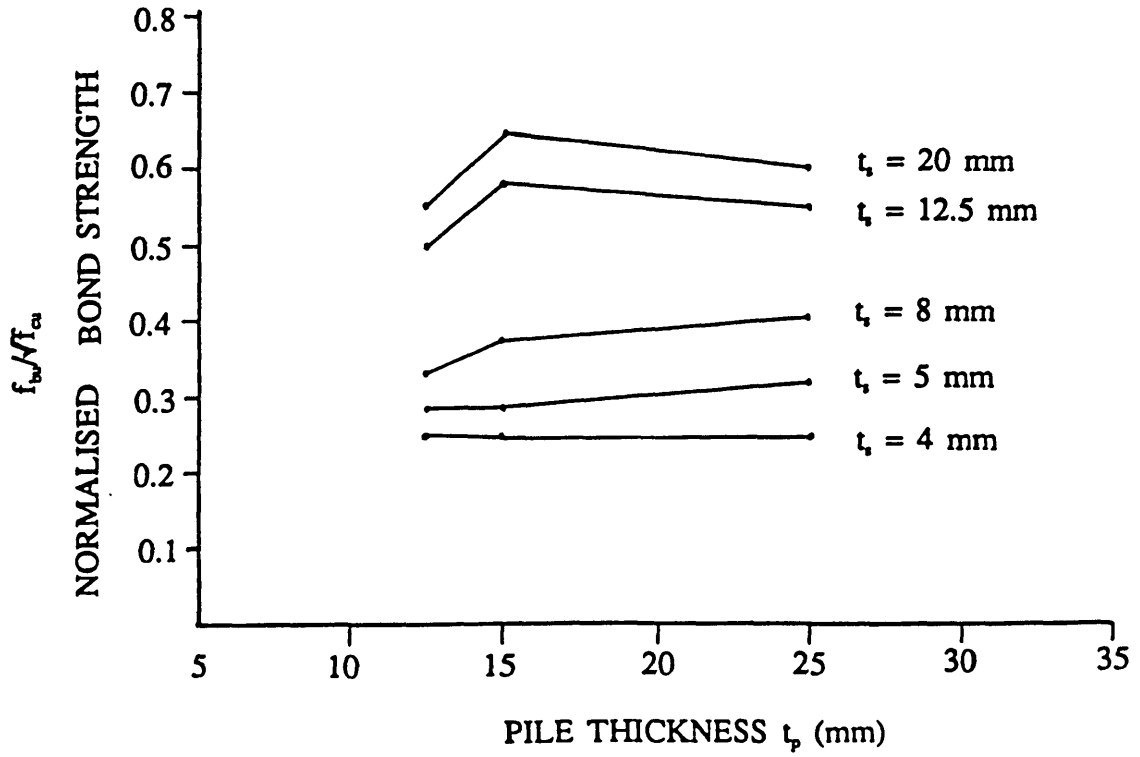
COMPARISON OF BOND STRENGTH PARAMETER FOR PLAIN CONNECTIONS

FIG 5.6



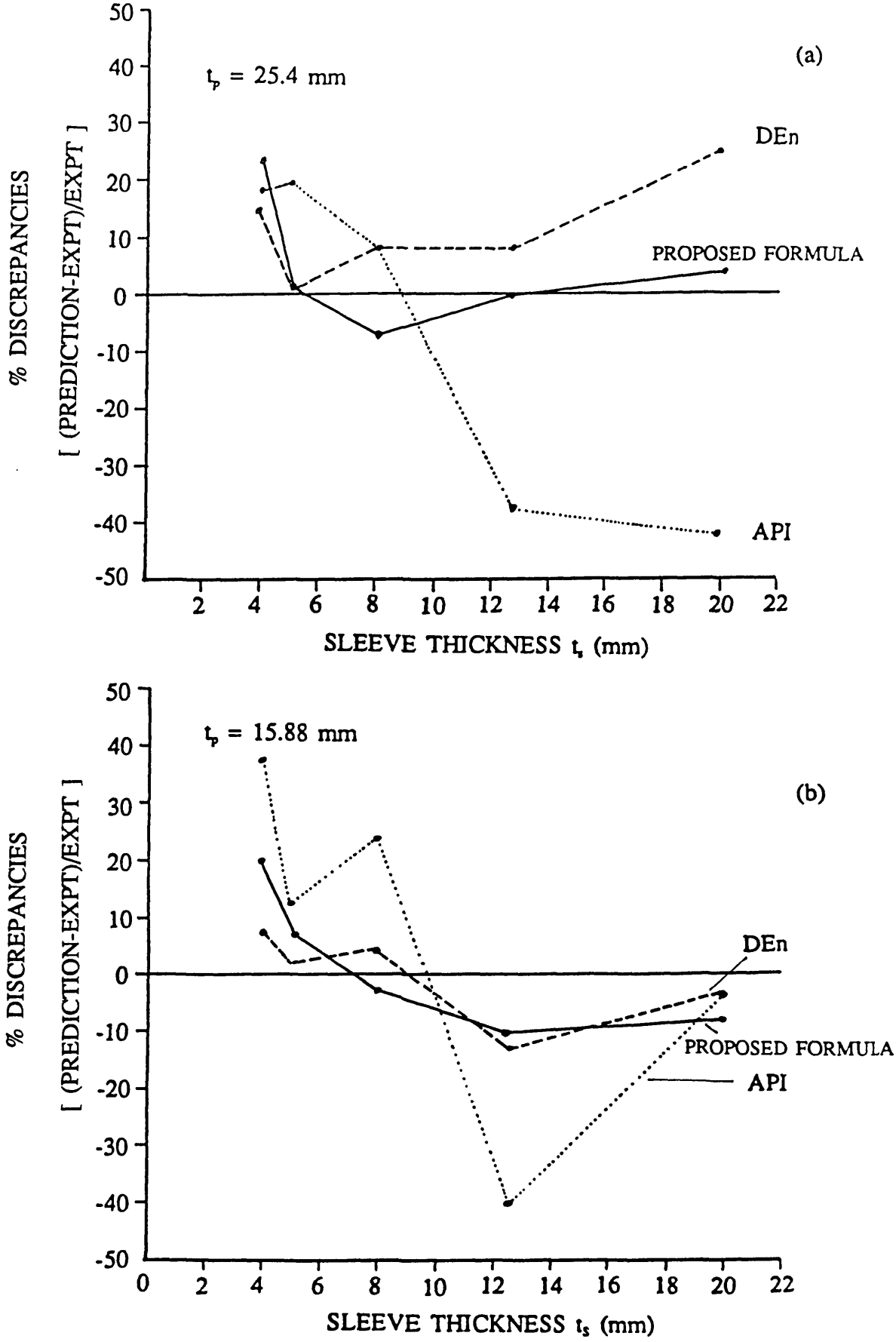
EFFECT OF SLEEVE THICKNESS, EXPERIMENTAL RESULTS

FIG 5.7



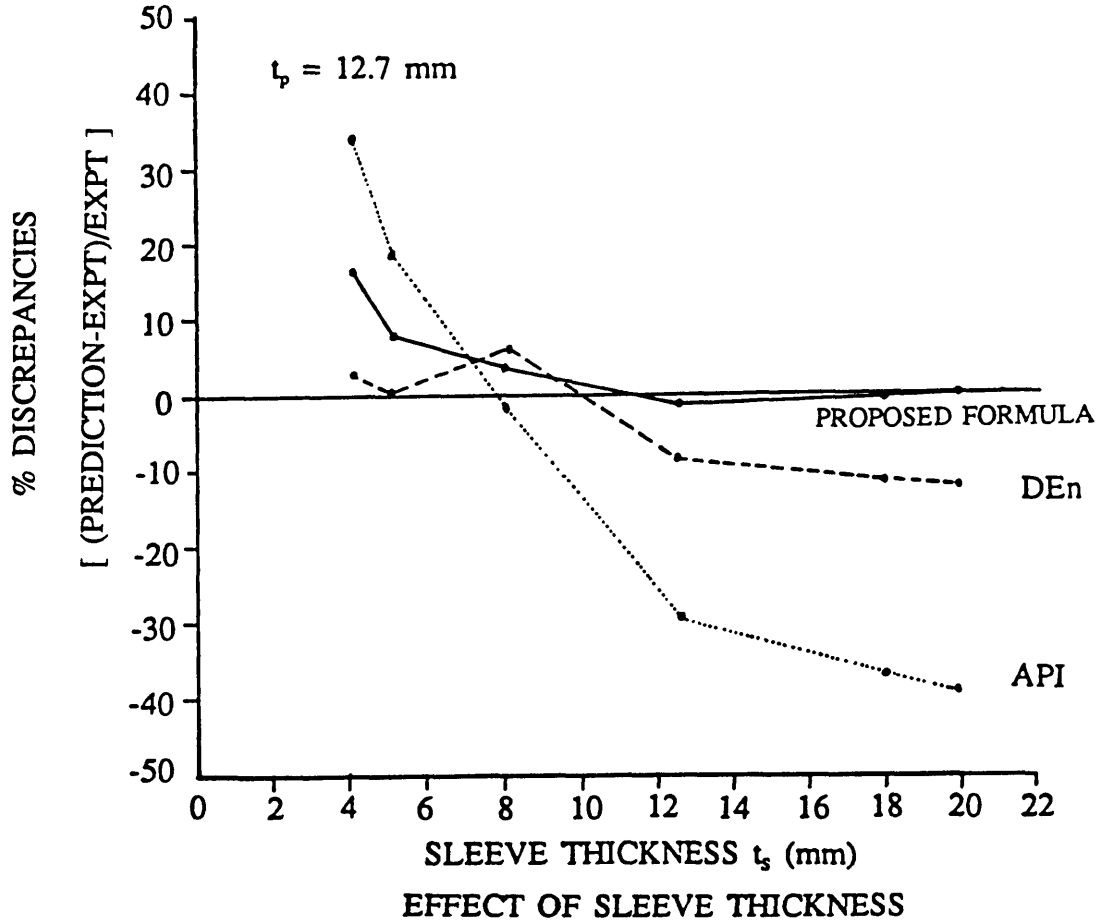
EFFECT OF PILE THICKNESS, EXPERIMENTAL RESULTS

FIG 5.8



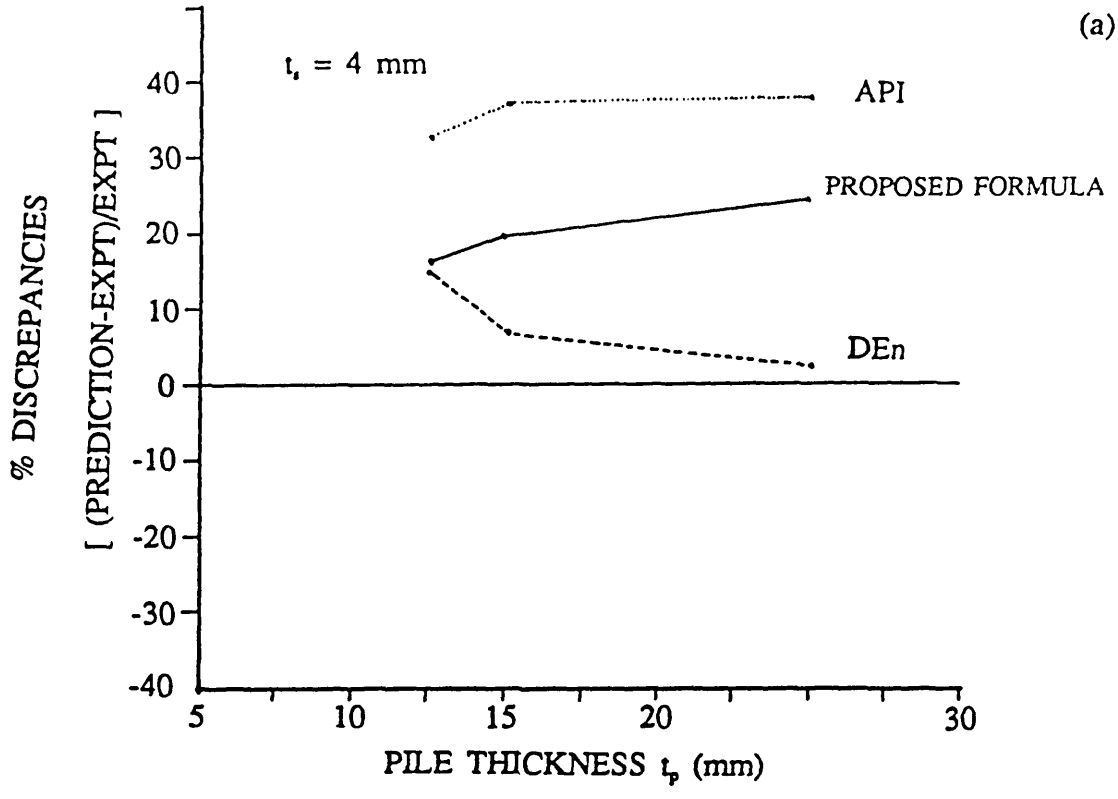
EFFECT OF SLEEVE THICKNESS

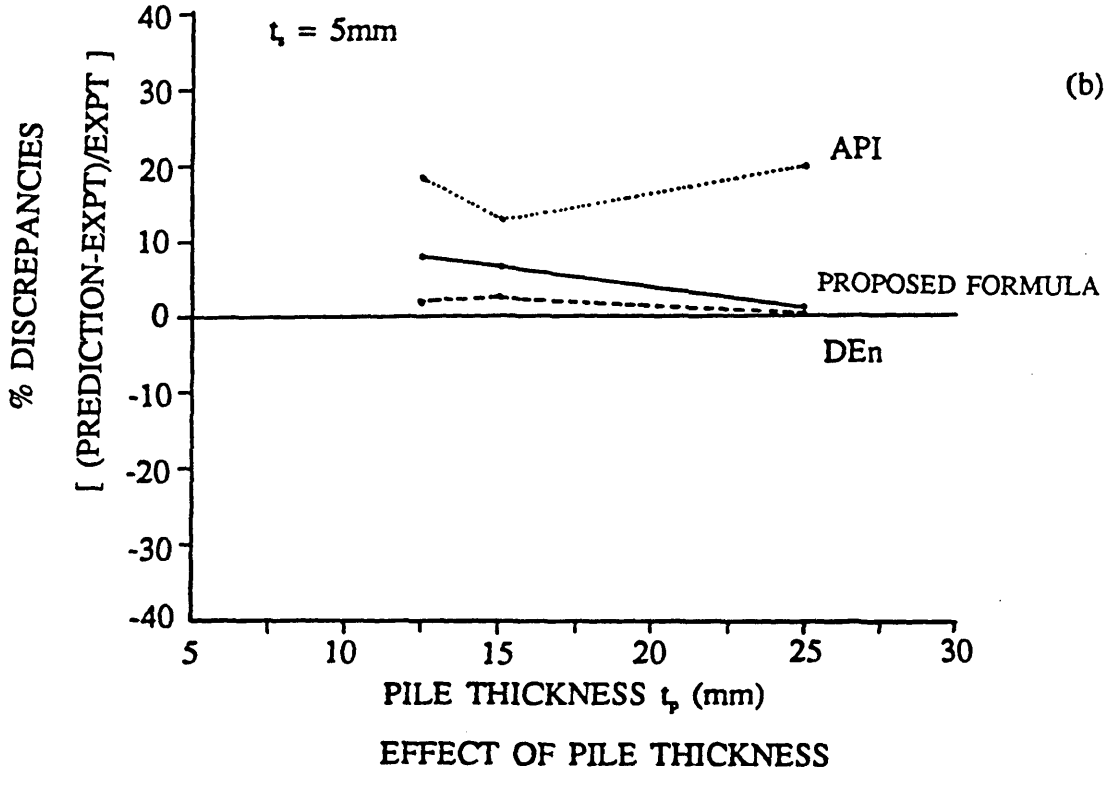
FIG 5.9



EFFECT OF SLEEVE THICKNESS

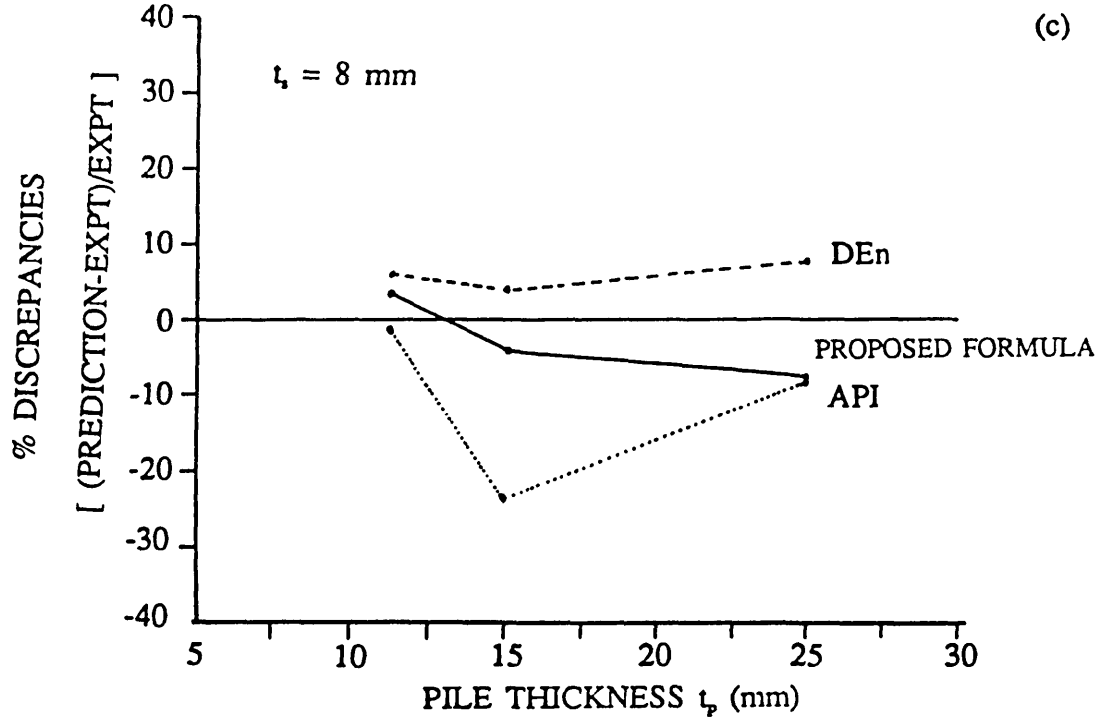
FIG 5.9 (c)

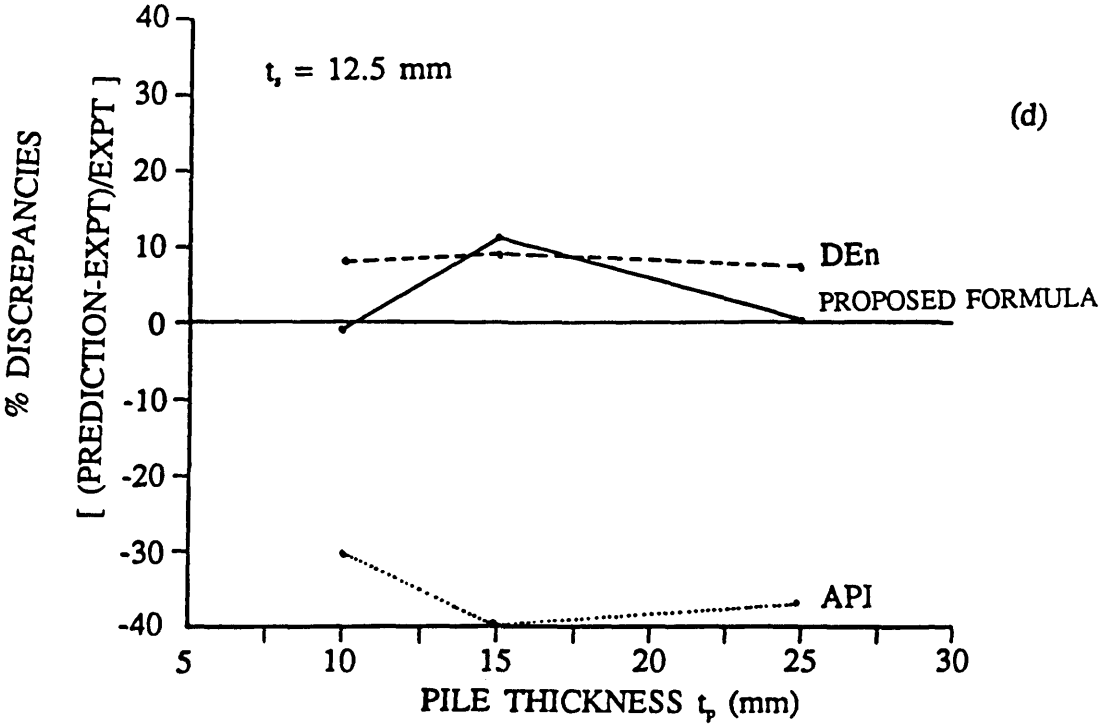




EFFECT OF PILE THICKNESS

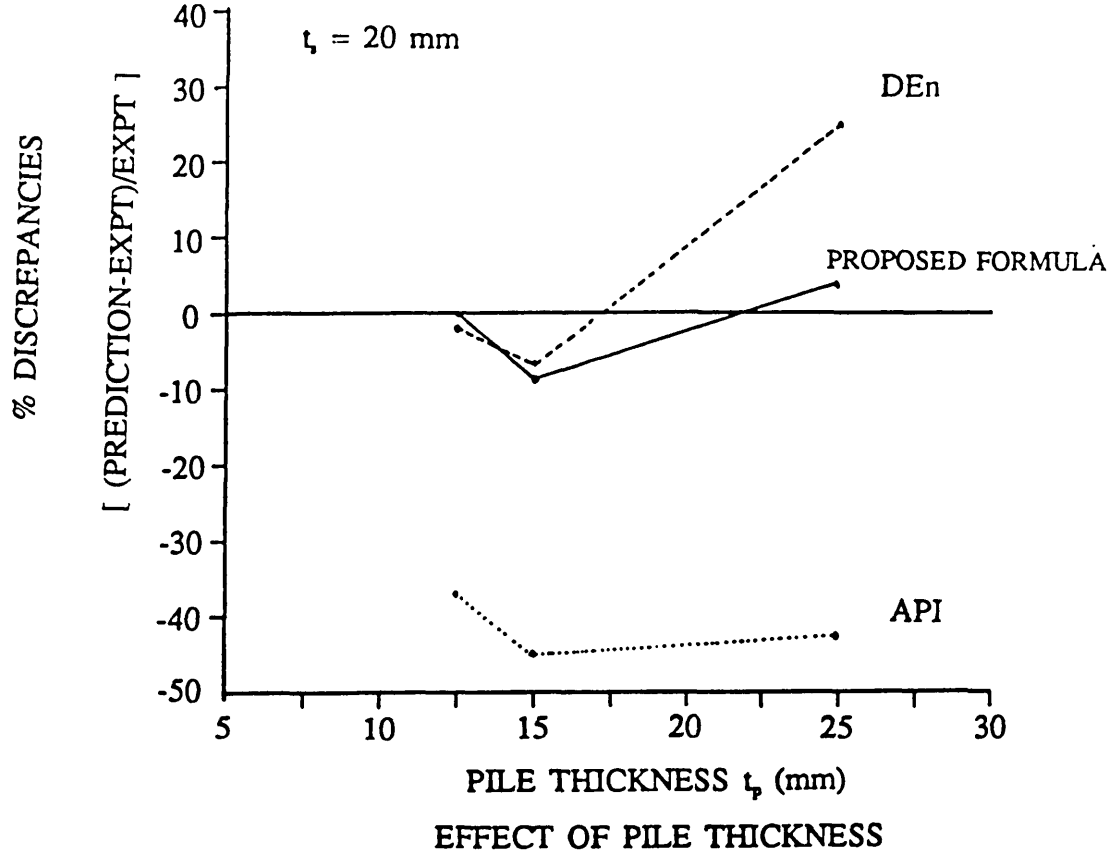
FIG 5.10





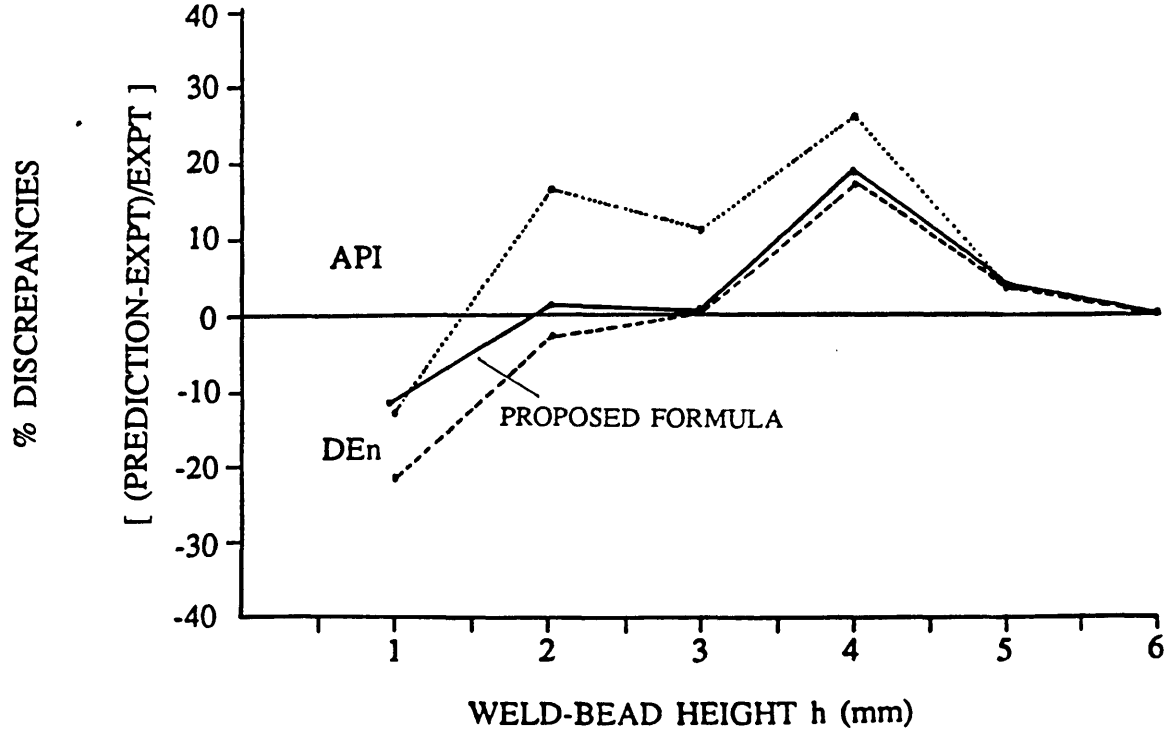
EFFECT OF PILE THICKNESS

FIG 5.10



EFFECT OF PILE THICKNESS

FIG 5.10(e)



EFFECT OF WELD-BEAD HEIGHT

FIG 5.11

CHAPTER SIX
GROUTED CONNECTIONS IN REPAIR

6.1 Causes of Defects

Repair of offshore platforms is increasing significance, firstly because more structures are being built, and secondly, since most of the existing platforms were built some years ago and may now be suffering from structural deterioration due to normal use and environmental factors. The causes of this damage have been studied and reported by some authors, including Winkworth et al (84) and The Underwater Engineering Group (85), the results of which can be summarized in the following :

i. Fatigue

Fatigue damage in an offshore structure can be caused by fabrication defects, such as welding faults and inadequate design calculations. A study of the fatigue life of members of an oil platform using advanced analysis has shown that simplified approachs, widely used in design in the late 1960's and early 1970's, overestimates the fatigue life of some members, especially those in the splash zone (84).

ii. Collision

Collision with the supply boats often occurs, although some precautions are taken to protect the platform. It is often necessary for the supply boat to approach close to the platform during loading and unloading, thus increasing the probability of collision. The resulting denting of tubular members can be serious and may affect the capacity of the affected member (86 and 87).

iii. Installation Damage

Offshore platforms are normally fabricated, towed to their permanent position offshore, then fixed to their foundations. Because of the difficulty of this process, it is possible that damage could occur in some parts of the structure.

iv. Dropped Objects

During installation and operation, heavy objects, such as piles and pipes dropped ccidentally can cause considerable damage to structural members (88).

6.2 Methods of Repair

Several options are available for repair of damaged tubulars (84, 89, 90, 91, 92 and 93). The decision to choose a particular method normally depends on factors such as the type of damage, the position of the member, weather conditions, and other practical considerations. The most common methods of repair are discussed below.

6.2.1 Welding

Because the design procedure for welding is well established, and often simpler than other methods, it has become the most common. If the damage is such that cracking occurs in the members , it is then necessary to grind the area before welding can be performed. If the crack is very serious, the work involves cutting out the section, providing a temporary support, and replacing the section with a new one. In this case, a well fitted assembly becomes necessary. If the member is badly damaged, the solution will be to replace the entire member with a new one. Welding is by means of dry welding in underwater habitats. The habitat is built around the member or joint under consideration. It has to be properly sealed and kept dry by means of hyperbaric air pressure, so that the welding process can be effected in a dry environment.

6.2.2 Grout Filling

Grout filling of the members can increase the stiffness and static strength. Tests (89) also showed that it could improve their fatigue lives by reducing stress concentration factors at hot-spot locations. However, if cracks exist in the member, grouting is not helpful since it does not stop the crack propagation.

6.2.3 Clamping

Two half circular cylinders may be clamped around the member under consideration. This is followed directly by bolting the two half-sleeves. This provides an alternative stress path through the clamp and hence the defective area

is by-passed. Two types of clamp repair scheme exist as discussed below.

6.2.3.1 Friction Clamp

In this type of clamp repair, the load from the member is transferred to the clamp by friction at the steel/steel interface. To achieve adequate friction strength, it is necessary for the clamp and member to be geometrically compatible, with very little tolerance. Because of geometrical imperfections in the member, it is often helpful to provide some kind of seal on its surface to accommodate any gaps which could occur on the contact surface, thereby improving friction strength. A more recent method of development for this type has been introduced by Williams (90).

6.2.3.2 Grouted Clamp

In grouted clamp repairs, the two half-sleeves have larger diameters than the members, and the annulus thus created is then filled with grout. The strength of the connection is due to the bond strength between the grout and the steel. This strength can be increased either by 'prestressing' or by providing the member and the clamps with mechanical shear-keys. Prestressing can be performed in one of two ways; either by actively prestressing, or by using expansive grout. The main advantage of this type of repair is that it can easily accommodate any gaps due to geometrical imperfection of the members and does not require accurate survey of the affected member underwater. Compared with other types, the grouted clamp has the following advantages.

- Can easily accomodate imperfections of the member.
- The technology of setting grout underwater is well developed.
- Does not need pre-treatment of the member surface, such as grinding.
- Does not need special installation conditions, such as a dry habitat.
- Divers requirements are less
- If needed, it can be used to strengthen the existing member or joint.
- The same principal can be used to install additional members.

Some applications of grouted clamp connections in repair of damaged tubular

Some applications of grouted clamp connections in repair of damaged tubular members are illustrated in figure (6.1). The clamps are provided with end flanges through which bolts are used to tie them together. The end gaps between the clamps and the member are sealed, and the annulus between the member and the clamps is then filled with cement grout. After a curing period, the bolts can be tightened. In the past, the flanges were usually directly attached at the clamp end, so that the two clamps could be fitted together using short bolts. This assembly, as shown in figure (6.3), is often known as a 'short bolt' type. In more recent developments the flanges are welded at some distance from the edge of the half-sleeve, and long bolts are used to tie the two halves. This 'long bolts' connection, as illustrated in figure (6.4), has the following advantages.

- Ease of tensioning.
- Preload control can be readily obtained since the elongation of the bolts is more likely to be in the elastic range.
- Easier to inspect.

With regard to ways of transferring loads from members to the clamps, there are three sub-types of grouted clamp connections.

6.2.3.2.1 Plain Connections

In plain connections the load is transferred entirely by friction between the grout and the steel. Until now, most of the connections used in offshore repairs employ this method. However, there are some disadvantages and problems in using plain connections.

- The average friction strength is usually very low, so that longer connections are usually required, whereas due to the members position, the available length is often very limited.
- The surface of the member has to be reasonably clean from marine growth to ensure that the friction strength can be developed.

6.2.3.2.2 Pre-stressed Connections

In long bolt connections, when the grout has cured, i.e. 7 days or more after casting, the bolts can be tightened in such a way that the clamps cause the

grout to be prestressed. By so doing, the friction strength can be significantly improved. The prestressing force should be carefully calculated, especially when the method is used for repairing damaged members, where high levels of stress may cause further damage to the affected member. The optimum applied prestress mainly depends on the residual strength of the damaged part of the member. Another method of prestressing has been studied by Carroll (63) at Imperial College. He studied the use of pressurised grout for prestressing in clamped connections. In this method, a thin steel membrane is welded to the inside of the sleeve, thus creating a 'pressure chamber'. After the grout annulus is set, high pressure grout is injected through an aperture in the sleeve wall and into the 'pressure chamber'. A secondary 'prestressing' annulus is thus created, and a radial, near uniform, pressure is applied. Tests at Imperial College demonstrated the superiority of this method over conventional bolted prestressed connections. The ratio of initial prestress to average friction strength for the pressurised method was 0.74 compared with 0.41 for the torque bolt method. However, these results have to be confirmed by more tests, since only one model for each type was tested.

6.2.3.2.3 Weld-beaded Clamps

As in the ordinary grouted pile-sleeve connections, the strength of grouted clamps can be increased substantially by providing mechanical shear-keys on the outer surface of the member and the inner surface of the clamps. Boswell and Mello (94 and 95) and Wimpey Laboratories (96) carried out some tests on weld-beaded clamp repairs. The former authors observed that the strength of weld-beaded clamps was much lower than that of ordinary weld-beaded connections, while the Wimpey tests showed that there was no significant difference between the two types of connections. The cause of the difference was probably the geometrical differences between the two test series.

The main difficulty in the application of weld-beaded clamp connections is to fabricate the weld-beads on the existing member, since this involves underwater welding. However, at least one application has been recorded by Conoco in 1980 (89). A research programme attempting to devise a shear-key which can be applied without the need for underwater welding habitat is under consideration (89).

6.3 Analytical Study

The following treatment concerns grouted weld-beaded clamp repairs. The strength of this type of connection will be analysed by using results of the stress-displacement relationship from the existing experiments discussed in chapters (3) and (4) above.

6.3.1 Assumptions

In grouted clamps with weld-beads, failure of the connection in most cases is due to crushing of the grout on the compression side of weld-beads. This failure mode will occur as long as the following conditions are maintained :

- The bolts are strong enough, so that there is no possibility of failure at the bolts.
- The bolts are stiff enough, so that elongation of the bolts does not cause substantial lateral movements.
- The member and the clamps have sufficient radial stiffness, so that a slipping failure mode will not occur.

It has been shown in the grouted clamp tests (94 and 95) that under loading, the pile will displace inwards. Due to the effect of bending produced by the bearing stress acting eccentrically at the weld-bead, the peak negative strain is at weld-beads locations, whilst the minimum values of hoop strain occurrs between weld-beads. This is a consequence of the restraining effect of the grout on radial dilation of the pile between weld-bead locations.

For analytical calculations, it can be assumed that inflection points occur every 1/4 S_p from the weld-bead. Therefore, to obtain the weld-bead strength, it is sufficient to consider a segment of length 1/2 S_p. Hinges are then 'inserted' at the ends to represent the inflection points. Since the radial stress is produced as a result of the confinement, its values must be proportional to the hoop strain. Therefore, the distribution of the radial stress should follow the same configuration

as the hoop strain. Based on these considerations, a reasonable representation of the problem in the axial direction will be as in figure (7.5).

Unlike conventional weld-bead connections, the grout in this case is not always continuous in the circumferential direction. If the connection is a 'short bolt' type, the grout may be cast continuously. On the other hand, for the 'long bolt' type, the grout is not normally continuous. In the latter case the grout stops at the clamp edges, thus forming a gap. The gap causes the distribution of the radial stress to be also discontinuous. This type of stress distribution leads to two important effects on the radial displacement :

- The maximum radial displacement is greater since bending occurs in the Z (axial) direction.
- The radial displacement is not constant along the circumference.

From the existing test results, it was concluded that failure of the connection was due to grout crushing. Furthermore, this crushing corresponded to yielding of the pile in the hoop direction. This mechanism of failure will be exemplified in the following section, and used to derive an analytical solution for the problem.

6.3.2 Analysis

6.3.2.1 Theory of Cylindrical Shells

The simplified equation for a laterally loaded cylindrical shell, as illustrated in figure (6.5), is given by:

$$\frac{\partial^2 u}{\partial x^2} + \frac{1-\mu}{2a^2}\frac{\partial^2 u}{\partial \phi^2} + \frac{1+\mu}{2a}\frac{\partial^2 v}{\partial x \partial \phi} - \frac{v}{a}\frac{\partial w}{\partial x} = 0 \qquad (6.1.a)$$

$$\frac{1+\mu}{2}\frac{\partial^2 u}{\partial x \partial \phi} + a\frac{1-\mu}{2}\frac{\partial^2 v}{\partial x^2} + \frac{1}{a}\frac{\partial^2 v}{\partial \phi^2} - \frac{1}{a}\frac{\partial w}{\partial \phi} = 0 \qquad (6.1.b)$$

$$\mu\frac{\partial u}{\partial x} + \frac{\partial v}{a\,\partial \phi} - \frac{w}{a} - \frac{h^2}{12}\left(a\frac{\partial^4 w}{\partial x^4} + \frac{2}{a}\frac{\partial^4 w}{\partial x^2 \partial \phi^2} + \frac{\partial^4 w}{a^3 \partial \phi^4}\right) = - \frac{a\,q\,(1-\mu^2)}{E\,h} \qquad (6.1.c)$$

The above formulae were given by Timoshenko (97) based on work by Reissner (98) and Wojtaszak (99). The equations will be referred to in the sections below.

6.3.2.2 Idealisation of the Problem

In the axial direction, the pile will be represented by a simply supported beam with a span of 1/2 S_p, as described in figure (6.6). The radial stress acting on it will be represented by a half sine distributed stress, and expressed in terms of a Fourier series, as given below :

$$q = \sum_{m=0}^{\infty} \sum_{n=0}^{\infty} D_{mn} \cos n\phi \sin m\pi x/l \qquad (6.2)$$

where,

l : length of the 'beam'

ϕ : angle at a point

D_{mn} : a constant which has to be determined

x : distance of the point of interest, measured from the beam end

The boundary conditions for expression (6.1) are :

$$q = q_0 \quad \text{for} \quad 0 < \phi < \alpha \tag{6.3.a}$$

$$q = 0 \quad \text{for} \quad \alpha < \phi < (\pi-\alpha) \tag{6.3.b}$$

$$q = q_0 \quad \text{for} \quad (\pi-\alpha) < \phi < (\pi) \tag{6.3.c}$$

6.3.2.3 Solution of the Differential Equations

D_{mn} can be determined as follows.

- Multiply both sides of equation (6.2) by cos $n\phi$ sin $m\pi x/l$.
- Integrate the equation along the circumference.

Since the distribution is symmetrical, the integration can be performed for a half cycle (π).

$$\int_0^l \int_0^{\pi} q \cos n\phi \sin m\pi x/l \, d\phi dx = \int_0^l \int_0^{\pi} \sum_{m=0}^{\infty} \sum_{n=0}^{\infty} D_{mn} \cos^2 n\phi \sin^2 m\pi x/l \, d\phi dx \tag{6.4}$$

After integration the equation becomes,

$$\frac{4\, q_0}{m\, n\, \pi} [\, \cos (n\pi/2) \sin (n\alpha - m\pi/2) \,] = (\pi/4l)\, D_{mn} \tag{6.5}$$

Therefore,

$$D_{mn} = [\frac{16\ q_0}{m\ n\ \pi^2}] \cos (\frac{m\pi}{2}) \sin n(\alpha - \pi/2) \tag{6.6.a}$$

(for $m \neq 0$, $n \neq 0$)

The procedure is repeated for $n = 0$, $m \neq 0$ and for $n \neq 0$, $m = 0$, thus giving :

$$D_{m0} = \frac{8\,\alpha\,q}{m\,\pi^2} \qquad (6.6.b) \quad , \quad \text{and} \quad D_{0n} = 0 \qquad (6.6.c)$$

Since the part of the cylinder under consideration can be represented by a simply supported cylinder with a symmetrical radial stress, the conditions of symmetry and the boundary conditions will be satisfied by assuming the displacement function as follows :

$$u = \sum_{m=0}^{\infty} \sum_{n=0}^{\infty} A_{mn} \cos n\phi \cos m\pi x/l \qquad (6.7.a)$$

$$v = \sum_{m=0}^{\infty} \sum_{n=0}^{\infty} B_{mn} \sin n\phi \sin m\pi x/l \qquad (6.7.b)$$

$$w = \sum_{m=0}^{\infty} \sum_{n=0}^{\infty} C_{mn} \cos n\phi \sin m\pi x/l \qquad (6.7.c)$$

By substituting the values of u, v, w and q into the general equation (6.1), the resulting expressions are,

$$A_{mn}\left[\left(\frac{m\pi}{l}\right)^2+\left(\frac{1-\mu}{2a^2}\right)n^2\right] - B_{mn}\left[\left(\frac{1+\mu}{2a}\right)n\left(\frac{m\pi}{l}\right)\right] + C_{mn}\left[\left(\frac{\mu}{a}\right)\left(\frac{m\pi}{l}\right)\right] = 0 \qquad (6.8.a)$$

$$A_{mn}\left[\left(\frac{1+\mu}{2}\right)n\left(\frac{m\pi}{l}\right)\right] - B_{mn}\left[a^2\left(\frac{1-\mu}{2}\right)\left(\frac{m\pi}{l}\right)^2+\left(\frac{n^2}{a}\right)\right] + C_{mn}\left(\frac{n}{a}\right) = 0 \qquad (6.8.b)$$

$$-A_{mn}\,\mu\left(\frac{m\pi}{l}\right) + B_{mn}\left(\frac{n}{a}\right) + C_{mn}\left[a\left(\frac{m\pi}{l}\right)^4 + \left\{\frac{2n^2(m\pi/l)+(12/h^2)}{a}\right\} + \left(\frac{n^4}{a^3}\right)\right]\frac{h^2}{12} =$$

$$D_{mn}\,\frac{a(1-\mu^2)}{Eh} \qquad (6.8.c)$$

These three equations contain three unknown parameters A_{mn}, B_{mn} and C_{mn}, which can be evaluated for each value of m and n. The solution procedure is described in figure (6.8) and the listing of the computer programme is given in appendix V. Once these constants are known, the displacements (u,v,w) at any point of interest under a given q can be calculated by substituting in all the corresponding values, and summing up for all values of m and n. The more values of m and n used in the series, the more accurate the solution will be. After the displacement is known, the stress and strain can be calculated using the following expressions,

$$\varepsilon_x = du/dx \qquad (6.10)$$

$$\varepsilon_\phi = a\, dv/d\phi - w/a \qquad (6.11)$$

Since the grout crushing corresponds to yielding in hoop direction, the value of the radial stress at that stage can be defined as, $\varepsilon_h = \varepsilon_y$. By substituting this value of hoop strain in the above equation, the corresponding maximum displacements can be obtained. And by substituting back the displacements, the corresponding radial stress is evaluated.

6.3.2.4 Strength of Grout beneath the Weld-bead

As in normal grouted connection problems, the stress state under the weld-bead is triaxial, comprising radial, hoop and axial stresses. The radial and hoop stresses resulting from confinement increase the bearing strength of the grout well above the uniaxial strength. Crushing of the grout occurs when the bearing stress exceeds the confined strength, and corresponds to the onset of hoop yielding, which

in turn corresponds to the maximum attainable confinement. Concequently, it is clear that to obtain the bearing strength of the weld-bead, this confining stress have to be evaluated. This can be achieved as follows.

- The radial stress can be evaluated by using the analytical procedure discussed above, and described in a flow chart as in figure (6.7).
- Unlike full sleeve grouted connections, the hoop stress in split sleeve assemblies cannot be related to or expressed as a function of radial stress since they are independent of each other. Figure (6.8) shows the principal difference between those types of connection. In a typical split sleeve connection, the grout is discontinuous in the circumferential direction, therefore there is no confinement in the hoop direction. Under loading, slip in the hoop direction may occur between the grout and the pile interface. In other words, there is no strain compatibility between the pile and the grout interface. The only resistance is due to friction between the grout and the pile, as well as grout and sleeve surfaces. The friction strength derived in the previous chapter for normal weld-beaded connection will be used here.

Following the evaluation of radial and hoop stress, the total strength of the grout at the weld-bead can be determined using a biaxial failure criterion.

6.4 Case Study

To study the validity of this analysis, comparisons with the models tested previously (94, 95 and 96), is undertaken. Because there is a very limited number of available test data in split sleeve connections extensive comparisons are not possible.

Model G1

L/D_p	D_p	t_p	D_s	t_s	h	S_p	f_{cu}	f_{bu} Exp	f_{bu} Analysis
2	406	12.5	405	5	2.87	135	43.71	2.11	2.01

(dimensions in Newton and mm)

Models G2 and G3 from the same reference, with a different applied prestress gives almost the same strength as G1. The same observation was found regarding models H and J. Boswell and Mello (94 and 95) observed that the ultimate load of the connection increased slightly with applied prestress, hence there is no clear advantage in applying higher prestressing forces. The reason for this may be explained as follows. Under the effect of prestressing, the friction strength increases between the steel and the grout, thus increasing the hoop stress that can be developed. This means that the confining stress will increase also, and therefore, the bearing strength. However, when the applied prestress is very high, the strength in the radial direction is reduced. Therefore, the combination of the above two components of stress causes no increases in the bearing strength.

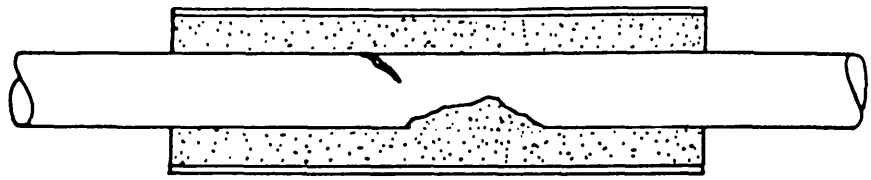
6.5 Discussion

Grouted clamp connections are a popular choice for offshore repairs. The main advantage of using such connections is the ease of accommodating geometric imperfections of the members. The most serious handicap of this connection is in-situ fabrication of the weld-beads on existing members. Although their geometric configurations are basically the same as their normal grouted connection counterparts, their behaviour, however, is quite different.

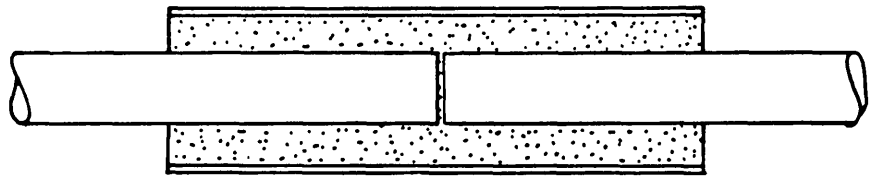
If the grout annulus is formed continuously, and the bolts are very stiff, the stress distribution is likely to be close to those in full sleeve connections, as demonstrated by Wimpey Labs (96 and 100). However, for semi-circular discontinuous annuli, such as in 'long bolt' connections, or when the bolts are not adequately stiff, the stress distribution becomes quite different. In the latter case, the hoop strength cannot be developed sufficiently, so that the strength of the connection will be significantly lower. This is likely to be the reason why tests by Boswell and Mello (94 and 95) gave lower connection strengths than those predicted using the normal grouted connection formula. In their tests, longitudinal cracks in the grout annulus occured along the joints of the clamps. These cracks caused discountinuity of the grout. Therefore, although the hoop stress in the sleeve was very high (due to prestressing and applied loading), the hoop stress could not

be developed in the grout.

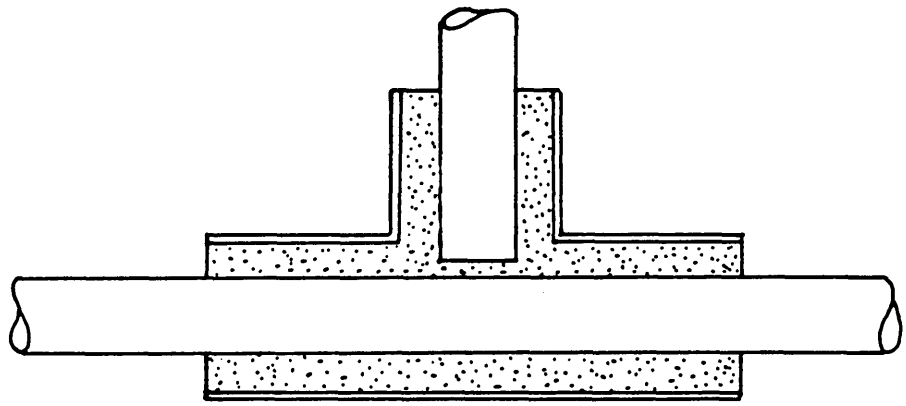
A simple analytical approach was developed for discontinuous grout clamp connections. To analyse the strength of the weld-bead, a simply supported equivalent beam was used. The beam represents part of the steel tubular, and the length was taken as the distance between the inflection points. The distributed load was assumed to be sinusoidal in the longitudinal direction, and uniformly distributed in the circumferential direction. The results from this method were compared to an actual test result, and are in very good agreement.



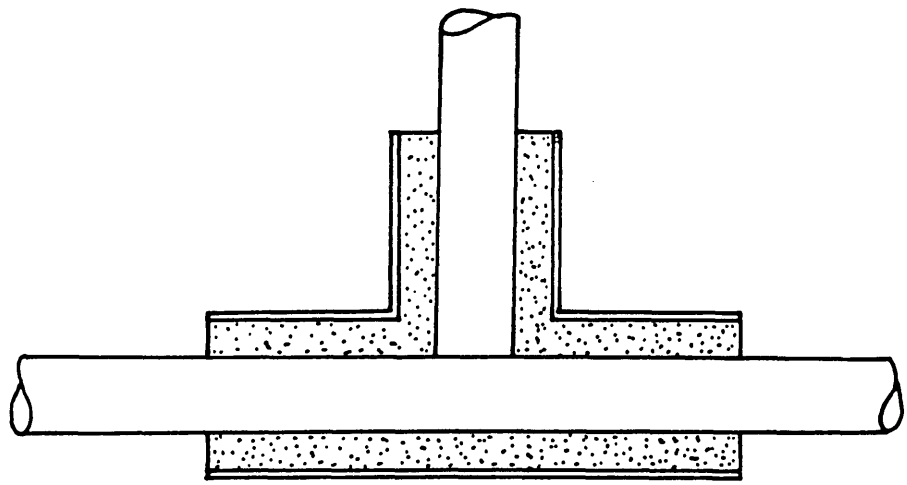
(a) TO BRIDGE A DISCONTINUITY



(b) TO JOIN TWO MEMBERS



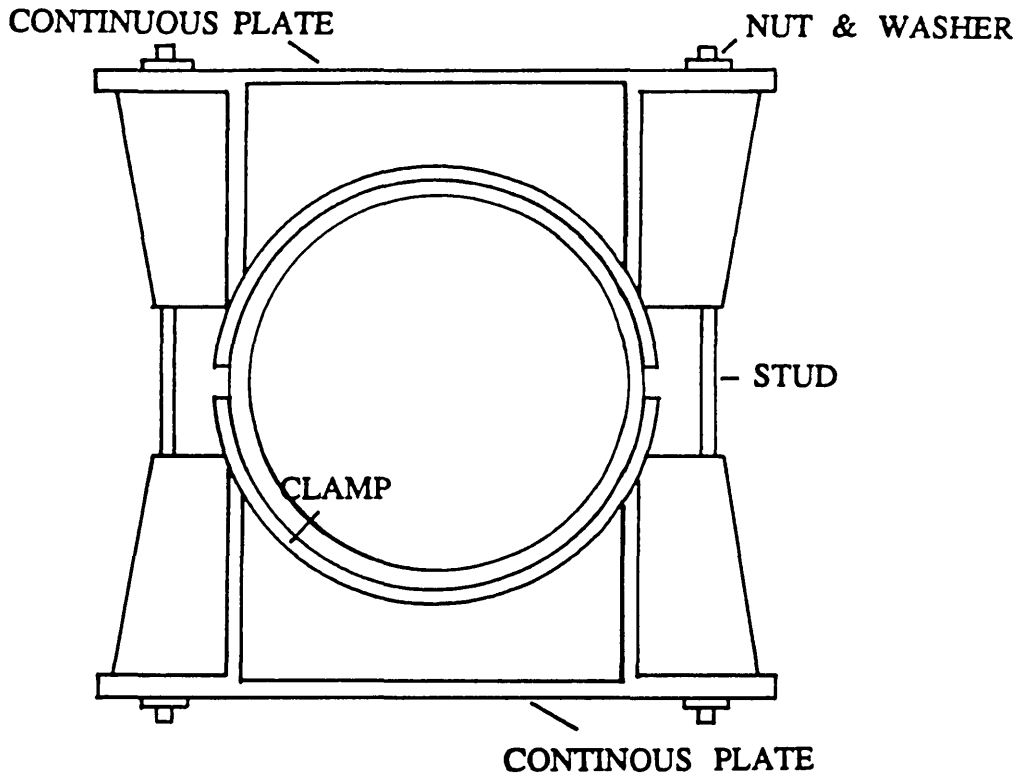
(c) TO FIX A NEW MEMBER TO AN EXISTING MEMBER

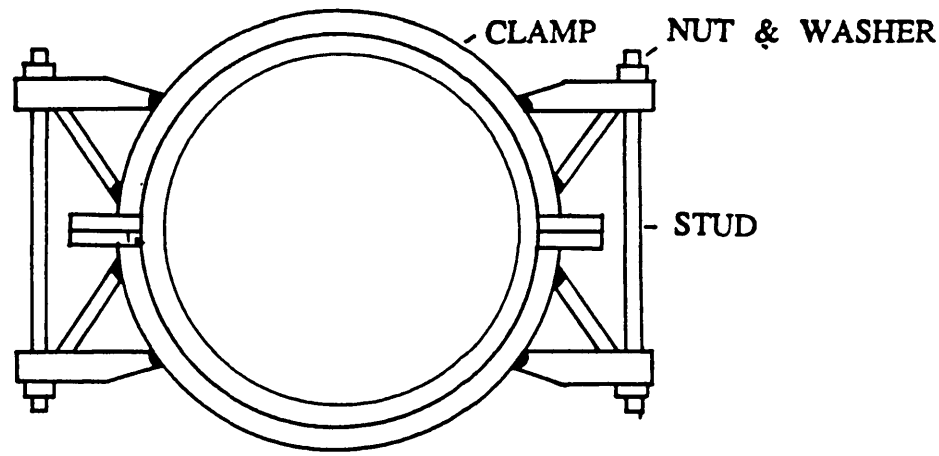


(d) TO REINFORCE AN EXISTING JOINT

APPLICATIONS OF GROUTED CLAMP CONNECTIONS IN REPAIR OF DAMAGED TUBULAR MEMBERS (HORDYK-92)

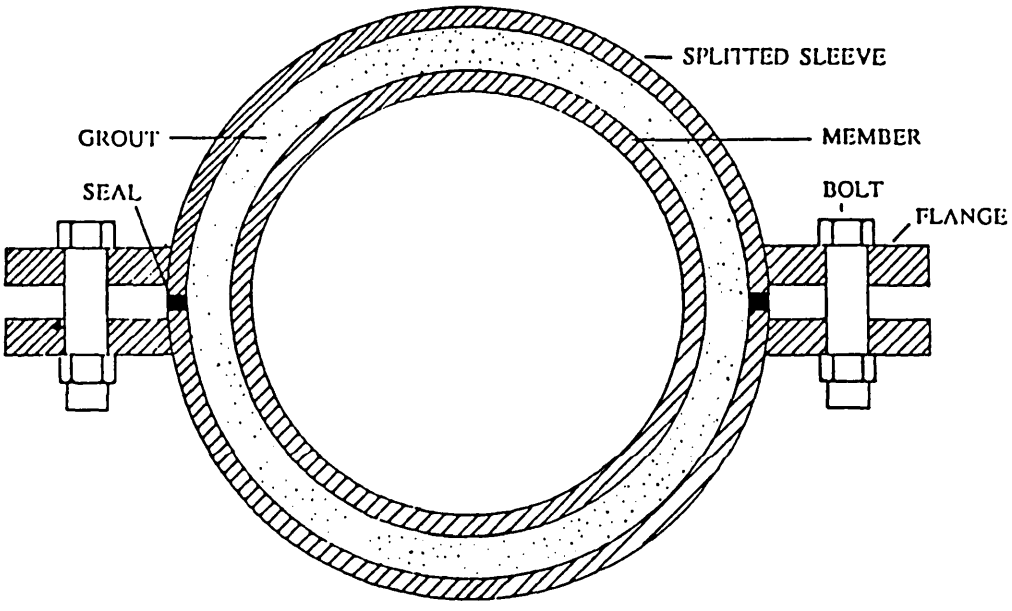
FIG 6.1





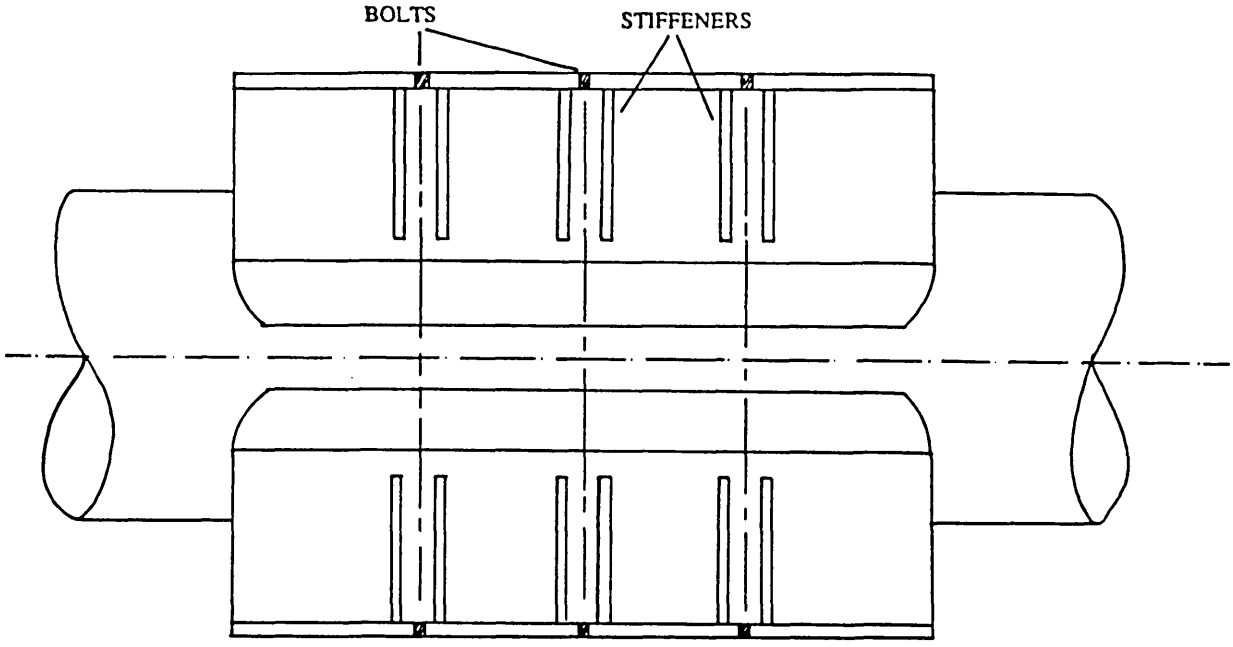
TYPICAL FRICTION CLAMP CONNECTIONS (SCOTT-91)

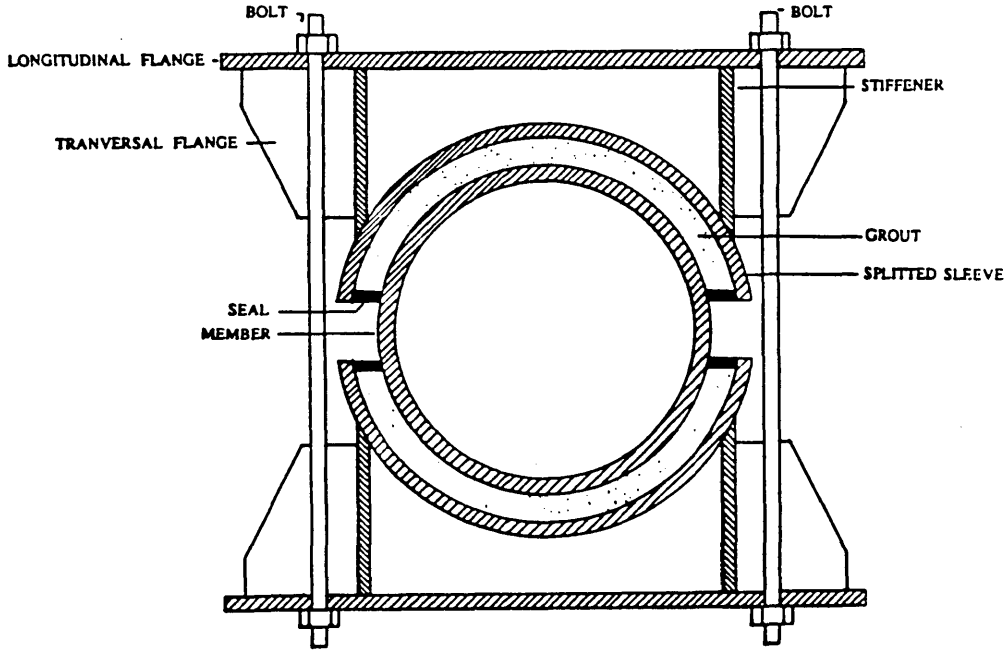
FIG 6.2



TYPICAL SHORT BOLT CONNECTION

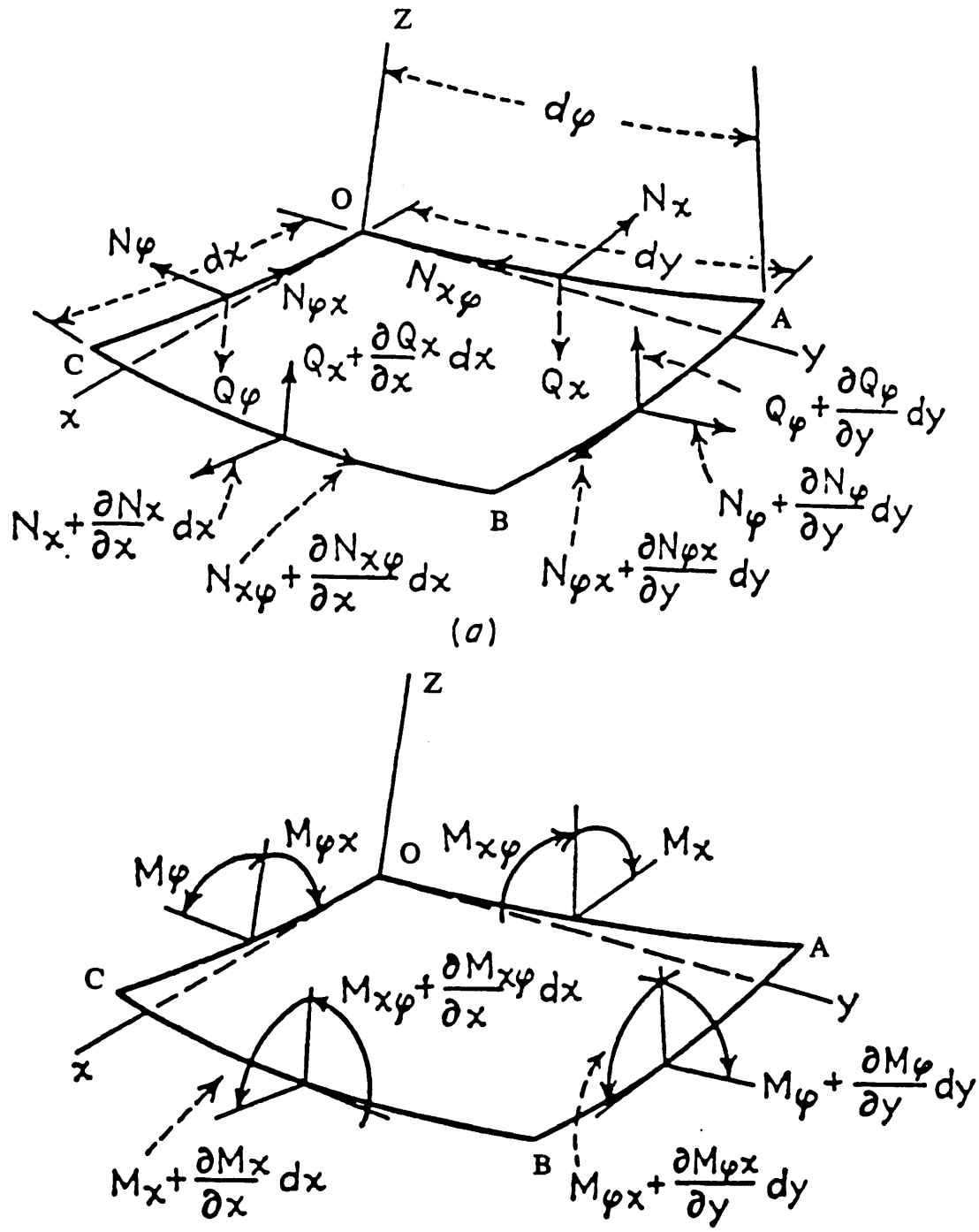
FIG 6.3





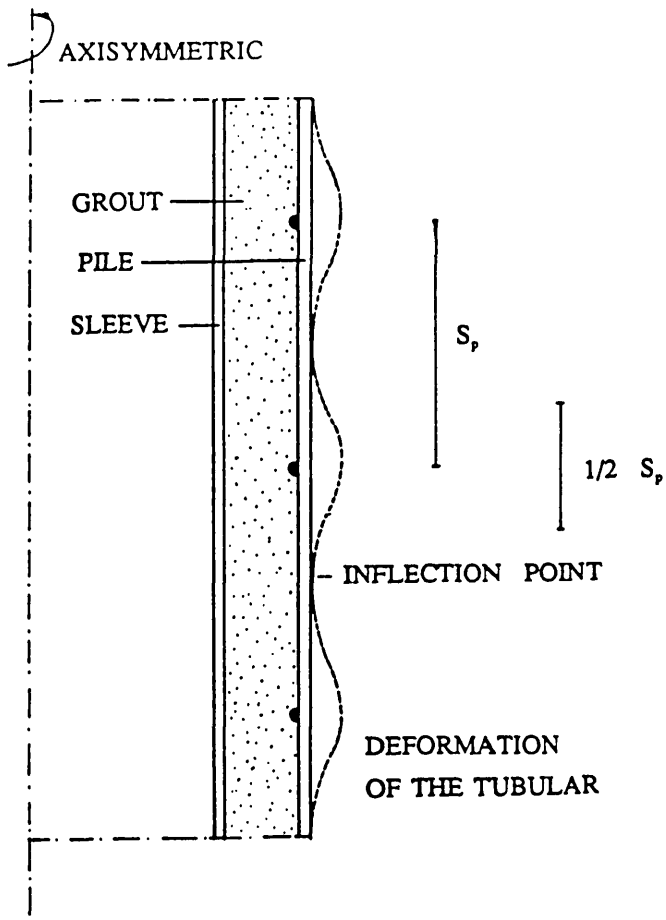
TYPICAL 'LONG BOLT' CONNECTION

FIG 6.4



STRESS STATE FOR GENERAL CYLINDRICAL SHELL (TIMOSHENKO-97)

FIG 6.5



IDEALISATION OF RADIAL STRESS DISTRIBUTION

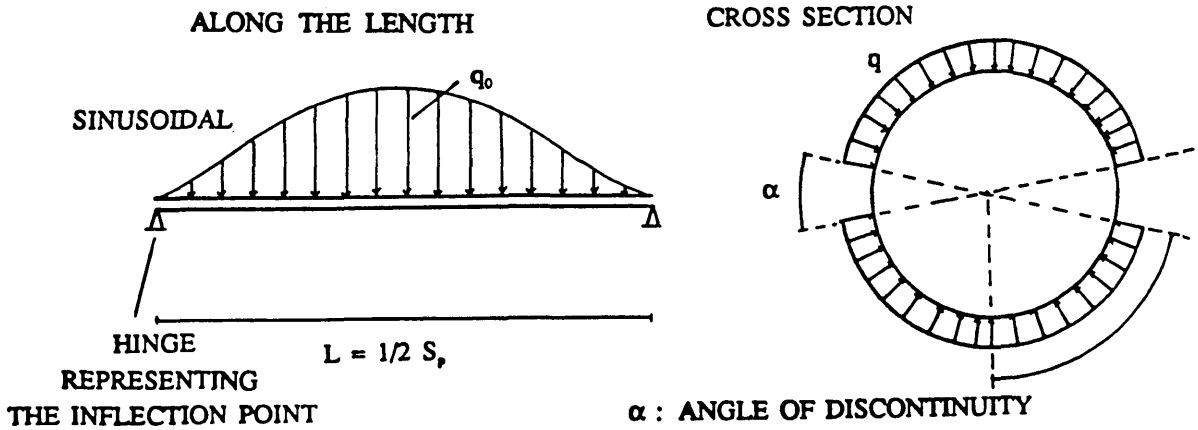
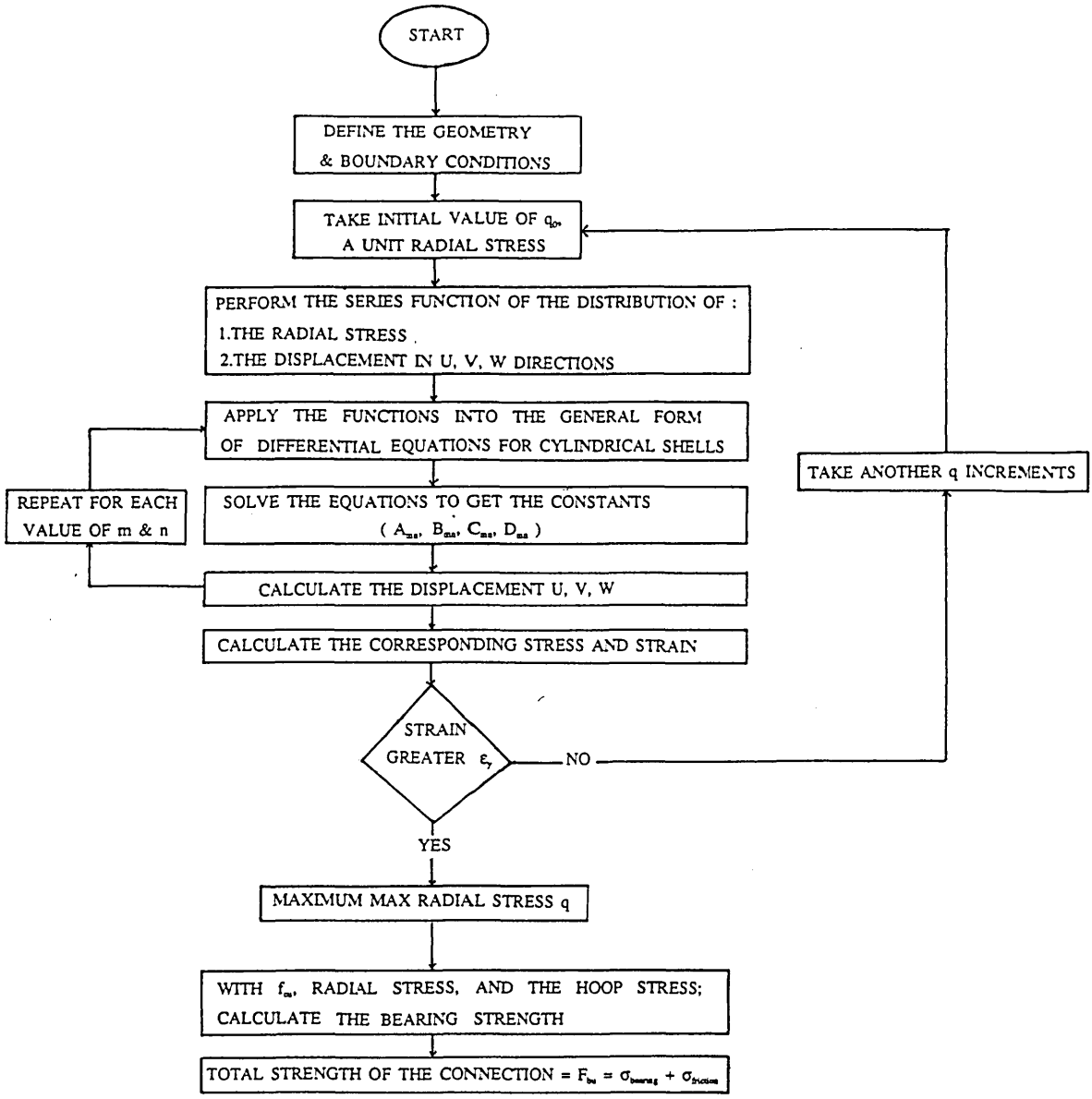
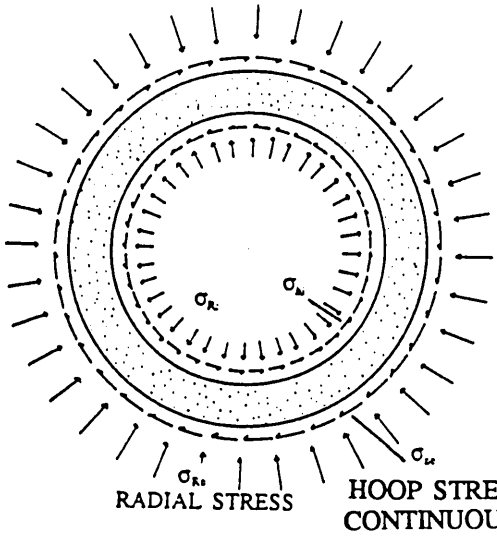


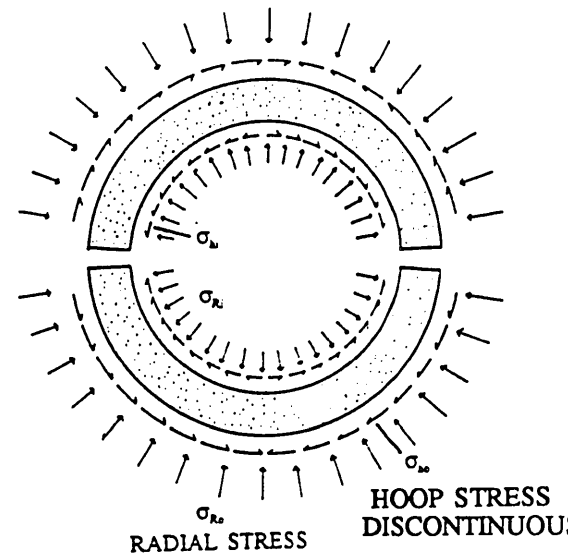
FIG 6.6

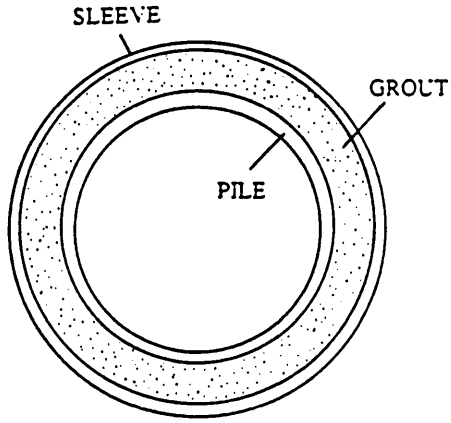


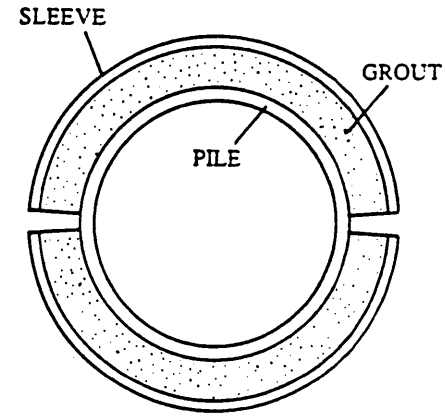
FLOW CHART FOR SOLVING THE DIFFERENTIAL EQUATIONS

FIG 6.7









STRESS STATE IN GROUTED CONNECTIONS

STRESS STATE IN SPLIT-SLEEVE CONNECTIONS

FIG 6.8

CHAPTER SEVEN
CONCLUSIONS AND SUGGESTIONS FOR FURTHER RESEARCH

7.1 Summary and Conclusion

Based on the experimental and numerical studies presented in the preceeding chapters, the summary and general conclusion drawn are as follows :

- Weld-beaded connection are the most widely used technique for improving the performance of grouted pile-to-sleeve connections in offshore structures.

- By providing weld-beads, the strength of grouted connections can be significantly increased. The present and previous programmes have shown that the strength of weld-beaded connections could be up to three times that of plain connections.

- The strength of weld-beaded connection is the sum of two components, namely the frictional bond due to friction between the grout and steel surface, and the bearing strength of the grout beneath the weld-bead.

- The friction strength is dependent upon the surface roughness of the tubular, the radial strength of the connection and the grout strength. For low grout strengths the friction component is significantly affected by changes in grout strength. However, this effect is much less for higher grout strengths. For connections with a grout strength of more than 35 N/mm^2, the effect of increasing grout strength on the friction strength is negligible.

- Depending on the radial stiffness of the connection, the bearing strength of the grout beneath the weld-bead can be more than four times that of its uniaxial strength. This is because the grout beneath the weld-bead is in a triaxial stress state. The confining stress produced by the steel tubular enhances the grout strength in such a way that an increase in radial stiffness of the steel tubular will increase the grout strength. In the present experimental programme, when strain gauges were provided, the failure of

the connection seemed to be associated with the yielding of the pile in the hoop direction.

- The specimens opened after testing showed that cracks occurred in the grout both diagonally and vertically. The diagonal cracks are not likely to be the primary cause of failure. Measurement of the cracks from the opened specimens showed that the point at which the diagonal cracks occured correspond to greater axial slip than the relative displacement recorded at the ultimate load.

- The occurence of vertical cracks may be considered to be related to the hoop yielding of the steel tubular at maximum load. However, it is also possible that the vertical cracks occured due to an energy release when the steel tubular was cut open.

- In the present programme the bottom weld-bead always failed at an early stage. This is because the failure at the bottom weld-bead is due to tension and shearing of the grout rather than grout crushing as in the upper weld-beads (although there is a possiblity that for a certain loading arrangement the loaded end could produce a prying force which could have a positive effect on the bottom weld-bead, thus improving its strength). This effect of earlier failure has not been considered before. The bottom weld-bead effect is significant for short connections which normally have few weld-beads, but the effect becomes less significant as the number of weld-beads increases, as in long connections.

- The above is significant in assessing the effect of L/D_p ratio. Depending on weld-bead and loading arrangements, the test results for $L/D_p = 2$ can have different bottom weld-bead effects. Therefore, different results are expected for the same L/D_p ratio.

- The variation in weld-bead height is not accurately predicted in the existing design formulae. The assumption of a linear relation between weld-bead height and average bond strength may result in a reduction in safety margins.

This is because for high values of weld-bead height and small pile thickness, the bending effect due to the eccentricity of the weld-bead stress will be more pronounced.

- The effect of weld-bead height and spacing should not be considered as a composite h/s parameter. This is because the effect of increasing the weld-bead height is not the same as that of reducing the spacing.

- If weld-bead spacing is very small, the total shearing strength of the grout between the weld-beads can be less than the bearing strength of the grout beneath the weld-bead. In this case, failure will be due to shear failure of an equivalent grout cylinder. On the other hand, when the spacing is sufficiently large, the effect of variation of weld-bead spacing is negligible.

- The exclusion of the radial stiffness parameter in the API design formula leads to poor predictions of the connection strength, and in some cases could reduce the safety margin.

- The use of longitudinal stiffeners in previous test programmes could be misleading in assessing the experimental results, especially for specimens with small sleeve thicknesses and long connections.

- The use of bond strength parameters in assessing the test results for specimens with low grout strength is not always reliable. This is because the assumption of a parabolic relation between grout strength and average bond strength is not applicable for low grout strengths.

- Stress-slip constitutive relations for weld-beaded connections have been formulated through a calibration process. The relationship was then implemented as the material model of the spring element, which is used to link the steel and grout nodes in the finite element analysis. The result of the analysis has been shown to agree well with experimental results, both with the present and previous programmes. The main advantages of using analytical models is that they can provide the stress distribution within the

connection and can easily accommodate any geometric variation without time consuming and costly experimental programmes.

- A design equation for both weld-beaded and plain connections was introduced. The formula for weld-beaded connection involves calculation of the confined grout strength which is developed under a triaxial stress condition. Comparisons with other formulae are presented, and as a whole the proposed method gave better agreement with experiments.

- An alternative approach to analyse the strength of split sleeve connections has been introduced. This takes into account the continuity or otherwise of the grout annulus in the circumferential direction.

It should be noted, however, that the above conclusions are based on a limited test programme. Although probably more than one hundred models of weld-beaded connections have been tested elsewhere, only about seventy models are available for use in comparison, due to the lack of information and publications. Therefore, it is realised that further confirmation of some of the above observations is required.

7.2 Suggestions for Further Research

Whereas the current project has resolved several outstanding issues, and yielded design expressions for grouted pile/sleeve and split-sleeve repair connnections, it has also highlighted several areas of concern.

Firstly, there is a growing need in the offshore industry to reduce the length of connections, hence effect an overall reduction in platform weight. Consequently, the use of larger weld-bead heights and/or smaller spacing is being considered. Due to the effect of local bending stresses in the pile (for increased h) and susceptibility to shear failure (for reduced s), research is urgently needed to quantify key thresholds. There is a limit on the increase of f_{bu} for an increase in h, which should be quantified. Moreover, a criterion for the onset of shear failure, as opposed to

crushing, needs to be established.

Another area of concern is the fatigue performance of grouted connections. Very few models were tested under a limited scope of applied displacement amplitude. The effect of early age cyclic loading on the subsequent fatigue performance should be studied. Furthermore, low cycle, high amplitude, fatigue testing should be conducted to ensure the safety of the connection under extreme cases.

The effect of increased L/D_p ratio is not adequately accounted for in the existing design codes. There is a large margin between tested specimens and L/D_p used in practice. Establishing a relation between f_{bu} and L/D_p up to 20 is very important.

Finally, only very limited work have been undertaken on the effect of combined axial force and bending on the connection behaviour. This may be of significance in certain cases, especially when a number of cycles of bending stresses are applied at an early age. The voids thus created may have a significant effect on subsequent load-displacement response of the connections.

It is hoped that the renewed interest in grouted connection, manifested in the recently launched joint industry research project, will address some of these issues, and will help advance existing experimental and analytical techniques that are needed, also to resolve the outstanding problems faced in designing safer and more reliable pile/sleeve grouted connections.

APPENDIX I

Bond-slip relationship from calibration results for plain connections :

For $\delta_a < 0.01$ mm :

$\sigma_f = 100\ \delta_a$

In this phase, the bond is given by chemical adhesion only.

For $0.01 \text{ mm} < \delta_a < 0.2$ mm :

$\sigma_f = 0.0819 + 33.35\ \delta_a - 513.34\ \delta_a^2 + 4404.4\ \delta_a^3 - 22099\ \delta_a^4 + 67346\ \delta_a^5 - 12623\ \delta_a^6 + 14206\ \delta_a^7 - 88016\ \delta_a^8$

In this phase, the bond consists of a combination of chemical adhesion and mechanical action.

For $0.2 \text{ mm} < \delta_a < 0.32$ mm :

$\sigma_f = 0.158\ \delta_a + 1.138$

In this phase, the bond consists of mechanical and friction action.

For $\delta_a > 0.32$ mm :

$\sigma_f = 1.314 - 0.376\ \delta_a$

Here, the bond is only due to friction, since the grout surface has been smoothed, and therefore does not provide any mechanical interlocking.

APPENDIX II

Bearing-slip relationship from calibration results for weld-beaded connections :

$\sigma_b = C_k\ C_h\ C_g\ f(\delta_a)$

$f(\delta_a) = 120.6\ \delta_a - 20.1\ \delta_a^2$ for $\delta_a < 2$ mm

$f(\delta_a) = 160.8 + 40.2\ (\delta_a - 2)$ for $\delta_a > 2$ mm

$C_k = -2.3 + 469.8\ K - 17165.2\ K^2$ for $0.008 < K < 0.013$

$C_k = 23.5048\ (K - 0.013) + 0.90648$ for $K > 0.013$

$C_h = 1 - 0.0833\ (h - 1.02)$ for $h < 5$ mm

$C_g = (f_{cu} / 36)^{0.2}$

APPENDIX III

Relationship between bearing and hoop stress :

$\sigma_{hi} = a_0 + a_1\ \sigma_b + a_2\ \sigma_b^2 + a_3\ \sigma_b^3 + a_4\ \sigma_b^4$

$a_0 = 0$

$a_1 = 5.384868$

$a_2 = 0.079137789$

$a_3 = -0.000573229$

$a_4 = 0.000002584$

APPENDIX IV

Computer Listing for Simplified Analytical Approach

```
      PROGRAM LDP(INPUT,OUTPUT,RESULT,TAPE5 = INPUT,
     &TAPE6 = OUTPUT, TAPE7 = RESULT)
C     ============================================================
C         PROGRAM OF THE SIMPLIFIED ANALYTICAL APPROACH
C         THIS PROGRAM HAS BEEN USED TO RUN MODELS SERIES P AND R
C         FROM OTP-11
C     ============================================================
C         TO RUN THE PROGRAM :
C         ====================
C         1.GET THE PROGRAM
C         2.COMPILE AND RUN IT (INTERACTIVELY)
C         3.EXAMPLE OF THE INPUT FOR MODEL P1 IS AS FOLLOWS;
C            - SPACING : 169.32
C            - NUMBER OF SHEARKEYS : 6
C            - SHEARKEY HEIGHT     : 2.83
C            - E STEEL             : 210000
C            - T PILE              : 25.4
C            - GROUT STRENGTH      : 54.21
C            - RADIUS PILE         : 254
C            - RADIAL STIFFNESS    : 0.0146
C
C          ============================================================
C         THE INPUT IS INTERACTIVE


C         THE OUTPUT IS IN THE FILE "RESULT"
C         ============================================================
C
C
      REAL K
      DIMENSION D (100), ESEC(100),ESECS (100), A(100)
      DIMENSION SB(100), BETA(100), EKADE(100), EHOOP(100), DELTA(100)
      DIMENSION GAMMA(100), SBN(100)
C
      WRITE (6,100)
  100 FORMAT (3X,'PLEASE GIVE  THE FOLLOWING INFORMATIONS',/,
     &3X,'SP : SHEAR KEY SPACING IN MM          ',/,
     &       3X,'N  : NUMBER OF SHEAR KEYS AT THE PILE     ',/,
     &       3X,'SKH: SHEARKEY HEIGHT                      ',/,
     &       3X,'ES : MODULUS ELASTICITY OF THE STEEL  ',/,
     &       3X,'TP : THICKNESS OF THE PILE           ',/,
     &       3X,'FC : GROUT UNIAXIAL STRENGTH    ',/,
     &       3X,'R : OUTER RADIUS OF PILE        ',/,
     &       3X,'K  : RADIAL STIFFNESS           ',/)
C
       READ (5,*) SP,N,SKH,ES,TP,FC,R,K
C
C      ------------------------------------------------


C      CALCULATE ES1
      ES1 = ( ES * TP ) / ( SP * SKH )
C
C     CALCULATE TAU
C
      TAU = 9 * (K)**0.5
C     ====================================================================
C     TAKE THE RELATIVE DISPLACEMENT AT THE TOP END, WHICH IS EQUAL WITH
C     THE  DISPLACEMENT OF THE PILE
C     AS AN INITIAL VALUE TAKE D(0) = 1 MM
C
C     DISPLACEMENT AT THE TOP WELD-BEAD IS INITIALLY
C     EQUAL WITH D (0)
C     ====================================================================
C
      D (1) = 1
C
C     INCREASE THE DISPLACEMENT GRADUALLY UNTILL P MAX IS REACHED
C     ==========================================================
```

```
C
      DO 11 L = 1,500
C
      D (1) = D(1) + 0.01

C     ------------------------------------------------------------
C     CALCULATE THE CORESPONDING STRESS AT EVERY WELD-BEAD POSITION
C     ------------------------------------------------------------
C
      DO 12 J = 1,N
C
C     ----------------------------------------------------
C     THE TOTAL DISPLACEMENT IS THE SUMMATION OF
C     DISPLACEMENT AND ELONGATION DUE TO ELASTICITY.
C     THE TOTAL DISPLACEMENT AT WELD-BEAD J ( D(J) ), IS EQUAL
C     WITH THE  DISPLACEMENT OF WELD-BEAD (J+1) WITHOUT
C     ELONGATION
C     ----------------------------------------------------
C
      IF (J.GT.1) D(J) = D(J-1)
C
C     ------------------------------------------------------------
C     CALCULATE ESEC, AND BEARING STRESS SB, AS FUNCTION OF RELA
C     TIVE DISPLACEMENT
C     CALCULATE THE STIFFNESS FACTOR CK, THE WELD-BEAD HEIGHT
C     FACTOR CH, AND THE GROUT STRENGTH FACTOR CG
C     ------------------------------------------------------------


C
      CK = -2.3 + 469.6*K - 17165.2*(K)**2
C
      CH =  1 - 0.0833*(SKH-1.02)
C
      CG = (FC/36)**0.2
C
      IF (D(J).LE.2) ESEC(J)=120.6067-20.101*(D(J))
C
      IF (D(J).GT.2.AND.D(J).LE.3.5) ESEC(J)=80.404/D(J) +
     & 40.2027
C
      IF (D(J).GT.3.5.AND.D(J).LE.11.167) ESEC(J)
     & = (221.11-28.75*(D(J)-3.5)+1.875*(D(J)-3.5)**2)/D(J)
C
      IF (D(J).GT.11.167) ESEC(J)=110.902/D(J)
C
      IF (D(J).GT.3.5) ESEC(J) = 0.7*221.11/D(J)
C
      ESEC(J) = ESEC(J) * CK * CH * CG
C
      ESECS(J) = ESEC(J) * SKH / TP
C


      SB(J) = ESECS(J) * D(J)
C
      BETA (J) = 0
C
      IF (J.EQ.1) GO TO 111
C
      DO 39 I = 1,(J-1)
C
      EKADE(I) = ESECS(I)*D(I)*(J+1-I)
C
      BETA(J) = BETA(J) + EKADE(I)
C
  39   CONTINUE
C
 111    FRICT = (0.5*TAU*J*SP)/(ES1*SKH)
C
```

```
C     ------------------------------------------------------
C     CALCULATE THE HOOP STRAIN EHOOP
C     ------------------------------------------------------
C
      EHOOP(J) = ( (5.385*SB(J)) + ((0.07913)*(SB(J))**2)
     &   -((0.00057)*(SB(J))**3) + ((0.0000025)*(SB(J))**4)
     &          ) * 0.000001
C
C     --------------------------------
C     YIELD STRAIN = 0.2 %
C     --------------------------------
C
      IF (EHOOP(J).GT.0.002) EHOOP(J) = 0.002
C
      DELTA(J) = ( FRICT+(0.3*EHOOP(J)*SP) ) * (ES1-ESEC(J))
C
      ALPHA = ES1 * D(1) * (1-0.3**2)
C
      GAMMA(J)= (ES1-ESECS(J))*(1-0.3**2)
C
C
      D(J) = (ALPHA + BETA(J) + DELTA(J))/(GAMMA(J))
C
 12   CONTINUE
C     ============================================
C     CALCULATE THE P MAX
C     ============================================
C
C     ------------------------------
C     CALCULATE THE BEARING STRESS SB(II)

C     ---------------------------------
C
      PB = 0
C
C
      DO 22 M = 1,N
C
      SBN(M) = ESEC(M) * D(M)
C
       IF(M.EQ.(N-1)) SBN(M) = 0.0
C
       IF(M.EQ.N) SBN(M) = 0.0
C
C
      PB =  PB + SBN(M)*SKN
C
 22   CONTINUE
C     ---------------------------------
C     CALCULATE THE TOTAL P MAX = PB + PFRICT
C     ---------------------------------------
      PMAX = ( PB + (TAU*(N)*SP))*3.14159*2*R
C
C     ---------------------------------------


C     CALCULATE THE BOND STRENGTH SBU
C     ---------------------------------------
      SBU = PMAX / ( 2*3.14159*R*(N)*SP)
C
C     GIVE INITIAL VALUE OF PULT
      IF (L.EQ.1) PULT = 0
C
C     CHECK WHETER P MAX IS EQUAL PULT
C     ---------------------------------------
C
      IF (L.GT.1.AND.PMAX.LT.PULT) GOTO 19
C
      PULT = PMAX
C
```

```
C
 11   CONTINUE
C
 19   SBUMAX = PULT/(2*3.14159*R*H*SP)
C
      WRITE (7,190) PULT,SBUMAX
190   FORMAT(3X,5HPMAX=,F10.2,1X,1HN,2X,4HSBU=,F6.3,1X,'N/MM2')
C
C

      STOP
      END
C     ============================================
C     THE OUTPUT, FILENAME "RESULT"
C     ============================================
      PMAX=4318425.55 N  SBU= 2.664 N/MM2
C    ============================================
```

Computer Listing for Grouted Clamp Connection Analysis

```
      PROGRAM REPAIR(INPUT,OUTPUT,RESULT,TAPE5 = INPUT,
     +TAPE6 = OUTPUT, TAPE7 = RESULT)
C
      REAL H,L,FI
C
      DIMENSION  A1(25,0:24),B(25,0:24),C(25,0:24),D(25,0:24)
C
      DIMENSION  U(25,0:24),V(25,0:24),W(25,0:24),FQ(25,0:24)
C
      DIMENSION  EQ(25,0:24), EX(25,0:24), FI(0:20)
C
      DIMENSION  C1(25,0:24), C2(25,0:24), C3(25,0:24), C4(25,0:24)
C
      DIMENSION  C5(25,0:24), C6(25,0:24), C7(25,0:24), C8(25,0:24)
C
      DIMENSION  C9(25,0:24), C10(25,0:24),C11(25,0:24),C12(25,0:24)
C
      DIMENSION  UF(0:20), VF(0:20), WF(0:20), QF(0:20), FBW (0:20)
C
C
C
C     ----------------------------------------------------
C


      U1 = 0.3
      E  = 210000.
      PHI= 3.14159265
C
      OPEN (UNIT=7,FILE='RESULT')
C
      REWIND 5
C
     WRITE (6,60)
C
  60  FORMAT (3X,'PLEASE GIVE THE FOLLOWING DATA',/,
     +        3X,'RADIUS OF PILE                ',/,
     +        3X,'THICKNESS OF PILE             ',/,
     +        3X,'LENGTH OF PILE                ',/,
     +        3X,'A HALF ANGLE OF THE SLEEVE        ',/,
     +        3X,'SHEARKEYS SPACING             ',/,
     +        3X,'WELD-BEAD HEIGHT              ',/,
     +        3X,'NUMBER OF WELD-BEAD           ',/,
     +        3X,'RADIAL STIFFNESS K            ',/,
     +        3X,'GROUT STRENGTH                ')
C
      READ (5,*) A, H, TL, ALP, SP, SKH, NW,AK, FC
C

C
      L = TL/NW
C
C
C
C      ------------------------------------------------
C      MAXIMUM DISPLACEMENTS WILL BE CALCULATED AT WELD-BEAD
C      POSITION, X = 1/2 SP
C      ------------------------------------------------
C
        X = (1/2)*SP
      IFAILS = 0
C
C
      WFW =0
C
      FBWW = 0
      DO 1001 KF = 0, 10
C
      FIX = (PHI/2 - ALP) / 10
C
      FI (KF) = FIX * KF
C
```

```
      IF (IFAILS.GE.3) GO TO 550
C
C
C
      Q = 5
C
      DO 10 I = 5,40,1
C
C
       Q = Q + 1
C
 550   DO 100 M = 1,20
C
      DO 200  N = 0,20
C
      IF ( M.GT.0) GO TO 400
C
      D (M,N) = 0
C
 400  IF (M.GT.0.AND.N.EQ.0) D(M,N) = (8*ALP*Q)/(M*PHI*PHI)
C
      IF (M.GT.0.AND.N.GT.0) D(M,N) = ((16*Q)/(M*N*PHI*PHI))*
     +        ((COS(N*PHI/2))*(SIN(N*(ALP-PHI/2))))


      IF (IFAILS.GE.3) GO TO 550
C
C
C
      Q = 5
C
      DO 10 I = 5,40,1
C
C
       Q = Q + 1
C
 550   DO 100 M = 1,20
C
      DO 200  N = 0,20
C
      IF ( M.GT.0) GO TO 400
C
      D (M,N) = 0
C
 400  IF (M.GT.0.AND.N.EQ.0) D(M,N) = (8*ALP*Q)/(M*PHI*PHI)
C
      IF (M.GT.0.AND.N.GT.0) D(M,N) = ((16*Q)/(M*N*PHI*PHI))*
     +        ((COS(N*PHI/2))*(SIN(N*(ALP-PHI/2))))
C      ------------------------------------------------------
C      CALCULATE THE COEFICIENT OF CONSTANTS, C1(M,N) UP TO C1(M,N)2
C      ------------------------------------------------------------
C
C
      C1(M,N) = ( (M*PHI/L)**2 + ((1-U1)/(2*A*A))*(N*N) )
C
      C2(M,N) =  - ( (1+U1)/(2*A) ) * (N)*(M*PHI/L)
C
      C3(M,N) = (U1/A)*(M*PHI/L)
C
      C4(M,N) = ((1+U1)/2)*(N)*(M*PHI/L)
C
      C5(M,N) = -( (A*(1-U1)/2)*((M*PHI/L)**2) + (N*N/A) )
C
      C6(M,N) = N/A
C
      C7(M,N) = -C3(M,N)
C
      C8(M,N) = C6(M,N)
C
      C9(M,N) = (-N*N/12) * ( (12/(A*N*N)) + A*((M*PHI/L)**4) +
```

```
     +     (2/A)*((N*M*PHI/L)**2) + ((N**4)/(A**3)) )
C
      C10(M,N) = (A*(1-U1**2))/(E*H)
C
C
      C11(M,N) = -(C4(M,N)-(C1(M,N))*(C6(M,N))/(C3(M,N))) /
     +           (C5(M,N)-(C2(M,N))*(C6(M,N))/(C3(M,N)))
C
      C12(M,N) = -(C1(M,N)+C2(M,N)+C11(M,N))/C3(M,N)
C
C     CALCULATE A1(M,N), B(M,N), C(M,N)
C
       A1(M,N) = D(M,N)*C10(M,N) / (C7(M,N)+C11(M,N)*C8(M,N)+
     +           C12(M,N)*C9(M,N))
C
      B(M,N) = C11(M,N)*A1(M,N)
C
      C(M,N) = C12(M,N)*A1(M,N)
C
 200  CONTINUE
 100  CONTINUE
C
C     SUBSITUTE TO THE EQUATION OF DISPLACEMENTS AND LOAD


C     DISTRIBUTION
C     ----------------------------------------------------
C
      UF(KF)= 0
C
      VF(KF) = 0
C
      WF(KF) = 0
C
      QF(KF)= 0
C
      DO 101 M = 1,20
C
      DO 201 N = 0,20
C
      U(M,N)  = - A1(M,N)*(COS(N*FI(KF)))*(COS(M*PHI*X/L))
C
      V(M,N) = B(M,N)*(SIN(N*FI(KF)))*(SIN(M*PHI*X/L))
C
      W(M,N) = C(M,N)*(COS(N*FI(KF)))*(SIN(M*PHI*X/L))
C
      FQ(M,N)= D(M,N)*(COS(N*FI(KF)))*(SIN(M*PHI*X/L))
C
      UF(KF)= UF(KF)+ U(M,N)
C
      VF(KF) = VF(KF) + V(M,N)
C
      WF(KF) = WF(KF) + W(M,N)
C
      QF(KF)= QF(KF)+ FQ(M,N)
C
  201 CONTINUE
C
  101 CONTINUE
C
C     CHECK THE CORRESPONDING STRESS OR STRAIN
C     EX = DU/DX  ; EQ = 1/A DV/DQ - W/A
C
C     EX = B(M,N)*(N)*(COS(N*FI(KF))*(SIN(M*PHI*X/L))
C
C     DV/DQ = -((A1(M,N)*COS(N*FI(KF)*SIN(M*PHI*X/L)) * (M*PHI/L)
C
      EQF1 = 0
C
      EXF  = 0
C
```

```
      DO 102 M = 1,20
C
      DO 202 N = 0,20
C
      EQ(M,N) = B(M,N)*(COS(N*FI(KF)))*(SIN(M*PHI*X/L))
C
      EQF1 = EQF1 + EQ(M,N)
C
      EX(M,N)=-A1(M,N)*(M*PHI/L)*(COS(N*FI(KF)))*
     +(SIN(M*PHI*X/L))
C
C
      EXF  = EXF + EX(M,N)
C
 202  CONTINUE
C
C
 102   CONTINUE
      EQF= (EQF1/A) -  WF(KF)/A
C
C
C     CHECK THE STRAIN IN HOOP DIRECTION
C     ----------------------------------


C
      IF ( EQF.GE.0.002) GO TO 404
C
      IF (IFAILS.GE.3) GO TO 404
C
C
  10  CONTINUE
C
 404  WRITE (7,700) UF(KF), VF(KF), WF(KF), QF(KF), Q
C
 700  FORMAT (3X,2HU=,F9.7,3X,2HV=,F9.7,3X,2HW=,F9.7,3X,2HQ=,F9.5
     +,2HQ=,F9.5)

C     ---------------------------------------------------
      CALL SURFAIX (FC, KF,QF, FBW ,IFAILS, AK )
C     ---------------------------------------------------
C
C
      FBWN = FBWN + FBW(KF)
C

C
      WFN  = WFN + WF(KF)

C
 1001  CONTINUE
C
      FBWNX=FBWN/11
C
      WFNX = WFN / 11
C

      PULT=( FBWNX)*(NW-1)*(SKH)*((2*ALP)*A)*2
C
C
      WRITE (7,701) FBWNX,PULT
C
 701  FORMAT (3X,5HFGUC=,F6.1,5HPULT=,F12.1)
C
      FBU = PULT/(2*PHI*A*TL)
      FBU = FBU +  9*(AK)**0.5
C
      WRITE (7,702) FBU
C
```

```
 702  FORMAT (3X,4HFBU=,F5.3)
C
      STOP
      END
C
C
      SUBROUTINE SURFAIX (FC, KF, QF, FB,IFAILS, AK )
C     ------------------------------------------------
C     PROGRAM TO CALCULATE FAILURE CRITERIA FOR TRIAXIAL
C     STRESS STATE OF CONCRETE
C     S(1)      : PRINCIPAL STRESS IN AXIAL DIRECTION
C     S(2)      : PRINCIPAL STRESS IN RADIAL DIRECTION
C     S(3)      : PRINCIPAL STRESS IN HOOP DIRECTION
C     SO(1)     : NORMAL OCTAHEDRAL STRESS
C     SO(2)     : SHEAR OCTAHEDRAL STRESS
C     SO(3)     : ROTATIONAL VARIABLE DEFINING DIRECTION
C                 OF SO(2) ON OCTAHEDRAL PLANE
C     ------------------------------------------------
C
C
      DIMENSION  S(3), SO(3), QF(0:20), FB(0:20)
C
C
      S(1) = FC
C
      IFAILS =0
C
      DO 20 I = 1,50
C
      S (2) = QF(KF)
C
      S (3) = 9*2*((AK)**0.5)
C
      S (1) = S(1) + 2
C
C
C     ------------------------------------------------
C     CALCULATE OCTAHEDRAL STRESS AND ROTATIONAL VARIABLE
C     ------------------------------------------------
      CALL OCTSTST ( S, SO )
C     ------------------------------------------------
C     CALCULATE SHEAR OCTAHEDRAL STRESS AT ONSET UNSTABLE
C     FRACTURE PROPAGATION (TOOUFP)
C     ------------------------------------------------


      CALL OUFPST ( FC, TOOUFP, SO, TOE, TOC)
      IF ( SO(2).GE.TOOUFP) IFAILS=3
C
      IF (IFAILS.GE.3) FB(KF) = S(1)
      IF (IFAILS.GE.3) GOTO22
C
C
      IF ( IFAILS.GE.4) WRITE(7,709) IFAILS, S(1), S(2), S(3), SO(3)
  709  FORMAT (2X,I2,3X,F7.2,3X,F7.2,3X,F7.2,F7.2)
   20   CONTINUE
C
   22   RETURN
C
      END
C
      SUBROUTINE OCTSTST ( S , SO )
C     ------------------------------------------------
C     CALCULATE OCTAHEDRAL STRESS AND ROTATIONAL VARIABLE
C     FROM PRINCIPAL STRESSES
C     ------------------------------------------------
      DIMENSION  S (3) , SO(3)
C     CALCULATE NORMAL OCTAHEDRAL STRESS
C
```

```
      SO (1) = ( S(1) + S(2) + S(3))/3
C
C     CALCULATE SHEAR OCTAHEDRAL STRESS
C
      DELS1   = S(1) - S(2)
      DELS2   = S(2) - S(3)
      DELS3   = S(3) - S(1)
      DELS11  = DELS1 ** 2
      DELS22  = DELS2 ** 2
      DELS33  = DELS3 ** 2
      SO (2)  = (( DELS11 + DELS22 + DELS33) ** 0.5)/3
C
C     CALCULATE ROTATIONAL VARIABLE (IN DEGRESS)
C
      A       = S(1) + S(2) - 2 * S(3)
      B       = 4.2426407 * SO (2)
      IF ( B.LT.1.0E-8) COSTHE = 1.
      COSTHE  = ABS ( A/B )
      IF ( COSTHE.GT.1 ) COSTHE = 1
      SO (3)  = ( ACOS (COSTHE)) * 57.295779
      RETURN
      END
C
      SUBROUTINE OUFPST ( FC , TOOUFP , SO , TOE , TOC )
C     ---------------------------------------------------
C     CALCULATE THE ULTIMATE SHEAR OCTAHEDRAL STRESS AT
C     OUFP ( TOOUFP ) WITH GIVEN ORIENTATION VARIABLE
C     SO (3) , GIVEN NORMAL OCTAHEDRAL STRESS SO (1) ,
C     AND GIVEN GROUT UNIAXIAL STRENGTH (FC)
C     ---------------------------------------------------
      DIMENSION  SO (3)
C
C     CALCULATE TOC : ULTIMATE SHEAR OCTAHEDRAL STRESS
C                     FOR ORIENTATION = 60 DEGREES
C
      SOREL  = SO(1)/FC
      IF( SOREL.LE.-0.05 ) SOREL = -0.049
      TOC    =( 0.944 * (( SOREL + 0.05 )) ** 0.724) * FC
C
C     CALCULATE TOE : ULTIMATE SHEAR OCTAHEDRAL STRESS
C                     FOR ORIENTATION = 0 DEGREE
C
      TOE    =( 0.633 * (( SOREL + 0.05 )) ** 0.857) * FC
C
C     CALCULATE TOOUFP FOR GIVEN SO (3)
C
C
      TOE    =( 0.633 * (( SOREL + 0.05 )) ** 0.857) * FC
C
C     CALCULATE TOOUFP FOR GIVEN SO (3)
C
      THETA = SO(3)/57.295779
      A     = 2*TOC*(TOC**2-TOE**2)*COS(THETA)
      B     = TOC * ( 2*TOE - TOC )
      C     = 4 * ( TOC**2 - TOE**2)*(COS(THETA))**2
      D     = 5 * ( TOE**2 ) - 4*TOC*TOE
      ATHETA= ABS ( SO(3)-60 )
      IF ( ATHETA.LE.1.0E-13) GO TO 10
      CD = C + D
      IF ( CD.LT.0) CD = 0
      E  = SQRT(CD)
      GO TO 20
 10   E  = ABS ( TOE - 2*TOC )
 20   F  = ( TOC-2*TOE )*(TOC-2*TOE)
      TOOUFP = ( A+B*E ) / ( C+F )
      RETURN
      END
```

REFERENCES

1 BOWDEN, F P, and TABOR, D
'The Friction and Lubrication of Solids', Clarendon Press, Oxford, 1964.

2 RABINOWICZ
'Friction and Wear of Materials', John Wiley and Sons Inc, 1965.

3 NEVILLE, A M
'Properties of Concrete', Pitman Publishing, Third edition, 1982.

4 BILLINGTON, C J and LEWIS, G H G
'The Strength of Large Diameter Grouted Connections', Offshore Technology Conference, paper 3083,Houston, 1978, pp. 291-297.

5 SHELSON, W
'Bearing Capacity of Concrete', ACI Journal, vol.54, no.5, November 1957, pp. 405-414.

6 TUNG, A U
'Bearing Capacity of Concrete', Discussion of paper by Shelson, W , proceeding vol.54, no.12, June 1958, pp. 1183-1189.

7 WILLIAMS, A
'The Bearing Capacity of Concrete Loaded Over a Limited Area', Cement and Concrete Association, Technical report no.526, August, 1979.

8 HAWKINS, N M
'The Bearing Strength of Concrete for Strip Loadings', Magazine of Concrete Research, vol.22, no.71, June 1970, pp. 87-98.

9 GRIFFITH, A A
'The Phenomena of Rupture and Flow in solids', Phil. Transaction, vol.221, 1921, pp. 163-198.

10 GRIFFITH, A A
'Theory of Rupture', Proceedings of The First International Congress for Applied Mechanics, 1924, pp. 55-63.

11 SACK, R A
'Extension of Griffith's Theory of Rupture to Three Dimensions', Proceeding of The Physical Society, vol.58, 1946, The Physical Society - London, pp. 729-736

12 MC CLINTOCK, F A and WALSH, J B
'Friction on Griffith's Cracks in Rock Under Pressure', 4th US National Congress of Applied Mechanic, 1962, pp. 1015-1021.

13 WRIGHT, P J F
'Crushing and Flexural Strength of Concrete made with Limestone Aggregate', Road Research Laboratory Note, RN/3320/PJFW, HMSO, October 1958.

14 SHUMAN, L and TUCKER, J
'Tensile and others Properties of Concrete made with various type of Cements ', Journal of Research National Bureau Standard, paper no.RP 1552, vol.31, 1943.

15 SAUL, A G A
'A Comparison of the Compressive, Flexural, and Tensile Strength of Concrete', Cement Concrete Association, Technical Report TRA/333, London, June 1960

16 SHACKLOCK, B W and KEENE, P W
'Comparison of The Compressive and Flexural Strength of Concrete with and without Entrained Air', Civil Engineering, vol.54, London, January 1959, pp. 77-80.

17 TEYCHENNE, D C
'Discussion on : The Design of Concrete mixes on The Basis of Flexural Strength, Proceeding of a Symposium on Mix Design and Quality Control of Concrete', Cement and Concrete Association, London, 1954, pp. 153.

18 GARDNER, N J and POON, S M
'Time and Temperature effects on Tensile, Bond, and Compressive Strength', Journal of American Concrete Institute, vol.73, no.7, 1976, pp. 405-409.

19 SOZEN, M A, ZWOYER, E M, and SIESS, C P
'Strength in Shear of Beams without Web Reinforcement', University of Illinois, Engineering Experiment Station, Bulletin no.452, April 1959.

20 BRANTDZAEGT, A, RICHART, F E and BROWN, R L
'A Study of The Failure of Concrete Under Combined Compressive Stresses', University of Illinois, Engineering Experiment Station, Bulletin no 185, 1928.

21 BELLAMY, C J
'Strength of Concrete Under Combined Stress', ACI Journal, vol.58, October 1961, pp. 367-381.

22 SUNDARA RAJA IYENGAR, K T, CHANDRASHEKHARA, K and KRISHNASWAMY, K T
'Strength of Concrete Under Biaxial Compression', ACI Journal, February 1965, pp. 239-249.

23 SUNDARA RAJA IYENGAR, K T, DESAYI, P and NAGI REDDY, K
'Stress-Strain Characteristic of Concrete Confined in Steel Binders', Magazine of Concrete Research, vol.22, no.72, September 1970, pp. 173-184.

24 DESAYI, P SUNDARA RAJA IYENGAR, K T and REDDY, T S
'Equation for Stress-Strain Curve of Concrete Confined in Circular Steel Spiral', Materiaux et Constructions, vol.11, no.65, 1978, pp. 339-345.

25 GERSTLE, K H
'Simple Formulation of Biaxial Concrete Behaviour', ACI Journal, vol.78, January-February 1981, pp. 62-67.

26 GERSTLE, K H
'Simple Formulation of Triaxial Concrete Behaviour', ACI Journal, vol.78, September-October 1981, pp. 382-387.

27 KUPFER, H, HILSDORF, H K, and RUSCH, H
'Behaviour of Concrete Under Biaxial Stresses', ACI Journal, vol.66, August 1969, pp. 656-666.

28 WANG CHUAN-ZHI, GHUO ZHEN-HAI and ZHANG XIU-QIU
'Experimental Investigation of Biaxial and Triaxial Compressive Concrete Strength', ACI Journal, vol.84, March-April 1987, pp. 92-100.

29 HOBBS, D W, POMEROY, CD and NEWMAN, JB
'Design Stresses for Concrete Structures Subject to Multi-axial Stresses', The Structural Engineer, vol.55, no.4, April 1977, pp. 151-164.

30 OTTOSEN, N S
'Constitutive Model for Short-time Loading of Concrete', ASCE journal, EM Div., vol.105, no.EM 1, 1979, pp. 127-139.

31 KOTSOVOS, M D
'A Mathematical Description of The Strength Properties of Concrete Under Complex Loading', Magazine of Concrete Research, vol.31, no.108, September 1979, pp. 151-157.

32 KOTSOVOS, M D and NEWMAN, J B
'Generalized Stress-Strain Relations for Concrete', ASCE Journal, EM Div., Vol 104, no EM 4, August 1978, pp. 845-855.

33 KOTSOVOS, M D
'Effect of Stress Path on The Behaviour of Concrete Under Triaxial Stress State', ACI Journal, vol 76, February 1979, pp. 213-223.

34 KOTSOVOS, M D
'A Mathematical Description of The Deformational Behaviour of Concrete Under Generalized Stress', Magazine of Concrete Research, vol.31, June 1979, pp. 79-90.

35 KOTSOVOS, M D and NEWMAN, J B
'Behaviour of Concrete Under Multiaxial Stress', ACI Journal, vol.74, September 1977, pp. 443-447.

36 KOTSOVOS, M D
'Effect of Boundary Conditions upon The Behaviour of Concrete Under Concentration of Load', Magazine of Concrete Research, vol.33, no.116, September 1981, pp. 161-170.

37 KOTSOVOS, M D
'Fracture Processes of Concrete Under Generalised Stress State', Materiaux et Constructions, vol.12, no.72, 1979, pp. 431-437.

38 KOTSOVOS, M D and NEWMAN, J B
'Fracture Mechanics and Concrete Behaviour', Magazine of Concrete Research, vol.33, no.115, June 1981, pp. 103-112.

39 BEDARD, C
'Non-linear Finite Element Analysis of Concrete Structures', Ph.D Thesis, Imperial College-University of London, 1983

40 LEFAS, I
'Behaviour of Reinforced Concrete Walls and its Implication for Ultimate Limit State Design', Ph.D Thesis, Imperial College-University of London, 1988.

41 NIWA, Y and KOBAYASHI, S
'Failure Criterion of Cement Mortar Under Triaxial Compression', Memoirs Faculty of Engineering, Kyoto University (Japan), vol.XXIX (part 1), January 1967, pp. 1-15.

42 BALMER, G G
'Shearing Strength of Concrete Under High Triaxial Stress', US Deaprtment of The Interior Bureau of Reclamation, Laboratory Report no.SP 23, October 1949.

43 LUTZ, L A and GERGELY, G
'Mechanisms of Bond Slip of Deformed Bars in Conrete', ACI Journal, vol.66, November 1967, pp. 711.

44 NILSON, A H
'Bond Stress-Slip Relations in Reinforced Concrete', School of Civil and Environmental Engineering - Cornell University, Report 345, December 1971.

45 NILSON, A H
'Internal Meausurement of Bond Slip', ACI Journal, vol.69, no.7, Jully 1972, pp. 439-441.

46 EDWARDS, A D and YANNOPOULOS, P J
'Local Bond-Stress to Slip Relationship for Hot Rolled Deformed Bars and Mild Steel Plain Bars', ACI Journal, vol.76, no.19, March 1979, pp.405-420.

47 MIRZA, S M and HOUDE, J
'Study of Bond Stress-Slip Relationship in Reinforced Concrete', ACI Journal, vol.76, no.2, January 1979, pp. 19-45.

48 SOMAYAJI, S and SHAH, S P
'Bond Stress-versus-Slip Relationship and Cracking Response of Tension Members', ACI Journal, vol.78, no.20, May-June 1981, pp. 217-225.

49 UNTRAUER, R E and HENRY, R L
'Influence of Normal Pressure on Bond Strength', ACI Journal, vol.62, no.5, May 1965, pp.577-585.

50 ROBINS, P J and STANDISH, I G
'Effect of Lateral Pressure on Bond of Reinforcing Bars in Concrete', Proceeding of The International Conference on Bond Concrete, Paisley-Scotland, 1982

51 VIRDI, K S and DOWLING, P J
'Bond Strength in Concrete Filled Circular Steel Tubes', Imperial College, CESLIC Report CC11, London, December 1975.

52 AMERICAN PETROLEUM INSTITUTE
'Recommended Practice for Planning, Designing, and Constructing Fixed Offshore Platforms', API RP2A, 7th edition, Texas, january 1976.

53 BILLINGTON, C J and TEBBET, I E
'Models Studies of Grouted Connections for Offshore Structures', Paper no 7 of Joint Institution of Structural Engineers/ Building Research Establishment Seminar, The Use of Physical Models in Their Design, Watford-UK, November 1977, pp. 299-312.

54 BILLINGTON, C J
'The Integrity of jacket to Pile Connections', Oceanology International, 1978, pp 79-88.

55 BILLINGTON, C J and TEBBET, I E
'The Basis for New Design Formulae for Grouted Jacket to Pile Connections', Offshore Technology Conference, 1980, paper 3788, pp. 449-454.

56 DEPARTMENT OF ENERGY - UK
'Report of The Working Party on The Strength of Grouted Pile/Sleeve Connections for Offshore Structures', Offshore Technology Publication, OTP-11, HMSO London, September 1982.

57 DEPARTMENT OF ENERGY - UK
'Guidance on The Design and Construction of Offshore Installation', 3rd Edition, HMSO London, 1984.

58 LOSET, O
'Grouted Connections in Steel Platform-Testing and Design Offshore Structures', The Use of Physical Models in Their Design, Watford-UK, November 1977, pp. 313-326.

59 YAMASAKI, T, HARA, M, and CHIYOMARU, T
'Static and Dynamic Test on Cement-Grouted Pipe-to-Pipe Connections', Offshore Technology Conference, paper no.3790, Houston, 1980, pp. 467-471.

60 DOWLING, P J, ELNASHAI, A S and CARROLL, B C
'A New Pressurised Grouted Connection for Steel Tubulars', Journal of Constructional Steel Research, vol.3, no.3, 1983, pp. 32-38.

61 ELNASHAI,A S, CARROLL,B C, DOWLING,P J and BILLINGTON,C J
'Full Scale Testing and Analysis of Prestressed Grouted Pile/Platform Connections', Offshore Technology Conference, paper 5325, Houston 1986, pp. 301-306.

62 ELNASHAI, A S
'Non-Linear Analysis of Composite Tubular Joints', Ph.D Thesis, Imperial College-University of London, 1984

63 CARROLL, B C
'Behaviour of Prestressed Grout Bond Joints', Ph.D Thesis, Imperial College-University of London, 1987.

64 CHILVERS, C
'Finite Element Analysis in Grouted Connection', Ph.D Thesis, The City University, 1986

65 KRAHL, N W and KARSAN D I
'Axial Strength of Grouted Pile-to-Sleeve Connections', ASCE, ST Div., April 1985, pp.889-905.

66 KARSAN, D I and KRAHL, N W
'New API Equation for Grouted Pile-to Sleeve Connections', Offshore Technology Conference, paper 4715, Houston, 1984, pp. 49-54.

67 LEWIS, G H G, LIVETT, I G, and MEAD, K C
'A Cost Saving Design for Pile to Structure Connections as Applied to BP Magnus', Offshore Technology Conference, paper 3789, Houston, 1980, pp. 459-463.

68 AMERICAN PETROLEUM INSTITUTE
'Recommended Practice for Planning, Designing, and Constructing Fixed Offshore Platforms', API RP2A, 16th edition, April 1986.

69 FORSYTH, P and TEBBET, I E
'New Test Data on The Strength of Grouted Connections with Closely Spaced Weld-Beads', Offshore Technology Conference, paper 5833, Houston 1988.

70 DEPARTMENT OF ENERGY - UK
'A Study of Length, Longitudinal Stiffening and Size Effects on Grouted Pile-Sleeve Connections', Offshore Technology Report, OTH 86 230, HMSO London, 1986.

71 DEPARTMENT OF ENERGY
'The Strength of Grouted Pile-Sleeve Connection', Offshore Technology Report, OTH 86 210, HMSO London, 1986.

72 DEPARTMENT OF ENERGY - UK
'The Strength of Grouted Pile-Sleeve Connections for Offshore Structures, Static Test Relating to Sleeve Buckling', Offshore Technology Report, OTH 85 223, HMSO London, 1985.

73 DET NORSKE VERITAS
'Rules for Design, Construction, and Inspection of Offshore Structures', Norway, 1977.

74 ELLINAS, CP, SUPPLE, W J and WALKER, A C
'Buckling of Offshore Structures, A State-of-the-art-review of the Buckling of Offshore Structures', Granada Publishing, 1984.

75 LAMPORT, W, JIRSA, M J and YURA, J A
'Grouted Pile-to Sleeve Connection Test', University of Texas, PMFSEL Report no 86-87, June 1986.

76 NGO, D and SCORDELIS, AC
'Finite Element Analysis of Reinforced Concrete Beams', ACI Journal, Proceeding vol.64, no.3, 1967, pp. 152-163.

77 NILSON, A H
'Non Linear Analysis of Reinforced Concrete by Finite Element Method', ACI Journal, Proceeding vol.65, no.9, September 1968, pp. 757-766.

78 LABIB, F
'Non Linear Analysis of The Bond and Crack Distribution in Reinforced Concrete Members', Ph.D Thesis, University of London, 1976.

79 DOWLING, P J, ELNASHAI, A S, ARITENANG, W and CARROLL, B
'Failure Mechanisms of Weld-beaded Connections', Grouts & Grouting for Construction & Repair of Offshore Structures, OTH 88 289, HMSO London, 1988, pp.158-176.

80 DOWLING, P J, ELNASHAI, A S, ARITENANG, W and CARROLL, B
'Failure Mechanisms of Composite Tubular Connections with Shear Keys', Proceeding of The International Conference on The Behaviour of Offshore, Structures, Norway, June 1988, pp. 1191-1202.

81 DOWLING, P J, ELNASHAI, A S, ARITENANG, W and CARROLL, B
'Failue Mechanisms of Weld-Beaded Connections', A Report Submitted to The Department of Energy - UK, Imperial College, Report CESLIC GC-04, London, 1988.

82 TIMOSHENKO, S P and GOODIER, J N
'Theory of Elasticity', 3rd Edition, Mc Grawhill, 1984, pp. 65-77.

83 CARROLL, B C, ELNASHAI, A S, and DOWLING P J
'Assessment of Design Recommendation for Offshore Composite Connections', Engineering Foundation Conference on Composite Construction, New Hampshire, 7 June 1987, pp.18-33.

84 WINKWORTH, W J, HARRIS, D and BOON, R
'Structural Repairs to Offshore Installations', Transaction - The Institute of Marine Engineers, vol.99, paper 23.

85 UNDERWATER ENGINEERING GROUP-UEG
'Repairs to North Sea Offshore Structures - a Review', CIRIA, Report UR 21, 1983.

86 ONIOFROU, A
'Collapse of Damaged Ring Stiffened Cylinders', Ph.D Thesis, Imperial College-University of London, 1987.

87 ONIOFROU, A, HARDING, J, and DOWLING, P J
'Impact Damaged on Ring Stiffened Tubulars', International Colloqium on Stability of Plate and Shell Structure, Belgium, 1987.

88 THOMPSON, J M and WHITE, A R
'The Heather Platform Leg Repair', Offshore Technology Conference, paper 3529, Houston, 1979, pp. 1503-1509.

89 TEBBET, I E and ROBERTSON, D A
'Novel Underwater Strengthening System for Tubular Joints', Offshore Technology Conference, paper 4110, Houston, 1981, pp. 411-418.

90 WILLIAMS, D J
'Recent Clamps on The Forties Platform', The Naval Architec, January 1988, pp. E32-34.

91 SCOTT, G A
'Studbolting Experience in The Underwater Environment of The North Sea', Offshore Technology Conference, paper 5050, Houston, May 1985, pp. 269-275.

92 HORDYK, M
'Grouted Clamps for Underwater Repair of Offshore Structures', Metal Construction, October 1983, pp. 602-605.

93 FERN, D T and SHEAR, L
'Bolted Repair of Tubular Joints', Proceeding of The International Symposium of Integrity of Offshore Structures, paper 23, Glasgow, 1981

94 BOSWELL, L F and D'MELLO, C
'Experimental Behaviour Of Grouted Connections for Construction and Repair', Proceeding of The 4th International Conference in Behaviour of Offshore Structures (BOSS), Delft-Netherlands, Jully 1985, pp. 835-844.

95 BOSWELL, LF and D'MELLO, C
'The Fatigue Strength of Grouted Repaired Tubular Members', Offshore Technology Conference, paper 5307, Houston, 1986, pp. 147-149.

96 DEPARTMENT OF ENERGY - UK
'Grouted Repairs to Steel Offshore Structures', Offshore Technology Report, OTH 84 202, HMSO London, 1984.

97 TIMOSHENKO, S P and KRIEGER, S W
'Theory of Plate and Shells', 2nd Edition, Mc Grawhill, 1984, pp.507-514.

98 REISSNER, V H
'Formanderung und Spannungen Einer Belateten Zylinderschale', Zeitschrift fur Angewandte Mathematik und Mechanik, vol.13, Berlin, 1933.

99 WOJTASZAK, I A
'Deformation of Thin Cylindrical Shells Subjected to Internal Loading', Philosophical Magazine and Journal of Science, vol XVII, 17th series, London, Jully-December 1934, pp. 1099-1115.

100 DEPARTMENT OF ENERGY - UK
'Grouted and Mechanical Strengthening and Repair of Tubular Steel Offshore Structures', Offshore Technology Report, OTH 88 283.